



UNIVERSITAT
POLITÈCNICA
DE VALÈNCIA



UNIVERSITAT POLITÈCNICA DE VALÈNCIA

School of Industrial Engineering

Design and integration of an innovative propulsion system
based on the association of a Compact Membrane Reactor
and a Fuel Cell System

Master's Thesis

Master's Degree in Industrial Engineering

AUTHOR: Richart Alcover, Bernat Salvador

Tutor: López Juárez, Marcos

ACADEMIC YEAR: 2023/2024

REPORT

AGRADECIMIENTOS

Este trabajo ha supuesto un viaje que me ha hecho crecer, como ingeniero y como persona. Hoy no estaría aquí escribiendo estas líneas sin un buen puñado de personas con las que he tenido la suerte de cruzarme en la vida. Me gustaría darles las gracias especialmente a:

Mi familia, especialmente a mi madre. Gracias por estar ahí.

A mi tutor Marcos. Gracias por enseñarme de cerca el mundo de la investigación y por darme una guía y consejos de valor incalculable.

A mis amigos. Gracias por permitirme desconectar en los momentos que más lo he necesitado, por las rutas, las horas de césped, los cafés, las tardes de cervezas y demás momentos inolvidables.

A mis compañeros del CMT: Isabel y Àlex. Sin ellos este trabajo no sería lo que es. También al resto de “los de la sala”, por los buenos momentos compartidos.

A Ricardo, por ofrecerme la oportunidad de participar en este proyecto y confiar en mí como pocas personas lo han hecho.

Y, por último, gracias al resto de personas que me han acompañado en algún momento de esta etapa y me han aportado su granito de arena.

RESUMEN

Con el objetivo de frenar el calentamiento global y reducir las emisiones, las llamadas energías limpias están en el foco de la investigación y del desarrollo de la industria y del transporte. Con el fin de prosperar en este contexto de crisis ambiental, el Hidrógeno se postula como uno de los principales agentes para garantizar una energía limpia y sostenible en el futuro. En el sector del transporte, las Pilas de Combustible (FCS) están generando interés como una de las opciones más prometedoras para alcanzar la descarbonización, alineándose con el progreso actual hacia la economía del Hidrógeno.

Este Trabajo Final de Máster se ha desarrollado en el marco del Proyecto Europeo ALL-IN Zero, cuyo principal objetivo es el desarrollo de un sistema que alimente múltiples combustibles con bajo contenido de carbono, cero emisiones o carbono negativo, como Amoníaco, Gas Natural o alcoholes a un Reactor Compacto de Membrana (CMR), generando Hidrógeno como vector energético intermedio. Éste será consumido in situ por Motores de Combustión Interna (ICE) y por FCS para generar energía eléctrica y mecánica con cero emisiones.

Este trabajo abarca algunos aspectos de las fases de Optimización, Integración y Escalado, contando con dos objetivos principales. El primero de ellos es desarrollar una plataforma de modelado para el CMR y el FCS para diseñar el sistema de recuperación de calor y maximizar la eficiencia global. El segundo objetivo es integrar el CMR y el FCS en una plataforma de simulación multiescala para Vehículos Heavy-Duty (HDV) para estimar el rendimiento del sistema propulsivo en condiciones realistas.

Además, se propone un diseño del layout que contiene todos los componentes involucrados en el sistema propulsivo para HDV, así como una selección de componentes para el sistema térmico.

RESUM

Amb l'objectiu de frenar el calfament global i reduir les emissions, les anomenades energies netes es troben al centre de la investigació i del desenvolupament de la indústria i del transport. Per prosperar en aquest context de crisi ambiental, l'Hidrogen es postula com un dels principals agents per garantir una energia neta i sostenible en el futur. En el sector del transport, les Piles de Combustible (FCS) estan generant interès com una de les opcions més prometedores per aconseguir la descarbonització, alineant-se amb el progrés actual cap a l'economia de l'Hidrogen.

Aquest Treball Final de Màster s'ha desenvolupat en el marc del Projecte Europeu ALL-IN Zero, el principal objectiu del qual és el desenvolupament d'un sistema que alimenta un Reactor Compacte de Membrana (CMR) amb múltiples combustibles de baix contingut de carboni, emissions zero o carboni negatiu, com Amoníac, Gas Natural o alcohols, generant Hidrogen com a vector energètic intermedi. Aquest serà consumit in situ per Motors de Combustió Interna (ICE) i per FCS per generar energia elèctrica i mecànica amb zero emissions.

Aquest treball cobreix alguns aspectes de les fases d'Optimització, Integració i Escalat, comptant amb dos objectius principals. El primer d'ells és desenvolupar una plataforma de modelatge per al CMR i el FCS que permeta dissenyar el sistema de recuperació de calor i maximitzar l'eficiència global. El segon objectiu és integrar el CMR i el FCS en una plataforma de simulació multiescala per a Vehicles Heavy-Duty (HDV) per tal d'estimar el rendiment del sistema propulsiu en condicions realistes.

A més, es proposa un disseny del layout que conté tots els components involucrats en el sistema propulsor per a HDV, així com una selecció de components per al sistema tèrmic.

ABSTRACT

Aiming to reduce global warming and emissions in general, cleaner technologies are the spotlight of research, industry and transport development. In order to thrive through environmental crisis, Hydrogen is postulated as one of the main agents to guarantee a clean and sustainable energy future. In the transport sector, Fuel Cell Systems (FCS) are gaining interest as promising options to decarbonize the sector in line with the current progress towards the Hydrogen economy.

This Final Master's Thesis has been developed within the framework of the European Project ALL-IN Zero, whose main objective is to develop a multi-fuel system that will feed low, zero or carbon negative fuels like Ammonia, natural gas or alcohols into a Compact Membrane Reactor (CMR), producing Hydrogen as an intermediate temporary energy vector. The temporary energy vector will be consumed in situ by Internal Combustion Engines (ICE) and FCS to generate electrical and mechanical power with zero emissions.

The Thesis covers some aspects of the Optimization, Integration and Scaling phases, having two main objectives. The first one is to develop a modelling framework for the CMR and a FCS to design the heat recovery system to maximize the global efficiency. The second one is to integrate the CMR+FCS models in a multiscale Heavy-Duty Vehicles (HDV) simulation platform to develop control strategies and estimate the powertrain performance in realistic conditions.

Furthermore, the design of a layout that contains all the components involved in the propulsion system is proposed for HDV. Finally, the selection of thermal components is also part of this Thesis.

TABLE OF CONTENTS

CHAPTER 1	1
1.1 Introduction.....	1
1.2 Context.....	2
1.3 Justification	4
1.4 Hydrogen as an energy carrier.....	6
1.5 Objectives and reach.....	7
1.6 General outline	8
1.7 References	9
CHAPTER 2	11
2.1 Fuel Cells.....	12
2.2 Compact Membrane Reactor	13
2.3 Heat Exchangers.....	15
2.4 References	18
CHAPTER 3	19
3.1 Methodology outline	19
3.2 Stage description	21
3.3 Tools.....	22
3.4 Initial CMR system model.....	22
3.5 CMR Dynamics	22
3.6 FC Models	27
3.7 Vehicles	30
3.8 References	33
CHAPTER 4	35
4.1 Stage 1 – Thermal Equilibrium.....	36
4.1.1 Fluid parameters.....	36
4.1.2 Flow parameters.....	41
4.1.3 Internal chemistry parameters	42
4.1.4 Energy parameters	43
4.1.5 Scaling Factor range and justification	44
4.1.6 Simulation parameters	45
4.1.7 Results.....	46
4.2 Stage 2 – Operating points	49
4.2.1 Introduction	49
4.2.2 Model modification.....	49

4.2.3 Results.....	53
4.3 Stage 3 – Heat Exchangers	60
4.3.1 Introduction	60
4.3.2 Commercial models – the need of a custom solution	60
4.3.3 Sizing methodology	61
4.3.4 Weight calculation	70
4.3.5 Hydrogen – Air heat exchanger	70
4.3.6 Summary of results	72
4.3.7 References	73
4.4 Stage 4 – Scaling Factor selection.....	74
4.4.1 Efficiency summary	74
4.4.2 Weight summary.....	74
4.4.3 Selection	75
4.4.4 Possible criteria changes	75
CHAPTER 5.....	77
5.1 Stage 5 – Driving Cycles.....	79
5.1.1 Introduction	79
5.1.2 CMR Dynamics results	80
5.1.3 Mean Value Models.....	82
5.1.4 Cycle simulations	85
5.1.5 Hydrogen tank pressure control	86
5.1.6 Results.....	87
5.1.7 References	97
5.2 Stage 6 – Final layout and specifications	98
5.2.1 Summary of the final system	98
5.3 Stage 7 – Benchmark against current systems.....	99
5.3.1 Pressurized Hydrogen.....	99
CHAPTER 6.....	102
CHAPTER 7.....	105
CHAPTER 8.....	109
ANNEX I.....	115
ANNEX II.....	119
II.1 Additional Tables	120
II.2 Additional Plots.....	129
II.2.1 Hydrogen Generation Specific Energy.....	129
II.2.2 Hydrogen Efficiency	130

ANNEX III	131
III.1 Additional HXN2 Temperature Tables	132
III.2 Additional HXN2 UA Calculation Tables.....	136
III.3 Additional Tube Number Calculation Tables for HXN2	140
III.4 Additional Results for HXH2	144
ANNEX IV	149
IV.1 CMR Dynamics Function.....	150
IV.2 Hydrogen Tank Pressure Control Function.....	150
IV.3 Ideal Gas Law for Tank mass calculation	151
Price Chart N°1	1
Decomposed Price Chart	2
Budget Summary.....	3

INDEX OF FIGURES

Figure 1.1. Global net energy generation by source 2010-2050. [3].....	2
Figure 1.2. Energy-related carbon emission reductions by sector. [4].....	2
Figure 1.3. Breakdown of 2020 well-to-wheel CO ₂ emissions fin the transportation. [5]	3
Figure 1.4. ALL-IN Zero framework.	4
Figure 1.5. ALL-IN Zero technology concept.....	5
Figure 1.6. ALL-IN Zero specific objectives.....	5
Figure 2.1. Single-cell PEMFC outline. [1]	12
Figure 2.2. View of the CMR System. Illustration of the phenomena.	14
Figure 2.3. Heat Transfer Modes. [14]	15
Figure 2.4. Heat Exchanger constructive types.	16
Figure 2.5. Flow disposition in a heat exchanger. Parallel (right) and Countercurrent (left). [14]	16
Figure 2.6. Temperature distribution for countercurrent and parallel flow configuration.....	17
Figure 2.7. Latent and Sensible heat in a heat exchanger.	17
Figure 3.1. Methodology outline.	20
Figure 3.2. CMR initial model - Layer 1.	23
Figure 3.3. CMR initial model - Layer 2.	24
Figure 3.4. CMR initial model - Layer 3.	25
Figure 3.5. Genetic Algorithm steps diagram. [1]	26
Figure 3.6. Simulink model to implement Genetic Algorithm transfer function parameters.....	26
Figure 3.7. Fuel Cell test room diagram at the IUI CMT. [2]	28
Figure 3.8. Power and Hydrogen inlet curves in each step of the polarization curve. [2].....	28
Figure 3.9. Toyota Mirai FC characterization methodology. [3].....	29
Figure 3.10. Toyota Mirai FC characterization testing rig. [3].....	29
Figure 3.11. Toyota Mirai FC characterization main results. [3]	30
Figure 3.12. HDFCV powertrain layout.	30
Figure 4.1. Input of Nitrogen properties.	36
Figure 4.2. Input of Water Vapor properties.....	36
Figure 4.3. Input of Hydrogen properties.....	37
Figure 4.4. Input of Ammonia general properties.	39
Figure 4.5. Input of liquid Ammonia properties.	40
Figure 4.6. Input of Ammonia vapor properties.	40
Figure 4.7. Concept of the CMR implementation into the vehicle's cabin.....	44
Figure 4.8. Thermal Efficiency summary for the Thermal Equilibrium condition.....	46
Figure 4.9. Revision of the Thermal Efficiency summary for the Thermal Equilibrium condition.	46
Figure 4.10. Operating zones.	49
Figure 4.11. Auxiliary thermal source implementation in the model.	50
Figure 4.12. System Identification Toolbox main screen.....	50
Figure 4.13. System Identification Toolbox - Input of model variables.....	51
Figure 4.14. Controller parameters.....	52
Figure 4.15. PID Tuner – Controller response.....	52
Figure 4.16. Anti-windup implementation.....	52
Figure 4.17. Stage 2 - Electric power summary.....	55
Figure 4.18. Stage 2 - Auxiliary Power summary.....	56
Figure 4.19. Stage 2 - Total Power Supplied summary.....	57
Figure 4.20. Stage 2 - Net power summary.	58
Figure 4.21. Stage 2 - Thermal Efficiency summary.....	59

Figure 4.22. Sketch of the preliminary design of the main heat exchangers. 61

Figure 4.23. T-Q diagram to represent ΔT_0 and ΔT_L 63

Figure 5.1. Results of a validation test of the Heuristic Identification of the CMR dynamics. 81

Figure 5.2. Detail of a validation test of the Heuristic Identification of the CMR dynamics. 81

Figure 5.3. Flow to Max Efficiency Operating Temperature 2-D Lookup Table. 82

Figure 5.4. Mean Values Model integrating the CMR and the FC for HDV applications. 83

Figure 5.5. Mean Values Model integrating the CMR and the Toyota Mirai FC. 84

Figure 5.6. HDDT cycle FCS Power demand profile. 85

Figure 5.7. VECTO LHR cycle FCS Power demand profile. 85

Figure 5.8. Intervals for the Hydrogen intermediate tank pressure control. 86

Figure 5.9. Ammonia flows demanded to the CMR for each pressure interval. 86

Figure 5.10. HDDT IUI CMT FC Power share summary. 87

Figure 5.11. HDDT IUI CMT FC Temperature summary. 87

Figure 5.12. HDDT IUI CMT FC Hydrogen balance. 88

Figure 5.13. HDDT IUI CMT FC Tank pressure. 88

Figure 5.14. HDDT IUI CMT FC 1025 K Power share summary. 89

Figure 5.15. HDDT IUI CMT FC 1025 K Temperature summary. 90

Figure 5.16. HDDT IUI CMT FC 1025 K Tank pressure. 90

Figure 5.17. HDDT MIRAI FC Power share summary. 91

Figure 5.18. HDDT MIRAI FC Temperature summary. 91

Figure 5.19. HDDT MIRAI FC Hydrogen balance. 91

Figure 5.20. HDDT MIRAI FC Tank pressure. 92

Figure 5.21. VECTO LHR IUI CMT FC Power share summary. 93

Figure 5.22. VECTO LHR IUI CMT FC Temperature summary. 93

Figure 5.23. VECTO LHR IUI CMT FC Hydrogen balance. 93

Figure 5.24. VECTO LHR IUI CMT FC Tank pressure. 94

Figure 5.25. VECTO LHR MIRAI FC Power share summary. 95

Figure 5.26. VECTO LHR MIRAI FC Temperature summary. 95

Figure 5.27. VECTO LHR MIRAI FC Hydrogen balance. 95

Figure 5.28. VECTO LHR MIRAI FC Tank pressure. 96

Figure II.1. Stage 2 – Hydrogen Generation Specific Energy summary. 129

Figure II.2. Stage 2 – Hydrogen Efficiency summary. 130

INDEX OF TABLES

Table 1.1. ALL-IN Zero partners.	6
Table 2.1. Representative Values of the Overall Heat Transfer Coefficient. [14].....	17
Table 3.1. CO ₂ emissions share from different HDV groups. [5]	31
Table 3.2. Hyundai XCIENT 4-RD HDFCV datasheet. [6].....	32
Table 3.3. HDV 5-LH and 4-RD additional data. [4].....	32
Table 4.1. Gas constant.....	37
Table 4.2. Diffusivity.....	37
Table 4.3. Hydrogen properties.	37
Table 4.4. Nitrogen properties.....	38
Table 4.5. Water properties.	38
Table 4.6. Ammonia properties.	39
Table 4.7. Summary of liquid and vapor common properties.	40
Table 4.8. General fluid properties.....	41
Table 4.9. Lower Heating Value for Hydrogen and Ammonia.	41
Table 4.10. CMR Scaling Factor range and characteristics.	44
Table 4.11. Input array breakdown.....	45
Table 4.12. Excerpt of Thermal Equilibrium simulations results.	48
Table 4.13. Stage 2 results summary for Scaling Factor 3.....	54
Table 4.14. Relevant tubes data for the heat exchangers design.	61
Table 4.15. HXN2 temperature summary for SF0.3.	62
Table 4.16. Thermal resistances and UA values for SF0.3.	66
Table 4.17. Number of tubes as a function of the U value for SF0.3.....	67
Table 4.18. HXH2 results for SF0.3.....	69
Table 4.19. Weights for different Heat Exchanger sizes.	70
Table 4.20. Summary of the Hydrogen-Air HX geometrical data.....	71
Table 4.21. Air-Hydrogen HX summary of results. Part 1.	71
Table 4.22. Air-Hydrogen HX summary of results.	71
Table 4.23. Stage 3 - Summary of final results.	72
Table 4.24. Maximum thermal efficiency operating points for different SFs.	74
Table 4.25. Weight summary.....	74
Table 5.1. Maximum efficiency operating temperature for each Ammonia flow.....	80
Table 5.5. Minimum requisites of FC number for the different combinations of cycle and FC.....	85
Table 5.6. HDDT IUI CMT FC Ammonia consumption.	88
Table 5.7. HDDT IUI CMT FC Hydrogen consumption.	89
Table 5.8. HDDT IUI CMT FC required Ammonia for an autonomy of 400 and 800 km.	89
Table 5.9. HDDT IUI CMT FC cycle conditions.....	89
Table 5.10. HDDT IUI CMT FC tank summary.....	89
Table 5.11. HDDT MIRAI FC Ammonia consumption.....	92
Table 5.12. HDDT MIRAI FC Hydrogen consumption.....	92
Table 5.13. HDDT MIRAI FC required Ammonia for an autonomy of 400 and 800 km.....	92
Table 5.14. HDDT MIRAI FC cycle conditions.	92
Table 5.15. HDDT MIRAI FC tank summary.....	92
Table 5.16. VECTO LHR IUI CMT FC Ammonia consumption.....	94
Table 5.17. VECTO LHR IUI CMT FC Hydrogen consumption.....	94
Table 5.18. VECTO LHR IUI CMT FC required Ammonia for 400 and 800 km of autonomy.....	94
Table 5.19. VECTO LHR IUI CMT FC cycle conditions.	94
Table 5.20. VECTO LHR IUI CMT FC tank summary.....	94

Table 5.21. VECTO LHR MIRAI FC Ammonia consumption.....	96
Table 5.22. VECTO LHR MIRAI FC Hydrogen consumption.....	96
Table 5.23. VECTO LHR MIRAI FC required Ammonia for 400 and 800 km of autonomy.....	96
Table 5.24. VECTO LHR MIRAI FC cycle conditions.	96
Table 5.25. VECTO LHR MIRAI FC tank summary.	96
Table 5.26. Powertrain summary.	98
Table 5.27. Powertrain benchmark.	99
Table I.1. Stage 1 additional results Part 1.	116
Table I.2. Stage 1 additional results Part 2.	117
Table II.1. Stage 2 – Results for SF0.05.	120
Table II.2. Stage 2 – Results for SF0.1.	121
Table II.3. Stage 2 – Results for SF0.2.	122
Table II.4. Stage 2 – Results for SF0.3.	123
Table II.5. Stage 2 – Results for SF0.4.	124
Table II.6. Stage 2 – Results for SF0.5.	125
Table II.7. Stage 2 – Results for SF1.....	126
Table II.8. Stage 2 – Results for SF1.5.	127
Table II.9. Stage 2 – Results for SF2.....	128
Table III.1. HXN2 Temperature results for SF0.2.....	132
Table III.2. HXN2 Temperature results for SF0.4.....	133
Table III.3. HXN2 Temperature results for SF0.5.....	134
Table III.4. HXN2 Temperature results for SF1.....	135
Table III.5. HXN2 UA calculation tables for SF0.2.....	136
Table III.6. HXN2 UA calculation tables for SF0.4.....	137
Table III.7. HXN2 UA calculation tables for SF0.5.....	138
Table III.8. HXN2 UA calculation tables for SF1.	139
Table III.9. HXN2 Tube number calculation tables for SF0.2.	140
Table III.10. HXN2 Tube number calculation tables for SF0.4.	141
Table III.11. HXN2 Tube number calculation tables for SF0.5.	142
Table III.12. HXN2 Tube number calculation tables for SF1.	143
Table III.13. HXH2 Additional results for SF0.2.	144
Table III.14. HXH2 Additional results for SF0.4.	145
Table III.15. HXH2 Additional results for SF0.5.	146
Table III.16. HXH2 Additional results for SF1.	147

NOMENCLATURE

AI	Artificial Intelligence
ASR	Area Specific ohmic Resistance
BCZY	$\text{BaZr}_{1-x-y}\text{Ce}_x\text{Y}_y\text{O}_{3-\delta}$
BEV	Battery Electric Vehicle
CH_4	Methane
CMR	Compact Membrane Reactor
DC	Direct Current
EIS	Electrochemical Impedance Spectroscopy
EMS	Energy Management Strategy
EV	Electric Vehicle
FC	Fuel Cell
FCS	Fuel Cell System
F_{H_2}	Hydrogen Flow
F_{NH_3}	Ammonia Flow
GCW	Gross Combined Weight
GHG	Greenhouse Gas
H_2	Hydrogen
HDDT	Heavy-Duty Diesel Truck
HDFCV	Heavy-Duty Fuel Cell Vehicle
HHDDT	Heavy Heavy-Duty Diesel Truck
HDV	Heavy-Duty Vehicle
HHV	Higher Heating Value
HX	Heat Exchanger
ICE	Internal Combustion Engine
IUI CMT	Instituto Universitario de Investigación CMT – Clean Mobility and Thermofluids
JRC	Joint Research Centre
LHR	Long Haul with Reference loading
LHV	Lower Heating Value
LMTD	Logarithmic Mean Temperature Difference
$L \times W \times H$	Length x Width x Height
MVM	Mean Values Model
N_2	Nitrogen
NH_3	Ammonia
NIST	National Institute of Standards
O_2	Oxygen
OCV	Open Circuit Voltage
P	Proportional
PI	Proportional Integral
PID	Proportional Integral Derivative
SDG	Sustainable Development Goal
SEM	Scanning Electron Microscope
SF	Scaling Factor
SMR	Steam Methane Reforming
SOC	State Of Charge
TGA	Thermogravimetric Analysis
TPR	Temperature Programmed Reduction
UPV	Universitat Politècnica de València
VECTO	Vehicle Energy Consumption calculation TOol
WLTC	World-wide harmonized Light duty Test Cycle
WLTP	Worldwide harmonized Light vehicle Test Procedure
XRD	X-Ray Diffraction

Chapter 1

Introduction

1.1 Introduction

The growing trend in energy demand, along with the urgent need to mitigate (and reverse) climate change by reducing greenhouse gas emissions, highlights the importance of improving the efficiency of all processes related to energy generation and transformation. Transportation is one of the main challenges to address in order to make this improvement and advance the transition toward a sustainable energy future.

This thesis was developed within the context of a university internship at IUI CMT – Clean Mobility and Thermofluids. One of the projects being carried out at the institution required the design of the layout and components for an innovative zero-emissions propulsion system. However, making the right decisions in this regard requires a meticulous study of the different possibilities in order to achieve an efficient and effective system and establish a clear pathway for future iterations.

The study of this novel powertrain has been chosen as the subject of this Master's Thesis.

1.2 Context

The recent advancements in Hydrogen fuel cell technology have emerged within a multifaceted context. While the advantages of utilizing Hydrogen in fuel cell systems (FCS) might appear sufficient to warrant their widespread adoption across various sectors, the reality is far more intricate. It has been the convergence of complex global factors and an urgent need for decisive action that has propelled this technology to the forefront of attention within the scientific, political, and industrial communities.

The political context and actions, as the drivers of the recent funding of research projects to develop FC technology, arise from the needs derived from the environmental, industrial, societal and financial contexts [1].

In 1990, the global population was 5.3 billion, a figure that has since risen to 7.7 billion, reflecting a 45% increase over the past 30 years. It is projected that, by 2050, the world population will exceed 9.5 billion and may reach 11 billion by 2100 [2]. This represents a doubling of the global population in just 100 years. According to the experts in the US's Energy Information Administration, this may lead to an increase in the global energy demand of 47% by 2050, that would probably be mostly covered by coal and other fossil fuels' energy (Figure 1.1), since only 27% of the global energy mix would be from renewable sources, thus implying a global increase in the CO₂ only motivated by the increase in the energy demand.

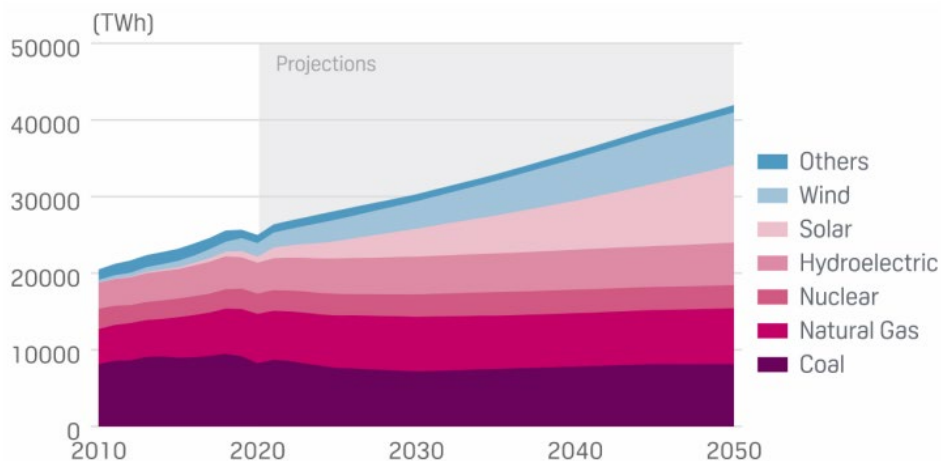
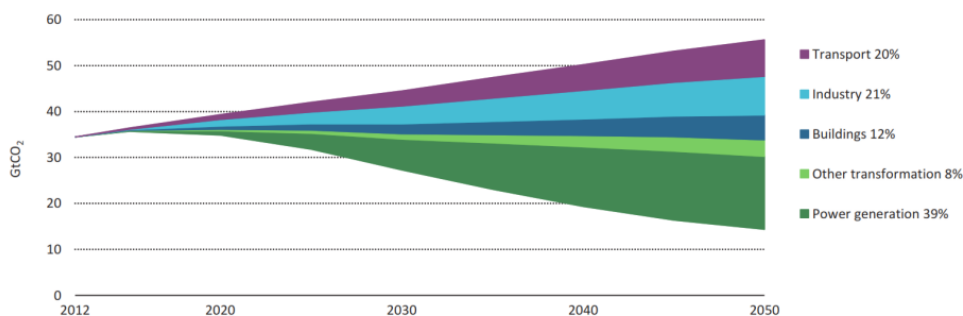


Figure 1.1. Global net energy generation by source 2010-2050. [3]

According to the International Energy Agency, the transportation sector could help mitigate or be responsible for 20% of the increment of the energy-related CO₂ emissions in 2050 (Figure 1.2) [4].



Note: GtCO₂ = gigatonnes of carbon dioxide.

Figure 1.2. Energy-related carbon emission reductions by sector. [4]

Particularly, for the transportation sector it is expected that the well-to-wheel GHG emissions would increase from 12000 Mt of CO₂ eq. in 2020 to 21000 Mt of CO₂ eq. in 2050 (+75%) [5]. Among the different applications within the transportation sector, heavy-duty vehicles (HDV) and light-duty vehicles (LDV) or passenger cars together with light commercial vehicles are responsible for 30% and 40% of the total well-to-wheel CO₂ emissions in 2020 respectively (Figure 1.3), which may be maintained in 2050 if no further action is taken.

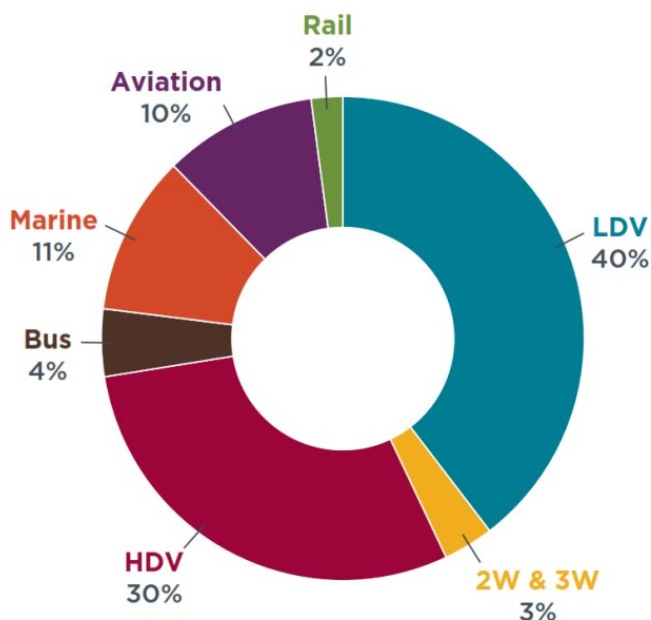


Figure 1.3. Breakdown of 2020 well-to-wheel CO₂ emissions in the transportation. [5]

The role of transport in sustainable development was first recognized at the United Nations Earth Summit in 1992 and reinforced in its final document, Agenda 21. During the five-year review of the implementation of Agenda 21 at the 19th Special Session of the United Nations General Assembly in 1997, it was further noted that, over the following 20 years, transport was expected to become the primary driver of growing global energy demand.

In recent years, global attention on transport has continued. At the United Nations Conference on Sustainable Development in 2012 (Rio+20), world leaders unanimously acknowledged that transport and mobility are essential for sustainable development. Sustainable transport can stimulate economic growth and improve accessibility. It achieves better integration of the economy while respecting the environment. Furthermore, it enhances social equity, health, urban resilience, rural-urban connections, and rural productivity.

In the 2030 Agenda for Sustainable Development, sustainable transport is integrated into various Sustainable Development Goals (SDGs) and targets.

The primary Sustainable Development Goal (SDG) is SDG 11, “Sustainable Cities and Communities”, specifically target 2: “By 2030, provide access to safe, affordable, accessible, and sustainable transport systems for all, improving road safety, notably by expanding public transport, with special attention to the needs of those in vulnerable situations, including women, children, persons with disabilities, and older persons”.

Other SDGs related to sustainable transport and the content of this thesis include:

- **SDG7.** Affordable and Clean Energy
- **SDG9.** Industry, Innovation and Infrastructure.
- **SDG12.** Responsible consumption and production.
- **SGD13.** Climate action.

1.3 Justification

This thesis is part of the framework of the European project ALL-IN Zero. The main objective of this project is to develop a multi-fuel system that will feed low, zero or carbon negative fuels like Ammonia, natural gas, biogas or alcohols among other easy-handling fuels, into a Compact Membrane Reactor (CMR) producing an intermediate temporary energy vector (i.e. Hydrogen). The temporary energy vector will be consumed *in situ* by ICE and FCS to generate electrical and mechanical power with zero emissions. In addition, this technology will implement efficient energy recovery strategies by means of thermal, mechanical and electrical energy exploitation to sustain CMR operation and will turn emissions of CO₂ stream coming from CMR (in case they exist due to the fuel type) into business opportunity by means of efficient Carbon Capture and Storage (CCS) techniques to produce synthetic fuels, among other high value uses. The project is part of the Horizon Europe framework (Figure 1.4).

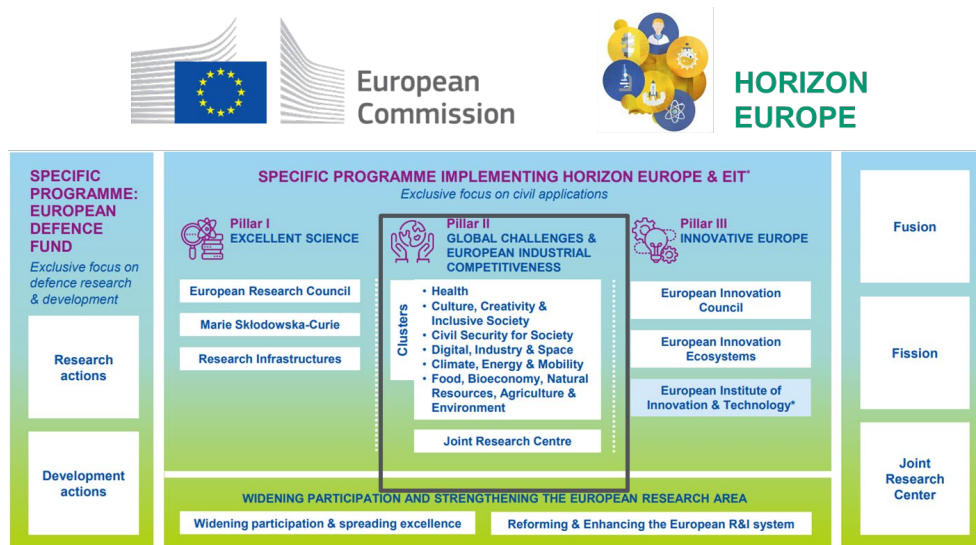


Figure 1.4. ALL-IN Zero framework.

The proposed system (Figure 1.5) comprises the joint operation of the CMR together with the power generation system that can be either an ICE or a FCS. The CMR is fed with any fuel and requires heat, to dissociate any molecule into H₂ and other components, and electricity, to capture the H₂ flow through the membrane by forcing a flow of protons (H⁺) through it. The H₂ is then introduced into the PGS to produce thermal or electrical energy that is partially fed back into the CMR. This propulsion system requires the complex interaction and control of both the CMR and the power generation system to achieve the maximum performance for each fuel and configuration.

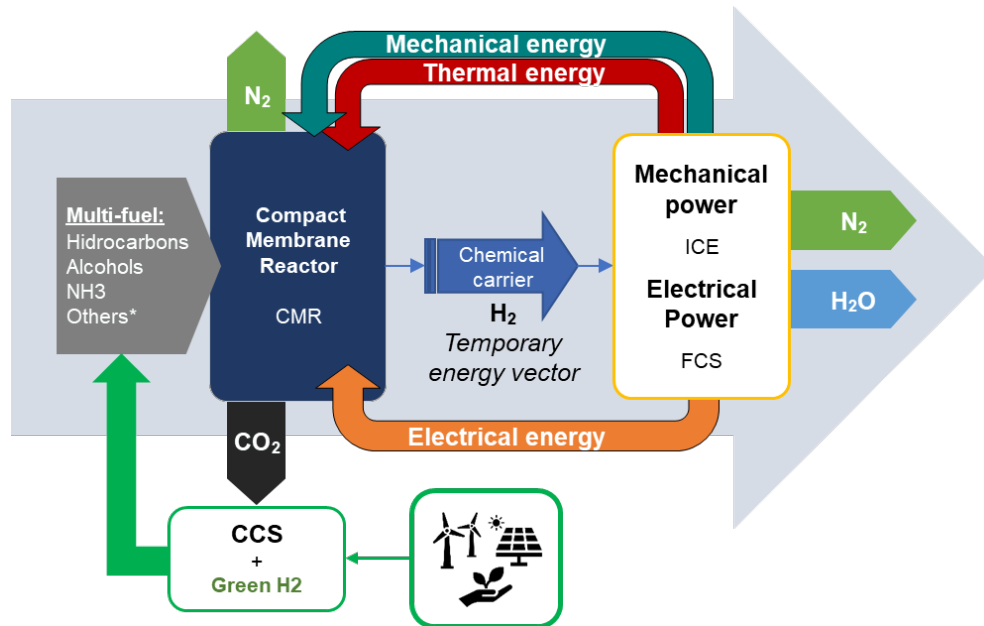


Figure 1.5. ALL-IN Zero technology concept.

ALL-IN Zero will contribute to the implementation of the EU policies and Directives on competitiveness and sustainability (e.g., Emerging technologies for a climate-neutral Europe), through the validation of a novel, clean and high-flexible power generation system with low capital expenditure and fast implementation due to the use of already well-implemented infrastructure for high energy density liquid fuels as well as ICE and FCS technologies and their related productive chains. However, this requires further research, development, and validation of our innovative multi-fuel feeder system to supply chemical energy from conventional fuels to a CMR, producing an intermediate temporary energy vector to generate power with zero emissions. This new technology will avoid the extra efforts associated with energy storage, waste elimination and purification processes thus enabling more efficient and sustainable power generation from the economic, social, energetic and environmental points of view. Considering these assumptions and previously obtained promising results, the specific objectives of the project are shown in Figure 1.6.

1. **Development:** Develop a planar CMR with a multi-functional catalyst to convert different fuels into the H₂ vector
2. **Optimization:** Optimize a H₂-powered ICE and FCS (Power Generation System or PGS) to be integrated with the CMR
3. **Integration:** Develop a modelling framework for the CMR and each PGS to design the heat recovery system to maximize the global efficiency
4. **Scaling-up:** Integrate the CMR+PGS models in a multiscale HDV simulation platform to develop control strategies and estimate the powertrain performance in realistic conditions
5. **Benchmarking:** Compare the developed powertrain (CMR+PGS) keeping the same target HDV and PGS but with H₂ stored in a tank in terms of LCA and TCO

Figure 1.6. ALL-IN Zero specific objectives.

Table 1.1 summarizes the partners that will perform the research, administrative and dissemination activities in the ALL-IN Zero project and their general role.

Table 1.1. ALL-IN Zero partners.

Partner N ^o	Name	Role
1	UPV (Universitat Politècnica de València)	Project Coordinator
2	CSIC (Consejo Superior de Investigaciones Científicas)	Partner
3	FZJ (Forschungszentrum Jülich)	Partner
4	AVL	Partner
5	AVL-I (AVL IBERICA)	Partner

1.4 Hydrogen as an energy carrier

Hydrogen (H_2) is seen as a promising solution for decarbonizing both light and heavy-duty transportation. While its energy density is lower than conventional fuels, particularly affecting vehicle range, the current high manufacturing costs of H_2 vehicles, due to high-pressure H_2 tanks and fuel cell (FC) systems, are expected to decrease with economies of scale in the future. H_2 offers flexibility in reducing emissions, as it can be produced from various sources, including renewable energy (green H_2), Steam Methane Reforming (SMR) with or without carbon capture (blue and grey H_2), and electrolysis using mixed energy sources (black H_2).

H_2 can power either internal combustion engines (ICE) or FC systems. While ICEs are cheaper to manufacture and more durable, they are less efficient and may emit pollutants like NOx. FCs, by contrast, offer higher efficiency, nearly double that of ICEs, with zero CO₂ emissions when used with H_2 . However, challenges remain, such as developing compact, affordable storage systems and improving H_2 infrastructure and handling. Current FC vehicles can achieve ranges of over 600 km for light-duty and 400 km for heavy-duty applications with refuelling times of 5-20 minutes, making them viable for long-distance trips [6].

Compared to batteries, H_2 has advantages such as higher energy density, shorter refuelling times (5 minutes versus up to 2 hours for batteries), fewer raw material requirements, and minimal energy loss during long-term storage. However, batteries are more efficient (90% vs. 50-60%) and quieter due to the absence of air compressors. Thus, H_2 's main advantages are higher energy density and faster refuelling, despite lower energy utilization efficiency.

In conclusion for the transportation sector, H_2 can provide higher energy density than batteries, hence enabling long-range operation (>600 km for passenger car and >400 km in heavy-duty vehicles), and potentially lower well-to-wheel and cradle-to-grave emissions than hydrocarbon-fuelled vehicles [7], given the large variety of H_2 production pathways. This makes H_2 a suitable option to decarbonize the operation of heavy-duty vehicles, ships, trains, and aircraft while it is a perfect fuel to complement and coexist with batteries and/or neutral CO₂ emissions ICE for light-duty vehicles, enabling high-enough-range and carbon-free transport applications [6, 8].

1.5 Objectives and reach

The main objective of this thesis is to **design the CMR layout and heat recovery system to maximize the global efficiency and integrate the CMR and FCS models in a multiscale HDV simulation platform to develop control strategies and estimate the powertrain performance in realistic conditions in order to collate it against traditional isolated FCS to gain some insight into this novel powertrain viability.** The conclusions extracted from each of the studies in this thesis are used, when possible, to extract recommendations for the industry in such a way that this work can contribute to help both the CMR and the FC technology penetrate the transportation sector. To achieve the main objective, a set of secondary targets must be fulfilled:

- **Partial Objective 1: Develop a CMR model.** This model must accomplish three main purposes. The first one is to integrate the chemical part of the CMR alongside the main fluid streams of the system: NH_3 side, H_2 side and N_2 side. The second one is to accurately represent the thermoelectric energy balances within the CMR. The third and last one is to model the thermodynamic phenomena occurring in each of the system's components.
- **Partial Objective 2: Explore different sizes and operating conditions to optimize the system.** Explore all the alternatives resulting from combining the range of possible SF of the CMR, limited by the vehicle cabin dimensions, with the different possible operating conditions, constrained by the CMR materials, to carry out an optimization of the system that maximizes thermoelectric efficiency with the minimum possible weight and volume.
- **Partial Objective 3: Integrate the CMR and the FCS models.** With the optimized CMR model, the next natural step is to integrate it with the models of the different fuel cells present in the study in the same simulation platform, allowing for the exploration of different control strategies and parametric analyses of the various system components without an excessively high computational cost.
- **Partial Objective 4: System requirements for different Driving Cycles.** Once the system model is complete, two reference driving cycles for HDVs are simulated: HDDT and VECTO LHR with different FCSs to obtain the system requirements in each case, optimize the size of the intermediate H_2 tank and compare the performance with traditional FC vehicles.

1.6 General outline

This thesis contents are divided in 8 Chapters, with the following structure:

- **Chapter 1:** Introduction and motivation, context, justification, Hydrogen as an energy Carrier and objectives and reach.
- **Chapter 2:** Theoretical foundations of the relevant components of the powertrain layout.
- **Chapter 3:** Methodology.
- **Chapter 4:** Results of the characterization of the CMR in steady state and selection of the Scaling Factor.
- **Chapter 5:** Results of the characterization of the CMR in transient response, results of the simulations of driving cycles and powertrain layouts and characteristics of each study case.
- **Chapter 6:** Conclusions.
- **Chapter 7:** Future works.
- **Chapter 8:** References.
- **Annexes:** Additional results and documentation considered as relevant.

1.7 References

- [1] López-Juárez, M. “Analysis of Hydrogen fuel cell powerplant architectures for future transport applications”, 2022.
- [2] United Nations, “D. of E. and S.A”. *World Population Prospects*, 2019.
- [3] U.S. Energy Information Administration. “International Energy Outlook 2021”, 10 2021.
- [4] International Energy Agency. “Technology Roadmap Hydrogen and Fuel Cells”.
- [5] International Council Of Clean Transportation. “Vision 2050: A strategy to decarbonize the global transport sector by mid-century”, 2020.
- [6] Fuel Cells & Hydrogen (FCH). “Hydrogen Roadmap Europe - a Sustainable Pathway for the European Energy Transition”. *Publications Office of the European Union*, 1st edition, 2019.
- [7] Desantes J. M., Molina S., Novella R. and Lopez-Juarez M. “Comparative global warming impact and NOX emissions of conventional and Hydrogen automotive propulsion systems”. *Energy Conversion and Management*, Vol. 221, pp. 113137, 2020.
- [8] International Energy Agency. “The Future of Hydrogen”. *Technical Report June*, 2019.

Chapter 2

Theoretical Foundation

Before delving into the detailed explanation of the tools and results obtained throughout this thesis, it is important to understand the current state-of-the-art of some fundamental concepts. This chapter intends to provide a general outlook of the basic knowledge to the reader to be able to comprehend the complex concepts used in the following chapters.

For that purpose, Section 2.1 explains the fundamental of H₂ FC technology, which is considered one of the most promising propulsion systems for sustainable transport, though more complex than internal combustion engines (ICEs) or battery electric vehicles (BEVs).

Section 2.2 focuses on the CMR, the key component of the powertrain explored in this thesis.

Lastly, Section 2.3 discusses heat exchangers, essential for the propulsion system's design, providing the foundational knowledge necessary to follow the calculation methodology detailed in Section 4.3.

2.1 Fuel Cells

FC technology can be regarded as a hybrid solution or an intermediary between ICEs and batteries.

In ICEs, chemical energy is extracted from fuel stored in a separate tank, meaning that the energy available in the vehicle is independent of the engine size. In these systems, chemical energy is initially converted into heat through combustion, which requires air, and subsequently transformed into mechanical energy through a thermodynamic cycle, with the maximum theoretical efficiency constrained by the Carnot cycle.

In contrast, batteries store reactants internally and convert chemical energy directly into electrical energy via electrochemical reactions. This electrical energy is then converted into mechanical energy using an electric motor, typically with around 5% power losses, including the inverter.

Fuel cells represent a synthesis of these two technologies. Similar to ICEs, they obtain chemical energy from a fuel stored in a tank, typically Hydrogen, which is then combined with air. The energy stored in the Hydrogen bonds is converted into electricity through an electrochemical process, resembling the mechanism in batteries. This design allows the energy storage to be independent of the fuel cell system size, as with ICEs, while achieving higher overall efficiency due to the direct electrochemical extraction of energy, paralleling the efficiency gains seen in batteries.

The structure of a low-temperature Hydrogen Proton-Exchange Membrane Fuel Cell (PEMFC), as illustrated in Figure 2.1, primarily consists of flow channels, which are shaped by the bipolar plates on both the anode and cathode sides, along with the membrane electrode assembly (MEA). The flow channels carry the reactants (H_2 in the anode and O_2 in the form of air in the cathode) to the MEA and evacuate the products of the reaction (H_2O) so that they do not obstruct the flow channels or any porous media in the MEA. The MEA is used to provide mechanical integrity to the FC, to separate the H_2 and the O_2 thus preventing combustion, and to carry out all the steps required in the electrochemical oxidation of H_2 [1].

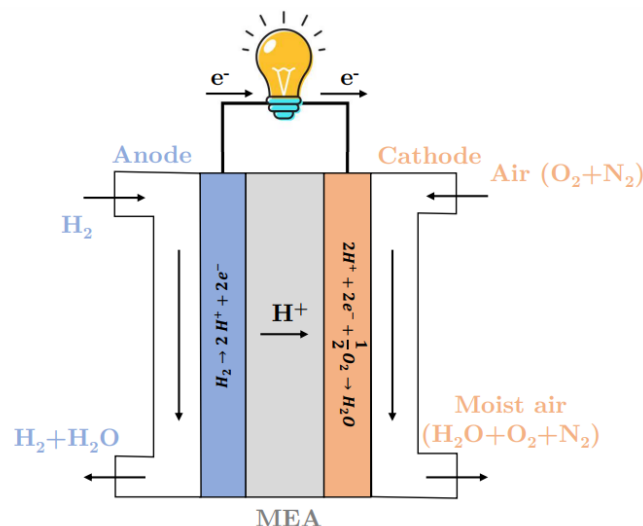
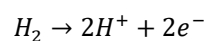
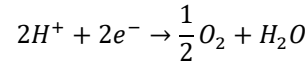


Figure 2.1. Single-cell PEMFC outline. [1]

When H_2 molecules interact with the Pt in the catalyst layer, they are broken down into H^+ ions or protons and e^- or electrons:



The split up of H^+ and e^- produces the voltage difference that is perceived as open-circuit cell voltage that is later measured as cell voltage after all the voltage losses are accounted for. Then, when H^+ reach the other side of the membrane, they interact with the e^- (from which they were separated at the anode catalyst layer) and the O_2 at the cathode catalyst layer, thus forming H_2O which is transported to the anode and the cathode flow channels:



The electrical power of the FC is produced by the circulation of e^- through the conducting material and the voltage difference resulting from the overall electrochemical process [1].

2.2 Compact Membrane Reactor

In the past, Hydrogen was mainly produced for use in Ammonia and Methanol synthesis, refining of hydrocarbons, and other industrial applications. In the present and near future, Hydrogen may also play a role as an energy carrier and in storage of chemical energy for fuel cell electric vehicles and other next-generation energy systems. [2]

Solid-oxide electrochemical cells operating at high temperature can be used as fuel cells [3], electrolyzers [4] or membrane reactors for direct conversion of low- to higher-value chemicals [5]. Potential application of high-temperature proton conductors as the functional membrane in energy conversion technologies dates back almost 40 years when proton conductivity in acceptor-doped $BaCeO_3$ was reported and its application to steam electrolysis was claimed [6]. In the years to follow, publications classified several acceptor-doped alkaline earth cerates and zirconates as proton conductors with diverse potential uses in electrochemical cells, membrane reactors for dehydrogenation, or sensors [7-10]. However, the cerates are vulnerable towards decomposition in CO_2 levels even as low as for ambient air, jeopardizing long-term durability. In comparison, acceptor-doped barium zirconates exhibit superior chemical stability, but it was not until their high bulk proton conductivity was resolved [11,12] that the true potential could be envisioned.

Proton ceramic reactors offer efficient extraction of Hydrogen from Ammonia, Methane, and biogas by coupling endothermic reforming reactions with heat from electrochemical gas separation and compression. Preserving this efficiency in scale-up from cell to stack level poses challenges to the distribution of heat and gas flows and electric current throughout a robust functional design. A 36-cell well-balanced reactor stack enabled by a new interconnect that achieves complete conversion of Ammonia with more than 99% recovery to pressurized Hydrogen, leaving a concentrated stream of carbon dioxide. The stacking of proton ceramic reactors into practical thermo-electrochemical devices demonstrates their potential in efficient Hydrogen production [13].

The CMR is a variation of this proton ceramic reactors. Its primary components are catalysts and electrochemical cell materials (electrolyte and electrodes), as can be observed in Figure 2.2. The progress in adapting materials formulation or textural properties in the reactor architecture is used to manufacture the integrated compact electrochemical reactors, which are modular by nature. To start with, this process involves the manufacturing of the electrochemical cells, and subsequent integration of the catalyst, ensuring good gas exchange between the electrodes and the catalyst surface as well as efficient current collection (with low ohmic losses). Moreover, proper fixation and excellent fluid-dynamics in the catalytic chamber are required.

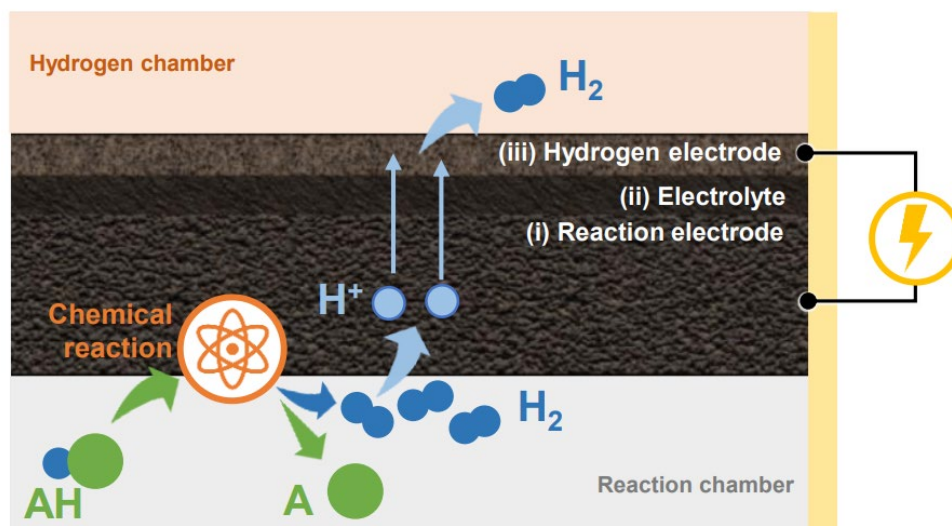


Figure 2.2. View of the CMR System. Illustration of the phenomena.

Electrolyte

The developed electrolytes will be based on $\text{BaZr}_{1-x-y}\text{Ce}_x\text{Y}_y\text{O}_{3-\delta}$ (BZCY) materials. An essential requirement for the dense electrolyte is the achievement of a proper transport of protons (H^+) and a negligible electronic contribution. The main method to manufacture the electrolyte will be solid-state sintering. The electrolyte should be compatible with the rest of materials and stable in the operating conditions. Structural and morphological characterization is performed by XRD and SEM. Electrochemical properties are evaluated by means of DC-conductivity and Electrochemical Impedance Spectroscopy (EIS).

Electrode

Electrode materials for the anode and cathode have been characterized and tested. The active transfer area of the electrodes must be maximized in order to optimize the gas exchange and to ensure the proper charge-transfer reaction distribution along the whole electrode surface. To achieve this, electrodes must possess high electronic and protonic conductivity and, on the other hand, both electrodes must present thermochemical stability in the operating conditions. In addition, the porous electrode layers should show good attachment onto the electrolyte as well as chemically compatible. Structural and morphological characterization is done in fresh and post-mortem states by XRD and SEM. Electrochemical characterization of the manufactured electrodes is performed in symmetrical cells (same electrode coated in both sides of the electrolyte) by EIS.

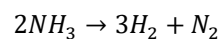
Catalysts

The catalysts must ensure an effective, full conversion of the different fuels to Hydrogen. Catalysts' performance and stability is evaluated in a fixed bed reactor where different operating conditions such as temperature and pressure and fuel type are studied for each catalyst. Structural and morphological characterization has been carried out in fresh and post-mortem states by conventional techniques such as XRD, TGA, TPR and SEM. The Hydrogen yield, stability and compatibility (by XRD and SEM) with the electrochemical cell will be thoroughly analysed and taken into account for the selection of the final set of optimized catalysts.

Relevant parameters for the model development

The main generic parameters of the CMR introduced in the model are listed below. Chapter 4 provides additional details and offers a more in-depth analysis of these specific aspects.

- **Volume [m³]:** CMR_V. Designed to maintain a constant relation between external area and volume.
- **Density [kg/m³]:** CMR_rho = 2696.96 kg/m³ [14]
- **Mass [kg]:** CMR_m = CMR_V · CMR_rho
- **Specific heat capacity [J/kgK]:** CMR_Cp = 440 · 0.1832 + 460 · 0.8048 + 720 · 0.012. This result is due to considering the composition of the CMR: [18.32% cell, 80.48% steel, 1.2% interconnector]
- **Operating pressure.** The nominal pressure for the CMR is 10 bar, but a difference of +5 bar between both sides of the membrane is possible.
- **Flow relations.** Hydrogen flow is 3/17 of the Ammonia flow. This is derived from the reaction taken place in the CMR and accounting the atomic masses for each element (17 and 2 units respectively):



2.3 Heat Exchangers

The process of heat exchange between two fluids that are at different temperatures and separated by a solid wall occurs in many engineering applications. The device used to implement this exchange is termed a heat exchanger, and specific applications may be found in space heating and air-conditioning, power production, waste heat recovery, and chemical processing.

Heat Transfer Modes

However, before diving in specific parameters, it is necessary to do a quick review of how this heat is exchanged. As shown in Figure 2.3, different types of heat transfer processes are referred as modes. When a temperature gradient is present in a stationary medium, whether solid or fluid, the heat transfer that occurs through the medium is referred to as conduction. Conversely, convection describes the heat transfer between a surface and a moving fluid when they possess differing temperatures. The third mode of heat transfer is known as thermal radiation, wherein all surfaces at a finite temperature emit energy in the form of electromagnetic waves. As a result, in the absence of an intervening medium, net heat transfer by radiation occurs between two surfaces at distinct temperatures.

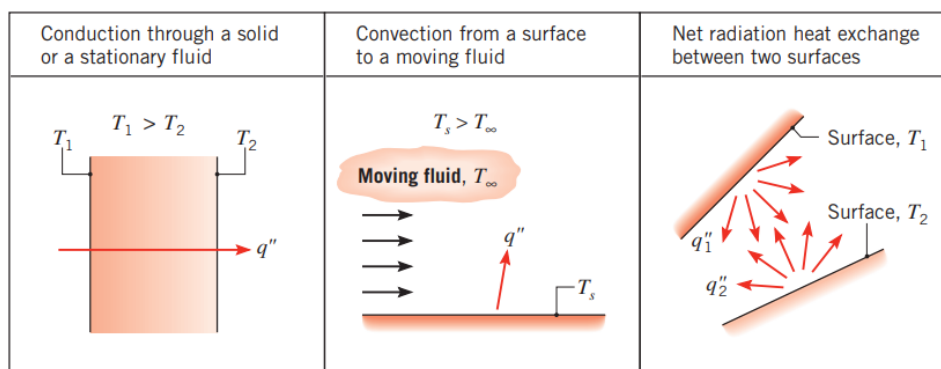


Figure 2.3. Heat Transfer Modes. [14]

Heat Exchangers Constructive Types

HXs can be found in various forms and designs, each fitting a range of purposes. In Figure 2.4, the most common types are shown.



Figure 2.4. Heat Exchanger constructive types.

A common configuration is the shell-and-tube heat exchanger. Specific forms differ according to the number of shell-and-tube passes. Baffles are usually installed to increase the convection coefficient of the shell-side fluid by inducing turbulence and a cross-flow velocity component relative to the tubes. In addition, the baffles physically support the tubes, reducing flow-induced tube vibration.

Another type is the plate heat exchanger. This consists of multiple heat-conducting plates that are welded, brazed, or bolted together, forming stacked corrugated chambers. Fluids flow through the spaces between these chambers.

A special and important class of heat exchangers is used to achieve a very large ($>400 \text{ m}^2/\text{m}^3$ for liquids and $>700 \text{ m}^2/\text{m}^3$ for gases) heat transfer surface area per unit volume [14]. Termed compact heat exchangers, these devices have dense arrays of finned tubes or plates and are typically used when at least one of the fluids is a gas and is hence characterized by a small convection coefficient.

Flow Disposition

Depending on the flow direction of each fluid within the heat exchanger, it is described as either parallel or countercurrent. Figure 2.5 illustrates parallel flow on the left and countercurrent flow on the right.

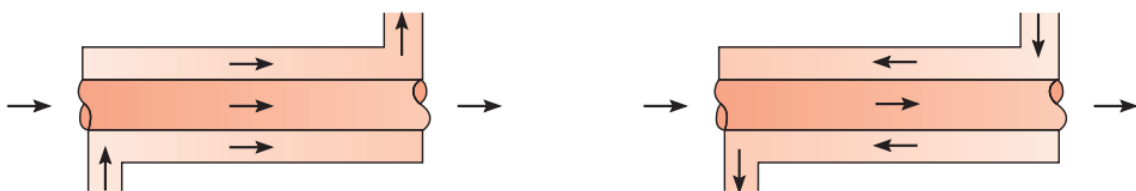


Figure 2.5. Flow disposition in a heat exchanger. Parallel (right) and Countercurrent (left). [14]

The countercurrent configuration is generally preferred because it allows for greater heat exchange efficiency. For the same length or surface area, it achieves a temperature distribution that maximizes the temperature difference between the fluids, promoting greater heat transfer. Figure 2.6 illustrates the temperature distribution for both configurations.

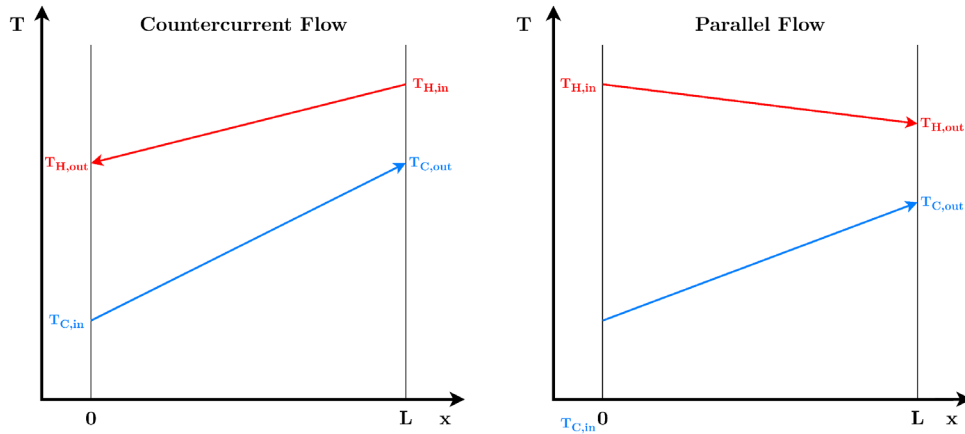


Figure 2.6. Temperature distribution for countercurrent and parallel flow configuration.

Sensible and Latent Heat

The internal energy consists of a sensible component, which accounts for the translational, rotational, and/or vibrational motion of the atoms/molecules comprising the matter; a latent component, which relates to intermolecular forces influencing phase change between solid, liquid, and vapor states [14]. Figure 2.7 shows the temperature distribution in a heat exchanger with a phase change. Q_S stands for sensible heat and Q_L is used for latent heat. The difference between them is relevant in Stage 4.3.

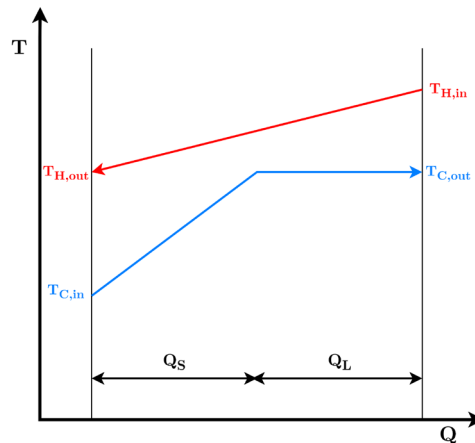


Figure 2.7. Latent and Sensible heat in a heat exchanger.

Overall Heat Transfer Coefficient

An essential, and often the most uncertain, part of any heat exchanger analysis is determination of the overall heat transfer coefficient. This coefficient is defined in terms of the total thermal resistance to heat transfer between two fluids. The details of its calculation will be explained for a specific case in Stage 4.3.

Table 2.1. Representative Values of the Overall Heat Transfer Coefficient. [14]

Fluid Combination	U [W/m ² ·K]
Water to water	850 - 1700
Water to oil	110 - 350
Steam condenser (water in tubes)	1000 - 6000
Ammonia condenser (water in tubes)	800 - 1400
Alcohol condenser (water in tubes)	250 - 700
Finned-tube heat exchanger (water in tubes, air in cross flow)	25 - 50

2.4 References

- [1] López-Juárez, M. “Analysis of Hydrogen fuel cell powerplant architectures for future transport applications”, 2022.
- [2] Malerød-Fjeld H., Clark D., Yuste-Tirados I., Zanón R., Catalán-Martínez D., Beeaff D., Morejudo S. H., Vest P. K., Norby T., Haugrud R., Serra J. M. and Kjølseth C. “Thermo-electrochemical production of compressed Hydrogen from Methane with near-zero energy loss”. *Nature Energy*, Vol. 2 n^o December, pp. 923-931, 2017.
- [3] Morejudo, S. H. et al. “Direct conversion of Methane to aromatics in a catalytic co-ionic membrane reactor”. *Science*, Vol. 353, pp. 563–566, 2016.
- [4] Sengodan, S. et al. “Layered oxygen-deficient double perovskite as an efficient and stable anode for direct hydrocarbon solid oxide fuel cells”. *Nature Materials*, Vol. 14, pp. 205–209, 2015.
- [5] Myung, J.-h, Neagu, D., Miller, D. N. & Irvine, J. T. S. “Switching on electrocatalytic activity in solid oxide cells”. *Nature*, Vol. 537, pp. 528–531, 2016.
- [6] Iwahara, H., Uchida, H., Ono, K. & Ogaki, K. “Proton conduction in sintered oxides based on BaCeO₃”. *Journal of the Electrochemical Society*, Vol. 135, pp. 529–533, 1988.
- [7] Hamakawa, S., Hibino, T. & Iwahara, H. “Electrochemical Methane coupling using proton conductors”. *Journal of the Electrochemical Society*, Vol. 140, pp. 459–462, 1993.
- [8] Bonanos, N., Knight, K. S. & Ellis, B. “Perovskite solid electrolytes: structure, transport properties and fuel cell applications”. *Solid State Ionics*, Vol. 79, pp. 161–170, 1995.
- [9] Norby, T. “Solid-state protonic conductors: principles, properties, progress and prospects”. *Solid State Ionics*, Vol. 125, pp. 1–11, 1999.
- [10] Kreuer, K. D. “On the development of proton conducting materials for technological applications”. *Solid State Ionics*, Vol. 97, pp. 1–15, 1997.
- [11] Kreuer, K. D. “Aspects of the formation and mobility of protonic charge carriers and the stability of perovskite-type oxides”. *Solid State Ionics*, Vol. 125, pp. 285–302, 1999.
- [12] Kreuer, K. D. “Proton-conducting oxides”. *Annual Review of Materials Research*, Vol. 33, pp. 333–359, 2003.
- [13] Kjølseth C. et al. “Single-step Hydrogen production from NH₃, CH₄, and biogas in stacked proton ceramic reactors”. *Science*, Vol. 367, pp. 390-393, 2022.
- [14] Elcogen. “Solid oxide stacks for fuel cell systems – Technical Data”.
- [15] Incropera F. P., DeWitt D. P., Bergman T. L. and Levine A. S. “Fundamentals of Heat and Mass Transfer”, 7th ed., 2011.

Chapter 3

Methodology

In this chapter, the tools, techniques and procedures followed in this thesis to obtain the results discussed in Chapters 4 and 5 are described.

3.1 Methodology outline

The process followed along this thesis is fairly linear. As can be perceived, the results in chapters 4 and 4 are based on simulations. As such, it is critical to ensure that the numerical tools are both representative of the physics and useful to extract meaningful conclusions.

In general terms, the first step of this work involved developing a functional model to characterize the CMR. This was built upon several prior iterations addressing various issues. Once the model is functional and the CMR is characterized, the next step is to integrate it with models of different FCs to create a simulation platform for driving cycles. This platform will enable the evaluation of powertrains with various characteristics at a low computational cost. Finally, the developed powertrain will be compared against conventional designs.

The outline of this thesis (Figure 3.1) can be clearly divided into 2 different parts, each of which addresses two partial objectives defined in Section 1.5:

1. **CMR system characterization.** The main objective of this part is to develop a model of the CMR system capable to provide accurate results in different operating conditions, both in thermal equilibrium and outside of it. This part integrates not only the development of the model, but also the element sizing and the selection of the steady-state operating points for the next part. The path to follow in order to be able to carry out this first part is detailed throughout the **Stages 1 to 4**, in **Chapter 4**. Finally, this part responds to the **Partial Objectives 1 and 2**.

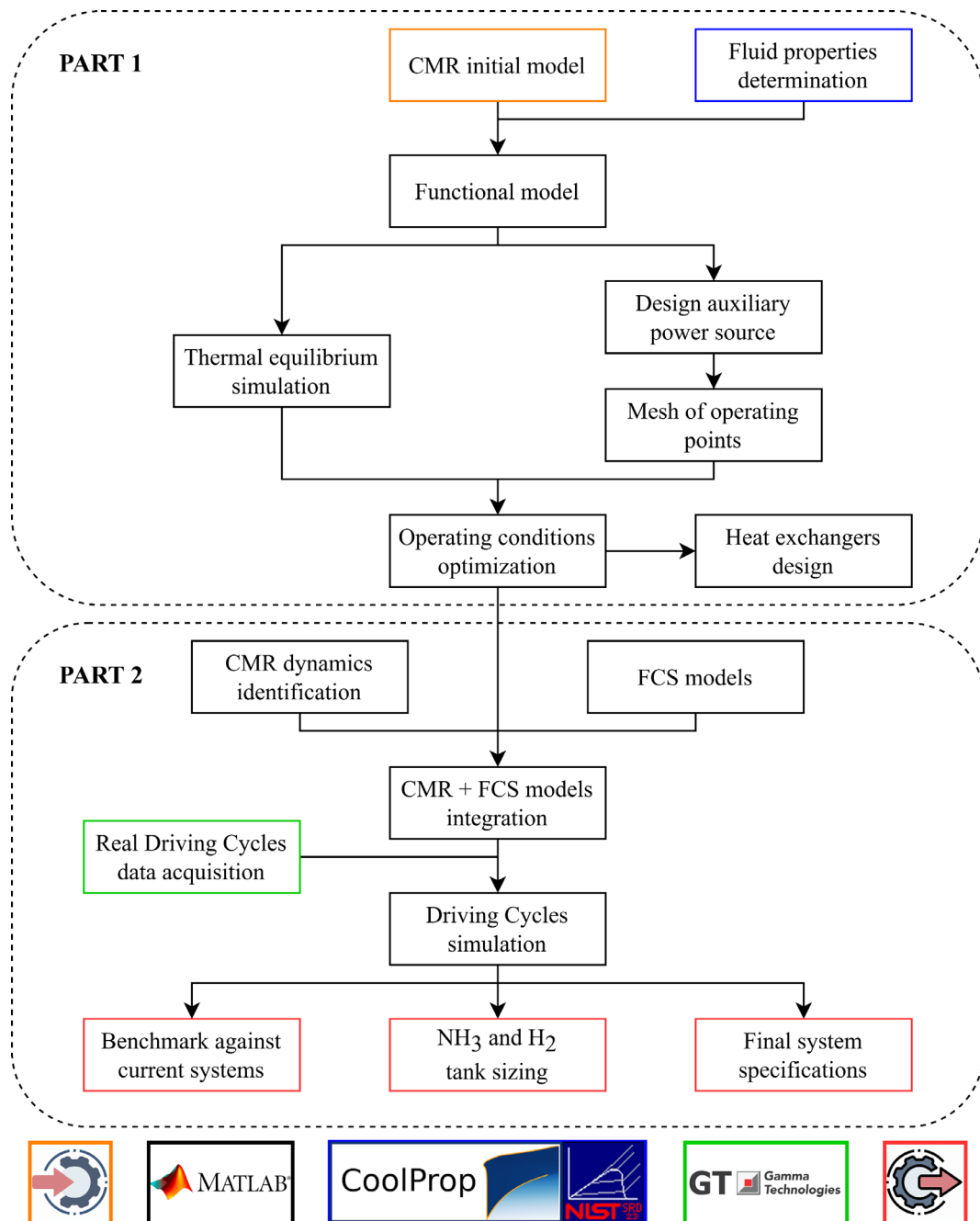


Figure 3.1. Methodology outline.

2. **CMR-FCS integration into HDV.** This part, comprising the analysis carried out in **Chapter 5, Stages 5 to 7**, is aimed at identifying the optimum sizing, operating conditions and control dynamics that satisfy the different performance requirements while maximizing efficiency and minimizing both system weight and volume. Since usually performance and weight/volume cannot be optimized simultaneously, the trade-off between them is what fixates that the performance of the system is fixed by the minimum requirements for each Driving Cycle and each particular layout of CMR-FCS. The research related to this part is in line with **Partial Objectives 3 and 4**.

3.2 Stage description

Chapters 4 and 5 of this thesis are divided in a total of 7 Stages:

- **Stage 1 – Thermal Equilibrium.** In this first stage, the objective is to understand the core mechanisms that govern the system's behaviour in order to characterize the CMR response in the most straightforward scenario, that is, thermal equilibrium.
- **Stage 2 – Operating points.** After exploring thermal equilibrium, it is necessary to ask whether operating outside of it is viable. That is, whether externally heating or cooling the CMR could improve the overall system efficiency.
- **Stage 3 – Heat Exchangers.** There are up to three heat exchangers in the powertrain system and they are a fundamental part of the powertrain layout. Their design is a key factor in the system performance and sizing them requires its own Stage.
- **Stage 4 – Scaling Factor selection.** Once the CMR is characterized in its different SFs and the system for each of them is designed, an evaluation of the advantages and disadvantages is carried over and a SF is selected for the simulations in the next stages.
- **Stage 5 – Driving cycles.** This stage includes the description of the FC models, its integration with the CMR developed in previous stages in a simplified Mean Values Model (MVM) and the simulation of various two driving cycles with different powertrain configurations.
- **Stage 6 – Final layout and specifications.** For each case simulated in Stage 5, a final layout is proposed and a summary of the specifications is made.
- **Stage 7 – Benchmark against current systems.** All the simulated systems in Stage 5 are compared with powertrains of two different HDFCV.

3.3 Tools

To develop the various models presented throughout this thesis, the following software programs have been employed:

- **MATLAB. Simulink/Simscape.** MATLAB is a programming and numerical computing platform widely used by engineers and scientists to analyse data, develop algorithms, and create models. Simulink is a block diagram environment designed for systems with multidomain models, allowing simulation before transitioning to hardware and deployment without the need for code. Simscape enables the rapid creation of physical system models within the Simulink environment. All models in this thesis have been developed using this platform, and MATLAB was also used for data management.
- **CoolProp & RefProp.** These are thermodynamic property databases for a wide range of fluids. RefProp, developed by NIST, and CoolProp, an open-source database, were both used to obtain fluid properties for the models discussed.
- **GT-Power.** This software, developed by Gamma Technologies, offers a real-time plant model solution for both vehicle system simulation and ECU calibration. It was employed to generate the driving cycle data used in the simulations throughout Chapter 5.

3.4 Initial CMR system model

The initial model for the CMR system has 3 different layers. The first two, shown in Figures 3.2 and 3.3, are actually at the same model level, but the second layer, in Figure 3.3, is embedded in a block to ease the handling and modifying of the different components. As they are part of the same actual model, they both share solver configuration among other properties.

Figure 3.4 shows the third layer, which is, in fact, an embedded different model that is responsible of all the calculations related to the electrochemical aspect of the CMR.

This first iteration of the model will be detailed in depth in throughout the Stage 1. The different modifications also will be discussed in the pertinent Stages.

3.5 CMR Dynamics

In Chapter 5, in order to integrate these FC models with the CMR model developed in Chapter 4, one of the most critical aspects of the CMR must be characterized: its dynamic behaviour. Conducting this analysis for all the possible SFs requires significant time investment, and the computational cost of each necessary simulation is quite high. For this reason, the analysis was only carried out after selecting a single SF. Three different methodologies were tested to characterize the dynamics.

MATLAB IDENTIFICATION TOOLBOX

This first methodology involves attempting to find a single transfer function that accurately represents the behaviour of the CMR using MATLAB's System Identification Toolbox. This methodology will be explained in depth, alongside the implementation in the model, in Section 4.2.2.

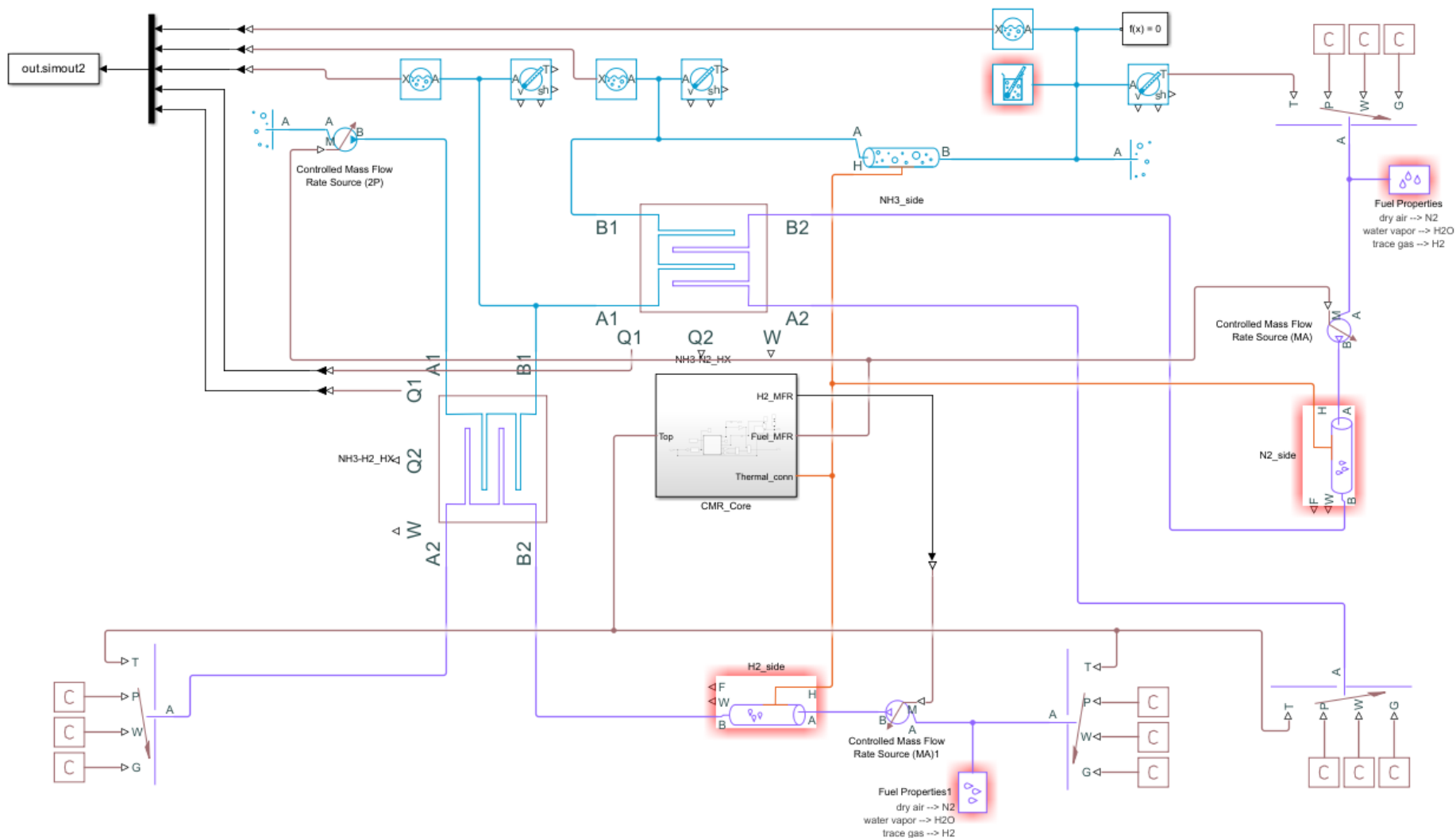


Figure 3.2. CMR initial model - Layer 1.

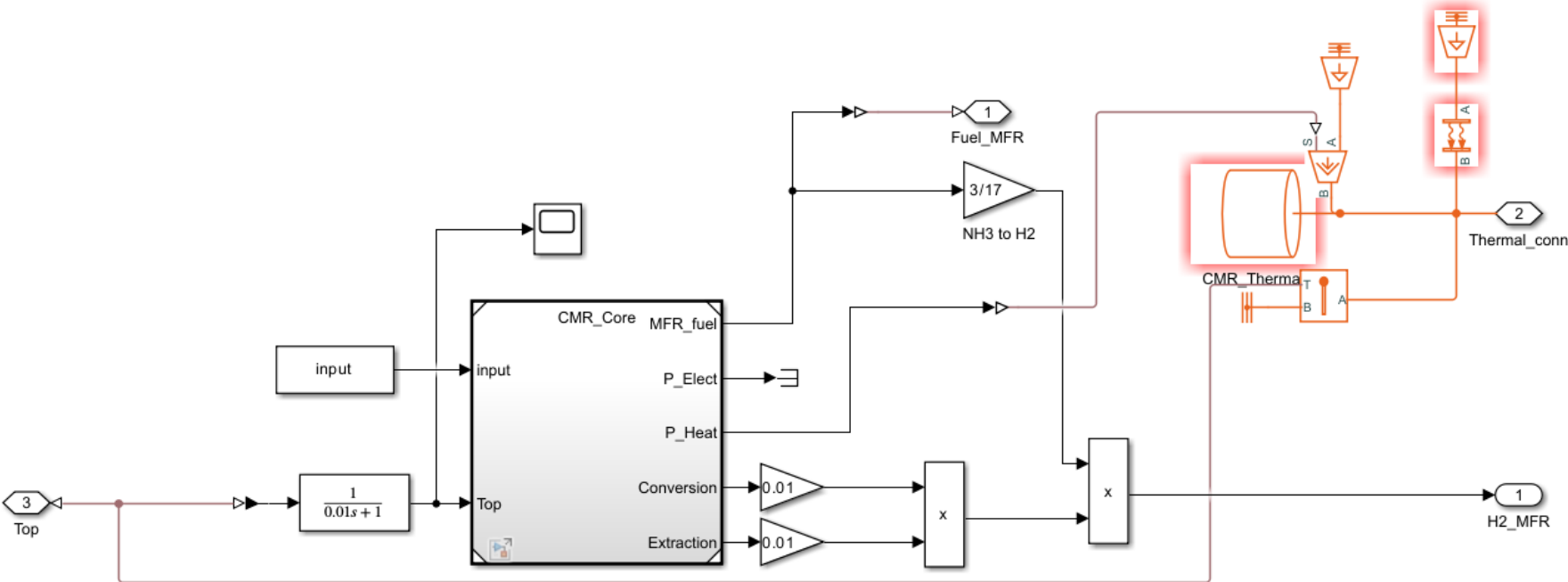


Figure 3.3. CMR initial model - Layer 2.

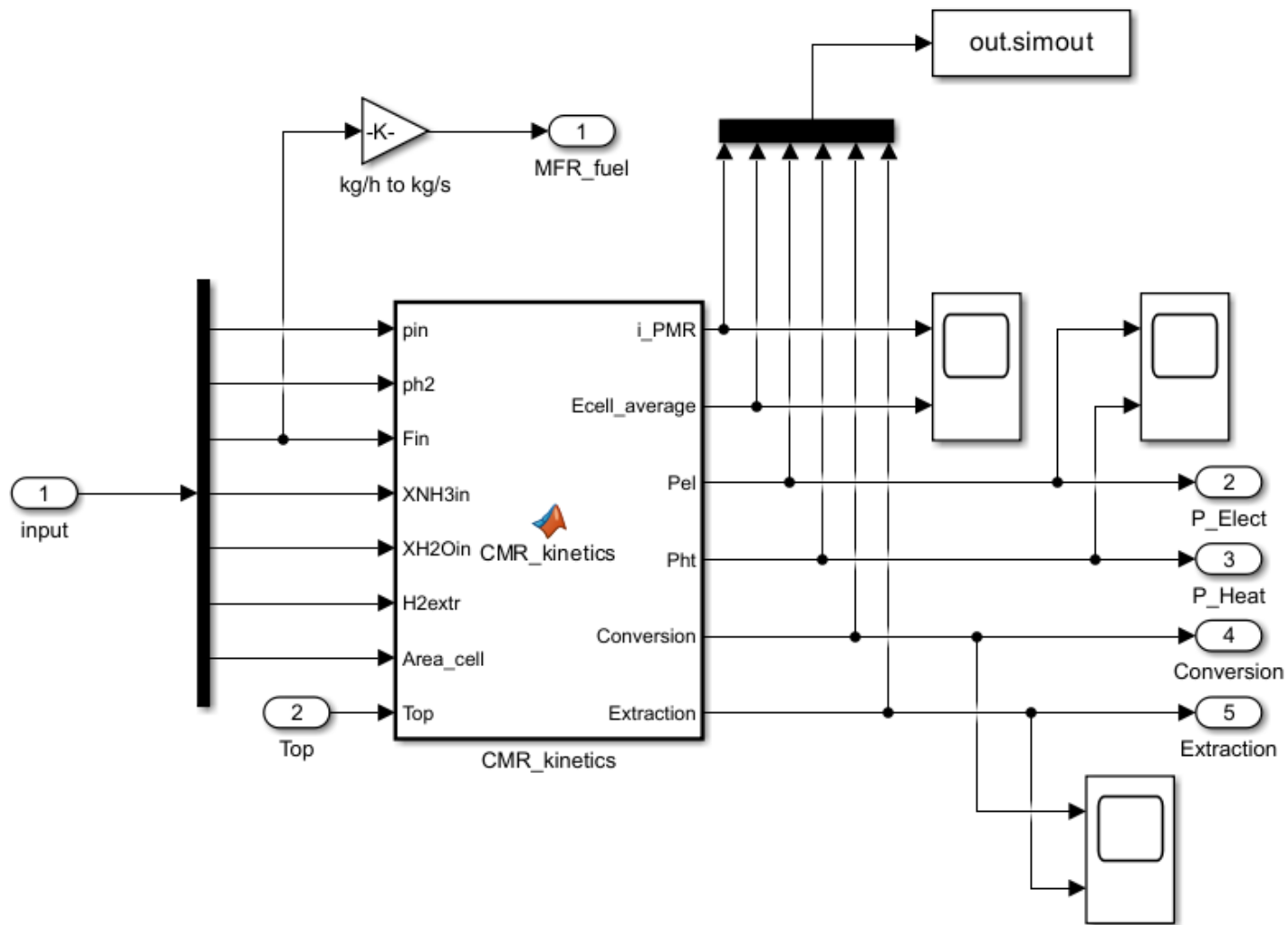


Figure 3.4. CMR initial model - Layer 3.

GENETIC ALGORITHM

The second methodology requires the application of the genetic algorithm, which is an optimization technique used to solve both constrained and unconstrained problems, inspired by the principles of natural selection in biological evolution. This algorithm iteratively modifies a population of potential solutions. At each iteration, it selects individuals from the current population to act as parents, which then generate offspring for the subsequent generation. Through this process of selection and reproduction over multiple generations, the population gradually evolves toward an optimal solution.

This technique is well-suited for tackling a wide range of optimization problems that traditional methods struggle with, particularly those where the objective function is discontinuous, nondifferentiable, stochastic, or highly nonlinear.

There are three main types of rules that are used at each step to create the next generation from the current population: [1]

- **Selection rules.** They select the individuals, called parents, which contribute to the population at the next generation. The selection is generally stochastic and can depend on the individuals' scores.
- **Crossover rules.** They combine two parents to form children for the next generation.
- **Mutation rules.** They apply random changes to individual parents to form children.

Figure 3.5 shows the flowchart of this algorithm.

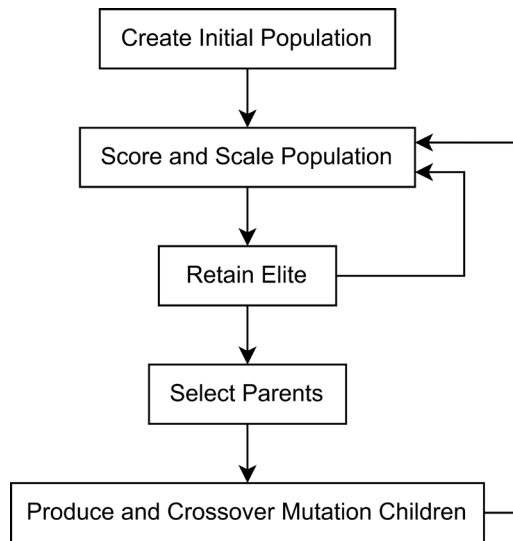


Figure 3.5. Genetic Algorithm steps diagram. [1]

The model used for the identification through this methodology is shown in Figure 3.6.

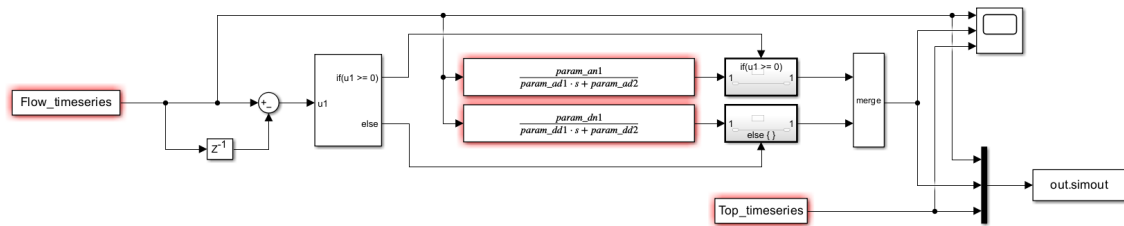


Figure 3.6. Simulink model to implement Genetic Algorithm transfer function parameters.

HEURISTIC IDENTIFICATION

This third method requires a certain level of modelling expertise and involves manually approximating functions to achieve sufficient fitness for the various behaviours of the CMR. In this case, the proposed operation calculates the operating temperature at each moment based on the operating temperature of the previous instant and a gain, as shown in the following equation:

$$T_{op,i} = T_{op,0} + Gain \cdot dt$$

However, this linear gain is defined differently depending on whether the maximum efficiency temperature for the flow at the time of calculation is higher or lower than the current CMR temperature.

Ascendent Gain

In cases where the maximum efficiency temperature is higher than the current temperature, the following gain is used, calculated as:

$$Gain_{asc,i} = \frac{T_{op_{max_eff}} - T_{op,0}}{2250 \cdot \left(1 - \frac{flow_i^{1.1}}{160}\right)}$$

Descendent Gain

Conversely, if the maximum efficiency temperature is lower than the current temperature, another gain is applied, calculated as:

$$Gain_{desc,i} = \frac{T_{op,0} - T_{op_{max_eff}}}{1400 \cdot \left(1 + \frac{5}{1.5 \cdot flow_i^{0.15}}\right)}$$

These gains are the result of several iterations of identification and validation with different Ammonia flow jumps within the range defined for the chosen SF.

3.6 FC Models

For the integration alongside the CMR, two possible FCS options have been considered: one FC designed for HDV applications, property of the IUI CMT, and the other is the one equipped in the Toyota Mirai. Each of these systems is described in detail below, along with how their respective models were developed.

FC designed for HDV applications – CMT FC

This FC is owned for the IUI CMT and its nominal power is 60 kW. The model data comes from an experimental test developed to evaluate the influence of ambient conditions on the performance of the system, plus information about both the anode and cathode circuits.

Additionally, the obtained data regarding the performance of an FCS is highly significant for HDV manufacturers in the transportation sector and eases the pathway to the optimization of these technologies, as the experimental campaign has shown that increasing relative humidity can improve the performance of the membrane up to a 2% for a 25% change in the humidity level [2]. Figure 3.7 shows the design of the lab where the various experiments were conducted to characterize this FC. The most relevant results from this experimental campaign for this thesis are the Power Curve and the Hydrogen Inlet Curve, presented in Figure 3.8.

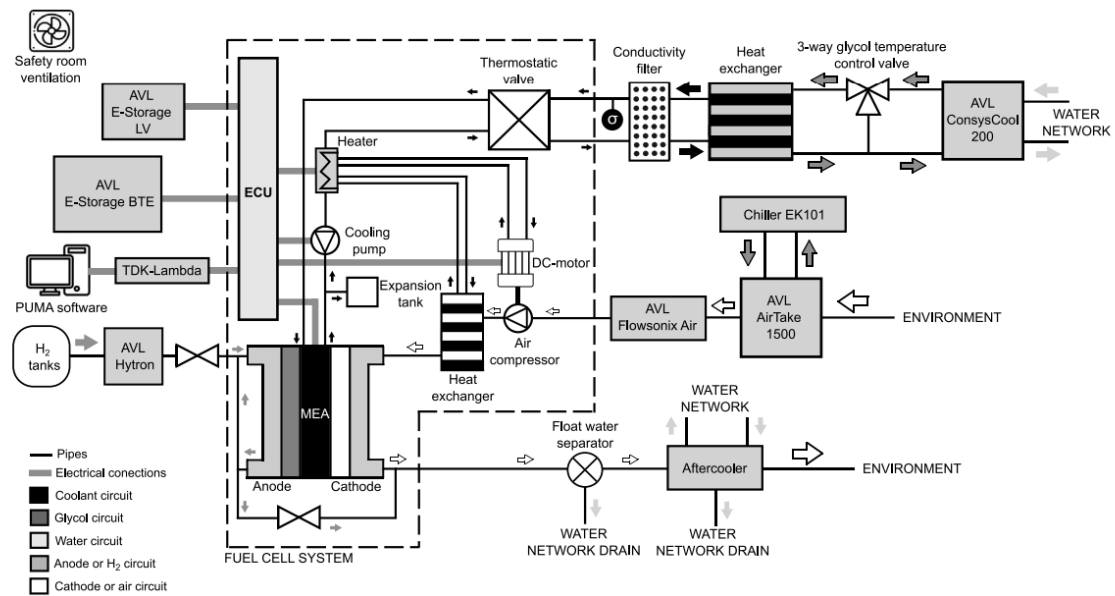


Figure 3.7. Fuel Cell test room diagram at the IUI CMT. [2]

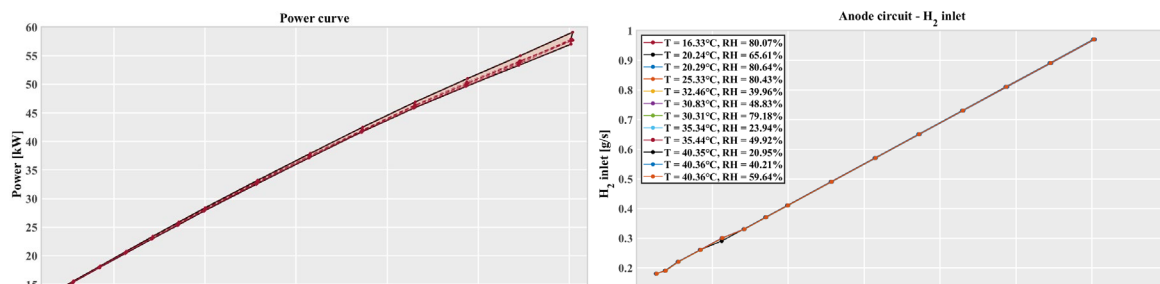


Figure 3.8. Power and Hydrogen inlet curves in each step of the polarization curve. [2]

Toyota Mirai FCS

This FC model results from a study aimed to develop a comprehensive methodology to calibrate and validate multi-physics dynamic FCS models.

The model was calibrated with the aid of experimental data from a Toyota Mirai FC electric vehicle, which was predominantly retrieved from the vehicle’s Controller Area Network (CAN) bus system thereby negating the need for major intrusion into the powertrain system. The validation process was deemed successful with the model being able to truthfully replicate the characteristics of the FC vehicle operated on the World-wide harmonized Light duty Test Cycle (WLTC) 3b and US06 driving cycle [3].

The time-resolved physical parameters, including cathode pressure, mass flow and FC stack temperature, were captured with high precision. Meanwhile, the overall performance metrics, such as Hydrogen consumption in the stack and system, as well as compressor energy consumption, were predicted with deviations of less than 0.47%, 1.75%, and 1.89% from the experimental data, respectively.

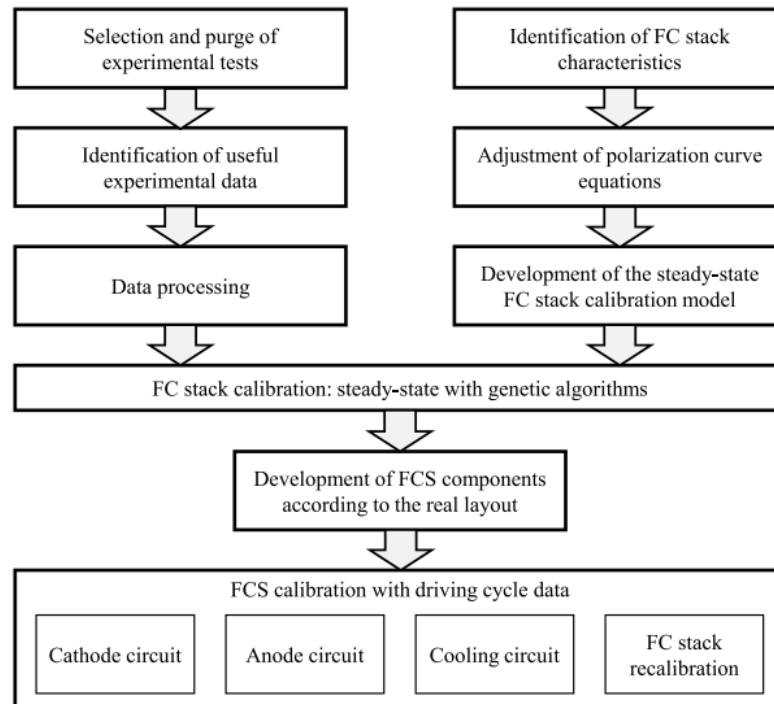


Figure 3.9. Toyota Mirai FC characterization methodology. [3]

Figure 3.9 shows the methodology used in this study, and its application in real-world industry scenarios offers significant benefits, primarily enhancing the FCV design process, accelerating the transition to a Hydrogen-based economy through the faster deployment of FCVs, and enabling precise forecasting of Hydrogen demand requirements.

Figure 3.10 shows a diagram of the testing rig, which is very similar to the experimental setup of the previous FC.

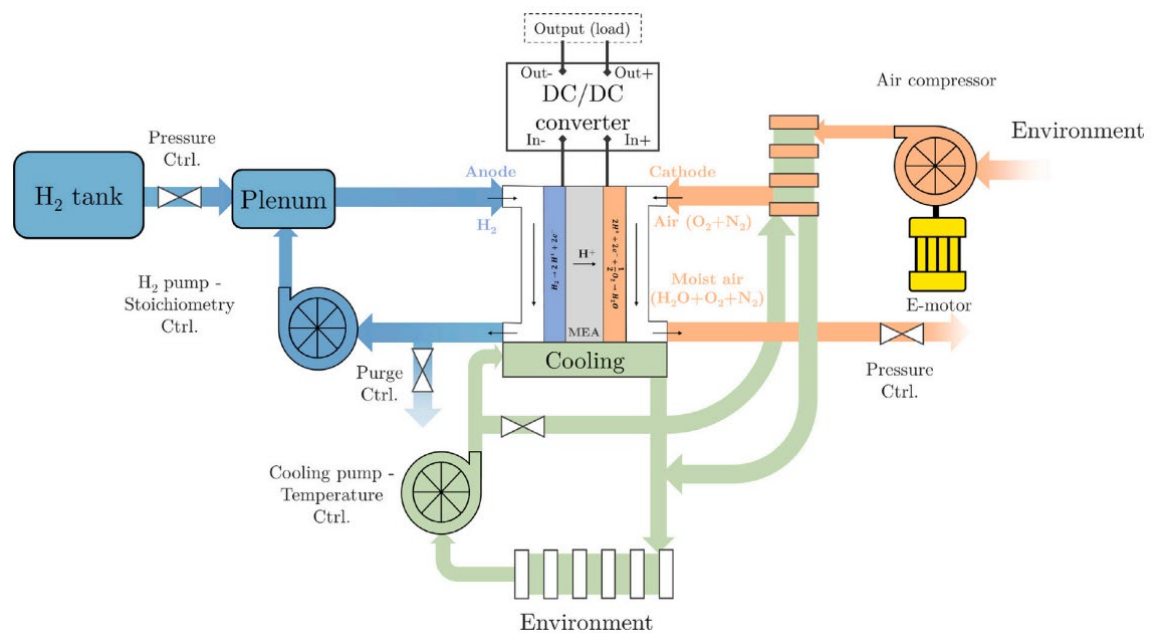


Figure 3.10. Toyota Mirai FC characterization testing rig. [3]

Figure 3.11 summarizes the key results of interest for the model used in this thesis.

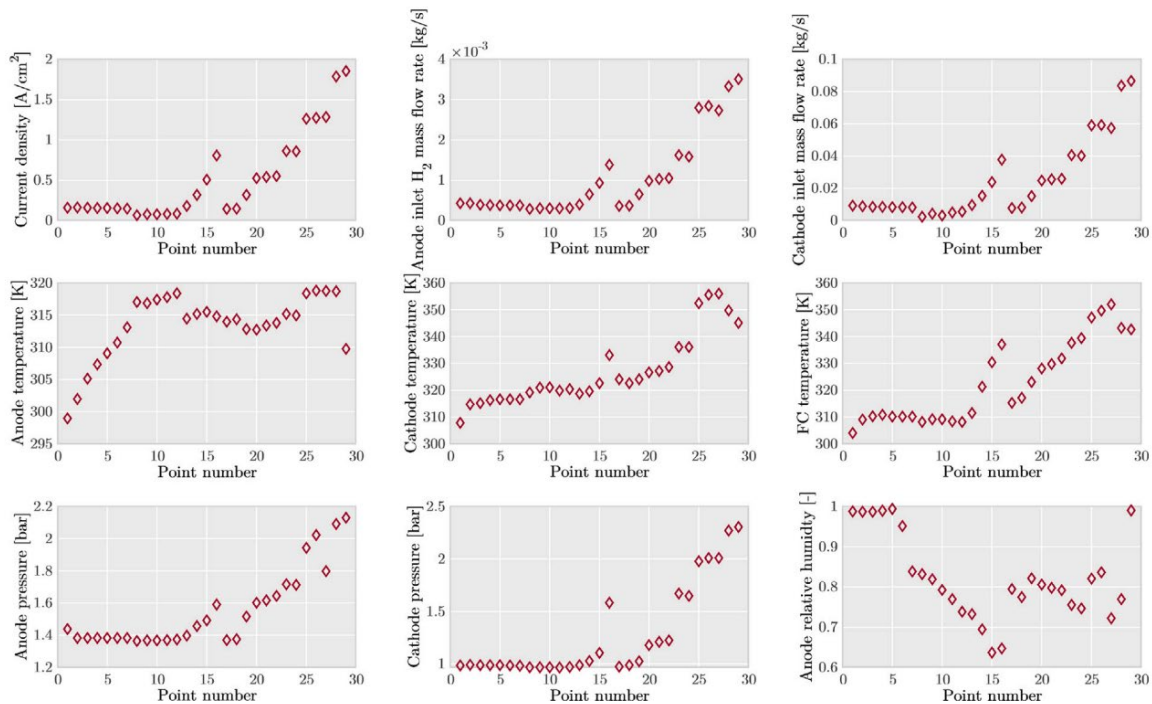


Figure 3.11. Toyota Mirai FC characterization main results. [3]

The Toyota Mirai FC has a nominal power of 114 kW.

3.7 Vehicles

For the integration of the CMR into the system, two typical FCVs will be considered. These vehicles were obtained from a fleet jointly characterized by the IUI CMT and the JRC. One of the main databases used to identify the reference vehicles is the European Parliament standard [4].

The powertrain of these FCVs is mainly composed of the e-motors, the transmission system, the battery system, the FCS, and the H₂ tanks, as shown in Figure 3.12. The connection between the FCS, the battery, and the e-motor is indirect, meaning that both the FCS and the battery have a DC/DC converter at their output. This architecture protects the FCS from oscillations originating from the bus and allows for downsizing the FC stack by boosting the voltage to the levels required by the e-motor without significantly increasing the number of cells.

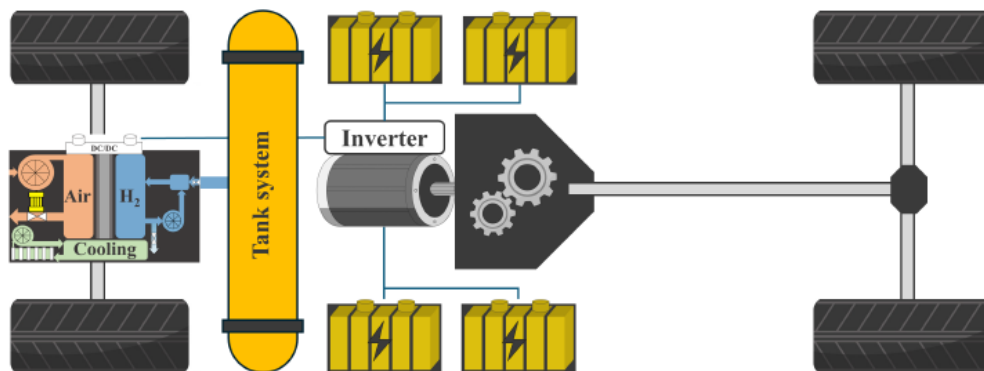






Figure 3.12. HDFCV powertrain layout.

The European Automobile Manufacturers Association has conducted studies on the distribution of CO₂ emissions among different HDV groups. The latest analysis shows that 68.2% of the CO₂ emissions from all the vehicles analysed can be attributed to just one subgroup, namely 5-LH (4x2 tractors, GCW>16t) [5], as shown in Table 3.1.

Table 3.1. CO₂ emissions share from different HDV groups. [5]

	Q3-Q4 share	Configuration	GCW [T]	Engine [kW]	Cabin	
	4-UD	0.4%	R 4x2	>16	<170	All
	4-RD	7.9%	R 4x2	>16	≥170 day cab ≥170 <265 sleeper cab	Day & sleeper
	4-LH	1.9%	R 4x2	>16	≥265	Sleeper
	5-RD	0.8%	T 4x2	>16	All-day cab <265 sleeper cab	Day & sleeper
	5-LH	62.8%	T 4x2	>16	≥265 sleeper cab	Sleeper
	9-RD	7.2%	R 6x2			Day
	9-LH	9.2%	R 6x2			Sleeper
	10-RD	0.1%	T 6x2			Day
	10-LH	9.7%	T 6x2			Sleeper

For this reason, the VECTO-LHR cycle has been simulated with a 5-LH vehicle. This vehicle, which is a HDFCV derived from a diesel HDV, has a total mass of 34595 kg, with a loading of 19300 kg. This vehicle does not actually exist; it is a reference vehicle for 5-LH, developed based on statistical data from the european vehicle fleet [4].

On the other hand, the HDDT cycle was simulated for the Hyundai XCIENT FCV, an HDFCV in the 4-RD group, whose main characteristics are shown in Table 3.2.

Table 3.2. Hyundai XCIENT 4-RD HDFCV datasheet. [6]

Item Model	Xcient Fuel Cell
Vehicle Type	Cargo (Chassis Cab)
Cab Type	Day Cab
Drive System	LHD / 4 x 2
Dimensions [mm]	
Wheel Base	5,130
Overall (Chassis Cab)	
Length	9,745
Width	2,515 (2,550 with side protector), Maximum allowable width 2,600
Height	3,730
Weight [kg]	
Max. Gross Combination Weight	36,000 as pull-cargo
Max. Gross Vehicle Weight	19,000 as rigid truck
Front / Rear	8,000 / 11,500
Empty Vehicle Weight (Chassis Cab)	9,795
Calculated Performance	
Drive Range	Accurate range to be confirmed later
Max. Speed	85 km/h
Powertrain	
Fuel Cell Stack	190 kW (95 kW x 2EA)
Battery	661V / 73.2 kWh - by Akasol
Motor / Inverter	250 kW / 3,400 Nm - by Siemens
Transmission	ATM S4500 - by Allison / 6 forward and 1 reverse speed
Rear Axle Ratio	4.875
Hydrogen Tank	
Filling Pressure	350 bar
Capacity	32.09 kgH ₂

Finally, Table 3.3 provides additional characteristics of both HDV groups. These are estimates and not fully rigid values.

Table 3.3. HDV 5-LH and 4-RD additional data. [4]

HDV Group	No-powertrain mass [kg]	E-motor n ^o x Power [kW]	Battery Capacity [kWh]	H ₂ capacity [kg]	LHR range [km]
5-LH	5599	2 x 166	73	43.7 - 48.2	600
4-RD	5014	1 x 122	73	20.0 - 21.1	265-276

3.8 References

- [1] Mathworks. “What Is the Genetic Algorithm?”.
- [2] Desantes J.M., Novella R., López-Juárez M., Nidáguila I. “Experimental assessment of a heavy-duty fuel cell system in relevant operating conditions”. *Applied Energy* Vol. 376, pp. 12493, 2024
- [3] López-Juárez M., Rockstroh T., Novella R., Vijayagopal R. “A methodology to develop multi-physics dynamic fuel cell system models validated with vehicle realistic drive cycle data”. *Applied Energy* Vol. 358, pp. 122568, 2024.
- [4] THE EUROPEAN PARLIAMENT, Commission regulation (EU) 2017/2400.
- [5] European Automobile Manufacturers’ Association. “CO2 emissions from heavy-duty vehicles”, 2020
- [6] Hyundai. “XCIENT Fuel Cell catalog”, 2020.

Chapter 4

CMR system characterization

The first step in developing a model is to characterize the system's behaviour in as much detail as possible. For this reason, this entire chapter focuses on developing a model of the CMR system capable of providing accurate results under different operating conditions, both in thermal equilibrium and outside of it. However, since it is closely linked to the system's implementation in the vehicle and its driving cycles, the characterization of the thermal dynamic response is covered in the following chapter.

This part integrates not only the development of the model, but also the element sizing and the selection of the steady-state operating points that are the most efficient for each SF. As mentioned in Section 3.2, this fourth chapter is divided into four stages:

- **Stage 1 – Thermal Equilibrium.**
- **Stage 2 – Operating points.**
- **Stage 3 – Heat Exchangers.**
- **Stage 4 – Scaling Factor Selection.**

The main results of this chapter should be the SF to be implemented in the vehicle, along with data on its operation in a steady state. These will serve as a basis for developing new CMR models that are less computationally expensive but still sufficiently accurate and that can be integrated with the models already developed for the other components of the propulsion system.

4.1 Stage 1 – Thermal Equilibrium

In this first stage, the model employed is the simplest one of this chapter and its objective is to serve as the foundation for the analysis. This basic model is crucial for understanding the core mechanisms that govern the system's reaction.

The operational conditions are set to the most straightforward scenario, that is, thermal equilibrium, which allowed for a clear analysis of the natural behaviour of the CMR. This equilibrium scenario is critical for establishing a baseline understanding of the system's response before introducing more dynamic or complex conditions.

The following sections describe the most important parameters to be introduced into the model, both for this stage and, more generally, for all the simulations conducted throughout this thesis.

4.1.1 Fluid parameters

One of the most important tasks to do is to obtain the properties of the different fluids which are relevant to the model and to format this data as required to create the input for the model.

The properties of these fluids are introduced into the "Fuel Properties" block, as illustrated in Figures 4.1, 4.2, and 4.3. This block is designed to model humid air with a trace gas, but it is not strictly limited to this configuration. To adapt it to the desired conditions within the model, Nitrogen will act as dry air, water steam will remain as such and Hydrogen will serve as the trace gas.

NAME	VALUE
▼ Dry Air	
> Dry air specific gas constant	N2_R 296.8 J/kg/K
Temperature vector	N2_T <1x131 double> K
Dry air specific enthalpy vector	N2_h <1x131 double> kJ/kg
> Dry air dynamic viscosity vector	N2_mu <1x131 double> s*uPa
> Dry air thermal conductivity vector	N2_k <1x131 double> mW/m/K
> Minimum valid pressure	1 kPa
> Maximum valid pressure	inf MPa
> Minimum valid temperature	min(N2_T) 200 K
> Maximum valid temperature	max(N2_T) 1500 K
Pressure and temperature outside valid r...	Error
> Atmospheric pressure	0.101325 MPa
> Atmospheric temperature	20 degC

Figure 4.1. Input of Nitrogen properties.

> Dry Air	
▼ Water Vapor	
> Water vapor specific gas constant	H2O_R 461.52 J/kg/K
> Water vapor saturation pressure vector	H2O_psat <1x131 double> MPa
> Water specific enthalpy of vaporization ve...	H2O_hv <1x131 double> kJ/kg
Water vapor specific enthalpy vector	H2O_h <1x131 double> kJ/kg
> Water vapor dynamic viscosity vector	H2O_mu <1x131 double> s*uPa
> Water vapor thermal conductivity vector	H2O_k <1x131 double> mW/m/K
> Water vapor diffusivity in air	H2O_D 25 mm^2/s

Figure 4.2. Input of Water Vapor properties.

NAME	VALUE
> Dry Air	
> Water Vapor	
▼ Trace Gas	
Trace gas model	Track mass fraction and gas properties
> Trace gas specific gas constant	H2_R 4124.5 J/kg/K
Trace gas specific enthalpy vector	H2_h <1x131 double> kJ/kg
> Trace gas dynamic viscosity vector	H2_mu <1x131 double> s ^u Pa
> Trace gas thermal conductivity vector	H2_k <1x131 double> mW/m/K
> Trace gas diffusivity in air	H2_D 74 mm ² /s

Figure 4.3. Input of Hydrogen properties.

Table 4.1 presents the constants for each fluid, and the Table 4.2 shows the diffusivity.

Table 4.1. Gas constant.

GAS CONSTANT [J/kgK]		
Hydrogen	Nitrogen	Water
4124.48	296.80	461.52

Table 4.2. Diffusivity.

DIFFUSIVITY [mm ² -s]	
Hydrogen	Water
74	25

The two most critical fluids for the model are Hydrogen and Nitrogen. An extract of the properties for Hydrogen is shown in Table 4.3, while Table 4.4 provides the corresponding data for Nitrogen.

Table 4.3. Hydrogen properties.

HYDROGEN						
Enthalpy	Temperature	Thermal Conductivity	Kinematic viscosity	Dynamic Viscosity	Density	Prandtl
[kJ/kg]	[K]	[mW/(m·K)]	[cm ² ·s]	[μPa·s]	[kg/m ³]	[-]
3533.8	270	173.10	0.0928	8.32	0.9042	0.6910
3672.8	280	175.99	0.0987	8.54	0.8720	0.6908
3815.3	290	180.97	0.1047	8.75	0.8421	0.6902
3958.3	300	185.76	0.1109	8.95	0.8141	0.6899
4101.6	310	190.56	0.1171	9.16	0.7879	0.6892
4245.2	320	195.17	0.1236	9.36	0.7634	0.6890
4389.0	330	200.28	0.1301	9.56	0.7404	0.6867
4533.0	340	205.30	0.1368	9.75	0.7187	0.6846
...						
16007.0	1120	585.79	0.1012	21.91	0.2190	0.5688
16159.0	1130	590.92	0.1028	22.04	0.2170	0.5680
16312.0	1140	596.05	0.1043	22.17	0.2151	0.5672
16464.0	1150	601.18	0.1058	22.30	0.2133	0.5664
16617.0	1160	606.33	0.1074	22.43	0.2114	0.5656
16770.0	1170	611.48	0.1089	22.56	0.2096	0.5648
16923.0	1180	616.63	0.1105	22.69	0.2079	0.5640
17076.0	1190	621.80	0.1120	22.82	0.2061	0.5632

Table 4.4. Nitrogen properties.

NITROGEN						
Enthalpy	Temperature	Thermal Conductivity	Kinematic viscosity	Dynamic Viscosity	Density	Prandtl
[kJ/kg]	[K]	[mW/(m·K)]	[cm ² ·s]	[μPa·s]	[kg/m ³]	[-]
3533.8	270	173.10	0.0928	8.32	0.9042	0.6910
3672.8	280	175.99	0.0987	8.54	0.8720	0.6908
3815.3	290	180.97	0.1047	8.75	0.8421	0.6902
3958.3	300	185.76	0.1109	8.95	0.8141	0.6899
4101.6	310	190.56	0.1171	9.16	0.7879	0.6892
4245.2	320	195.17	0.1236	9.36	0.7634	0.6890
4389.0	330	200.28	0.1301	9.56	0.7404	0.6867
4533.0	340	205.30	0.1368	9.75	0.7187	0.6846
...						
16007.0	1120	585.79	0.1012	21.91	0.2190	0.5688
16159.0	1130	590.92	0.1028	22.04	0.2170	0.5680
16312.0	1140	596.05	0.1043	22.17	0.2151	0.5672
16464.0	1150	601.18	0.1058	22.30	0.2133	0.5664
16617.0	1160	606.33	0.1074	22.43	0.2114	0.5656
16770.0	1170	611.48	0.1089	22.56	0.2096	0.5648
16923.0	1180	616.63	0.1105	22.69	0.2079	0.5640
17076.0	1190	621.80	0.1120	22.82	0.2061	0.5632

As can be observed, there are additional properties beyond those strictly required by the "Fluid Properties" block. This is because these properties will be necessary in future sections.

Table 4.5. Water properties.

WATER					
Temperature	Saturation Pressure	Enthalpy	Thermal Conductivity	Dynamic Viscosity	LHV
[K]	[MPa]	[kJ/kg]	[mW/(m·K)]	[μPa·s]	[kJ/kg]
200	1.63E-07	20.0	500.00	1500.00	2833.0
210	7.02E-07	21.0	510.00	1490.00	2835.5
220	2.66E-06	22.0	520.00	1480.00	2837.3
230	8.95E-06	23.0	530.00	1470.00	2838.3
240	2.73E-05	24.0	540.00	1460.00	2838.7
250	7.60E-05	25.0	550.00	1450.00	2838.5
260	1.96E-04	26.0	560.00	1440.00	2837.4
...					
1440	21.4874	5064.7	161.36	53.76	547.6
1450	21.4974	5090.6	162.88	54.11	547.6
1460	21.5074	5116.4	164.40	54.45	547.6
1470	21.5174	5142.4	165.93	54.80	547.6
1480	21.5274	5168.4	167.45	55.14	547.6
1490	21.5374	5194.4	168.98	55.48	547.6
1500	21.5474	5220.6	170.51	55.82	547.6

As the final fluid in this group, water requires other specific properties for this block. An excerpt of these properties is provided in Table 4.5.

Lastly, it is essential to discuss Ammonia. Ammonia is the fuel used in the case study that encompasses this entire thesis and is the most critical fluid in terms of properties, as it requires a greater number of properties and a higher level of detail. A summary of Ammonia's properties is presented in Table 4.6, similar to the previous group of fluids:

Table 4.6. Ammonia properties.

AMMONIA					
Temperature	Thermal conductivity	Kinematic Viscosity	Dynamic viscosity	Density	Prandtl
[K]	[mW/(m·K)]	[cm ² ·s]	[μPa·s]	[kg/m ³]	[-]
290	509.41	0.0023	142.94	0.7146	1.3242
295	494.72	0.0022	135.90	0.7019	1.3070
300	26.33	0.0126	9.90	0.6897	1.1673
305	26.76	0.0132	10.11	0.6780	1.1288
310	27.21	0.0138	10.31	0.6666	1.0970
315	27.68	0.0145	10.51	0.6557	1.0702
320	28.17	0.0151	10.72	0.6451	1.0475
325	28.67	0.0157	10.92	0.6349	1.0280
...					
855	66.67	0.1276	31.01	0.2395	1.5363
860	65.46	0.1291	31.19	0.2382	1.5788
865	64.19	0.1306	31.37	0.2368	1.6245
870	62.86	0.1321	31.55	0.2354	1.6738
855	66.67	0.1276	31.01	0.2395	1.5363
860	65.46	0.1291	31.19	0.2382	1.5788
865	64.19	0.1306	31.37	0.2368	1.6245
870	62.86	0.1321	31.55	0.2354	1.6738

However, the element where the fuel properties are input into the model differs from the previous one. In this case, the “Two-Phase Fluid Properties” block is used, with its structure for the inputs illustrated in Figures 4.4, 4.5, and 4.6.

NAME	VALUE	
Parameters		
Minimum valid specific internal energy	AmmoniaTables.u_min	kJ/kg
Maximum valid specific internal energy	AmmoniaTables.u_max	kJ/kg
Pressure vector	AmmoniaTables.p	MPa
Critical pressure	AmmoniaTables.p_crit	MPa
Thermal transport properties near critical ...	Clip peak values	
Fraction above and below Critical pressur...	0.12	
Atmospheric pressure	0.101325	MPa
Configurability	Compile-time	
Pressure and specific internal energy outs...	Error	
Dynamic pressure threshold for flow reve...	0.01	Pa
Configurability	Compile-time	

Figure 4.4. Input of Ammonia general properties.

NAME	VALUE	
Parameters		
Liquid Properties		
Normalized liquid internal energy vector	AmmoniaTables.liquid.unorm	
Liquid specific volume table	AmmoniaTables.liquid.v	m ³ /kg
Liquid specific entropy table	AmmoniaTables.liquid.s	kJ/(K*kg)
Configurability	Compile-time	
Liquid temperature table	AmmoniaTables.liquid.T	K
Configurability	Compile-time	
Liquid kinematic viscosity table	AmmoniaTables.liquid.nu	mm ² /s
Configurability	Compile-time	
Liquid thermal conductivity table	AmmoniaTables.liquid.k	W/(K*m)
Liquid Prandtl number table	AmmoniaTables.liquid.Pr	
Saturated liquid specific internal energy v...	AmmoniaTables.liquid.u_sat	kJ/kg

Figure 4.5. Input of liquid Ammonia properties.

NAME	VALUE	
Parameters		
Liquid Properties		
Vapor Properties		
Normalized vapor internal energy vector	AmmoniaTables.vapor.unorm	
Vapor specific volume table	AmmoniaTables.vapor.v	m ³ /kg
Vapor specific entropy table	AmmoniaTables.vapor.s	kJ/(K*kg)
Configurability	Compile-time	
Vapor temperature table	AmmoniaTables.vapor.T	K
Configurability	Compile-time	
Vapor kinematic viscosity table	AmmoniaTables.vapor.nu	mm ² /s
Configurability	Compile-time	
Vapor thermal conductivity table	AmmoniaTables.vapor.k	W/(K*m)
Vapor Prandtl number table	AmmoniaTables.vapor.Pr	
Saturated vapor specific internal energy v...	AmmoniaTables.vapor.u_sat	kJ/kg

Figure 4.6. Input of Ammonia vapor properties.

Therefore, the data must be stored in a struct and the way to generate this data is by using MATLAB’s “twoPhaseFluidTables” function. Once the data is generated, the properties shown in Table 4.7 are obtained for both the liquid and gaseous phases:

Table 4.7. Summary of liquid and vapor common properties.

FIELD	CONTENTS	DIMENSIONS	UNITS
unorm	Normalized specific internal energy	mLiquid- or mVapor-by-1	-
v	Specific volume	mLiquid- or mVapor-by-n	m ³ /kg
s	Specific entropy	mLiquid- or mVapor-by-n	kJ/kgK
T	Temperature	mLiquid- or mVapor-by-n	K
nu	Kinematic viscosity	mLiquid- or mVapor-by-n	mm ² /s
K	Thermal conductivity	mLiquid- or mVapor-by-n	W/m·K
Pr	Prandtl number	mLiquid- or mVapor-by-n	-
u_sat	Saturation specific internal energy	mLiquid- or mVapor-by-1	kJ/kg
u	Specific internal energy	mLiquid- or mVapor-by-1	kJ/kg

Here “mLiquid” and “mVapor” are the number of rows to include in the liquid and vapor tables respectively and “n” is the number of rows for each table. Certain phase-independent properties are also generated, which are listed in Table 4.8:

Table 4.8. General fluid properties.

FIELD	CONTENTS	DIMENSIONS	UNITS
p	Normalized specific internal energy	n-by-1	MPa
u_min	Specific volume	1-by-1	kJ/kg
u_max	Specific entropy	1-by-1	kJ/kg
p_min	Temperature	1-by-1	MPa
p_max	Kinematic viscosity	1-by-1	MPa
p_crit	Thermal conductivity	1-by-1	MPa
u_crit	Prandtl number	1-by-1	kJ/kg
n_sub	Saturation specific internal energy	1-by-1	-

Note that the field column is the label the function assigns to each property.

To conclude this section, it is necessary to briefly discuss the heating value of Hydrogen and Ammonia. This parameter refers to the amount of energy per unit mass or unit volume of material that can be released during a chemical oxidation reaction. In common practice, two values have been defined: the higher heating value (HHV) and the lower heating value (LHV).

The HHV is the total amount of heat released during the complete combustion of a unit mass of fuel when the water vapor produced in the combustion is condensed, thereby accounting for the heat released during this phase change. It is measured using a calorimeter.

The LHV is the total amount of heat released during the complete combustion of a unit mass of fuel, excluding the portion corresponding to the latent heat of the water vapor generated during combustion, as no phase change occurs and the vapor is expelled. This value is of interest in industrial applications, such as furnaces or turbines, where the combustion gases exiting the chimney or exhaust are at high temperatures, and the water remains in the vapor phase without condensing. This latter value is which will be used in future sections to calculate efficiencies and other magnitudes. Table 4.9 sums up the LHV for NH₃ and H₂.

Table 4.9. Lower Heating Value for Hydrogen and Ammonia.

LHV			
Hydrogen		Ammonia	
[MJ/kg]	[kWh/kg]	[MJ/kg]	[kWh/kg]
120	33.33	18.72	5.2

4.1.2 Flow parameters

This group of parameters is fundamental to understand how the flow behaves and why some decisions are taken, as most of them are critical to the proper operation of the CMR.

Pressure of the system

One of the main parameters of the flow is pressure. As discussed in Section 2.2, the operating pressure range of the CMR is from 5 to 15 bar. To standardize and streamline the simulations while maintaining a good approximation of the order of magnitude of the different results, a standard pressure of 10 bar has been agreed upon as a compromise solution.

However, this pressure will not always remain constant, as friction losses with the pipes and localized losses in each component are inevitable. The primary pressure losses are associated with the heat exchangers, due to both pipe length and changes in flow path. To simplify the model, the decision has been made not to model the piping between the various system components and to consider only the losses occurring within these components, commonly referred to as localized or minor losses,

although this latter term is increasingly falling out of use, as localized losses often exceed other types of losses (friction, gravity and acceleration).

Flow Rate

Another important parameter is flow rate. The pumps are modelled using the "Controlled Mass Flow Rate Source" element. These pumps will operate with a constant flow rate setpoint in the case of steady-state operation, and this flow rate will be one of the inputs established at the beginning of each simulation.

Therefore, despite not being a closed circuit, the pumps will perform a similar function, as they will be responsible for supplying only the pressure necessary to overcome pressure losses throughout the system, up to the intermediate Hydrogen tank.

Temperatures

The next flow parameter to consider is the initial temperature. In this case, the entire system will initially be at 290 K.

Steam quality and requirements

Steam quality, also known as static quality, is defined as the mass fraction of vapor and is given by:

$$x_s = \frac{\rho_g \cdot A_g}{\rho_g \cdot A_g + \rho_l \cdot A_l}$$

Where ρ_g is the vapor density, A_g is the sum of the areas occupied by the vapor, ρ_l is the liquid density, and A_l is the sum of the areas occupied by the liquid.

For the proper functioning of the CMR, it is essential that the vapor quality reaches a value equal to the unit after the pipe connected to the thermal mass (NH₃ side). It is highly recommended to achieve this value at the exit of the second heat exchanger (NH₃-N₂_HX) or the membranes of the CMR could be damaged.

4.1.3 Internal chemistry parameters

Another set of relevant parameters are the those related to the internal chemistry of the CMR. The most important ones are listed below:

- **Current density:** Current is derived and proportional to the H₂ flow and the extraction. To obtain the current density, current is divided by the area of each individual cell from the CMR.
- **Voltage:** Obtained from the sum of the OCV and the product of the ASR and the current.
- **Conversion:** Parameter that shows how much NH₃ is converted to H₂.
- **Extraction:** Parameter that represents how much of the H₂ generated is actually recovered from the CMR, thus being able to be fed to the FCS.
- **Thermal Power:** Heat that is generated in the chemical reaction that takes place in the CMR.
- **Electric Power:** Power that needs to be supplied to the CMR in order to maintain its operation. Is the sum of the Thermal Power and the product of the average cell voltage and the total current.

4.1.4 Energy parameters

Energy parameters are also fundamental to analyse. The main ones are listed and detailed below.

NH₃ Power

This parameter shows the amount of energy that can be extracted from Ammonia. Its value is derived by:

$$P_{NH_3} = F_{NH_3} \cdot LHV_{NH_3}$$

H₂ Power

Similarly to the previous parameter, it represents the energy that Hydrogen can supply and its value is derived by:

$$P_{H_2} = F_{H_2} \cdot LHV_{H_2}$$

FCS Power

From all the energy available from Hydrogen, a FC can only extract a portion. To simplify calculations and obtain a reasonably accurate estimate of the system's performance, the FC efficiency is assumed to be constant and equal to 50%. Therefore, the electrical power that the FCS can supply is given by the following equation:

$$P_{FCS} = P_{H_2} \cdot 0.5$$

Net Power

Following the same train of thought, the Net Power represents the electric power that reaches the electric motor in the vehicle, that is, the FC Power minus the electric power consumed by the CMR.

$$P_{Net} = P_{FCS} - P_{Cons}$$

Thermal Efficiency

Once the net power is obtained, it is only natural to ask which part of the initial available energy reaches this final state. This is what thermal efficiency represents and it is derived from the following equation:

$$\eta_{Thermal} = \frac{P_{Net}}{F_{NH_3} \cdot LHV_{NH_3}}$$

Hydrogen Efficiency

Another type of efficiency that can illustrate an interesting aspect of the CMR under a different approach is the Hydrogen efficiency. This parameter shows how effective is the CMR in generating Hydrogen from a fuel, in this case Ammonia. Hydrogen efficiency is derived from the following equation:

$$\eta_{Thermal} = \frac{F_{H_2} \cdot LHV_{H_2}}{F_{NH_3} \cdot LHV_{NH_3} + P_{Cons}}$$

4.1.5 Scaling Factor range and justification

The SF (scaling factor) is simply the ratio of cells between different sizes of the CMR and, therefore, the ratio of volumes. For the calculation of the dimensions for each SF, it has been ensured that the External Surface/Volume ratio remains constant. The various SFs considered throughout this thesis are presented in Table 4.10:

Table 4.10. CMR Scaling Factor range and characteristics.

SF	NUMBER OF CELLS	EXTERNAL AREA [m ²]	VOLUME [m ³]	MASS [kg]
2	4046	9.73	1.156	3117
1.5	3035	7.58	0.867	2338
1	2023	5.36	0.578	1558
0.5	1012	3.04	0.289	780
0.4	810	2.54	0.231	624
0.3	607	2.03	0.173	468
0.2	405	1.50	0.116	312
0.1	203	0.91	0.058	156
0.05	102	0.57	0.029	79

The range of SF spans from 0.05 to 2, with both values being justified.

The upper limit is defined by the dimensions of the rear part of the vehicle's cabin. It is estimated that the entire system at the standard SF, that means SF1, occupies approximately 0.5 m³ and has a prismatic shape with an estimated side ratio of 1:8:8 (LxWxH), as shown in Figure 4.7. Given that the cabin has a maximum width of 2.5 m and standard Hydrogen tanks for HDFCV are 2.15 m, it is logical to establish a maximum width, and thus, height, of 2 meters. That results in an upper SF limit of 2.



Figure 4.7. Concept of the CMR implementation into the vehicle's cabin.

The lower limit is determined by the requirement to satisfy an HDDT cycle for a HDFCV. In this cycle, the average Hydrogen consumption is 1.48 g/s, which, using the equations from the previous section, results in a P_{H_2} of 178.2 kW and, consequently, a P_{FCs} of approximately 90 kW. This implies that, applying the flow rate ratio of 17/3 shown in Section 2.2, the reference Ammonia flow rate is 30.3 kg/h. The smallest SF that meets this condition is 0.05. It should be noted that these calculations are a preliminary approximation; the HDDT cycle is explored in greater detail in Stage 5.

Another important point is that, for the first stage, only the blue highlighted SFs have been simulated, as one of the objectives is to obtain a general understanding of the CMR's behaviour and to establish an SF range within which the desired system performance can be achieved, allowing for more detailed exploration within this range in subsequent iterations.

4.1.6 Simulation parameters

Time step

This is the first input of the model and one of the most important. Like the vast majority of mathematical models, this model does not simulate continuously but rather operates in a quasi-static manner. That is, the simulation period is discretized into different steady states separated by a time step dt . An initial dt of 1 second was chosen, but after performing a sensitivity analysis to determine the steady-state conditions for each calculated operating point, it was observed that the model remains robust even with time steps of up to 500 seconds. Beyond this, the model becomes unstable.

For the simulations of the system dynamics in Chapter 5, this limit is lower, and smaller time steps have been used, as will be discussed in that section.

Simulation time

In this chapter, the simulation time only needs to be larger than the settling time for each simulation.

Initial temperature

This parameter represents the initial CMR temperature. To shorten simulation times, it is set close to the estimated steady-state final temperature.

CMR physical data

Another important input for the model is the set of physical properties of the CMR. In addition to those listed in Table 4.10, the C_p and the density must also be included.

Input array

The last relevant input pack is an array conformed by the following elements:

Table 4.11. Input array breakdown.

ARRAY POSITION	MAGNITUDE	VALUE	UNITS
1	Fuel input pressure	10	bar
2	H ₂ side pressure	10	bar
3	NH ₃ flow	2.5 – 100	kg/h
4	NH ₃ mole fraction	1	-
5	Water inlet mole fraction	0	-
6	H ₂ extraction target	99	%
7	Total cell area	$N_{\text{cells}} \cdot A_{\text{cell}} \cdot 10^4$	cm ²

Where N_{cells} is defined in the Table 4.10 and the A_{cell} is 0.04 cm².

4.1.7 Results

To conclude this stage, it is necessary to discuss the simulation results for thermal equilibrium.

The first point to mention is that certain data points are invalid. This is because the operating temperature does not reach the lower operating limit, which is 400 °C, or 673 K. As shown in Figure 4.8, these points, which do not meet the minimum temperature requirement, are located within the red-coloured area and display values outside the general trend. Therefore, they have been removed to create Figure 4.9 in order to provide a clearer view of the system's behaviour.

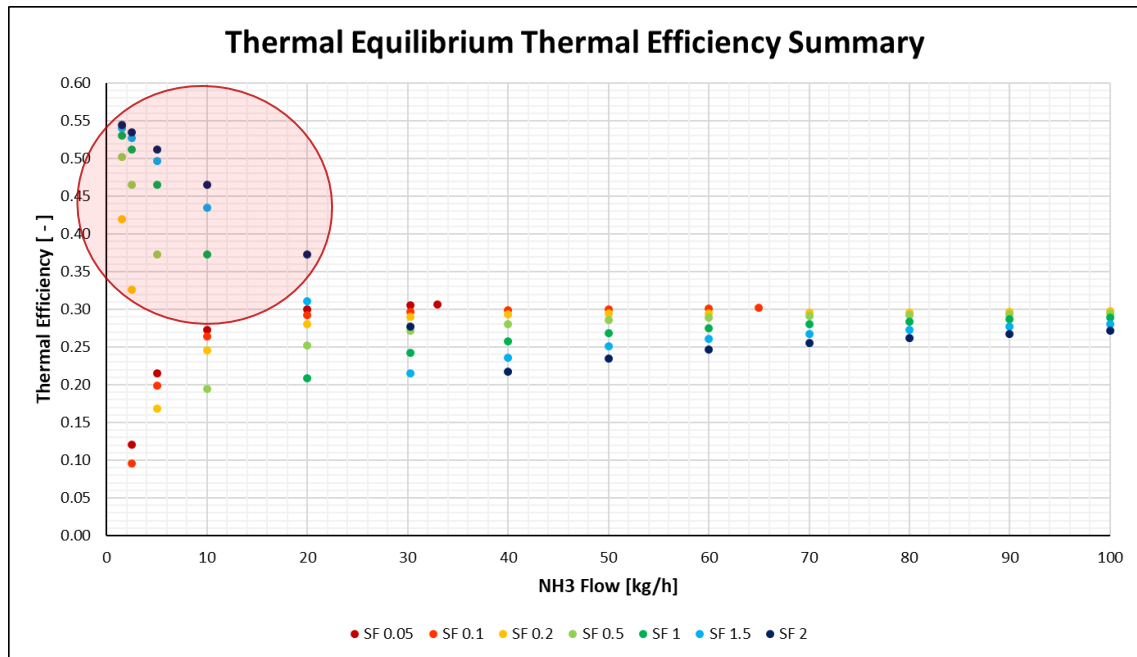


Figure 4.8. Thermal Efficiency summary for the Thermal Equilibrium condition.

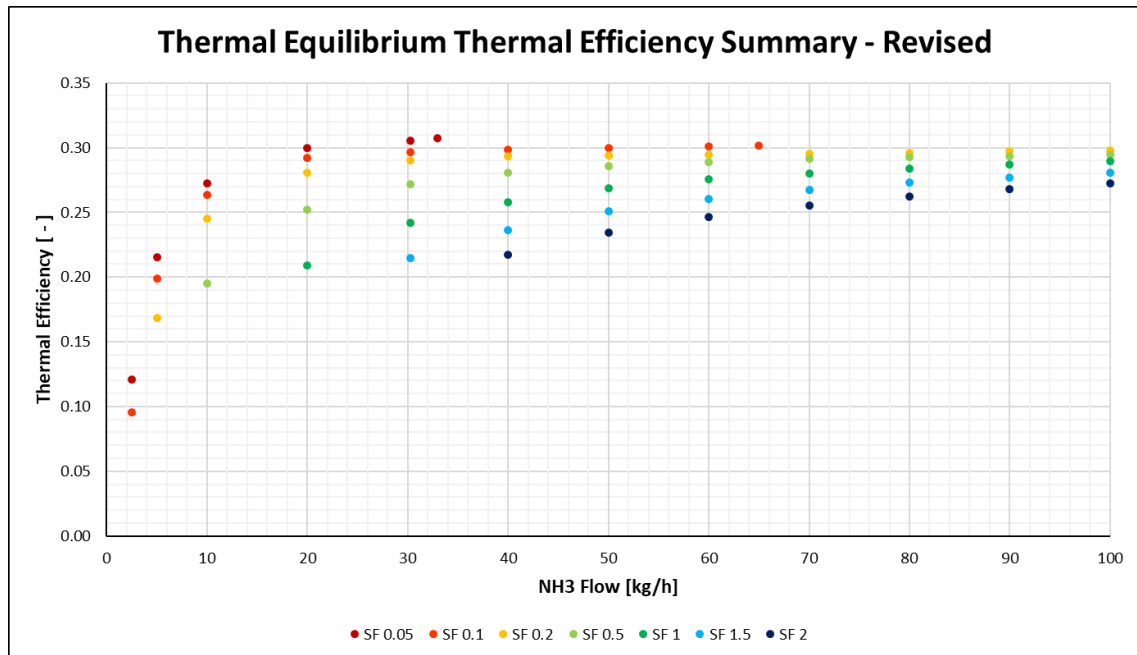


Figure 4.9. Revision of the Thermal Efficiency summary for the Thermal Equilibrium condition.

The second one is that, as it can be observed in Figure 4.9, smaller SFs show better efficiency values, but their maximum Ammonia flow rate is substantially lower compared to larger SFs and the operating temperature usually exceeds the upper limit of 900 °C, that is, 1173 K. Although this upper limit is as restrictive as the 400 °C one, next iterations of the CMR with different or enhanced materials could allow its operation at higher temperatures, and, therefore, giving meaning to the fact of giving greater importance to these points compared to those previously eliminated.

However, bigger SF not only exhibit poorer performance values but also fail to reach minimum operating temperature at low Ammonia flow rates, which could pose a challenge for system regulation once integrated into the HDFCV.

The reason smaller SFs naturally operate at higher temperatures is that, with larger SFs, the number of cells in the CMR increases, which results in a greater total surface area. The heat released is determined solely by the operating Ammonia flow rate, remaining constant as the SF varies. However, with a larger SF, the increased number of cells leads to a greater overall surface area. This increase in surface area enhances heat transfer to the environment through convection, resulting in greater thermal losses and, consequently, a lower operating temperature for the same flow rate.

This phenomenon is modelled through a “Convective Heat Transfer” block in the second layer of the model, visible in Figures 3.3 (Section 3.4) y 4.11 (Section 4.2.2).

Table 4.12 shows an excerpt of the results for the smallest SFs. The complete results for Thermal Equilibrium simulations can be found in Annex I.

Table 4.12. Excerpt of Thermal Equilibrium simulations results.

SF	NH3 Flow [kg/h]	T_op [K]	I_cell [A/cm2]	E_cell [V]	P_el [kW]	Ph_CMV [kW]	Q_HXN2 [kW]	Q_HXH2 [kW]	P H2 [kW]	P FCS [kW]	P net [kW]	Eff_thermal [-]	Eff_H2 [-]
0.05	2.5	752	0.2861	0.4948	5.78	3.63	0.15	0.80	14.7	7.4	1.6	0.121	0.783
	5	881	0.5722	0.3904	9.11	4.74	0.23	2.04	29.4	14.7	5.6	0.215	0.838
	10	1051	1.1444	0.3264	15.24	6.27	0.41	4.92	58.8	29.4	14.2	0.272	0.875
	20	1275	2.2889	0.2963	27.67	9.15	0.84	11.38	117.6	58.8	31.1	0.299	0.893
	30.3	1446	3.4676	0.2896	40.98	12.27	1.32	18.58	178.2	89.1	48.1	0.305	0.898
	33	1488	3.7766	0.2879	44.36	12.92	1.42	20.61	194.1	97.0	52.7	0.307	0.899
0.1	2.5	673	0.1438	0.5233	6.11	3.99	0.17	0.66	14.7	7.4	1.2	0.096	0.769
	5	776	0.2875	0.4082	9.53	5.22	0.20	1.62	29.4	14.7	5.2	0.199	0.828
	10	908	0.5750	0.3362	15.70	6.91	0.38	4.12	58.8	29.4	13.7	0.264	0.869
	20	1070	1.1501	0.3043	28.41	10.42	0.88	9.30	117.6	58.8	30.4	0.292	0.888
	30.3	1185	1.7424	0.2993	42.35	14.65	1.53	14.64	178.2	89.1	46.8	0.297	0.891
	40	1275	2.3001	0.2974	55.54	18.51	2.18	20.01	235.3	117.6	62.1	0.299	0.893
	50	1359	2.8752	0.2962	69.16	22.35	2.88	25.91	294.1	147.0	77.9	0.300	0.893
	60	1436	3.4502	0.2949	82.61	25.84	3.52	32.22	352.9	176.5	93.8	0.301	0.894
65	1473	3.7377	0.2938	89.17	27.37	3.78	35.58	382.3	191.2	102.0	0.302	0.895	
0.2	1.5	297	0.0432	0.1631	1.14	-0.13	0.00	0.00					
	2.5	319	0.0721	0.2665	3.11	0.99	0.01	0.04					
	5	690	0.1441	0.4427	10.33	6.08	0.28	1.37	29.4	14.7	4.4	0.168	0.809
	10	794	0.2882	0.3566	16.65	8.00	0.35	3.41	58.8	29.4	12.8	0.245	0.857
	20	919	0.5765	0.3170	29.60	12.00	0.84	7.65	117.6	58.8	29.2	0.281	0.881
	30.3	1005	0.8733	0.3069	43.41	16.41	1.47	10.82	178.2	89.1	45.7	0.290	0.887
	40	1071	1.1529	0.3035	56.68	20.70	2.13	16.14	235.3	117.6	61.0	0.293	0.889
	50	1129	1.4411	0.3022	70.56	25.21	2.85	20.60	294.1	147.0	76.5	0.294	0.890
	60	1180	1.7294	0.3014	84.45	29.63	3.53	25.23	352.9	176.5	92.0	0.295	0.890
	70	1228	2.0176	0.3008	98.31	33.93	4.18	30.10	411.7	205.9	107.6	0.295	0.891
	80	1273	2.3058	0.3000	112.08	38.05	4.81	35.27	470.5	235.3	123.2	0.296	0.891
	90	1316	2.5941	0.2992	125.75	41.98	5.42	40.72	529.4	264.7	138.9	0.297	0.892
100	1357	2.8823	0.2982	139.22	41.61	5.99	46.60	588.2	294.1	154.9	0.298	0.892	

4.2 Stage 2 – Operating points

4.2.1 Introduction

After exploring thermal equilibrium, it is necessary to ask whether operating outside of it is viable. That is, whether externally heating or cooling the CMR could improve the overall system efficiency. Figure 4.10 provides a simplified illustration of the three possible operating zones.

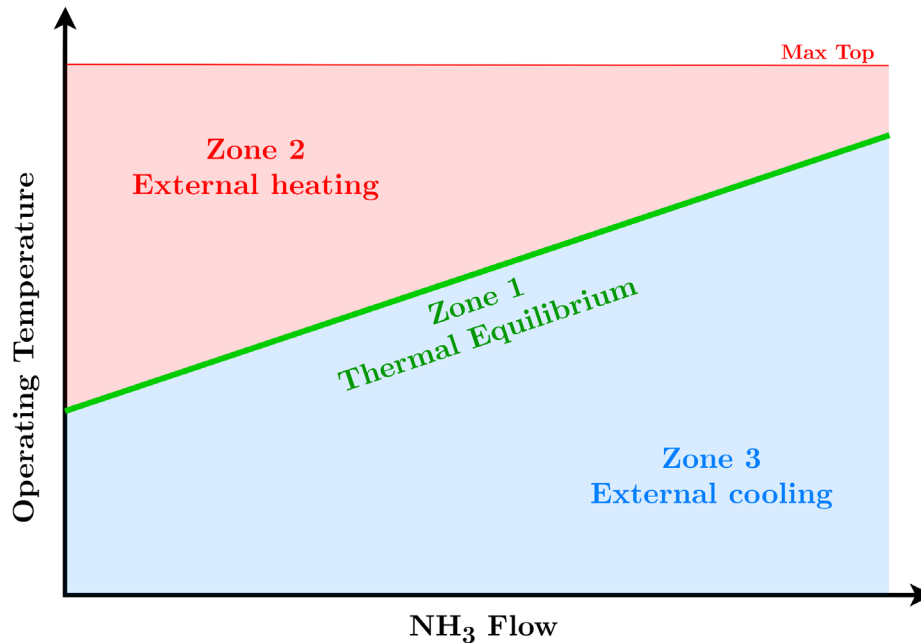


Figure 4.10. Operating zones.

The graph represents the Ammonia flow rate, but the x-axis could also be interpreted as the current density of each CMR cell, resulting in the same graph, as both parameters are directly proportional.

Each point will thus have a pair of [Flow, Temperature] coordinates that result from combining the following values:

- **Temperature range:** [673 775 900 1025 1150] K
- **Flow range:** [2.5 5 10 20 30.3 40 50 60 80 100] kg/h

4.2.2 Model modification

Throughout this section, the steps to modify the original model will be outlined to capture the system's response at all operating points. Specifically, how to ensure that the operating temperature remains fixed and equal to a setpoint temperature.

Auxiliary thermal source

The first step to being able to set the temperature at will is to add a thermal source capable of both heating and cooling the system. This new thermal source must work in conjunction with the thermal mass modelled in Layer 2. The method for implementing this in the model is shown in Figure 4.11.

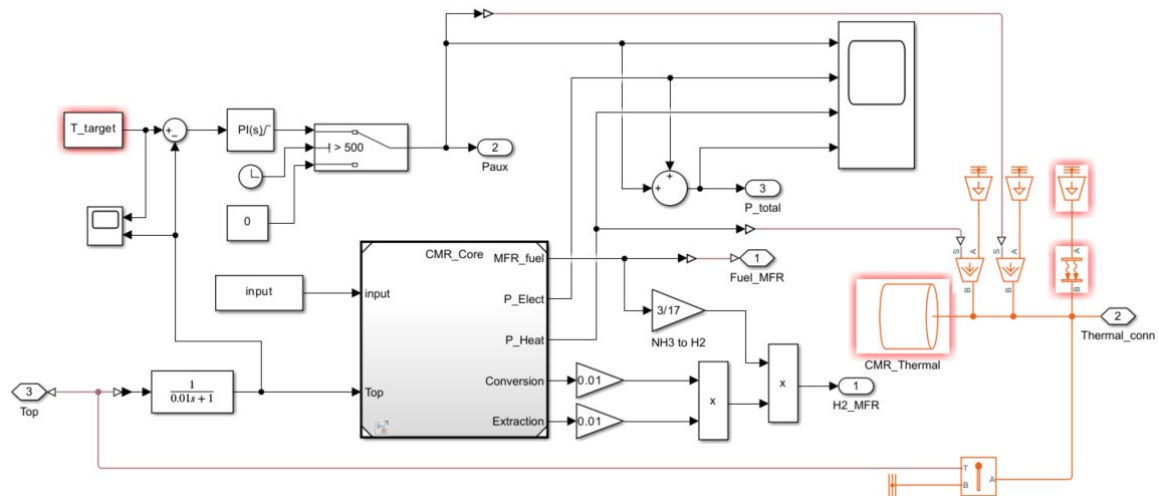


Figure 4.11. Auxiliary thermal source implementation in the model.

As can be observed, an additional “Heat Flow Rate Source” component is added and connected to the CMR_Thermal thermal mass.

PID implementation

This thermal source is controlled by a PID, which activates at the second 500 of the simulation to avoid initialization issues. Since the objective is to capture a "photo" of the final state, this delay has no undesirable consequences. The PID regulates the thermal power of the source, which is subsequently converted into heat flow through the combination of the “Temperature Source” and “Controlled Heat Flow Rate Source” blocks.

This is a closed-loop control system, and the input to the PID will be the difference between the target temperature, an input to this new version of the model, and the resulting temperature from the total thermal flow applied in the previous time step.

System identification

To properly control the system using the PID, the first step is to obtain the system’s transfer function, that is, its identification. This is done using MATLAB’s System Identification Toolbox, the main window of which is shown in Figure 4.12.

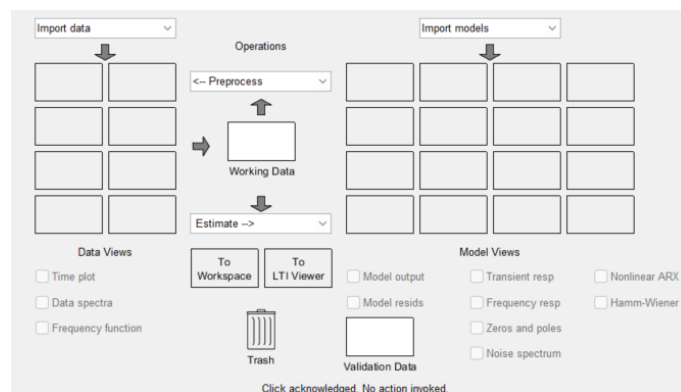


Figure 4.12. System Identification Toolbox main screen.

Before proceeding to the next step, it is necessary to obtain the typical data for this process. To achieve this, a step change in the flow rate will be simulated once the steady-state operating temperature of the first run is reached. In the "Import Data" tab, the "Time domain data..." option is selected, and the corresponding variables related to the model and simulation are entered, as shown in Figure 4.13.

Figure 4.13. System Identification Toolbox - Input of model variables

The input is the Ammonia flow rate, and the output is the operating temperature of the CMR.

Once this is set, the "Transfer Function Models..." option is selected, and after importing the data, the number of poles and zeros is chosen to calculate the transfer function. For this case, several options were tested, and the best fit was obtained with the following transfer function:

$$\frac{0.0833 s^2 + 2.77 \cdot 10^{-4} s + 2.78 \cdot 10^{-8}}{s^2 + 1.77 \cdot 10^{-4} s + 8.08 \cdot 10^{-9}}$$

Thus, it is a second-order system with two zeros and the TF provides a fit of 98.17%.

PID parameters

The next step is to tune the PID controller to properly control the system. MATLAB's PID Tuner tool is used for this purpose. Although this task can be done manually or using other utilities within MATLAB, given that the control specifications are fairly straightforward and do not require particularly robust or complex control, there is no need to resort to more advanced methods. The simplicity of PID Tuner is therefore an advantage.

The system must meet the following control specifications:

- Steady-state position error (ep) should be zero.
- No overshoot.

The process begins with a P controller, but it fails to achieve the specification of zero steady-state position error. Therefore, a PI controller is employed. In this case, as shown in Figure 4.14, both specifications are met.

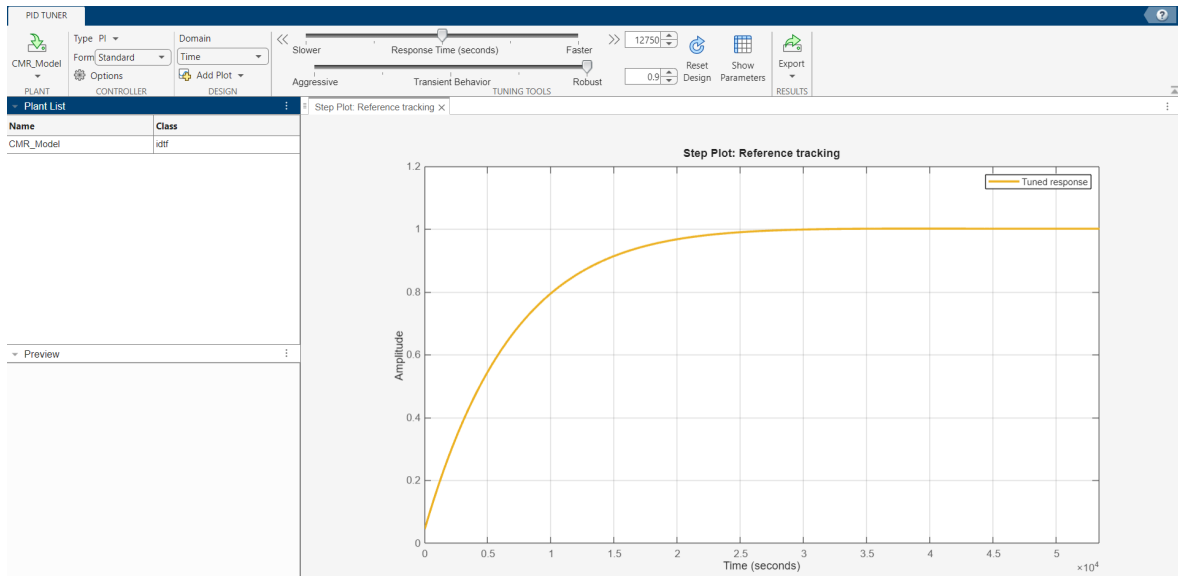


Figure 4.15. PID Tuner – Controller response.

The controller parameters are entered as shown in Figure 4.15.

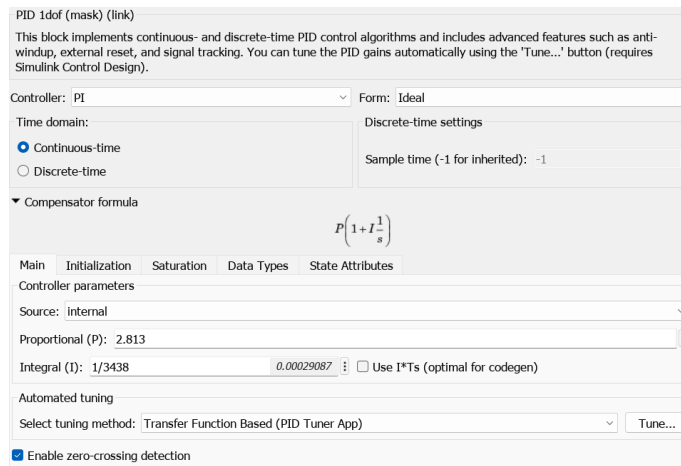


Figure 4.14. Controller parameters.

For operational reasons and based on the magnitude of the electrical power consumed by the CMR, a limitation has been set, restricting the maximum thermal power provided or extracted by this additional source to 100 kW. Consequently, the controller’s output is capped at this value. However, since the CMR exhibits slow thermal dynamics, it is necessary to activate the anti-windup option to prevent the accumulation of integral action and avoid undesirable control actions. The anti-windup method is set to clamping, as shown in Figure 4.16.



Figure 4.16. Anti-windup implementation.

As a final comment on the PI controller before moving on to the results of this section, it is worth noting that the system's transfer function is only used to initially tune a controller that can correctly set the operating temperature in each case. In this instance, the transfer function was derived solely for the reference SF, this is, SF1. However, it has been verified that the resulting controller functions properly across the entire range of SFs explored. Had this not been the case, a readjustment would have been required for those SFs that presented issues.

4.2.3 Results

Regarding the results of this section, the first point to mention is that Zone 3, external cooling, is completely ruled out. In many cases, more auxiliary power is required than what is generated by the FCS, resulting in a net negative power output. This means the system shifts from generating energy to consuming it, which clearly makes it unsuitable as a propulsion system. Besides the auxiliary power, which meaning is obvious and is a direct result obtained from simulations, an additional parameter has been introduced in this section.

Hydrogen Generation Specific Energy

Measured in kWh/kg, this parameter represents how much energy the CMR consumes to produce 1 kg of Hydrogen. It is calculated as follows:

$$E_{sp} = \frac{P_{Cons}}{F_{H_2}} = \frac{P_{El} + P_{Aux}}{F_{H_2}}$$

Table 4.13 presents an excerpt of the results, while the complete tables can be found in Annex II. As shown in the table, there are instances where the thermal power of the CMR is negative. This indicates that the CMR operates in an endothermic regime, absorbing heat instead of providing it. This behavior is entirely undesirable because the auxiliary thermal power source must supply more heat to compensate for the CMR operating outside the desired range, leading to a reduced overall system efficiency.

At first glance, the conclusions drawn from these results are quite similar to those from Section 4.1.7.

On one hand, smaller SFs, such as 0.05 and 1, have fewer operating points in Zone 2, as they heat up more easily and typically operate at higher equilibrium temperatures, around 1150 K, which is the upper operating limit of the CMR. For this reason, as shown in Tables II.1 and II.2 in Annex II, the temperature range was not refined further since preliminary simulations ruled them out.

On the other hand, while most SFs show endothermic operation points below thermal equilibrium, that is, in Zone 3 as defined earlier in this section and thus are disregarded, SF2 presents a unique situation. In this case, many points where the CMR operates endothermically also occur in Zone 2, as seen in Table II.9 of Annex II. For several NH3 flow rates, regardless of the operating temperature, the CMR never contributes heat, significantly limiting the operation of this SF in a real HDFCV. Consequently, the temperature range was not refined further for this case either.

Next, a scan will be made of the evolution of the most relevant parameter results for the different SF values.

Table 4.13. Stage 2 results summary for Scaling Factor 3.

SF	NH3 Flow [kg/h]	T_target [K]	I_cell [A/cm2]	E_cell [V]	P_el [kW]	Ph_CMV [kW]	Conversion [-]	Extraction [-]	P_total [kW]	P_aux [kW]	X_3 [-]	X_2 [-]	X_1 [-]	Q_HXN2 [kW]	Q_HXH2 [kW]	P_H2 [kW]	P_FCS [kW]	P_net [kW]	E_sp [kWh/kgH2]	Eff_thermal [-]	Eff_H2 [-]	
0.3	5	673	0.0962	0.3530	8.24	4.00	99.9000	99.0000	11.19	2.94	1.000	1.000	0.764	269.52	1231.74	29.41	14.70	3.52	12.68	0.135	0.791	
	5	775	0.0962	0.1441	3.36	-0.95	99.9003	99.0000	13.68	10.32	1.000	1.000	1.000	218.53	1673.52	29.41	14.70	1.02	15.51	0.039	0.741	
	5	900	0.0962	0.0676	1.58	-2.81	99.9000	99.0000	16.12	14.54	1.000	1.000	1.000	235.51	2105.57	29.41	14.70					
	5	1025	0.0962	0.0418	0.98	-3.49	99.9002	99.0000	18.48	17.50	1.000	1.000	1.000	252.94	2529.66	29.41	14.70					
	5	1150	0.0962	0.0314	0.73	-3.81	99.9001	99.0000	20.75	20.01	1.000	1.000	1.000	277.75	2830.38	29.41	14.70					
	10	673	0.1923	0.6981	32.60	24.10		99.9000	99.0000	15.98	-16.62	1.000	1.000	0.716	385.42	2413.53	58.82	29.41				
	10	775	0.1923	0.2789	13.02	4.40		99.9002	99.0000	18.31	5.28	1.000	1.000	0.986	353.24	3283.69	58.82	29.41	11.10	10.38	0.213	0.837
	10	900	0.1923	0.1246	5.82	-2.96		99.9002	99.0000	20.87	15.06	1.000	1.000	1.000	378.31	4073.86	58.82	29.41	8.53	11.83	0.164	0.807
	10	1025	0.1923	0.0715	3.34	-5.60		99.9000	99.0000	23.33	19.99	1.000	1.000	1.000	403.54	4772.71	58.82	29.41	6.08	13.22	0.117	0.781
	10	1150	0.1923	0.0493	2.30	-6.80		99.9001	99.0000	25.61	23.31	1.000	1.000	1.000	406.01	5479.77	58.82	29.41	3.80	14.51	0.073	0.758
	20	673	0.3830	1.3670	127.11	110.20		99.4706	98.9478	27.11	-100.00	1.000	0.919	0.674	826.03	4648.67	117.64	58.82				
	20	775	0.3846	0.5487	51.24	34.00		99.9001	99.0000	29.08	-22.16	1.000	1.000	0.883	1070.05	5962.88	117.64	58.82				
	20	900	0.3846	0.2385	22.27	4.71		99.9002	99.0000	31.80	9.53	1.000	1.000	1.000	840.20	7441.42	117.64	58.82	27.01	9.01	0.260	0.866
	20	1025	0.3846	0.1308	12.22	-5.66		99.9002	99.0000	34.31	22.09	1.000	1.000	1.000	874.95	8789.04	117.64	58.82	24.51	9.72	0.236	0.851
	20	1150	0.3846	0.0849	7.93	-10.27		99.9001	99.0000	36.66	28.74	1.000	1.000	1.000	882.54	10087.59	117.64	58.82	22.15	10.39	0.213	0.836
	30.3	673	0.5827	0.9908	140.18	114.15		99.9000	99.0000	40.18	-100.00	1.000	0.991	0.739	1676.23	7759.13	178.22	89.11				
	30.3	775	0.5827	0.8266	116.94	90.82		99.9000	99.0000	40.62	-76.32	1.000	1.000	0.781	1823.10	8158.78	178.22	89.11				
	30.3	900	0.5827	0.3558	50.34	23.73		99.9003	99.0000	43.83	-6.50	1.000	1.000	1.000	1411.18	10393.90	178.22	89.11				
	30.3	1025	0.5827	0.1920	27.16	0.08		99.9002	99.0000	46.81	19.65	1.000	1.000	1.000	1493.97	12237.77	178.22	89.11	42.30	8.75	0.268	0.872
	30.3	1150	0.5827	0.1216	17.20	-10.36		99.9000	99.0000	49.45	32.25	1.000	1.000	1.000	1545.14	14100.66	178.22	89.11	39.66	9.25	0.252	0.861
	40	673	0.7692	0.8175	152.68	118.00		99.9001	99.0000	52.68	-100.00	1.000	1.000	0.780	2587.09	10843.29	235.27	117.64				
	40	775	0.7692	0.8175	152.68	118.00		99.9001	99.0000	52.68	-100.00	1.000	1.000	0.780	2587.09	10843.29	235.27	117.64				
	40	900	0.7692	0.4663	87.09	51.97		99.9001	99.0000	55.26	-31.82	1.000	1.000	0.947	2220.54	12821.83	235.27	117.64				
	40	1025	0.7692	0.2495	46.61	10.85		99.9000	99.0000	58.75	12.14	1.000	1.000	1.000	2102.69	15276.86	235.27	117.64	58.88	8.32	0.283	0.882
	40	1150	0.7692	0.1561	29.16	-7.23		99.9001	99.0000	61.73	32.57	1.000	1.000	1.000	2199.66	17598.51	235.27	117.64	55.91	8.75	0.269	0.872
	50	673	0.9616	0.7106	165.90	122.21		99.9000	99.0000	65.90	-100.00	1.000	1.000	0.819	3246.79	14217.63	294.09	147.04				
	50	775	0.9616	0.7106	165.90	122.21		99.9000	99.0000	65.90	-100.00	1.000	1.000	0.819	3246.79	14217.63	294.09	147.04				
	50	900	0.9616	0.5802	135.45	91.55		99.9000	99.0000	67.03	-68.42	1.000	1.000	0.883	3117.98	15124.20	294.09	147.04				
	50	1025	0.9616	0.3089	72.11	27.42		99.9001	99.0000	71.16	-0.96	1.000	1.000	1.000	2734.51	18249.81	294.09	147.04				
	50	1150	0.9616	0.1918	44.77	-0.71		99.9001	99.0000	74.55	29.78	1.000	1.000	1.000	2894.90	21060.22	294.09	147.04	72.49	8.45	0.279	0.879
	60	673	1.1539	0.6402	179.36	126.58		99.9003	99.0000	79.36	-100.00	1.000	1.000	0.855	3837.23	17724.30	352.91	176.45				
	60	775	1.1539	0.6402	179.36	126.58		99.9003	99.0000	79.36	-100.00	1.000	1.000	0.855	3837.23	17724.30	352.91	176.45				
	60	900	1.1539	0.6402	179.36	126.58		99.9003	99.0000	79.36	-100.00	1.000	1.000	0.855	3837.23	17724.30	352.91	176.45				
	60	1025	1.1539	0.3682	103.16	49.53		99.9002	99.0000	83.51	-19.65	1.000	1.000	1.000	3310.18	21063.27	352.91	176.45				
	60	1150	1.1539	0.2274	63.71	9.13		99.9001	99.0000	87.33	23.62	1.000	1.000	1.000	3514.37	24385.97	352.91	176.45	89.12	8.25	0.286	0.884
	80	673	1.5385	0.5537	206.84	135.62		99.9001	99.0000	106.84	-100.00	1.000	1.000	0.934	4841.40	25261.90	470.54	235.27				
	80	775	1.5385	0.5537	206.84	135.62		99.9001	99.0000	106.84	-100.00	1.000	1.000	0.934	4841.40	25261.90	470.54	235.27				
	80	900	1.5385	0.5537	206.84	135.62		99.9001	99.0000	106.84	-100.00	1.000	1.000	0.934	4841.40	25261.90	470.54	235.27				
	80	1025	1.5385	0.4869	181.89	110.38		99.9000	99.0000	108.13	-73.76	1.000	1.000	0.990	4573.28	26385.52	470.54	235.27				
	80	1150	1.5385	0.2987	111.57	38.79		99.9001	99.0000	112.81	1.24	1.000	1.000	1.000	4673.89	30855.22	470.54	235.27	122.46	7.99	0.294	0.890
100	673	1.9231	0.5028	234.76	144.82		99.9001	99.0000	134.76	-100.00	1.000	1.000	1.000	5652.97	33614.62	588.18	294.09					
100	775	1.9231	0.5028	234.76	144.82		99.9001	99.0000	134.76	-100.00	1.000	1.000	1.000	5652.97	33614.62	588.18	294.09					
100	900	1.9231	0.5028	234.76	144.82		99.9001	99.0000	134.76	-100.00	1.000	1.000	1.000	5652.97	33614.62	588.18	294.09					
100	1025	1.9231	0.5028	234.76	144.82		99.9001	99.0000	134.76	-100.00	1.000	1.000	1.000	5652.97	33614.62	588.18	294.09					
100	1150	1.9231	0.3699	172.73	81.76		99.9001	99.0000	138.11	-34.62	1.000	1.000	1.000	5791.75	37320.60	588.18	294.09					

Electric Power

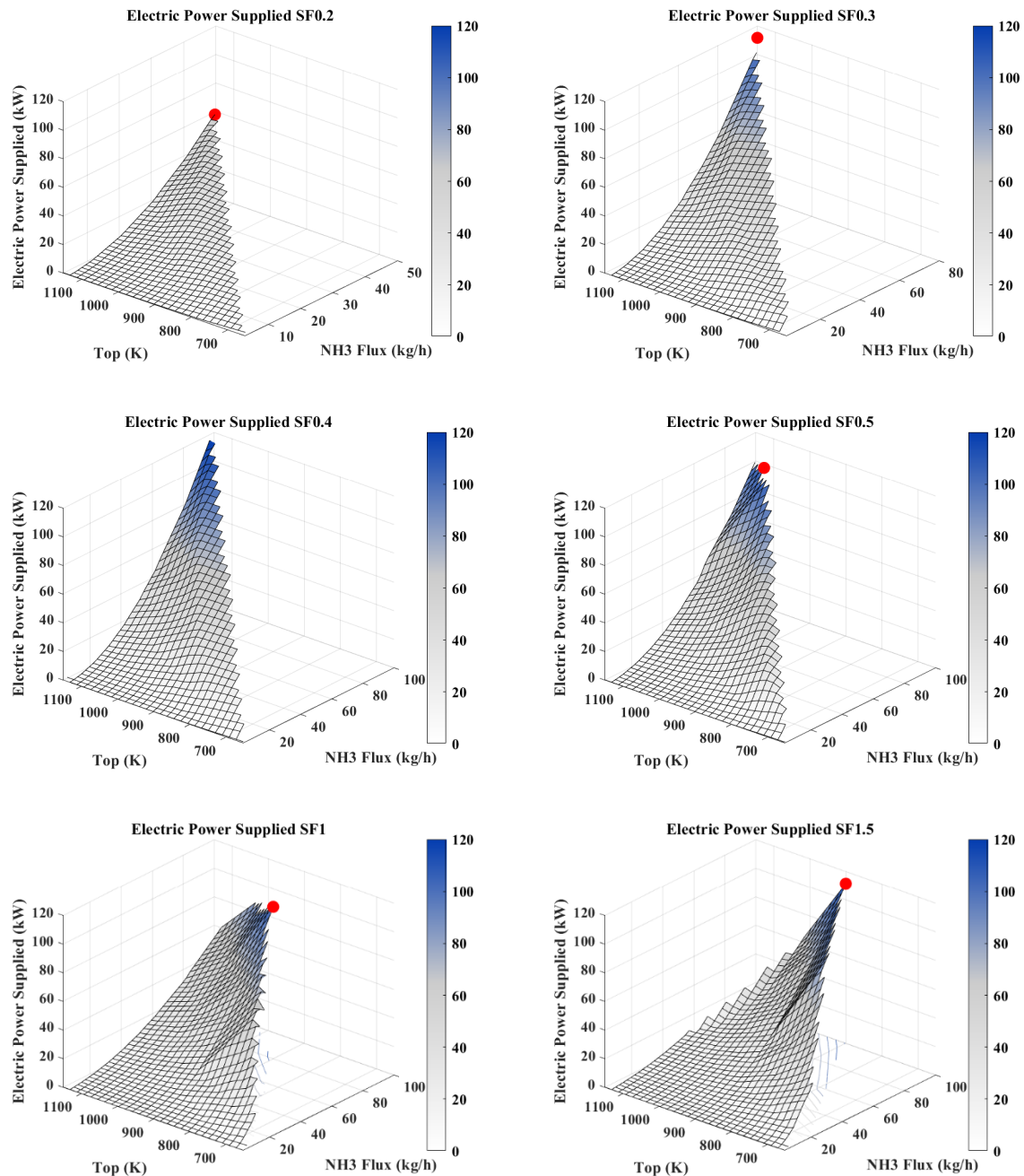


Figure 4.17. Stage 2 - Electric power summary.

Regarding the electrical power consumed by the CMR, as shown in Figure 4.17, two conclusions can be drawn, which are also supported by the results from Stage 1.

The first and most expected conclusion is that the main factor determining the electrical power consumption is the Ammonia flow rate. The higher the flow rate, the greater the consumption.

The second, more subtle conclusion is that electrical power consumption increases slightly as the SF increases. Although this nuance is difficult to distinguish in the graphs, it can be observed more clearly in Annexes I and II.

Auxiliary Power

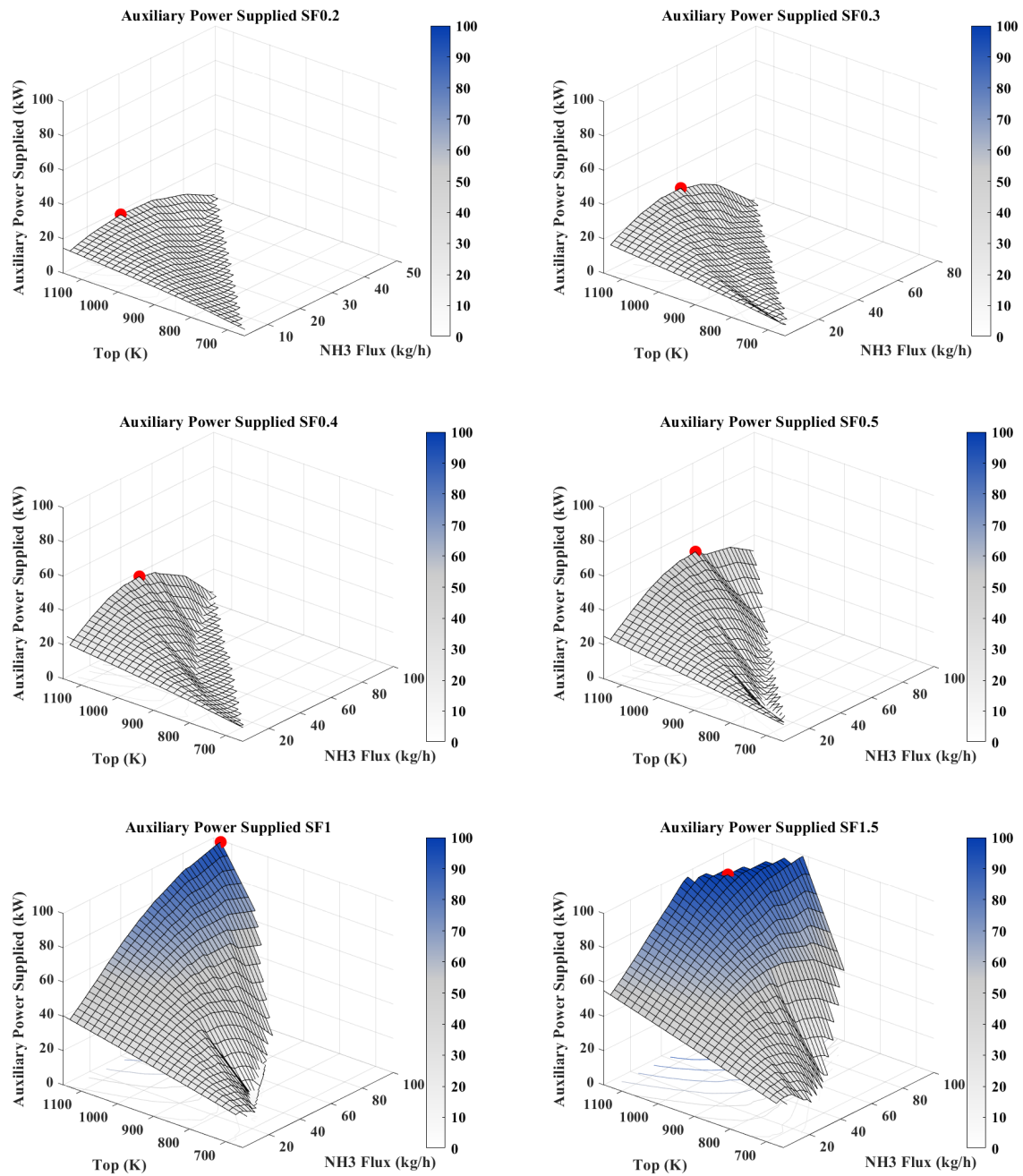


Figure 4.18. Stage 2 - Auxiliary Power summary.

As shown in Figure 4.18, the auxiliary power supplied by the additional thermal source increases with SF, and the peak shifts to higher Ammonia flow rates as SF increases.

The first phenomenon is due to smaller SFs operating at higher equilibrium temperatures, requiring less external heat to reach the target temperatures.

The second phenomenon is less significant, as most of the points driving it involve the CMR operating in an endothermic regime, which are not desirable operating conditions.

Total Consumed Power

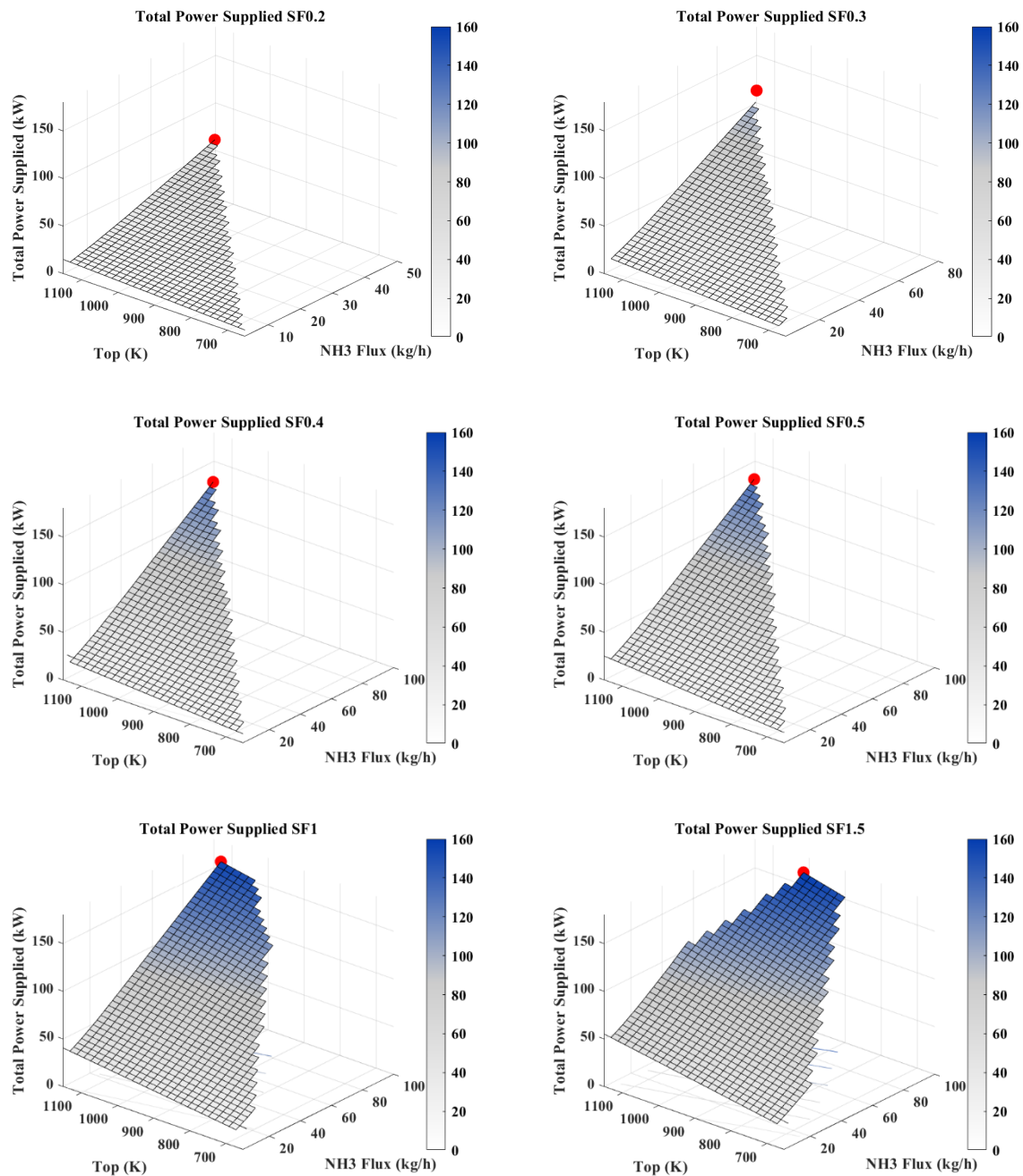


Figure 4.19. Stage 2 - Total Power Supplied summary.

The results for total power consumption are quite predictable: for all SFs, they evolve linearly up to the maximum NH₃ flow rate and the maximum operating temperature, as shown in Figure 4.19.

In the case of SF1.5, the 100 kW from the thermal source is not sufficient to reach all temperature values within the range, which is why the graph takes on a different shape. This SF will be discarded onwards for this reason.

Again, it is evident that smaller SFs operate at higher equilibrium temperatures, requiring less total power under the same operating conditions.

Net Power

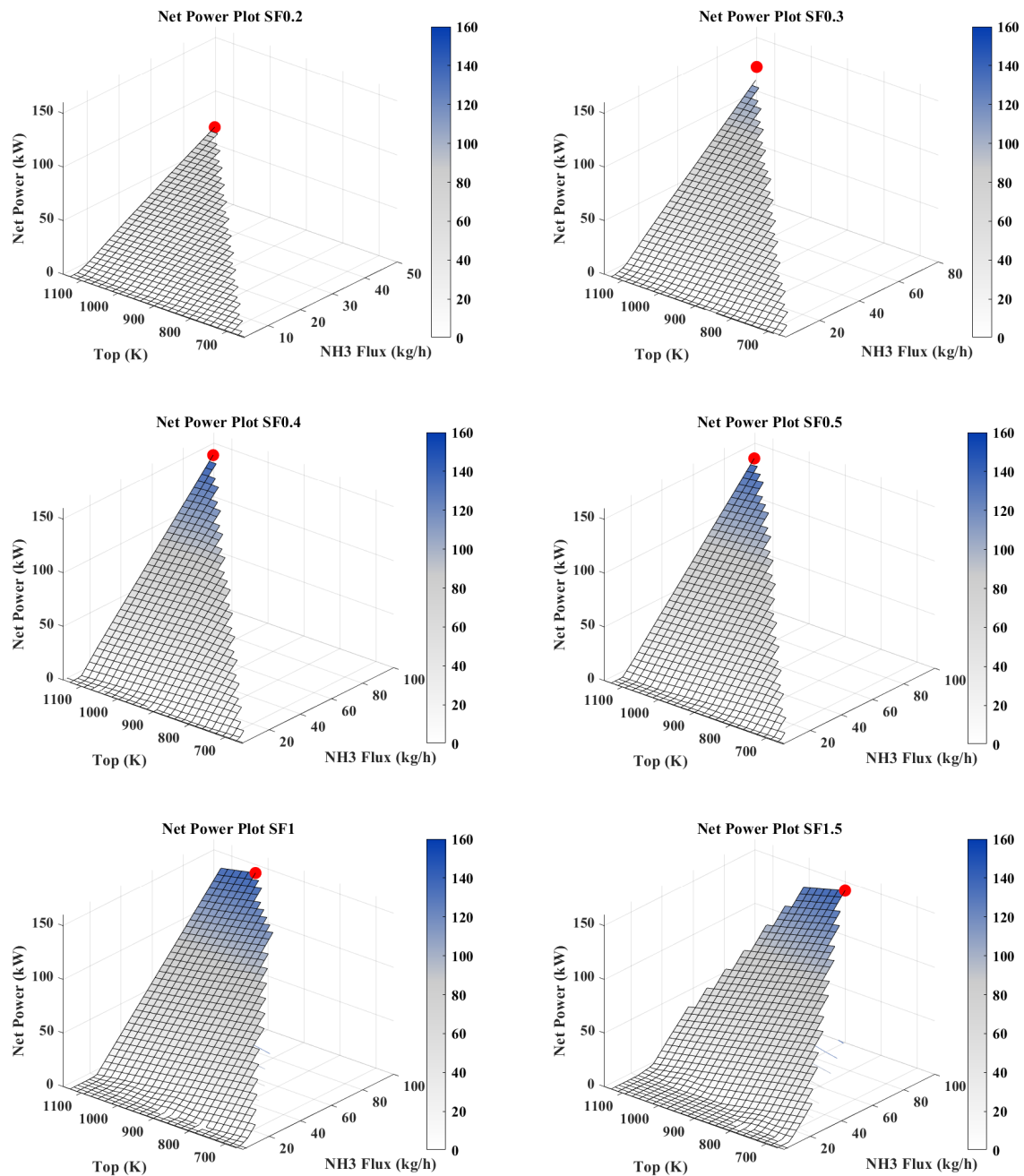


Figure 4.20. Stage 2 - Net power summary.

Figure 4.20 presents the results for Net Power. For all SFs, the highest Net Power is achieved at the maximum flow rate and near thermal equilibrium.

Another relation that can be inferred from these results is that, in general, a larger SF allows the CMR to provide higher Net Power. Therefore, as will be discussed in Stage 4, the power requirement of the FCS is a key factor when selecting an SF.

This, combined with the results from Figure 4.19, suggests the area where optimal thermal efficiency is expected to be obtained. This will be further detailed in the following analysis.

Thermal Efficiency

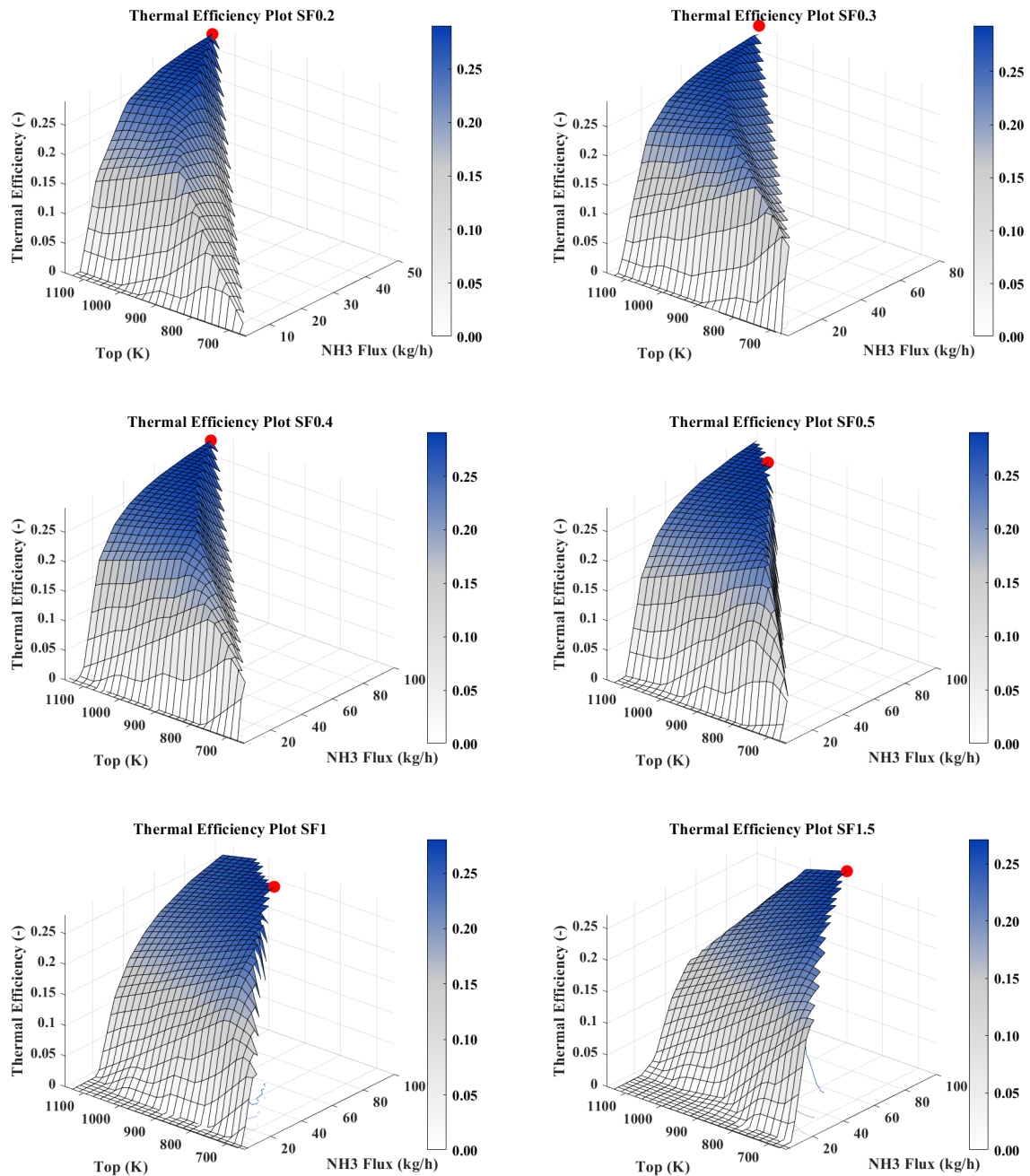


Figure 4.21. Stage 2 - Thermal Efficiency summary.

In Figure 4.21, a phenomenon similar to that observed in Figure 4.9 (Thermal Equilibrium Thermal Efficiency Summary – Revised) can be seen. Thermal efficiency approaches 30% asymptotically in all cases. However, for smaller SFs, there is a larger range where this occurs, whereas for larger SFs, it only happens at higher Ammonia flow rates.

Another key point is that the highest efficiency is achieved at the highest NH3 flow rates and at temperatures closest to equilibrium. Combining the efficiency results from Stage 1 and Stage 2, although it cannot be definitively stated that the best operating condition is thermal equilibrium, it does appear that the optimal zone is near it.

4.3 Stage 3 – Heat Exchangers

Heat exchangers are a fundamental part of the system, and their design is an aspect that cannot be neglected. Section 2.3 compiled the most important concepts to consider throughout this stage.

4.3.1 Introduction

The system includes three heat exchangers:

- **HXH2:** This is a shell-and-tube heat exchanger and the first in the circuit. The cold fluid is Ammonia, which flows through the tubes, initially in a liquid phase, while Hydrogen circulates through the shell as the hot fluid. Latent heat predominates in this heat exchanger, where most of the Ammonia evaporation occurs.
- **HXN2:** Another shell-and-tube heat exchanger and the second in the circuit. Ammonia is again the cold fluid, flowing through the tubes, but in this case, it enters in a two-phase or even gas-only state. Nitrogen serves as the hot fluid, circulating through the shell. In this exchanger, sensible heat predominates, although in some cases, there is also a portion of latent heat.
- **Hydrogen-Air HX:** A compact finned-tube heat exchanger for automotive applications. This exchanger has not been included in this first model as it does not interact with Ammonia. Its purpose is to cool the Hydrogen exiting the HXH2 to 60 °C before it reaches the intermediate tank and, from there, feeds into the FCS.

4.3.2 Commercial models – the need of a custom solution

The first two heat exchangers present certain challenges that make it difficult to find commercial models capable of ensuring safe and efficient operation:

- In both, one of the fluids is Ammonia, which means that heat exchangers with rubber gaskets or other materials sensitive to corrosion cannot be used. It is recommended that all components be made of stainless steel or materials with similar properties.
- The inlet temperature of the Nitrogen and Hydrogen in the exchangers is very high, often exceeding 650°C. Commercial models generally cannot withstand these operating conditions.

This combination of characteristics rules out the possibility of using a plate heat exchanger, which is usually the most compact and convenient option for low-power applications. However, no shell-and-tube exchanger models were found in commercial catalogs that meet the operational requirements. For this reason, a custom solution for these heat exchangers is necessary.

The design is based on the Wrema Type M model from FUNKE [1], which is the closest commercial exchanger to meeting the operational needs. Figure 4.22 shows a schematic of the design. As seen, it is a single-pass shell-and-tube heat exchanger. Adding bends and other components to increase the number of passes makes the system more fragile, as there are more delicate elements exposed to high thermal stresses, and more expensive, due to the need for higher-quality materials and machining. The exchangers are designed for countercurrent flow to enhance heat transfer. The total length of the exchanger is 1 meter.

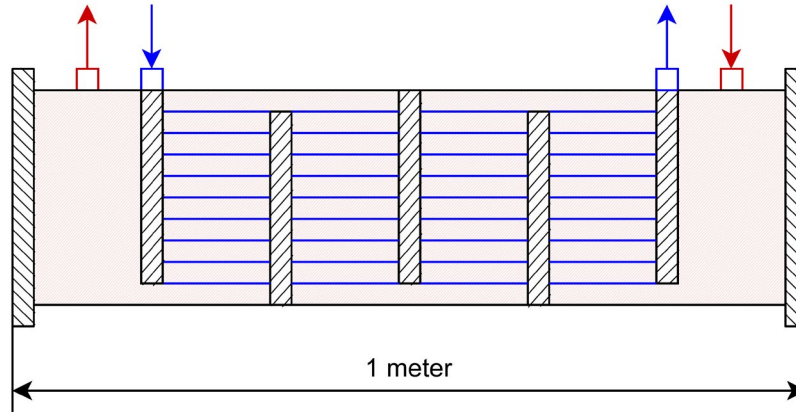


Figure 4.22. Sketch of the preliminary design of the main heat exchangers.

For the tubes and the shell, the Swagelok catalog [2] was used. Table 4.14 shows the two most relevant models for the calculations described in the following sections.

Table 4.14. Relevant tubes data for the heat exchangers design.

MODEL	O_{ext} [mm]	Tube Wall [mm]	O_{int} [mm]	Weight [kg/m]	Working Pressure [bar]
SS-T3M-S-0,5M-6ME	3	0.5	2	0.021	330
SS-T18M-S-1,0M-6ME	18	1	16	0.425	120

4.3.3 Sizing methodology

This section discusses the method used to size the HXH2 y HXN2 heat exchangers. The first step in sizing any heat exchanger is to divide it into two fictitious exchangers, one for latent heat and the other for sensible heat. By summing the surface areas of both, the total area required for the real heat exchanger is obtained. For most sizing methods, the focus is primarily on sensible heat.

$\text{N}_2 - \text{NH}_3$ Heat Exchanger

The first heat exchanger to be sized is the HXN2. The reason for this is that, as shown in Table 4.13 from Section 4.2.3 and Tables II.1 to II.9 from Annex II, the fluid combination in this exchanger almost always involves Gas \Leftrightarrow Gas, thus there is no phase change, which means that all the heat can be considered as sensible heat. This significantly simplifies the calculation process and the considerations regarding the overall heat transfer coefficient.

Table 4.15 shows the temperatures for SF0.3. The rest of the results for this heat exchanger can be found in Annex III, Section III.1.

To determine the necessary heat exchange area, the results obtained through two different methods will be compared. One of the most widely used methods for sizing heat exchangers is through the LMTD (Logarithmic Mean Temperature Difference) method. This parameter is calculated as follows:

$$LMTD = \frac{\Delta T_0 - \Delta T_L}{\ln(\Delta T_0 / \Delta T_L)}$$

Table 4.15. HXN2 temperature summary for SF0.3.

SF	Flow [kg/h]	T_target [K]	X_3 [-]	X_2 [-]	X_1 [-]	Q_HXN2 [kW]	T_NH3in [K]	T_NH3out [K]	T_N2in [K]	T_N2out [K]	$\Delta T1_{N2}$ [K]	$\Delta T2_{N2}$ [K]	LMTD_N2 [K]
0.3	2.5	673	1.000	1.000	0.822	179.90	298.64	438.28	562.38	316.26			
	2.5	775	1.000	1.000	1.000	152.78	312.11	555.88	680.52	475.46			
	2.5	900	1.000	1.000	1.000	176.98	413.58	664.54	797.79	565.15			
	2.5	1025	1.000	1.000	1.000	201.25	516.86	754.83	912.28	653.40			
	2.5	1150	1.000	1.000	1.000	235.66	590.50	818.85	1023.33	725.84			
	5	673	1.000	1.000	0.764	269.52	299.09	381.85	499.64	314.64	15.55	117.79	50.49
	5	775	1.000	1.000	1.000	218.53	307.58	511.12	613.51	465.79	158.21	102.39	128.29
	5	900	1.000	1.000	1.000	235.51	419.10	629.00	721.55	565.48			
	5	1025	1.000	1.000	1.000	252.94	525.90	724.92	821.34	657.12			
	5	1150	1.000	1.000	1.000	277.75	607.12	794.54	911.82	734.71			
	10	673	1.000	1.000	0.716	385.42	300.57	305.63	452.94	320.44			
	10	775	1.000	1.000	0.986	353.24	301.37	424.82	558.14	437.94	136.56	133.32	134.93
	10	900	1.000	1.000	1.000	378.31	402.42	550.57	671.58	545.32	142.89	121.01	131.65
	10	1025	1.000	1.000	1.000	403.54	502.60	650.25	766.60	634.51	131.91	116.36	123.97
	10	1150	1.000	1.000	1.000	406.01	597.53	733.64	847.48	716.90	119.37	113.84	116.58
	20	673	1.000	0.919	0.674	826.03	305.32	298.45	492.03	350.40			
	20	775	1.000	1.000	0.883	1070.05	307.20	367.67	587.01	405.00			
	20	900	1.000	1.000	1.000	840.20	354.57	463.10	682.56	542.47	187.90	219.46	203.28
	20	1025	1.000	1.000	1.000	874.95	450.69	561.17	769.76	626.48	175.79	208.60	191.73
	20	1150	1.000	1.000	1.000	882.54	541.55	646.03	843.60	701.39	159.83	197.57	178.04
	30.3	673	1.000	0.991	0.739	1676.23	312.71	298.45	580.16	391.71			
	30.3	775	1.000	1.000	0.781	1823.10	313.28	316.81	601.66	397.13			
	30.3	900	1.000	1.000	1.000	1411.18	324.01	405.42	701.18	546.23			
	30.3	1025	1.000	1.000	1.000	1493.97	403.58	499.66	791.30	630.27	226.68	291.64	257.80
	30.3	1150	1.000	1.000	1.000	1545.14	490.12	586.78	866.91	703.00	212.89	280.14	244.98
	40	673	1.000	1.000	0.780	2587.09	320.03	316.41	646.92	428.37			
	40	775	1.000	1.000	0.780	2587.09	320.03	316.41	646.92	428.37			
	40	900	1.000	1.000	0.947	2220.54	322.99	374.20	717.77	533.17			
	40	1025	1.000	1.000	1.000	2102.69	378.57	461.60	808.86	637.63	259.06	347.27	301.01
	40	1150	1.000	1.000	1.000	2199.66	458.10	547.49	885.34	709.04	250.94	337.84	292.24
	50	673	1.000	1.000	0.819	3246.79	327.48	329.60	694.09	476.51			
	50	775	1.000	1.000	0.819	3246.79	327.48	329.60	694.09	476.51			
	50	900	1.000	1.000	0.883	3117.98	328.81	351.69	722.89	515.28			
	50	1025	1.000	1.000	1.000	2734.51	363.11	433.34	820.75	642.94			
	50	1150	1.000	1.000	1.000	2894.90	436.39	519.20	902.94	717.84	281.46	383.74	329.96
	60	673	1.000	1.000	0.855	3837.23	334.44	340.55	731.29	518.64			
	60	775	1.000	1.000	0.855	3837.23	334.44	340.55	731.29	518.64			
	60	900	1.000	1.000	0.855	3837.23	334.44	340.55	731.29	518.64			
	60	1025	1.000	1.000	1.000	3310.18	353.70	409.61	819.20	639.73			
	60	1150	1.000	1.000	1.000	3514.37	421.17	495.52	905.80	718.62	297.45	410.28	350.85
80	673	1.000	1.000	0.934	4841.40	346.99	361.50	791.53	593.09				
80	775	1.000	1.000	0.934	4841.40	346.99	361.50	791.53	593.09				
80	900	1.000	1.000	0.934	4841.40	346.99	361.50	791.53	593.09				
80	1025	1.000	1.000	0.990	4573.28	348.15	377.24	813.07	626.73				
80	1150	1.000	1.000	1.000	4673.89	404.82	461.54	902.52	715.69	310.87	440.98	372.14	
100	673	1.000	1.000	1.000	5652.97	363.59	384.03	840.55	657.43				
100	775	1.000	1.000	1.000	5652.97	363.59	384.03	840.55	657.43				
100	900	1.000	1.000	1.000	5652.97	363.59	384.03	840.55	657.43				
100	1025	1.000	1.000	1.000	5652.97	363.59	384.03	840.55	657.43				
100	1150	1.000	1.000	1.000	5791.75	400.24	440.88	899.00	713.68				

Where ΔT_0 and ΔT_L are shown in Figure 4.23:

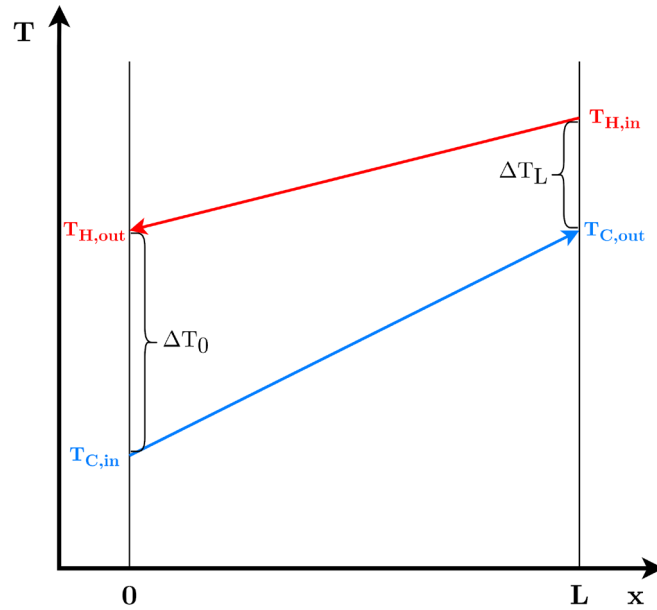


Figure 4.23. T-Q diagram to represent ΔT_0 and ΔT_L .

Once the LMTD is calculated, the heat exchanged, expressed in W, is obtained as:

$$\dot{Q} = UA \cdot LMTD$$

Where U is the overall heat transfer coefficient, measured in W/m^2K , and A is the heat exchange surface area in m^2 . This method provides different values of UA , and by estimating U based on the operating conditions, the area can be determined, allowing for the calculation of the number of tubes needed.

The other method involves using the fundamentals of heat transfer to obtain the UA value through the thermal resistance method. Following this approach, UA can be calculated using the following equation [3]:

$$UA = \frac{1}{\sum R_i} = \frac{1}{R_{internal\ convection} + R_{conduction} + R_{external\ convection}}$$

Since these are shell and tube heat exchangers, the control volume for applying this equation is one of the tubes, and the equations for thermal resistances in cylinders are applied.

The first thermal resistance to address is the internal convection resistance. Given that this is forced convection due to the velocity of the fluid, it can be obtained as follows [3]:

$$R_{conv,int} = \frac{1}{2\pi \cdot L \cdot r_{int} \cdot h_{int}}$$

Where L is the tube length (1 m), r_{int} is the internal radius of the tube (1 mm) and h_{int} is the internal convection coefficient. To obtain this coefficient, the following procedure is followed:

The first step is to calculate the average temperature of the fluid circulating inside the tubes, in this case, Ammonia, between the inlet and outlet of the heat exchanger:

$$T_{m,NH3} = \frac{T_{in,NH3} + T_{out,NH3}}{2}$$

Using this temperature, the following properties are obtained from the complete Table 4.6 in Section 4.1.1:

- Conductivity (k)
- Dynamic viscosity (μ)
- Prandtl number (Pr)

The next step is to calculate the Reynolds number (Re), which can be obtained using the following equation:

$$Re_D = \frac{4\dot{m}}{\pi\phi\mu}$$

The subscript D indicates that the magnitude is measured at a distance D from the wall, outside the boundary layer, where the flow is fully developed.

Once the Reynolds and Prandtl numbers are known, the Nusselt number (Nu) can be determined using the Dittus-Boelter correlation [3]:

$$Nu_D = 0.023Re_D^{0.8}Pr^{0.4}$$

The exponent of the Prandtl number is 0.4 because the NH_3 is being heated. It is important to note that this correlation is only valid if:

- $0.7 \leq Pr \leq 16700$
- $Re \geq 10000$
- $L/D \geq 10$

As shown in Table 4.16 of this section and in Tables III.5 to III.8 of Annex III, all these conditions are met.

Finally, based on the definition of the Nusselt number [3], the internal convection coefficient is obtained as:

$$Nu_D = \frac{h\phi}{k}$$

The second thermal resistance to calculate is conduction, which is the simplest to determine and is obtained as follows [3]:

$$R_{cond} = \frac{\ln(r_{ext}/r_{int})}{2\pi \cdot k \cdot L} = \frac{\ln(1.5/1)}{2\pi \cdot 16 \cdot 1} = 0.004 \text{ K/W}$$

Where L is the tube length (1 m), r_{ext} is the external radius of the tube (1.5 mm), r_{int} is the internal radius of the tube (1 mm) and k is the conduction coefficient of the steel (16 W/mK) [3].

The third and final thermal resistance is that corresponding to external convection. In this case, forced convection is also considered, as the outer shell of the heat exchanger has been designed to facilitate this phenomenon, thus improving heat transfer. This resistance is calculated as follows [3]:

$$R_{conv,ext} = \frac{1}{2\pi \cdot L \cdot r_{ext} \cdot h_{ext}}$$

Where L is the tube length (1 m), r_{ext} is the external radius of the tube (1.5 mm) and h_{ext} is the external convection coefficient. To obtain this coefficient, the following procedure is followed.

First, the density of N_2 is calculated at the average temperature between the inlet and outlet:

$$T_{m,N_2} = \frac{T_{in,N_2} + T_{out,N_2}}{2}$$

Next, a series of initial estimates are made regarding the following data:

- **Inner and outer diameters of the heat exchanger shell.** An inner diameter of 16 mm is estimated for the shell. With a thickness of 1 mm, resulting in an outer diameter of 18 mm, this is sufficient to meet the pressure and temperature requirements of operation [3].
- **Initial number of tubes.** It is estimated that there are initially 10 tubes.

Depending on the discrepancy between the initial estimates and the final results, the relevance of external convection for calculating UA, and the difference between this and the coefficient obtained through the LMTD method, additional iterations may or may not be necessary.

These estimates are necessary to calculate the free cross-sectional area within the heat exchanger, given by:

$$S = \frac{\pi}{4} (\phi_{int,shell}^2 - 10 \cdot \phi_{tubes}^2)$$

From this section, the velocity of N_2 is calculated using the following equation:

$$v_{N_2} = \frac{\dot{m}_{N_2}}{\rho \cdot S}$$

This velocity corresponds to the fully developed flow, equivalent to u_∞ . Using this value, and assuming that Nitrogen behaves similarly to air, the external convection coefficient can be calculated as follows [3]:

$$h_{ext} = 2.38 \cdot u_\infty^{0.89}$$

With this, the UA values from both methods are obtained. It is observed that the LMTD method yields higher values, so, as it represents the most conservative scenario, this value will be selected for sizing the heat exchanger.

The final step is to determine the heat transfer area. To do this, the value of U must be estimated, typically ranging from 100 to 1500 W/m²K [3,4]. Using this value and the area of each tube calculated in the previous section, the number of tubes can be determined. An extract of the results for this heat exchanger is shown in Tables 4.16 and 4.17, while the complete results are presented in Section III.2 of Annex III.

H₂ – NH₃ Heat Exchanger

The procedure for sizing this second heat exchanger is simpler. To achieve this, a relationship is established between the exchanged heats, the overall heat transfer coefficients, and the LMTDs.

The first step, as with the previous heat exchanger, is to obtain the inlet and outlet temperature data for both the Hydrogen and Ammonia, and then calculate the LMTD using the equation provided earlier.

The next step is to estimate the value of the overall heat transfer coefficient. In this case, since there is a phase change, a value of 1500 W/m²K is used [3,4].

Finally, the relationship between heat transfer rates is established using the following equation:

$$\frac{\dot{Q}_{HXH2}}{\dot{Q}_{HXN2}} = \frac{U_{HXH2}}{U_{HXN2}} \cdot \frac{A_{HXH2}}{A_{HXN2}}$$

From this equation, the required heat exchange area is determined, and consequently, the number of tubes for this heat exchanger is calculated.

The results of this section can be found in Table 4.18 for SF0.3 and in Section III.4 of Annex III for the rest of SFs.

Table 4.18. HXH2 results for SF0.3

SF	Flow [kg/h]	T _{target} [K]	X ₃ [-]	X ₂ [-]	X ₁ [-]	Q _{HXH2} [kW]	T _{NH3in} [K]	T _{NH3out} [K]	T _{H2in} [K]	T _{H2out} [K]	ΔT1 [K]	ΔT2 [K]	LMTD [K]	A _{H2} [m ²]	Tube Number [-]	h _{H2out} [kJ/kg]	Q _{H2-Air} [kW]	HX
0.3	2.5	673	1.000	1.000	0.822	617.77	298.72	298.64	649.99	298.30						3931	-0.11	
	2.5	775	1.000	1.000	1.000	839.40	298.81	312.11	774.99	298.23						3930	-0.11	
	2.5	900	1.000	1.000	1.000	1059.78	298.93	413.58	900.00	300.01						3955	-0.10	
	2.5	1025	1.000	1.000	1.000	1326.18	299.04	516.86	1025.00	276.64						3623	-0.14	
	2.5	1150	1.000	1.000	1.000	1467.62	299.12	590.50	1149.99	327.42						4348	-0.06	
	5	673	1.000	1.000	0.764	1231.74	299.33	299.09	650.00	299.31	0.02	350.91	36.01	0.02	3	3945	-0.21	
	5	775	1.000	1.000	1.000	1673.52	299.68	307.58	775.00	299.64	0.05	467.42	50.72	0.01	2	3950	-0.21	
	5	900	1.000	1.000	1.000	2105.57	300.20	419.10	900.00	303.89						4011	-0.19	
	5	1025	1.000	1.000	1.000	2529.66	300.64	525.90	1025.00	311.97						4126	-0.17	
	5	1150	1.000	1.000	1.000	2830.38	300.94	607.12	1150.00	357.25						4778	-0.01	
	10	673	1.000	1.000	0.716	2413.53	299.11	300.57	650.01	306.49						4048	-0.37	
	10	775	1.000	1.000	0.986	3283.69	301.79	301.37	775.01	308.74	6.96	473.64	110.57	0.02	3	4080	-0.35	
	10	900	1.000	1.000	1.000	4073.86	303.70	402.42	900.02	323.61	19.91	497.59	148.41	0.02	3	4293	-0.25	
	10	1025	1.000	1.000	1.000	4772.71	304.94	502.60	1025.02	353.03	48.09	522.42	198.85	0.03	4	4717	-0.04	
	10	1150	1.000	1.000	1.000	5479.77	306.09	597.53	1150.02	382.92	76.84	552.49	241.11	0.03	4	5151	0.17	
	20	673	1.000	0.919	0.674	4648.67	292.91	305.32	674.24	342.25						4562	-0.24	
	20	775	1.000	1.000	0.883	5962.88	293.65	307.20	775.10	352.17						4705	-0.10	
	20	900	1.000	1.000	1.000	7441.42	295.31	354.57	900.12	374.18	78.87	545.55	241.31	0.02	4	5023	0.22	
	20	1025	1.000	1.000	1.000	8789.04	297.75	450.69	1025.15	406.99	109.24	574.47	280.28	0.03	4	5499	0.68	
	20	1150	1.000	1.000	1.000	10087.59	300.21	541.55	1150.18	445.21	144.99	608.63	323.20	0.04	5	6052	1.23	
	30.3	673	1.000	0.991	0.739	7759.13	291.70	312.71	753.05	389.73						5249	0.66	
	30.3	775	1.000	1.000	0.781	8158.78	291.78	313.28	775.30	393.46						5303	0.74	
	30.3	900	1.000	1.000	1.000	10393.90	292.31	324.01	900.37	415.75						5626	1.22	
	30.3	1025	1.000	1.000	1.000	12237.77	293.23	403.58	1025.45	457.95	164.72	621.87	344.11	0.03	5	6237	2.13	
	30.3	1150	1.000	1.000	1.000	14100.66	294.20	490.12	1150.55	501.10	206.90	660.43	390.76	0.04	5	6863	3.06	
	40	673	1.000	1.000	0.780	10843.29	291.08	320.03	813.55	429.69						5828	2.01	
	40	775	1.000	1.000	0.780	10843.29	291.08	320.03	813.55	429.69						5828	2.01	
	40	900	1.000	1.000	0.947	12821.83	291.29	322.99	900.74	448.16						6095	2.54	
	40	1025	1.000	1.000	1.000	15276.86	291.73	378.57	1025.90	489.67	197.95	647.33	379.27	0.03	5	6697	3.72	
	40	1150	1.000	1.000	1.000	17598.51	292.21	458.10	1151.09	537.80	245.59	692.99	431.29	0.04	6	7395	5.08	
	50	673	1.000	1.000	0.819	14217.63	290.73	327.48	867.68	465.89						6352	3.80	
	50	775	1.000	1.000	0.819	14217.63	290.73	327.48	867.68	465.89						6352	3.80	
	50	900	1.000	1.000	0.883	15124.20	290.78	328.81	901.27	474.41						6476	4.10	
	50	1025	1.000	1.000	1.000	18249.81	291.03	363.11	1026.54	514.42						7056	5.52	
	50	1150	1.000	1.000	1.000	21060.22	291.34	436.39	1151.87	565.27	273.93	715.49	459.91	0.04	6	7794	7.33	
	60	673	1.000	1.000	0.855	17724.30	290.70	334.44	916.08	499.62						6841	6.00	
	60	775	1.000	1.000	0.855	17724.30	290.70	334.44	916.08	499.62						6841	6.00	
	60	900	1.000	1.000	0.855	17724.30	290.70	334.44	916.08	499.62						6841	6.00	
	60	1025	1.000	1.000	1.000	21063.27	290.88	353.70	1027.36	535.10						7356	7.51	
	60	1150	1.000	1.000	1.000	24385.97	291.13	421.17	1152.88	587.30	296.18	731.71	481.56	0.05	6	8114	9.74	
80	673	1.000	1.000	0.934	25261.90	290.86	346.99	1001.34	558.30						7693	11.34		
80	775	1.000	1.000	0.934	25261.90	290.86	346.99	1001.34	558.30						7693	11.34		
80	900	1.000	1.000	0.934	25261.90	290.86	346.99	1001.34	558.30						7693	11.34		
80	1025	1.000	1.000	0.990	26385.52	290.90	348.15	1029.60	567.59						7827	11.86		
80	1150	1.000	1.000	1.000	30855.22	291.12	404.82	1155.56	619.55	328.43	750.74	510.82	0.06	8	8583	14.83		
100	673	1.000	1.000	1.000	33614.62	291.09	363.59	1076.69	607.43						8406	17.67		
100	775	1.000	1.000	1.000	33614.62	291.09	363.59	1076.69	607.43						8406	17.67		
100	900	1.000	1.000	1.000	33614.62	291.09	363.59	1076.69	607.43						8406	17.67		
100	1025	1.000	1.000	1.000	33614.62	291.09	363.59	1076.69	607.43						8406	17.67		
100	1150	1.000	1.000	1.000	37320.60	291.25	400.24	1159.13	640.99						8895	20.06		

4.3.4 Weight calculation

To calculate the weight, the heat exchanger will be divided into its individual components: tubes, shell, lids, supports, and fittings.

The weight of the tubes and shell is directly obtained from the Swagelok catalog [2].

For the supports and lids, steel density ($8\text{g}/\text{cm}^3$) is used as a reference, and the weight is calculated by assuming a thickness of 1 cm, using the outer diameter of the shell for the lids and the inner diameter for the supports. The equation is as follows:

$$W = \frac{\pi}{4} \cdot \rho_{steel} \cdot [5 \cdot \varnothing_{int,shell}^2 + 2 \cdot \varnothing_{ext,shell}^2]$$

The weight of the fittings is estimated as 15% of the combined weight of the shell and tubes.

Table 4.19 presents a breakdown for all possible numbers of tubes.

Table 4.19. Weights for different Heat Exchanger sizes.

NT	Tubes weight [kg]	Shell \varnothing_{int} [mm]	Shell width [mm]	Shell weight [kg]	Shell and tubes weight [kg]	Supports and lids weight [kg]	Fittings weight [kg]	Total weight [kg]
1	0.021	6	1	0.175	0.196	1.935	0.029	2.161
2	0.042	10	1	0.275	0.317	4.951	0.048	5.316
3	0.063	10	1	0.275	0.338	4.951	0.051	5.340
4	0.084	10	1	0.275	0.359	4.951	0.054	5.364
5	0.105	16	1	0.425	0.530	12.114	0.080	12.723
6	0.126	16	1	0.425	0.551	12.114	0.083	12.748
7	0.147	16	1	0.425	0.572	12.114	0.086	12.772
8	0.168	16	1	0.425	0.593	12.114	0.089	12.796
9	0.189	16	1	0.425	0.614	12.114	0.092	12.820
10	0.210	16	1	0.425	0.635	12.114	0.095	12.844
11	0.231	18	2	1	1.231	16.261	0.185	17.677
12	0.252	18	2	1	1.252	16.261	0.188	17.701
13	0.273	18	2	1	1.273	16.261	0.191	17.725
14	0.294	18	2	1	1.294	16.261	0.194	17.749
15	0.315	23	2	1.15	1.465	25.780	0.220	27.465
16	0.336	23	2	1.15	1.486	25.780	0.223	27.489
17	0.357	23	2	1.15	1.507	25.780	0.226	27.513
18	0.378	23	2	1.15	1.528	25.780	0.229	27.537
19	0.399	23	2	1.15	1.549	25.780	0.232	27.561
20	0.420	23	2	1.15	1.570	25.780	0.236	27.585

4.3.5 Hydrogen – Air heat exchanger

This heat exchanger has been sized using the design methodology for compact heat exchangers employed in intercooling and recovery systems for Hydrogen-fuelled aero engines [5].

Table 4.18 shows the outlet enthalpies of the Hydrogen and the heat to be dissipated by this third heat exchanger for SF0.3. The remaining results can be found in Section III.4 of Annex III.

The heat to be dissipated was calculated considering that the Hydrogen must reach the intermediate tank at 60°C, with the maximum heat load across all operating points being 20.8 kW. This third heat exchanger will be sized with this target in mind. The sizing process was carried out using a MATLAB script.

The inputs for this program are listed below:

- **Max P_{FCS} .** This represents the maximum total gross power that the group of FCs has to provide to the complete system, both to feed the CMR and the electric motors that move the HDFCV.
- **Eff $_{FCS}$.** Average efficiency of the FCS. In this case it's 0.5.
- **Cruise speed.** Average speed of the HDFCV in the diving cycles.
- **Air inlet temperature.** It is considered to be 300 K.
- **Hydrogen temperatures.** Hydrogen inlet is at 652 K, the highest one obtained from the results of the HXH2. The desired Hydrogen temperature is 60 °C, that is, 333 K.
- **Fluid properties.** They are imported from REFPROP.
- **Material.** The material selected is stainless steel 321.

The geometrical data of this HX is summarized in Table 4.20.

Table 4.20. Summary of the Hydrogen-Air HX geometrical data.

A_{Fin}/A_{Total} [-]	k_{Fin} [W/mK]	Fin spacing [mm]	Fin thickness [mm]	Tube thickness [mm]
0.813	14	2.794	0.1	0.5

RESULTS

The results of the sizing process for this third HX are shown in Tables 4.21 and 4.22.

Table 4.21. Air-Hydrogen HX summary of results. Part 1.

N. Tubes [-]	N. Fins [-]	Total Weight [kg]	Cooling Power [kW]	Power/Weight [kW/kg]	Power/Volume [kW/m ³]
40	76	2.062	25.05	12.16	10168.11

Table 4.22. Air-Hydrogen HX summari of results.

HYDROGEN				AIR			
T_0 [K]	T_F [K]	ΔT [K]	ΔP [kPa]	T_0 [K]	T_F [K]	ΔT [K]	ΔP [kPa]
652.00	300.74	-351.26	0.542	300.00	322.30	22.30	23.1354

This third heat exchanger is very lightweight and compact. For this reason, the design that is capable of meeting the most demanding operating conditions in all cases will be adopted, as the difference is not significant.

4.3.6 Summary of results

The final results for this Stage 3 are summarized in Table 4.23.

Table 4.23. Stage 3 - Summary of final results.

SF	HXH2		HXN2		H ₂ - AIR	TOTAL HX
	N. Tubes [-]	Weight [kg]	N. Tubes [-]	Weight [kg]	Weight [kg]	WEIGHT [kg]
0.2	4	5.36	6	12.75	2.06	20.17
0.3	6	12.75	8	12.80	2.06	27.61
0.4	7	12.77	9	12.82	2.06	27.65
0.5	7	12.77	9	12.82	2.06	27.65
1	9	12.82	9	12.82	2.06	27.70

It can be observed that the weight derived for the different HX sizes for each SF is almost negligible, the only accountable difference being that the SF0.2 is around 7 kg lighter than the other SF. For this reason, the weight of the system will be impacted almost exclusively by the weight of the CMR itself.

4.3.7 References

- [1] FUNKE. “Shell-and-Tube Heat Exchanger Datasheet”.
- [2] Swagelok. “Stainless Steel Seamless Tubing and Tube Support Systems”.
- [3] Incropera F. P., DeWitt D. P., Bergman T. L. and Levine A. S. “Fundamentals of Heat and Mass Transfer”, 7th ed., 2011.
- [4] Engineers Edge. “Overall and Convective Heat Transfer Coefficients Table Chart”.
- [5] Capitao Alexandre, Jonsson Isak, Xisto Carlos, Lundbladh Anders, Grönstedt Tomas. “Compact heat exchangers for Hydrogen-fueled aero engine intercooling and recuperation”. *Applied Thermal Engineering*, Vol. 243 April, pp. 122538, 2024.

4.4 Stage 4 – Scaling Factor selection

The last stage of this first chapter is a brief summary of the key aspects to consider when selecting the system's SF and implementing it in the HDFCV.

4.4.1 Efficiency summary

Table 4.24 provides a recap of the maximum efficiencies achievable according to Stage 2, as well as the operating point at which they occur and the maximum Ammonia flow rate that the CMR can handle within the operational range defined in Stages 1 and 2.

Table 4.24. Maximum thermal efficiency operating points for different SFs.

SF	Max thermal efficiency [-]	NH3_Flow [kg/h]	T_op [K]	Máx NH3_Flow [kg/h]
0.2	0.292	50	1150	50
0.3	0.294	80	1150	80
0.4	0.293	100	1150	100
0.5	0.292	80	1025	100
1	0.282	80	900	100

As shown, the efficiencies are quite similar for SF values between 0.2 and 0.5, being higher than in the case of SF1. By comparing this information with the results from Stage 1, it can be reaffirmed that lower SF values result in higher thermal efficiencies.

Additionally, the maximum Ammonia flow rate is another crucial parameter, as it can be a limiting factor depending on the powertrain demands.

4.4.2 Weight summary

Table 4.25 summarizes the total weights for the different SF considered.

Table 4.25. Weight summary.

SF	Combined HX Weight [kg]	CMR Weight [kg]	TOTAL WEIGHT [kg]
0.2	20.17	311.97	332.15
0.3	27.61	467.58	495.18
0.4	27.65	623.95	651.60
0.5	27.65	779.55	807.21
1	27.70	1558.33	1586.04

As anticipated in the previous section, the weight of the CMR itself ultimately determines the weight of each SF, with the smaller ones being substantially lighter.

4.4.3 Selection

To correctly select the appropriate SF, in addition to considering the efficiency and weight results, it is necessary to briefly review the requirements of the next chapter to ensure that the operational criteria are met.

As a reference cycle for this quick verification, the HDDT cycle will be used. This cycle was developed for a set of two fuel cells owned by IUI CMT, with a maximum power output of 60 kW each FC, and a 80 kW battery. After analysing the power demands of the cycle, an initial simplified estimate concludes that the maximum Ammonia consumption peak for the CMR is 80 kg/h.

Therefore, the lightest and most efficient SF that meets the maximum Ammonia flow rate requirement is SF0.3.

4.4.4 Possible criteria changes

The choice of SF0.3 as the optimal size is not set in stone. There are three scenarios in which the selection could differ:

- **Maximum flow requirement.** If the system were to be integrated into another powertrain intended for a lower-power vehicle, it might be worth exploring the lower end of the SF range. In such cases, the optimal choice would likely be an SF smaller than 0.3.
- **Changes in efficiency.** In future iterations of the CMR, the design could evolve. On one hand, the design may improve in such a way that the overall efficiency increases. On the other hand, new geometries could be explored, resulting in different efficiency distributions. In both cases, the analysis carried out in this chapter should be revisited to make the correct decision.
- **Changes in volume and/or weight.** This possibility is also linked to the development of the CMR. If different materials are used or if the geometry and auxiliary systems are modified, a CMR with lower volume and weight may result. This could imply that, given that smaller SFs offer better efficiency, it might be feasible to combine two CMR systems in a single vehicle and explore different control possibilities. As seen in previous sections, the CMR operates best near the upper flow limit. Given this, if two systems were available, one could operate at high load during low power demand, and when higher power is needed, the second system could be incorporated. This mode of operation is similar to the regulation of many pumping systems, among other installations.

Chapter 5

CMR – FCS

integration into HDV

Once the system is characterized and its main components are sized, the next step is to integrate it into the HDFCV and analyse its performance under different scenarios, followed by a comparison with traditional FCS configurations.

Additionally, the connection between the system and the FCS must be designed, taking into account the power supply requirements and the differences in the dynamics of each system, ensuring that no bottlenecks are created.

As mentioned in Section 3.2, this fifth chapter is divided into three stages:

- **Stage 5 – Driving Cycles.**
- **Stage 6 – Final Layout and Specifications.**
- **Stage 7 – Benchmark Against Current Systems.**

The main outcomes of this chapter should include the method for implementing the system in the HDFCV, the sizing of additional components, and the powertrain's performance across different

driving cycles. Additionally, the final layout and the selection and arrangement of fuel tanks for different autonomy objectives will be obtained.

5.1 Stage 5 – Driving Cycles

The primary objective of this stage is to determine the dimensions of the Ammonia and Hydrogen tanks. To achieve this, the system's behaviour will be evaluated through simulations of driving cycles, which will establish the minimum requirements that these tanks must meet.

5.1.1 Introduction

For ICE vehicles, driving cycles are primarily used to assess performance and measure emissions. The implementation of standardized cycles allows for direct comparison of test results with data from other vehicles. In the case of EVs, driving cycles serve to simulate the propulsion system and estimate the energy consumption required to maintain a specific speed over a set duration. During testing, ICE or electric vehicles are placed on a dynamometer, with either new or used vehicles of varying mileage being tested. These tests, conducted according to driving cycle standards, measure parameters such as traction force, engine heat generation, emissions, fuel consumption (for ICE vehicles), and battery SOC for EVs. Additionally, driving cycles are valuable for simulating and comparing various electric vehicle propulsion systems and their components prior to manufacturing. They provide estimates of energy consumption across different speed conditions and predict vehicle behaviour during acceleration, deceleration, traffic scenarios, or sustained speeds. The time component of the driving cycle also predicts the duration an EV can operate with its remaining energy under specific conditions.

The driving cycle has many standards that are usually regulated differently in each country. The difference is usually due to different driving environments, such as traffic, road, and weather condition in each country [1]. Another key objective of introducing driving cycles is to facilitate the comparison and evaluation of vehicle performance across different types of vehicles. To fairly compare the testing results, the European Union has created world-standard driving cycles so that the comparison of the propulsion system for each vehicle can be more uniform, namely the Worldwide harmonized Light vehicle Test Procedure (WLTP).

The WLTP driving cycle, which was introduced in 2017, is a series of speed data against time adjusted to different countries' driving cycles [2].

For this second chapter, two driving cycles will be taken into account:

- **HDDT – Heavy-Duty Diesel Truck.** Also known as HHDDT, is a chassis dynamometer test fruit of a collaboration between California Air Resources Board and West Virginia University. It is a standardized driving cycle that consists of four speed-time modes: idle, creep, transient and (high-speed) cruise. The latter mode is the one that will be used for subsequent simulations.
- **VECTO LHR – Long-Haul with Reference loading.** The cycle is derived from realistic driving data and can be considered a real driving cycle that has recently been established as a reference for evaluating the performance of HDFCVs. It incorporates statistical behaviours related to inertia and driver response. It is worth noting that there is no VECTO available for FCVs; instead, the one used in this chapter is an adaptation of the conventional cycle developed through a collaboration between UPV and JRC. This cycle is more demanding in the FC dynamics than the HDDT.

These two driving cycles will be simulated using the FCS models explained in Section 3.6. As a reminder, these FCS are:

- A 60 kW one owned by the IUI CMT designed for HD applications.
- The FCS from the Toyota Mirai, which has a nominal power of 114 kW.

As initial conditions for each cycle, two additional parameters will be introduced:

- **Initial operating temperature of the CMR.** The range of values for this parameter corresponds to the CMR's operating range, from 673 to 1150 K. Since it is not feasible to test all values, the same discretization used in Stage 4 has been applied, specifically: [673 775 900 1025 1150] K.
- **Size of the intermediate Hydrogen tank.** The tank capacities evaluated range from 100 to 1000 litres.

In addition to these two parameters, the pressure control of the intermediate tank, as detailed in Section 5.1.5, must also be considered. Since it is impossible to optimize the system for all parameters simultaneously and achieve a system that operates at a single flow rate, starts at a low temperature, and has a small intermediate tank, trade-off solutions must be reached.

5.1.2 CMR Dynamics results

As described in Section 3.5, the characterization of the thermal dynamics of the CMR has been carried over by using 3 different ways. In this Section, the results of each method are discussed.

MATLAB IDENTIFICATION TOOLBOX

As opposed to what happened in Stage 2, this time the temperature at maximum efficiency coincides for several Ammonia flow rates, as shown in Table 5.1. This results in different static gains, making it challenging for a single transfer function to be sufficient.

Table 5.1. Maximum efficiency operating temperature for each Ammonia flow.

NH3 Flow [kg/h]	5	10	20	30.3	40	50	60	80
Max Eff. T_{op} [K]	673	775	900	1025	1025	1150	1150	1150

After testing various options for the number of zeros and poles in the TF, a satisfactory result for the model was not achieved. The conclusion from the analysis is that to capture the behaviour of the CMR in the model, it would be necessary to develop a matrix with a TF for each flow step characterized in Chapter 4, for both increasing and decreasing flows.

GENETIC ALGORITHM

As a second approach to finding a sufficiently accurate transfer function, the genetic algorithm was used to determine the various parameters.

To run the simulations in MATLAB, the “ga()” function is used. In this case, the simulation was performed with a population size of 15 individuals and a maximum of 80 generations.

In the first test of the algorithm, a similar issue to the previous method was observed. Consequently, a second test was performed by separating the dynamics into two transfer functions, one for ascending dynamics and another for descending dynamics. Assuming conventional first-order functions, this resulted in six parameters to be determined by the genetic algorithm.

However, the results remained unsatisfactory, leading to the same conclusion as in the previous section. Therefore, the next method was explored.

HEURISTIC IDENTIFICATION

This third methodology has been proven successful to accomplish the modelling of the thermal dynamics of the CMR. Figure 5.1 shows the response of the estimated function (Top estimated) compared to the full CMR model (Top CMR). The complete function can be consulted in Section IV.1 of Annex IV.

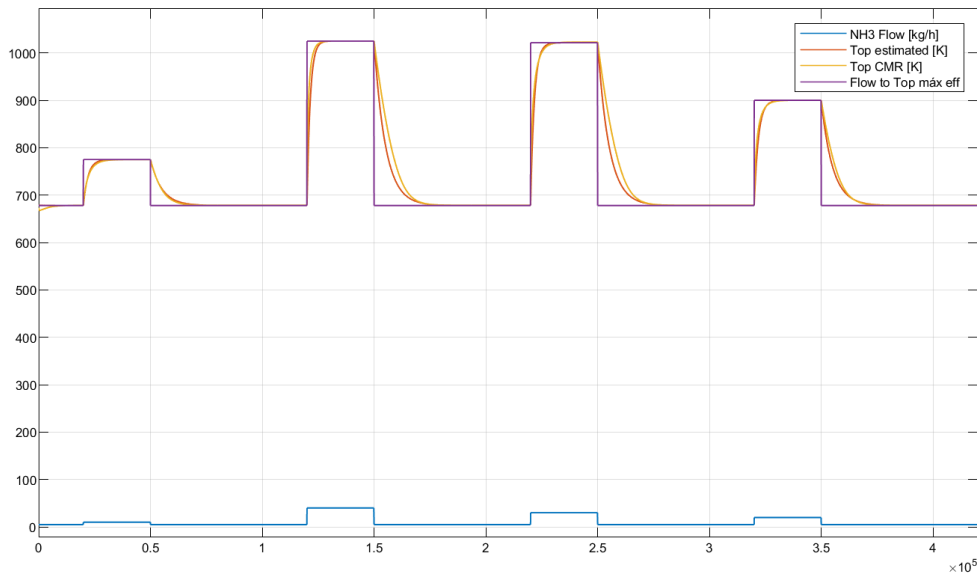


Figure 5.1. Results of a validation test of the Heuristic Identification of the CMR dynamics.

Figure 5.2 provides a more detailed view of the fit between the actual and calculated responses. The aim was to ensure that any slight mismatch would always occur in the least favourable way, meaning that the estimated dynamics are slower than the real ones when the CMR heats up and faster when it cools down.

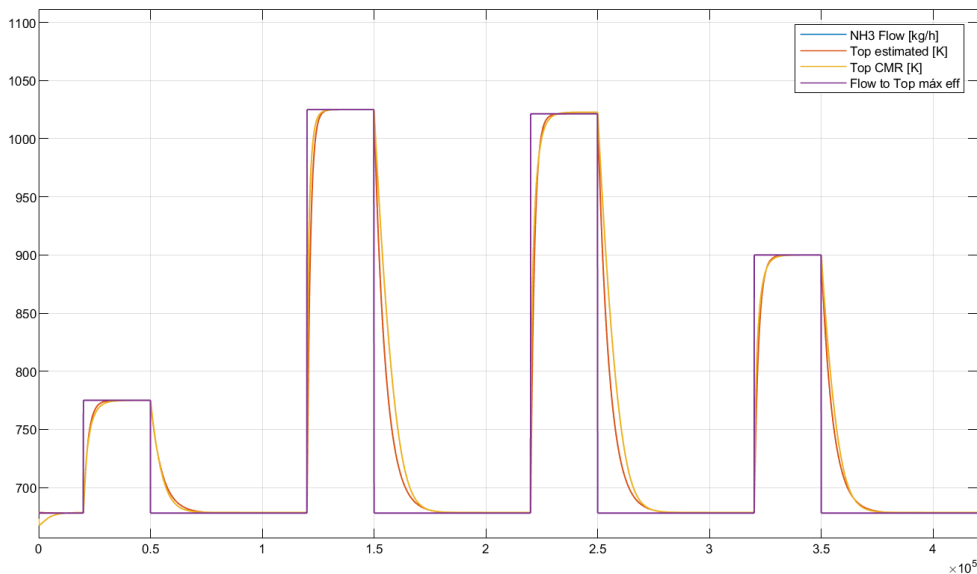


Figure 5.2. Detail of a validation test of the Heuristic Identification of the CMR dynamics.

5.1.3 Mean Value Models

In this section, we will demonstrate how to implement the models of both FCs alongside the CMR model, in order to develop a simplified yet accurate model that allows for low computational cost simulations. This enables iterative model refinement. In addition to offering greater versatility and ease for making changes and exploring new possibilities for the FC or CMR SF, this model allows for running large volumes of simulations to perform sensitivity analyses on FCV behaviour across different driving cycles.

This simplified model is known as a Mean Values Model, and to implement it in MATLAB, the “n-D Lookup Table” block is used. This block evaluates a sampled representation of a function with n variables. The block maps inputs to an output value by looking up or interpolating a table of values defined by the block parameters. Figure 5.3 shows the implementation of one of the tables incorporated into the model.

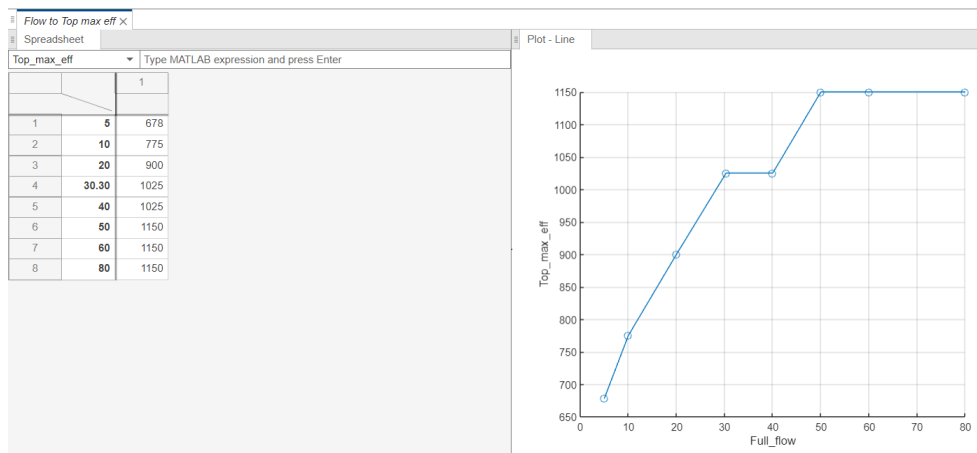


Figure 5.3. Flow to Max Efficiency Operating Temperature 2-D Lookup Table.

Figure 5.4 shows the integrated model of the CMR and FC from CMT, while Figure 5.5 presents the same for the Toyota Mirai FC. As can be seen in both figures, the models are quite similar in both cases, differing only in the red-marked area, which represents the implementation of each FC’s consumption curves. Since the models are different, the relationships between variables are not exactly the same, meaning that in each case, the results must be handled according to the specific characteristics of each FC model when integrating with the CMR.

In both diagrams, the driving cycle is implemented as a total power input. In this case, it refers to the gross power of the stack, as it allows for the calculation of the number of FCs needed to meet the cycle’s requirements. The gross power data already includes the consumption of the compressor and electric motors, so it only remains to add the consumption of the auxiliary thermal source and that of the CMR itself before converting to Hydrogen consumption.

Both models include three integrated functions:

- **Top_Dynamics.** This function represents the dynamic characterization of the CMR, as discussed in Section 5.1.3 and detailed in Section IV.1 of Annex IV.
- **PressureControl.** This manages the pressure control of the intermediate Hydrogen tank. It is thoroughly explained in Section 5.1.5 and can be further reviewed in Section IV.2 of Annex IV.
- **CMR_IdealGas.** This function recalculates the mass and pressure of the intermediate Hydrogen tank, based on a straightforward application of the ideal gas law, as outlined in Section IV.3 of Annex IV.

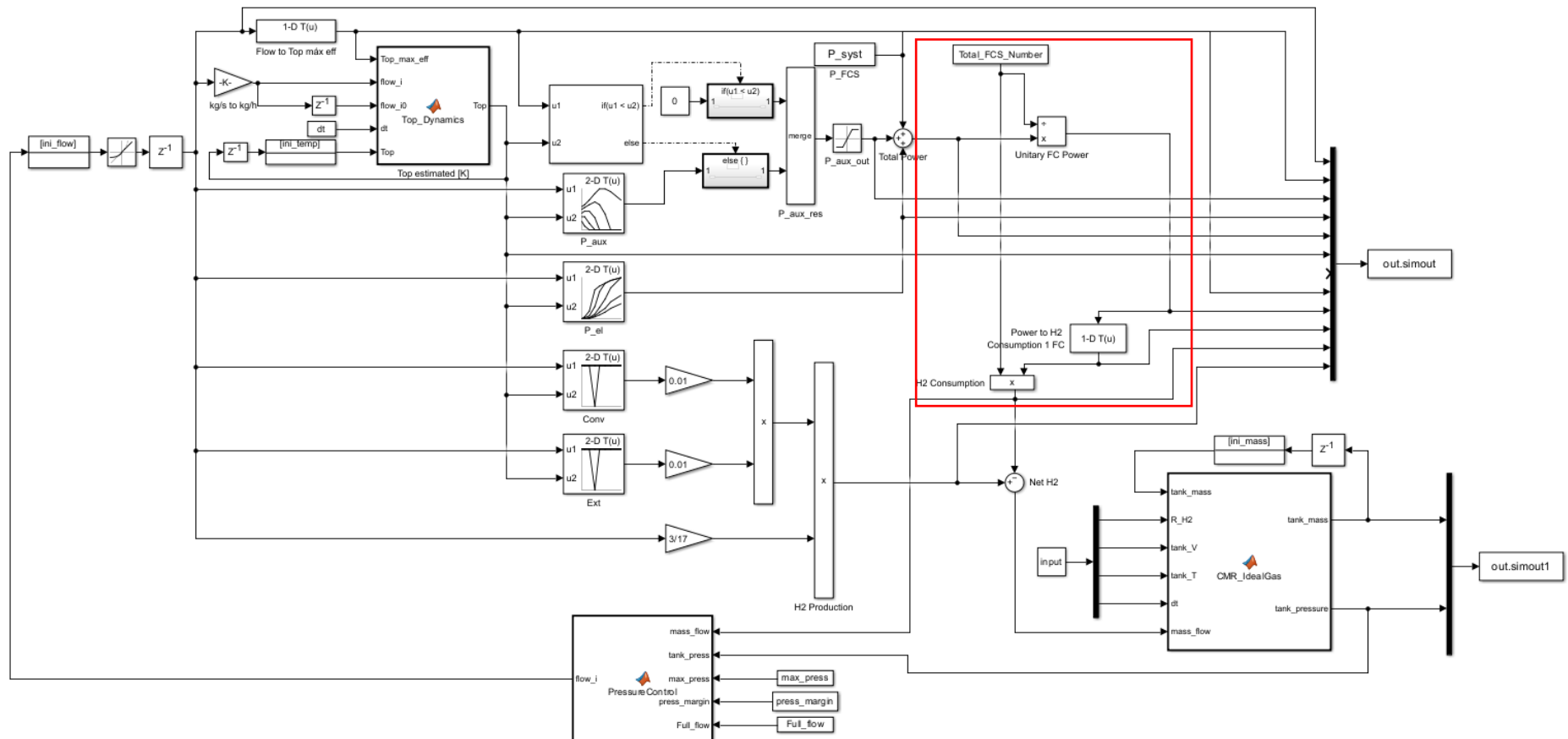


Figure 5.4. Mean Values Model integrating the CMR and the FC for HDV applications.

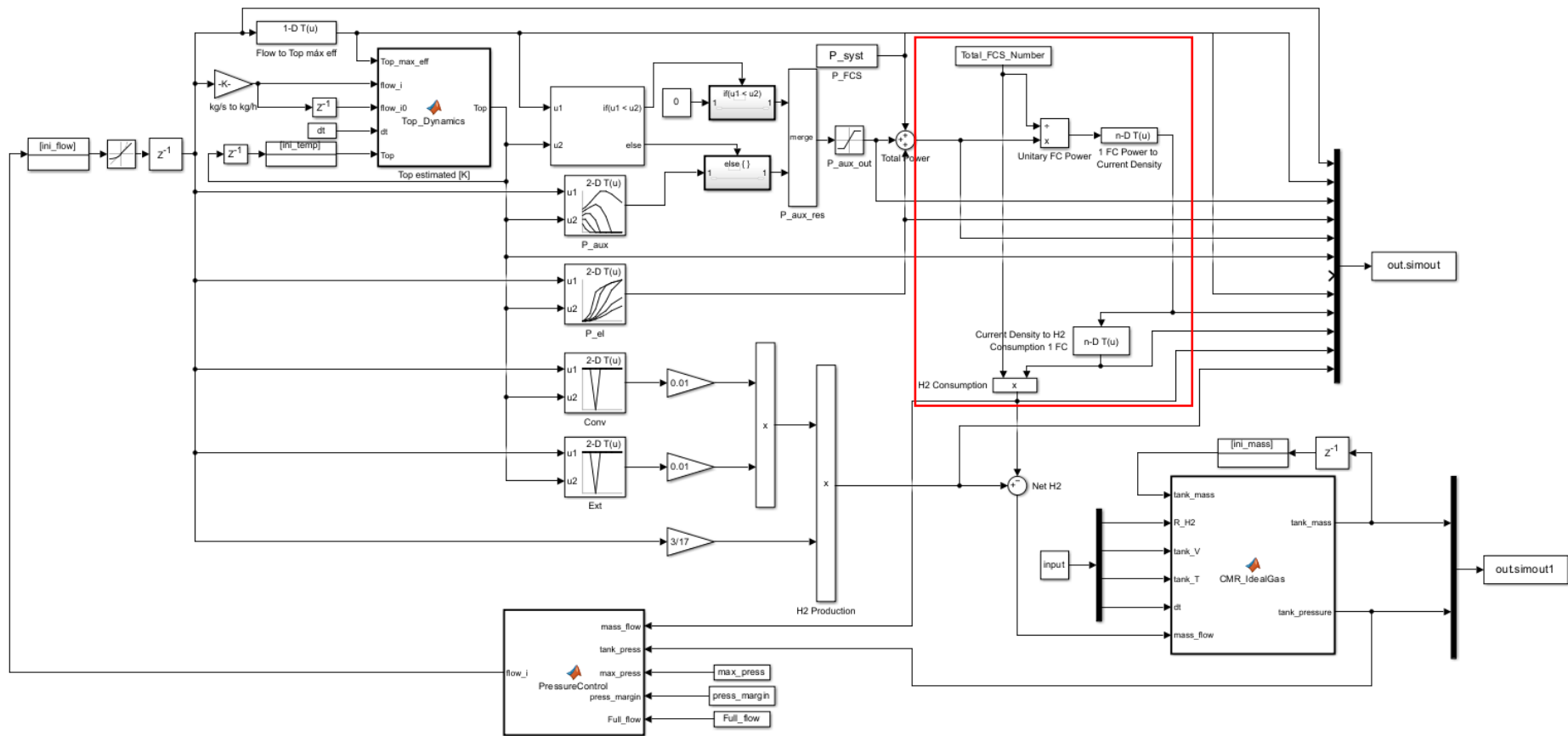


Figure 5.5. Mean Values Model integrating the CMR and the Toyota Mirai FC.

5.1.4 Cycle simulations

The primary objective of running these simulations is to size both the intermediate Hydrogen tank located between the CMR and the FCS, as well as the Ammonia tank that supplies the CMR. Figures 5.6 and 5.7 show the gross power profiles (P_{FCS}) demanded for the HDDT and VECTO LHR cycles, respectively.

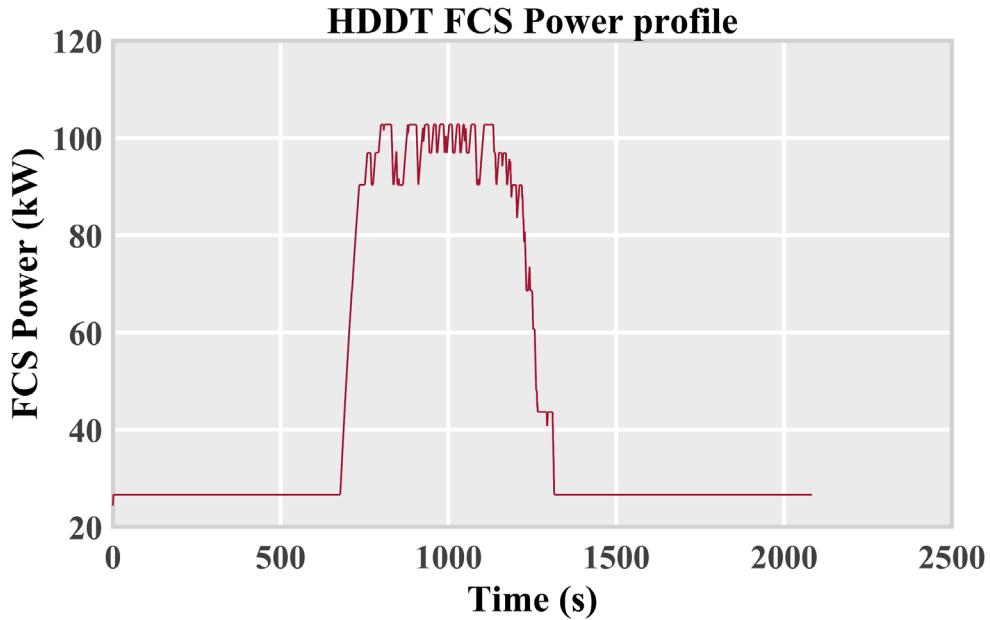


Figure 5.6. HDDT cycle FCS Power demand profile.

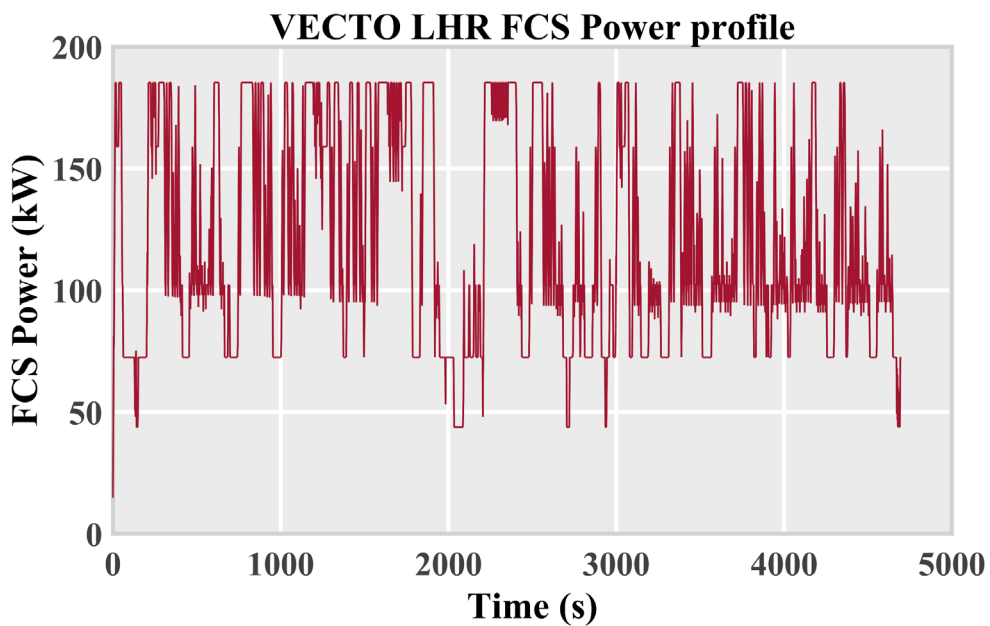


Figure 5.7. VECTO LHR cycle FCS Power demand profile.

Table 5.2 shows the number of FCs needed for each cycle to satisfy the minimum requisites.

Table 5.2. Minimum requisites of FC number for the different combinations of cycle and FC.

Cycle	Max P_{FCS} demanded [kW]	N of IUI CMT FC [-]	N of Toyota Mirai FC [-]
HDDT	102.79	2 +	1 +
VECTO LHR	185.32	4 +	2 +

5.1.5 Hydrogen tank pressure control

The maximum pressure difference between the two sides of the CMR membrane is 5 bar. This means that, with the system operating at a reference pressure of 10 bar, the maximum pressure on the H₂ side is 15 bar, and the minimum pressure is 5 bar. These limits are directly applied to the intermediate Hydrogen tank.

Under normal conditions, the CMR would produce Hydrogen based on the FCS demand, but since the dynamics of the CMR are significantly slower (mainly to ensure that only vapor enters the reactor and to protect the membrane, as discussed in Section 4.1.2), this synchronization is not feasible, and there will always be some mismatch. Therefore, the function of the intermediate Hydrogen tank, common to almost all tanks, is to decouple demand from production while ensuring the appropriate supply conditions for the FCS.

To maintain the pressure in this tank, two functions have been developed for variable calculation, both mentioned in Section 5.1.2 and implemented in Annex IV.

The first of these is the application of the ideal gas law to relate the mass and pressure in the tank. This is applicable because the compressibility factor of Hydrogen under the operating conditions is 1.006, which is essentially 1. For calculation purposes, the tank is assumed to remain at a constant 60 °C.

The second is a pressure control law that adjusts the Ammonia demand from the CMR. This was developed using a methodology similar to that employed in pumping stations for potable water supply [3]. The procedure is summarized as follows:

In first place, two absolute limits are set, one upper and one lower.

In second place, a safety margin is defined, which can be the same or different for each limit. This results in the intervals shown in Figure 5.8.

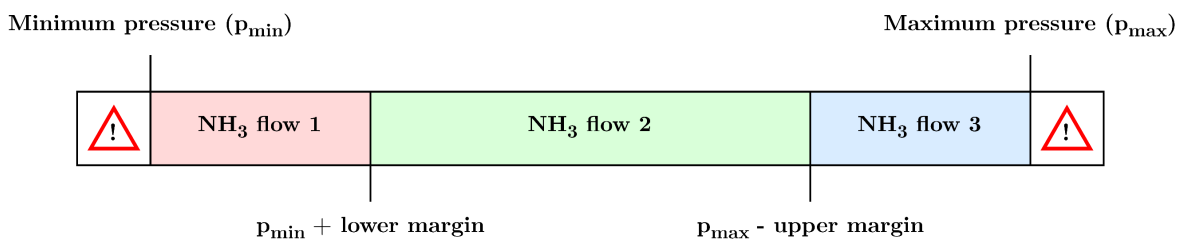


Figure 5.8. Intervals for the Hydrogen intermediate tank pressure control.

Finally, specific flow rates are assigned based on the operating zone, as shown in Figure 5.9.

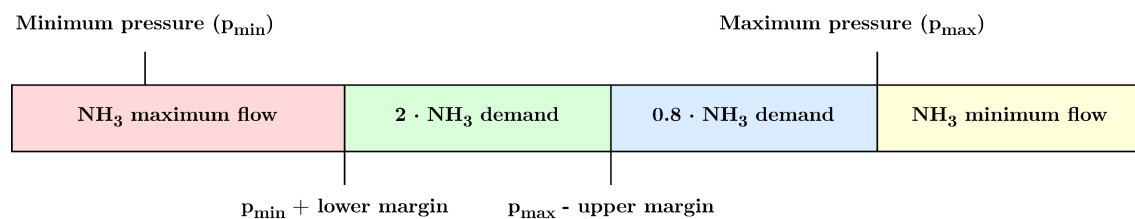


Figure 5.9. Ammonia flows demanded to the CMR for each pressure interval.

5.1.6 Results

For all simulations, an initial Ammonia flow rate of 5 kg/h is considered, and the Hydrogen tank is assumed to be full, meaning at a pressure of 15 bar. Additionally, the pressure margin for the control of the intermediate tank is set to 2 bar, both for the upper and lower limits.

The initial temperature of the CMR in each of the four simulations was determined by finding a compromise solution between this temperature and the size of the intermediate Hydrogen tank.

HDDT – IUI CMT FC

In this first simulated combination, the effect of the initial CMR temperature before starting the cycle will be demonstrated. For this, two temperatures will be simulated: 900 K and 1025 K.

Initial CMR Temperature as 900 K

Figures 5.10 to 5.13 show the most relevant results from this simulation.

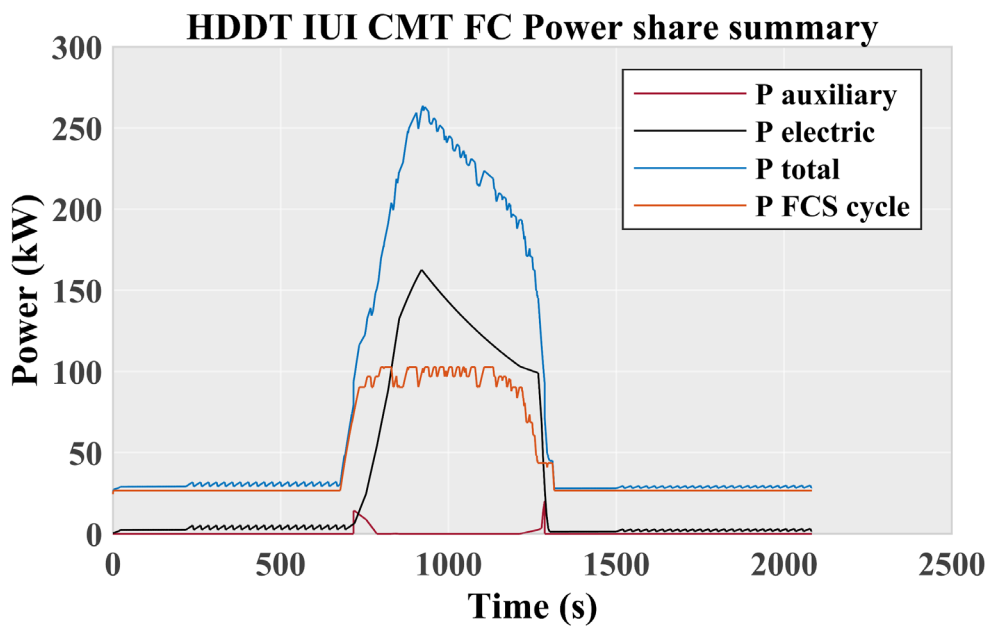


Figure 5.10. HDDT IUI CMT FC Power share summary.

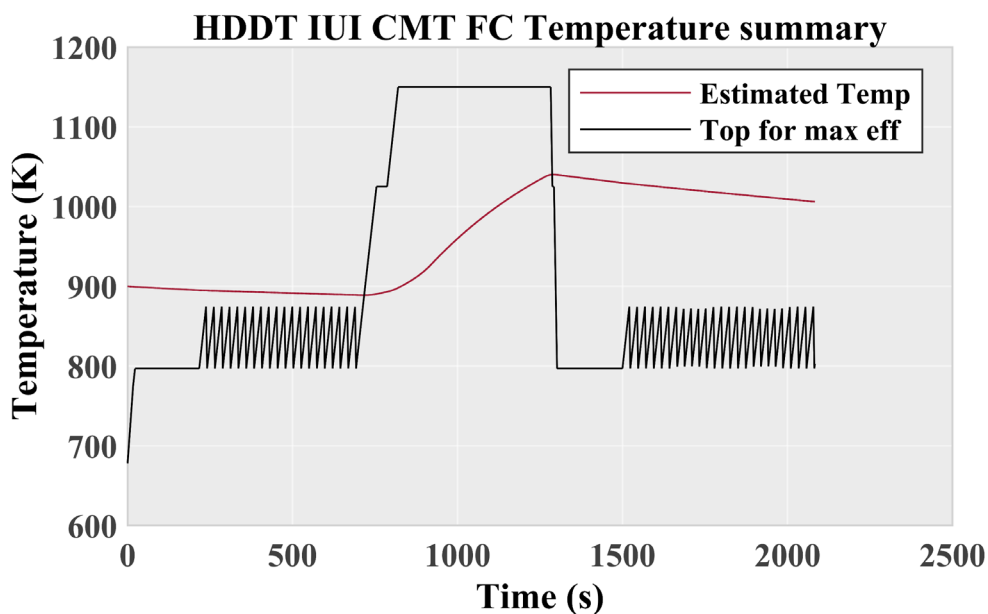


Figure 5.11. HDDT IUI CMT FC Temperature summary.

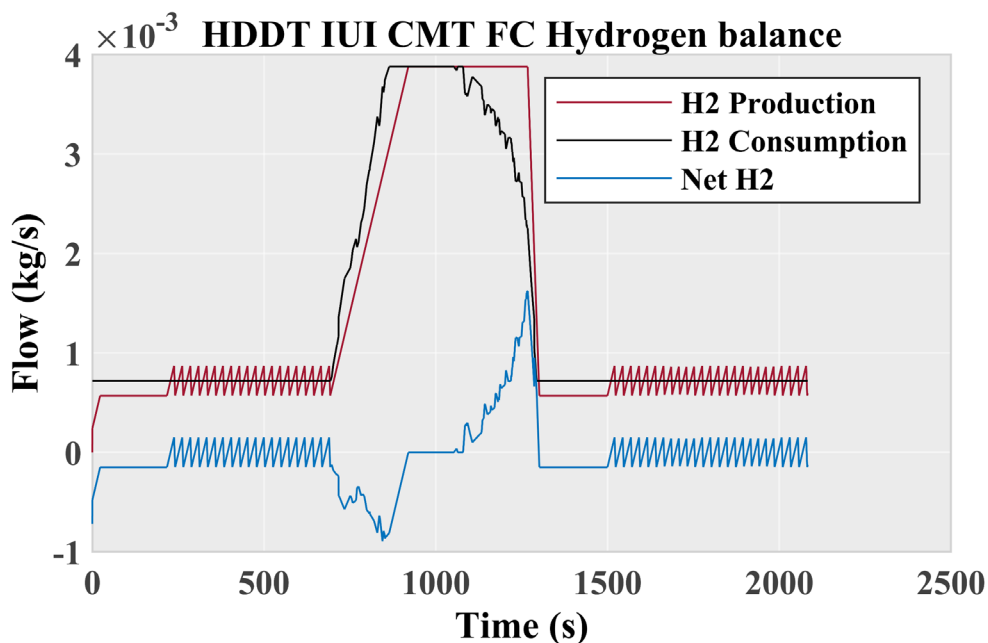


Figure 5.12. HDDT IUI CMT FC Hydrogen balance.

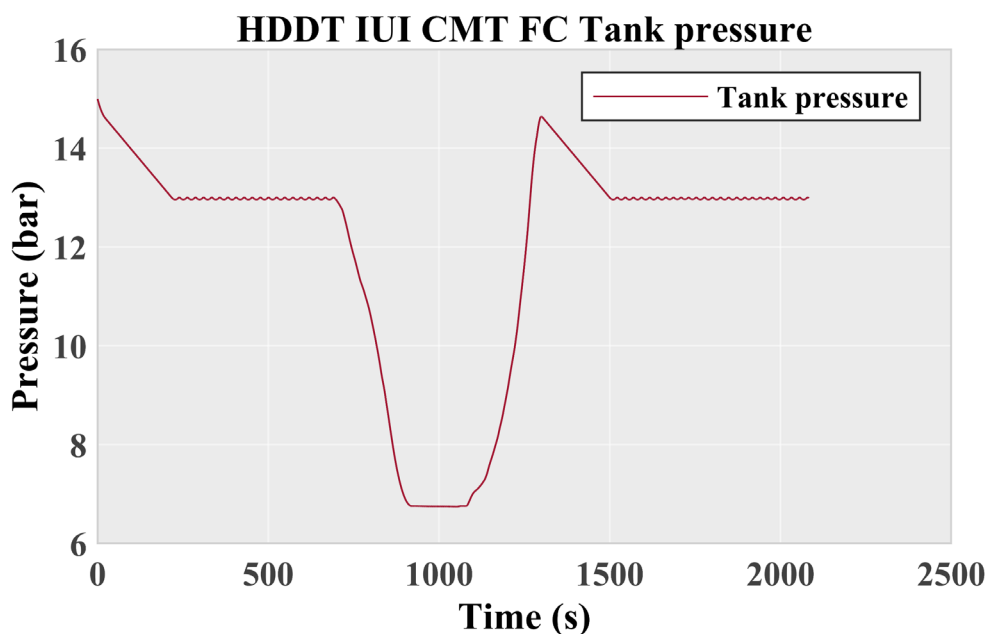


Figure 5.13. HDDT IUI CMT FC Tank pressure.

In the first three figures, certain oscillations or ripples can be observed. This is due to the pressure margins. If this phenomenon were to pose a risk to the system, a more relaxed pressure control could be implemented, but at the cost of requiring a larger intermediate Hydrogen tank. Tables 5.3 and 5.4 present the Ammonia and Hydrogen consumption data for this cycle, as well as the amounts required to ensure a range of 400 and 800 km, respectively. In the case of Hydrogen, it is produced entirely by the CMR.

Table 5.3. HDDT IUI CMT FC Ammonia consumption.

Ammonia Consumption [kg]		
HDDT Cycle	400 km	800 km
16.75	180.54	361.08

Table 5.4. HDDT IUI CMT FC Hydrogen consumption.

Hydrogen Consumption [kg]		
HDDT Cycle	400 km	800 km
2.96	31.90	63.81

Table 5.5 shows the volume occupied by the Ammonia for each autonomy scenario.

Table 5.5. HDDT IUI CMT FC required Ammonia for an autonomy of 400 and 800 km.

400 km		800 km	
Vol [l]	mass [kg]	Vol [m3]	mass [kg]
299.40	180.54	598.81	361.08

Finally, Tables 5.6 and 5.7 provide a summary of the requirements and initial conditions for the driving cycle and the different tanks, respectively.

Table 5.6. HDDT IUI CMT FC cycle conditions.

FC Number	FC Unitary Power	Initial Temperature
	[kW]	[K]
4	60	900

Table 5.7. HDDT IUI CMT FC tank summary.

TANK VOLUME [l]			EMPTY TANK MASS [kg]		
HYDROGEN	AMMONIA		HYDROGEN	AMMONIA	
	400 km	800 km		400 km	800 km
250	300	250	104.0	428.2	706.1

Initial CMR Temperature as 1025 K

The main results for comparison are presented in Tables 5.14, 5.15, and 5.16.

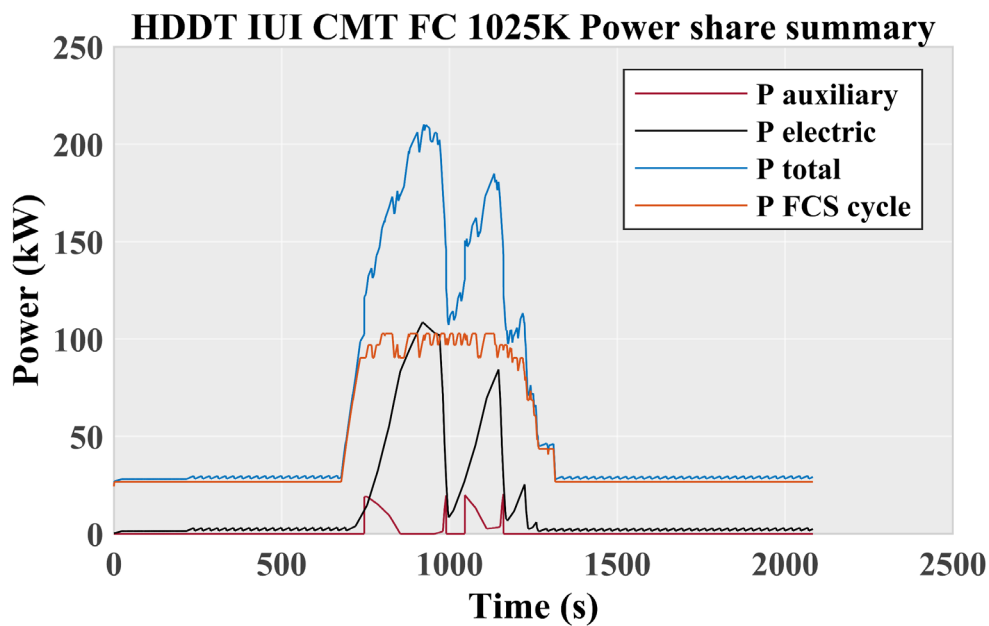


Figure 5.14. HDDT IUI CMT FC 1025 K Power share summary.

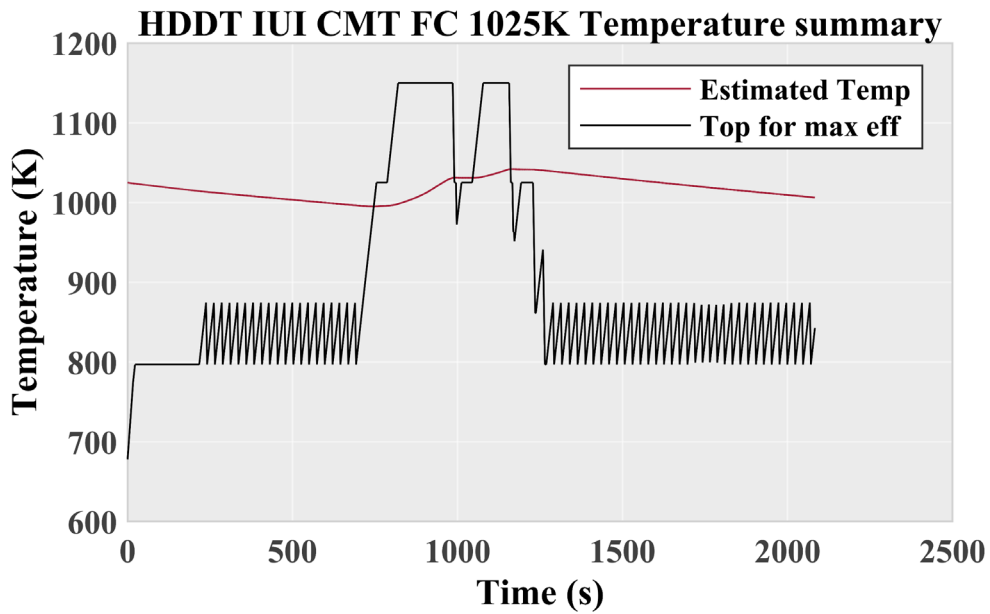


Figure 5.15. HDDT IUI CMT FC 1025 K Temperature summary.

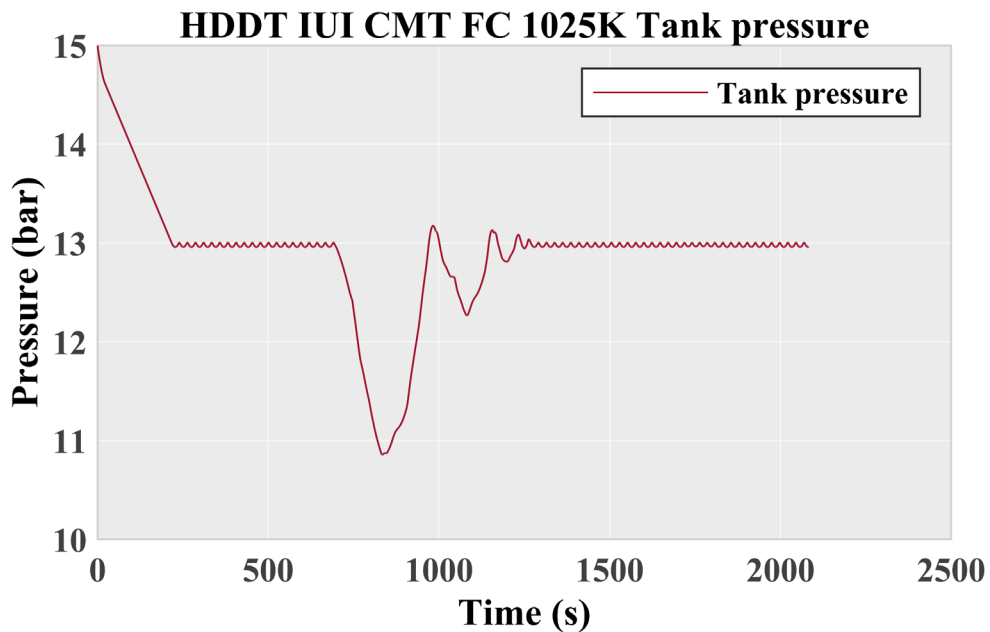


Figure 5.16. HDDT IUI CMT FC 1025 K Tank pressure.

As can be observed, when the system is started at 1025 K, performance improves, and the system operates more comfortably in relation to the cycle demands. This is evident in the reduced pressure oscillations in the intermediate tank, as well as a greater margin before reaching minimum pressures, and significantly lower stack power levels. The Hydrogen production graph, following a very similar trend to the power graph, has not been included in this case.

However, operating at higher initial temperatures imply a greater initial energy investment and this also requires longer setup times before starting the driving cycle. A compromise solution is needed then.

HDDT – TOYOTA MIRAI FCS

In this case and the subsequent ones, the main graphs and result tables will be presented, analogous to the previous case. Once all cases are reviewed, they will be discussed collectively in Stage 6.

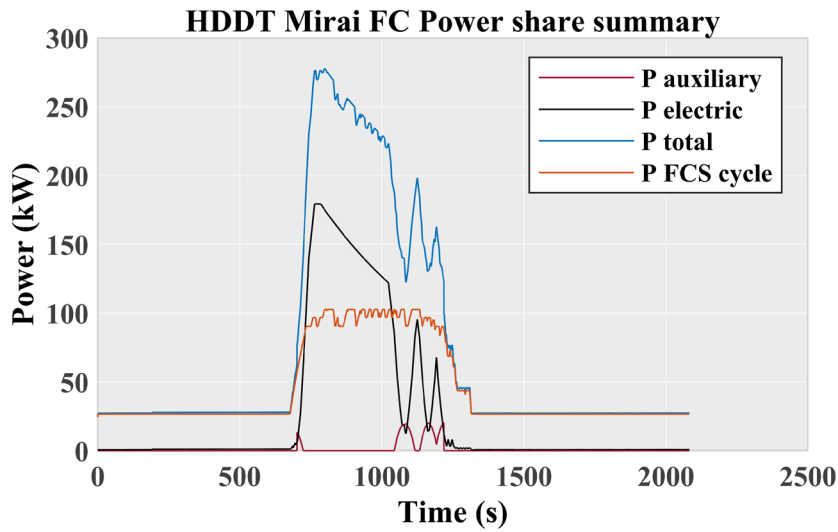


Figure 5.17. HDDT MIRAI FC Power share summary.

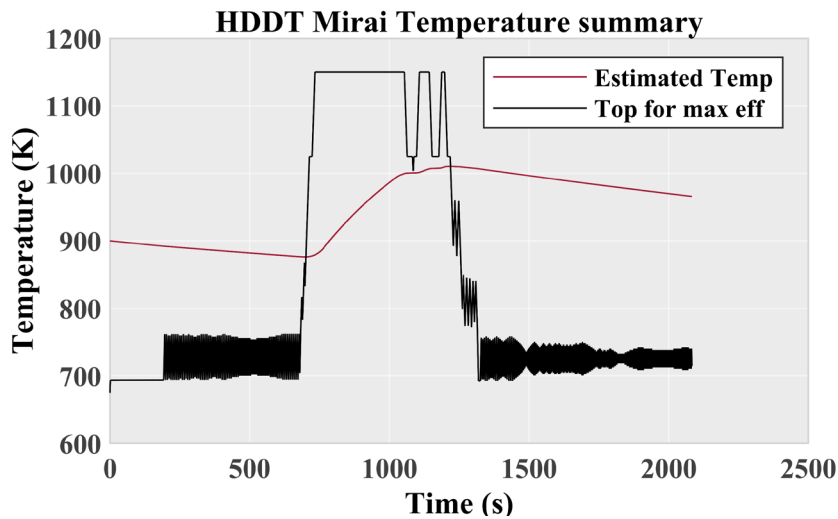


Figure 5.18. HDDT MIRAI FC Temperature summary.

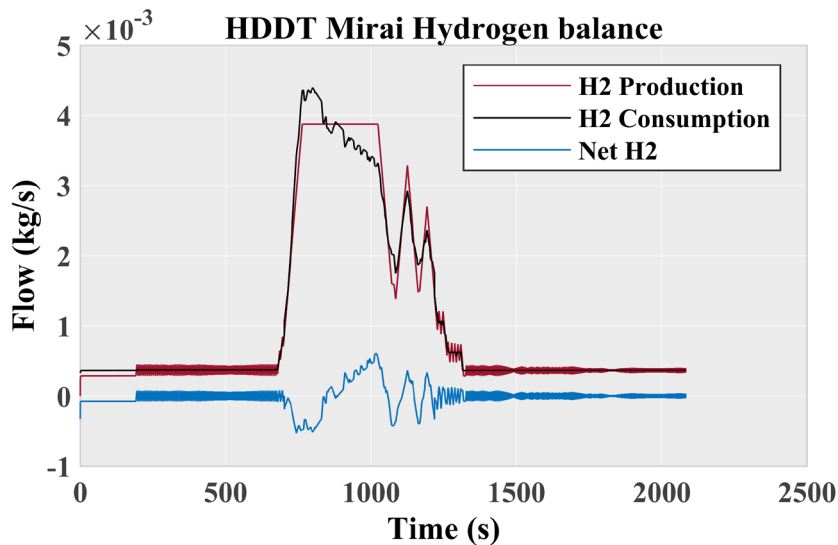


Figure 5.19. HDDT MIRAI FC Hydrogen balance.

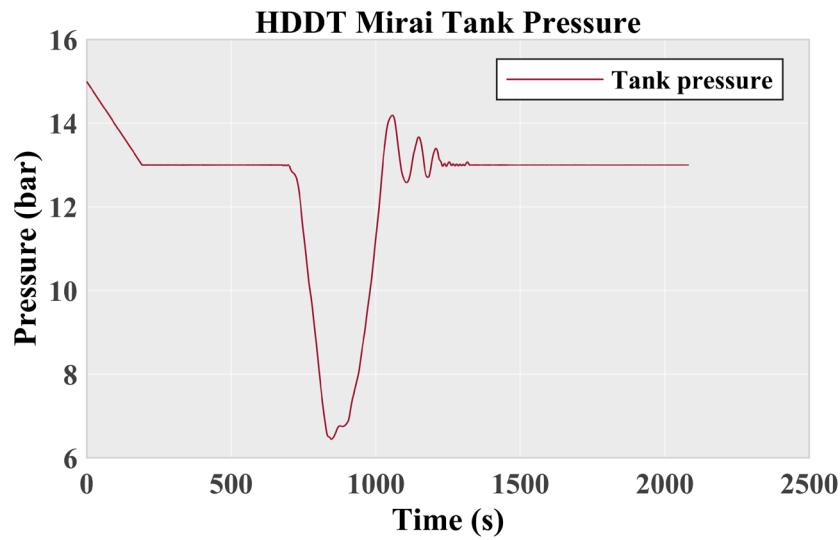


Figure 5.20. HDDT MIRAI FC Tank pressure.

Table 5.8. HDDT MIRAI FC Ammonia consumption.

Ammonia Consumption [kg]		
HDDT Cycle	400 km	800 km
12.66	136.47	272.95

Table 5.9. HDDT MIRAI FC Hydrogen consumption.

Hydrogen Consumption [kg]		
HDDT Cycle	400 km	800 km
2.22	23.98	47.95

Table 5.10. HDDT MIRAI FC required Ammonia for an autonomy of 400 and 800 km.

400 km		800 km	
Vol [l]	mass [kg]	Vol [m ³]	mass [kg]
226.32	136.47	452.65	272.95

Table 5.11. HDDT MIRAI FC cycle conditions.

FC Number	FC Unitary Power [kW]	Initial Temperature [K]
3	114	900

Table 5.12. HDDT MIRAI FC tank summary.

TANK VOLUME [l]			EMPTY TANK MASS [kg]		
HYDROGEN	AMMONIA		HYDROGEN	AMMONIA	
	400 km	800 km		400 km	800 km
100	250	500	75.8	231.4	312.57

VECTO LHR IUI CMT FC

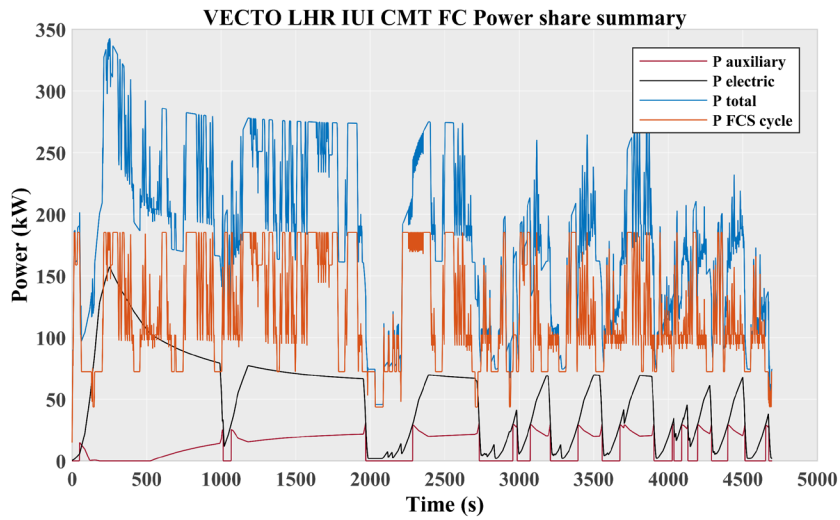


Figure 5.21. VECTO LHR IUI CMT FC Power share summary.

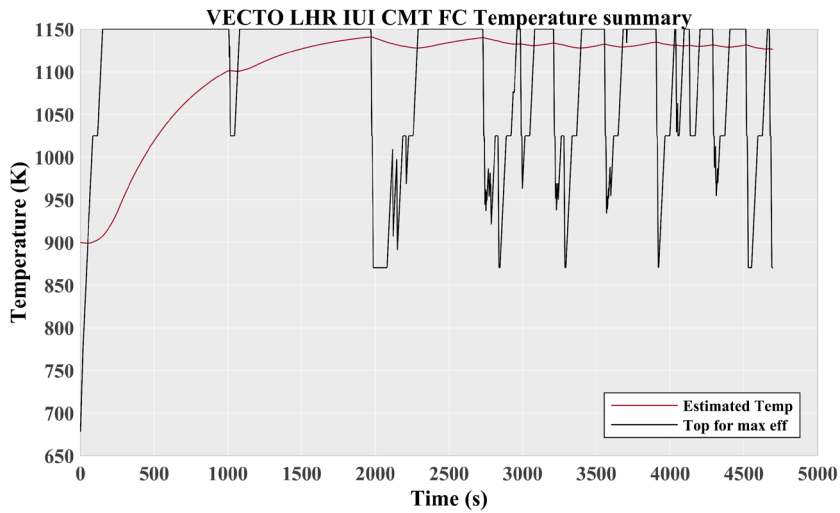


Figure 5.22. VECTO LHR IUI CMT FC Temperature summary.

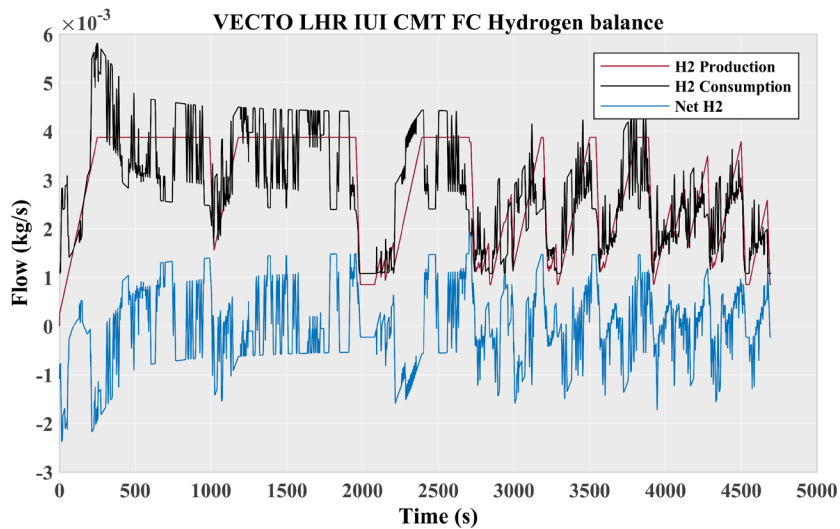


Figure 5.23. VECTO LHR IUI CMT FC Hydrogen balance.

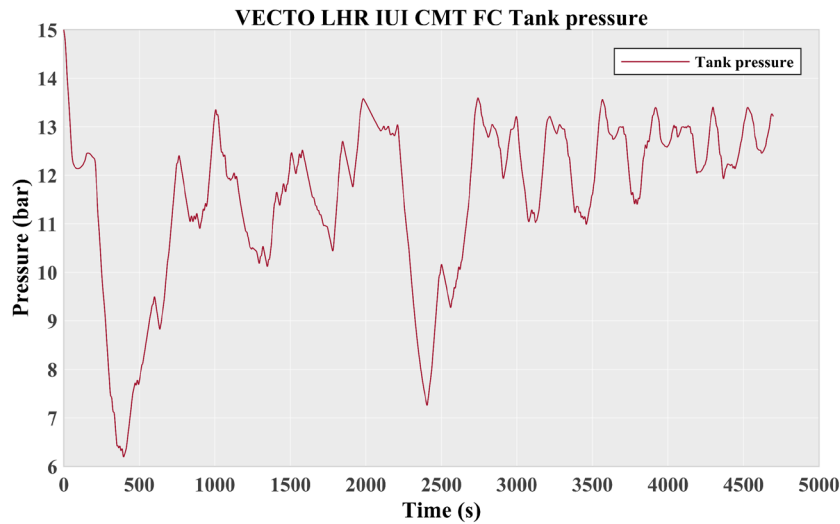


Figure 5.24. VECTO LHR IUI CMT FC Tank pressure.

Table 5.13. VECTO LHR IUI CMT FC Ammonia consumption.

Ammonia Consumption [kg]		
VECTO LHR Cycle	400 km	800 km
76.82	306.72	613.43

Table 5.14. VECTO LHR IUI CMT FC Hydrogen consumption.

Hydrogen Consumption [kg]			
VECTO LHR Cycle	400 km		800 km
13.47	53.79	107.58	

Table 5.15. VECTO LHR IUI CMT FC required Ammonia for 400 and 800 km of autonomy.

400 km		800 km	
Vol [l]	mass [kg]	Vol [m ³]	mass [kg]
508.65	306.72	1017.30	613.43

Table 5.16. VECTO LHR IUI CMT FC cycle conditions.

FC Number	FC Unitary Power [kW]	Initial Temperature [K]
6	60	900

Table 5.17. VECTO LHR IUI CMT FC tank summary.

TANK VOLUME [l]			EMPTY TANK MASS [kg]		
HYDROGEN	AMMONIA		HYDROGEN	AMMONIA	
	400 km	800 km		400 km	800 km
500	550	1100	163.0	328.0	507.43

VECTO LHR TOYOTA MIRAI FC

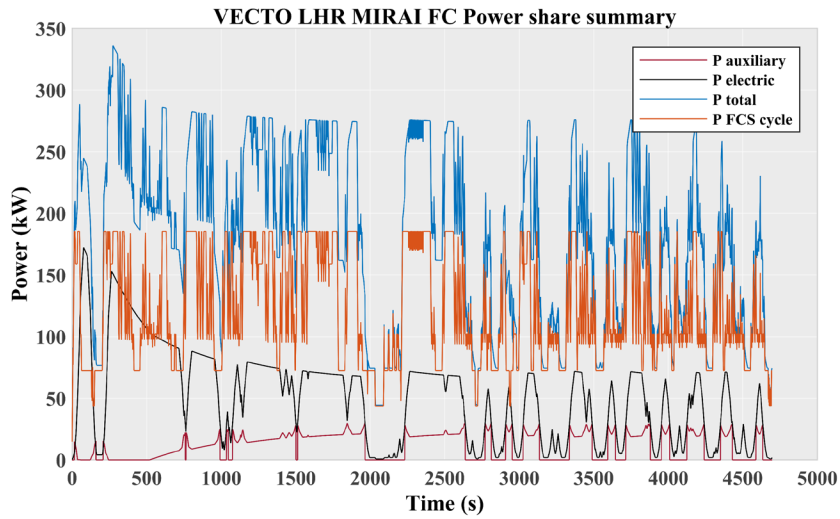


Figure 5.25. VECTO LHR MIRAI FC Power share summary.

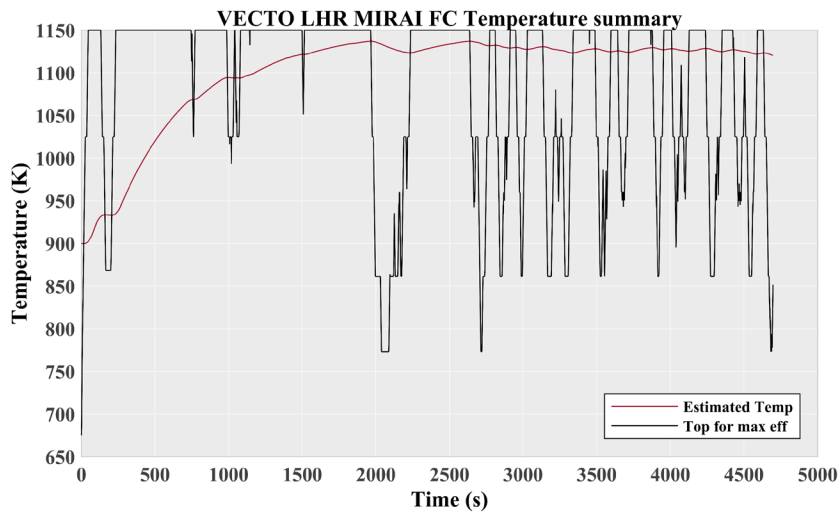


Figure 5.26. VECTO LHR MIRAI FC Temperature summary.

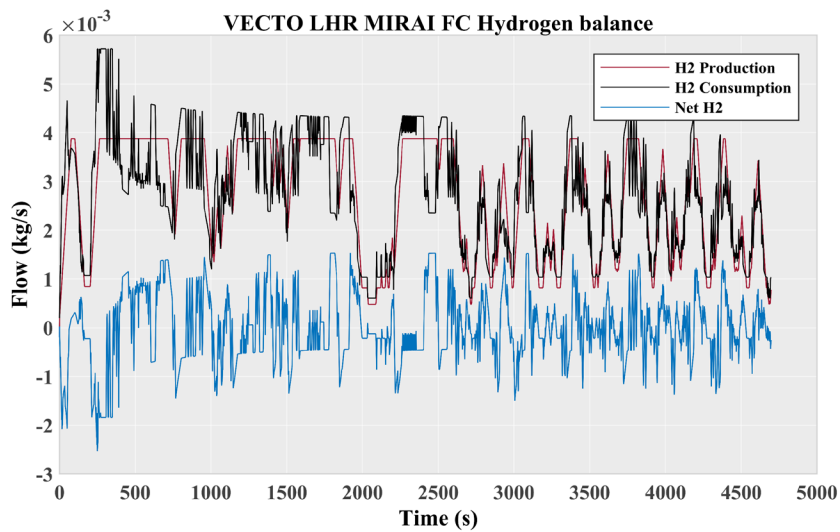


Figure 5.27. VECTO LHR MIRAI FC Hydrogen balance.

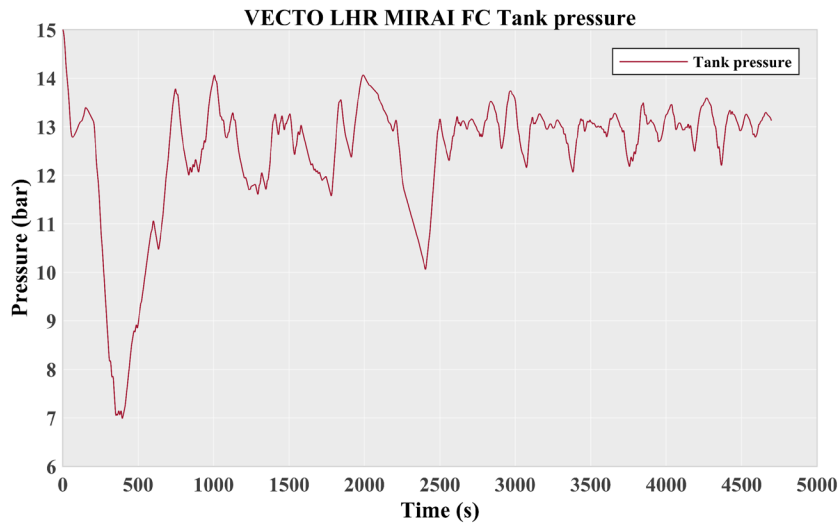


Figure 5.28. VECTO LHR MIRAI FC Tank pressure.

Table 5.18. VECTO LHR MIRAI FC Ammonia consumption.

Ammonia Consumption [kg]		
VECTO LHR Cycle	400 km	800 km
73.59	293.81	587.62

Table 5.19. VECTO LHR MIRAI FC Hydrogen consumption.

Hydrogen Consumption [kg]		
VECTO LHR Cycle Cycle	400 km	800 km
12.91	51.55	103.10

Table 5.20. VECTO LHR MIRAI FC required Ammonia for 400 and 800 km of autonomy.

400 km		800 km	
Vol [l]	mass [kg]	Vol [m ³]	mass [kg]
487.24	293.81	974.49	587.62

Table 5.21. VECTO LHR MIRAI FC cycle conditions.

FC Number	FC Unitary Power [kW]	Initial Temperature [K]
3	114	900

Table 5.22. VECTO LHR MIRAI FC tank summary.

TANK VOLUME [l]		EMMPTY TANK MASS [kg]			
HYDROGEN	AMMONIA		HYDROGEN	AMMONIA	
	400 km	800 km		400 km	800 km
500	500	1000	163.0	606.4	475.0

5.1.7 References

- [1] Islameka M., Budiman B.A., Juangsa F.B., Aziz M. “Energy management systems for battery electric vehicles”. *Emerging Trends in Energy Storage Systems and Industrial Applications*, 2023.
- [2] European Automobile Manufacturers’ Association. “What is WLTP and How Does It Work?”, 2017.
- [3] Richart B.S. “Análisis y propuestas de mejora de la red de abastecimiento de agua potable del Área Metropolitana de València en el subsistema Paterna-Bétera”, 2022.

5.2 Stage 6 – Final layout and specifications

After analysing the results from the different scenarios, several key points need to be highlighted:

1. The first is that, as mentioned in Section 5.1.1, the VECTO LHR cycle is significantly more demanding in terms of powertrain performance.
2. The second is that a critical factor is designing the combination of the fuel cell (FC) and battery to meet the demands of the vehicle's most likely driving cycle. In the following section, it is shown that three Toyota Mirai fuel cells are required for both the HDDT and VECTO LHR cycles. The HDDT cycle has much lower power demands, meaning the Toyota fuel cell configuration is considerably oversized for this cycle. If the vehicle is primarily expected to operate under conditions similar to the HDDT cycle, this can be addressed by adjusting the battery capacity, the energy management strategy (EMS), or by selecting a different FC model to better suit the vehicle's needs.
3. The third point is that, in this case, an SF for the CMR has been selected to satisfy the maximum Hydrogen demand based on the powertrain control of a conventional HDFCV. However, other controls and even changes to the powertrain layout can be explored, including testing different battery capacities, control regulations, and SF configurations for the CMR.

5.2.1 Summary of the final system

Table 5.23 provides a summary of the key aspects of the powertrain for each of the explored options.

Table 5.23. Powertrain summary.

PARAMETER	MIRAI FC		IUI CMT FC	
	HDDT	VECTO LHR	HDDT	VECTO LHR
CMR SF	0.3	0.3	0.3	0.3
Number of FC	3	3	4	6
FC Unitary Power [kW]	114	114	60	60
Initial CMR temperature [K]	900	900	900	900
Hydrogen				
Cycle consumption [kg]	2.22	12.91	2.96	13.47
400 km autonomy [kg]	23.98	51.55	31.90	53.79
800 km autonomy [kg]	47.95	103.10	63.81	107.58
Intermediate tank [l]	100	500	250	500
Intermediate tank weight [kg]	75.81	163.00	103.95	163.00
Ammonia				
Cycle consumption [kg]	12.66	73.59	16.75	76.82
400 km consumption [kg]	136.47	293.81	180.54	306.72
400 km consumption [l]	272.95	487.24	299.40	508.65
400 km Tank [l]	250	500	300	550
400 km Empty tank weight [kg]	231.37	312.57	247.61	328.80
800 km consumption [kg]	272.95	587.62	361.08	613.43
800 km consumption [l]	452.65	974.49	598.81	1017.30
800 km Tank [l]	500	1000	600	1100
800 km Empty tank weight [kg]	312.57	474.95	345.04	507.43

5.3 Stage 7 – Benchmark against current systems

At this stage, the powertrain incorporating the CMR will be compared to conventional FC powertrains.

5.3.1 Pressurized Hydrogen

Table 5.24. Powertrain benchmark.

DRIVING CYCLE POWERTRAIN FC MODEL	HDDT			VECTO LHR		
	CMR SYSTEM		CONV.	CMR SYSTEM		CONV.
	IUI CMT	MIRAI	IUI CMT	IUI CMT	MIRAI	MIRAI FC
FCS						
Unitary Power [kW]	60	114	60	60	114	114
Number of FC	4	3	2	6	3	2
Unitary Weight [kg]	190	230	190	190	230	230
Total Weight [kg]	760	690	380	1140	690	460
Battery						
Capacity [kWh]	73	73	73	79	79	79
Weight [kg]	714	714	714	750	750	750
CMR						
SF	0.3	0.3	-	0.3	0.3	-
Volume [m3]	0.173	0.173	-	0.173	0.173	-
Mass [kg]	468	468	-	468	468	-
HX weight [kg]						
HXH2	12.75	12.75	-	12.75	12.75	-
HXN2	12.80	12.80	-	12.80	12.80	-
Hydrogen-Air	2.03	2.03	-	2.03	2.03	-
Total Weight	27.58	27.58	-	27.58	27.58	-
Ammonia Tanks						
400 km - Volume [l]	300	250	-	550	500	-
400 km - Empty Weight [kg]	247.6	231.4	-	328.8	312.6	-
400 km - Full Weight [kg]	428.2	367.8	-	635.5	606.4	-
800 km - Volume [l]	600	500	-	1000	1100	-
800 km - Empty Weight [kg]	345.0	312.6	-	507.4	475.0	-
800 km - Full Weight [kg]	706.1	585.5	-	1120.9	1062.6	-
Hydrogen						
Cycle consumption [kg]	3.0	2.2	1.6	13.5	12.9	7.9
400 km - Consumption [kg]	31.9	24.0	16.9	53.8	51.6	31.6
400 km - Tank Weight [kg]	-	-	341.1	-	-	638.9
400 km - Full Weight [kg]	-	-	357.9	-	-	670.5
800 km - Consumption [kg]	63.8	48.0	33.7	107.6	103.1	63.2
800 km - Tank Weight [kg]	-	-	682.1	-	-	1277.8
800 km - Full Weight [kg]	-	-	715.8	-	-	1340.9
Intermediate tank volume [l]	250.0	100.0	-	500.0	500.0	-
Intermediate tank weight [kg]	103.9	75.8	-	163.0	163.0	-
400 km total weight [kg]	2501.7	2343.2	1451.9	3184.1	2705.0	1880.5
800 km total weight [kg]	2779.6	2560.9	1809.8	3669.4	3161.2	2550.9

Table 5.24 presents a comparison of all systems designed to operate with the CMR against a conventional FC system. It is important to highlight that all weight data have been obtained from databases property of IUI CMT.

Table 5.25 shows the percentual weight comparison across the different powertrains.

Table 5.25. CMR powertrains percentual weight increase.

DRIVING CYCLE POWERTRAIN FC MODEL	HDDT			VECTO LHR		
	CMR SYSTEM		CONV.	CMR SYSTEM		CONV.
	IUI CMT	MIRAI	IUI CMT	IUI CMT	MIRAI	MIRAI
400 km autonomy	72.30	61.39	Reference	69.33	43.85	Reference
800 km autonomy	53.59	41.50	Reference	43.85	23.92	Reference

As can be observed, the powertrains incorporating the CMR are heavier in all cases, with a smaller difference in those using the Toyota Mirai FC. A weight increment between 24 and 73 % can be quite notorious, however, considering that the vehicles weights 19 and 35 tons, a difference of 600 kg is not unmanageable. Table 5.26 provides a summary of the percentual weight difference of the vehicle that carries CMR powertrains compared to the conventional ones.

Table 5.26. CMR vehicle percentual weight increase.

DRIVING CYCLE POWERTRAIN FC MODEL	HDDT			VECTO LHR		
	CMR SYSTEM		CONV.	CMR SYSTEM		CONV.
	IUI CMT	MIRAI	IUI CMT	IUI CMT	MIRAI	MIRAI
400 km autonomy	5.01	4.25	Reference	3.53	2.24	Reference
800 km autonomy	4.55	3.52	Reference	2.98	1.63	Reference

The difference in this case is just 5% of the vehicle's total mass in the worst-case scenario. That means, the mass of the HDFCV carrying the CMR powertrain is on the same order of magnitude of its competitors. This may be a key factor when analysing the competitiveness of this system.

The key point is that the increase in weight for the CMR systems is mainly due to the need for greater stack power, and therefore, a higher number of FCs, along with the weight of the CMR itself. When comparing the weight of the tanks, it can be observed that in the case of CMR systems, especially when using the Toyota Mirai FC, the weight is lower than that of a conventional FC powertrain. From this observation, several important conclusions can be drawn.

The first is that the technological maturity of the CMR is relatively low, as these are novel technologies, and the FCs technology, although not that novel as there are already commercial solutions, still has room for improvement, particularly in their application to HDFCVs.

A more advanced CMR that:

1. Allows operation at higher pressures, reducing the weight of the intermediate Hydrogen tank.
2. Withstands higher temperatures, enabling smaller SFs to operate with greater Ammonia flow, thereby improving flexibility.
3. Is more efficient and consume less energy to operate, reducing the need for additional power compared to an equivalent system without the CMR.
4. Exhibits better thermal dynamics by heating up faster while maintaining slower cooling, enhancing system performance during transient conditions.

Would be greatly beneficial for the implementation of this powertrain concept. Additionally, the development of FCs with higher specific power would improve both powertrain designs, though systems incorporating the CMR would benefit more, as they require a greater number of FCs to achieve the same performance levels.

Secondly, it is essential to explore layout changes, that is, assessing the system's flexibility to operate with different battery capacities, or even without batteries, compared to the limitations faced by conventional systems. In this thesis, the CMR-based powertrains have been designed based on existing powertrains to provide an initial viability assessment. However, they have not been designed from scratch, nor have all system components, including unmodeled auxiliaries, been fully optimized. One example of potential energy improvement is the incorporation of a turbocharging stage, utilizing the Nitrogen released after Ammonia passes through the CMR, which could, for instance, increase the pressure of the intermediate storage tank, thereby lightening the overall system.

There are many possibilities to explore.

Chapter 6

Conclusions

This last chapter is written with two main purposes. On one hand, the general conclusions of each of the results and discussion chapters (4 and 5) are gathered and summarized. On the other hand, to summarize the work of this thesis and present a final conclusion regarding the viability of this novel powertrain architecture.

A model has been developed that accurately represents the behaviour of the CMR across different SF values ranging from 0.05 to 2. This model integrates the CMR with the three fluid streams of the system: NH_3 , H_2 , and N_2 . Additionally, the thermoelectric energy balance has been defined, allowing the model to determine each term of the balance at any given moment and under any operating condition. Furthermore, the model incorporates all the auxiliary components of the system and represents the various thermodynamic phenomena occurring within each of them.

The CMR has been characterized under steady-state conditions, both in thermal equilibrium and out of equilibrium. This has enabled a comparison of the different SF values under conditions of maximum efficiency and operational limits. After this analysis, it was determined that SF0.3 was the optimal value for the defined operating conditions: it is the lowest weight SF (468 kg) with maximum thermal efficiency (0.293) and capable of operating with an Ammonia flow rate of 80 kg/h. Subsequently, the thermal dynamics of the CMR for this specific SF were characterized.

Once the CMR was fully characterized, it was integrated with two previously calibrated and validated FC models: one FC owned by IUI CMT for HD applications and the Toyota Mirai FCS. The integration was carried out using Mean Value Models (MVM), resulting in a computationally efficient model with sufficient accuracy, allowing the analysis of different control strategies and parametric studies on various components of the powertrain.

Using this MVM, two reference driving cycles, HDDT and VECTO-LHR, were simulated to size the Ammonia and Hydrogen tanks for each powertrain configuration considered: CMR + IUI-CMT FC and CMR + Toyota Mirai FCS. These powertrains were compared with traditional FCS that operate with pressurized Hydrogen, leading to two main conclusions: although the powertrain incorporating the CMR is heavier, between 24% and 73%, the absolute difference is just 5% of the vehicle's total mass in the worst-case scenario; moreover, as the range requirements increase, these weight differences tend to diminish, as the conventional system is penalized by the significant weight of the Hydrogen tanks.

As a final conclusion, as discussed in Stage 7, the HDFCV incorporating the CMR, although heavier than alternatives using conventional FCS, remains within the same order of magnitude. Should the CMR be adapted to other fuels, the operational flexibility this offers, without excessively penalizing weight, could represent a competitive advantage over rivals and secure a market share if the design and implementation are executed correctly.

Chapter 7

Future Works

The scope of any research work, such as the one contained in this thesis, is finite and constrained by the tools, the previous state-of-the-art and the timeframe. This makes possible, and even necessary, to identify and describe the activities that could not be carried out in the final report of any research work. This last section of this thesis serves the purpose of presenting the activities that could arise using this work as the baseline for future research. Given the structure of this thesis, the advancements can be classified based on the optimization field and the level of innovation achieved.

While maintaining the current design, the optimization of the CMR can be approached in several ways:

- Conducting detailed studies on the CMR's efficiency at various operational points to more precisely identify the region of maximum efficiency, thus further optimizing the operating range. This could involve increasing resolution in the range of flow rates for Stage 1, adding more [flow-temperature] coordinate pairs for Stage 2, and testing additional power outputs for the auxiliary thermal source.
- Improving the characterization of dynamic performance. Now that the CMR's operational behaviour is better understood, investing the necessary computational resources would allow for a more refined analysis of the efficiency variation across different flow transitions, both ascending and descending, leading to the development of an appropriate transfer matrix.
- To verify that all the conclusions of this thesis are accurate, it is highly recommended to have a physical version of the CMR in order to validate both the static and dynamic models before carrying out more in-depth studies.

On the other hand, new CMR designs could result in a significant performance improvement:

- Size and pressure limitations. The size and weight of the intermediate Hydrogen storage tank are constrained by the CMR's operating pressure. Developing alternative CMR designs, either by using different materials or by reconfiguring internal components to allow for higher pressures without increasing the overall volume, could be a promising solution to address this limitation.
- Exploring alternative fuels. Although Ammonia has been the sole fuel used to feed the CMR in this thesis, the literature cited throughout the document supports the idea of using other fuels for Hydrogen synthesis. Methane, methanol and even water are proposed as some of the most promising alternatives.

Furthermore, a similar approach can be applied to the complete powertrain without altering the layout, improving its performance in several ways:

- Evaluating the response of the two configurations simulated in this thesis across various driving cycles would provide more comprehensive data on system performance in different environments. This would allow for finer tuning of the EMS and the pressure control of the intermediate storage tank. The recent surge in Artificial Intelligence within technological development and its spread across various sectors, could be leveraged here: AI could be employed to develop tailored control strategies for each driving route if pre-programmed in advance.
- In Section 5.1.6, the effect of starting a driving cycle at different temperatures is discussed. A topic that fell outside the scope of this section, however, is the calculation of the time required for the system to reach different initial temperatures for the CMR prior to driving cycles, as well as the energy required in each case. This analysis would assess the feasibility of starting the cycle without long setup delays for the powertrain.

It is also worth exploring alternative layouts:

- In this thesis, the CMR has only been combined with two FC models. Currently, there are numerous commercial solutions across different power ranges that deserve exploration. The powertrain resulting from integrating the CMR with the Toyota Mirai FCS has proven to be a better solution than the case involving the IUI CMT FC. This could also be the case with other FC systems.
- The battery used in the CMR powertrains was the same as in the conventional HDFCV. However, the intermediate Hydrogen tank can serve as an energy regulation mechanism similar to batteries. Given that incorporating the CMR requires additional FC stacks to meet its energy consumption, when the CMR operates at high efficiency points during the cycle (the CMR is cooling, and its current temperature exceeds the setpoint), and there is no demand from the auxiliary heat source, the extra 100 kW can be directed to the electric motors. This implies that, with sufficiently precise and robust control, smaller batteries could be used compared to current FC powertrains.

- As mentioned in Stage 7, it would be worth studying the feasibility of adding a turbocharging stage to harness the pressure energy from released Nitrogen and reduce the power consumed by the air compressor in the FCS. Another possible solution following this same philosophy is incorporating a turbine connected to a generator to help charge the battery.

Finally, although this thesis has focused on land transportation, specifically on HD applications, the CMR can be employed in various other fields. As demonstrated in Stage 7, the performance of the CMR improves compared to conventional FC powertrains as the autonomy requirement increases, opening up new avenues for application:

- Within transportation itself, its use in long-distance trains or maritime transport applications could be interesting to explore in terms of the performance of powertrains incorporating the CMR.
- Another possible application is its use in energy generation. Building Hydrogen pipelines to every location is expensive and complex, and sometimes the terrain makes it unfeasible. If Hydrogen needs to be transported by truck to a power plant, its appeal is diminished. Using Ammonia or other fuels would allow for transporting greater energy content per truckload, increasing the availability and flexibility of these plants.

Chapter 8
References

Bonanos, N., Knight, K. S. & Ellis, B.

Perovskite solid electrolytes: structure, transport properties and fuel cell applications.
Solid State Ionics, Vol. 79, pp. 161–170, 1995.

Capitao Alexandre, Jonsson Isak, Xisto Carlos, Lundbladh Anders, Grönstedt Tomas.

Compact heat exchangers for Hydrogen-fueled aero engine intercooling and recuperation.
Applied Thermal Engineering, Vol. 243 April, pp. 122538, 2024.

Desantes J. M., Molina S., Novella R. and Lopez-Juarez M.

Comparative global warming impact and NOX emissions of conventional and Hydrogen automotive propulsion systems.
Energy Conversion and Management, Vol. 221, pp. 113137, 2020.

Desantes J.M., Novella R., López-Juárez M., Nidáguila I.

Experimental assessment of a heavy-duty fuel cell system in relevant operating conditions.
Applied Energy Vol. 376, pp. 12493, 2024.

Elcogen.

Solid oxide stacks for fuel cell systems – Technical Data.

Engineers Edge.

Overall and Convective Heat Transfer Coefficients Table Chart.

European Automobile Manufacturers' Association.

CO2 emissions from heavy-duty vehicles.
2020.

European Automobile Manufacturers' Association.

What is WLTP and How Does It Work?
2017.

Fuel Cells & Hydrogen (FCH).

Hydrogen Roadmap Europe - a Sustainable Pathway for the European Energy Transition.
Publications Office of the European Union, 1st edition, 2019.

FUNKE.

Shell-and-Tube Heat Exchanger Datasheet.

Hamakawa, S., Hibino, T. & Iwahara, H.

Electrochemical Methane coupling using proton conductors.
Journal of the Electrochemical Society, Vol. 140, pp. 459–462, 1993.

Hyundai.

XCIENT Fuel Cell catalog
2020.

Incropera F. P., DeWitt D. P., Bergman T. L. and Levine A. S.

Fundamentals of Heat and Mass Transfer, 7th ed.
2011.

International Council Of Clean Transportation.

Vision 2050: A strategy to decarbonize the global transport sector by mid-century.
2020.

International Energy Agency.

Technology Roadmap Hydrogen and Fuel Cells.

International Energy Agency.

The Future of Hydrogen.

Technical Report June, 2019.

Islameka M., Budiman B.A., Juangsa F.B., Aziz M.

Energy management systems for battery electric vehicles.

Emerging Trends in Energy Storage Systems and Industrial Applications, 2023.

Iwahara, H., Uchida, H., Ono, K. & Ogaki, K.

Proton conduction in sintered oxides based on BaCeO₃.

Journal of the Electrochemical Society, Vol. 135, pp. 529–533, 1988.

Kjølseth C. et al.

Single-step Hydrogen production from NH₃, CH₄, and biogas in stacked proton ceramic reactors.

Science, Vol. 367, pp. 390–393, 2022.

Kreuer, K. D. Aspects of the formation and mobility of protonic charge carriers and the stability of perovskite-type oxides.

Solid State Ionics, Vol. 125, pp. 285–302, 1999.

Kreuer, K. D.

On the development of proton conducting materials for technological applications.

Solid State Ionics, Vol. 97, pp. 1–15, 1997.

Kreuer, K. D.

Proton-conducting oxides.

Annual Review of Materials Research, Vol. 33, pp. 333–359, 2003.

López-Juárez, M.

Analysis of Hydrogen fuel cell powerplant architectures for future transport applications.

2022.

López-Juárez M., Rockstroh T., Novella R., Vijayagopal R.

A methodology to develop multi-physics dynamic fuel cell system models validated with vehicle realistic drive cycle data.

Applied Energy Vol. 358, pp. 122568, 2024.

Malerød-Fjeld H., Clark D., Yuste-Tirados I., Zanón R., Catalán-Martínez D., Beeff D., Morejudo S. H., Vest P. K., Norby T., Haugsrud R., Serra J. M. and Kjøseth C.

Thermo-electrochemical production of compressed Hydrogen from Methane with near-zero energy loss.

Nature Energy, Vol. 2 n^o December, pp. 923-931, 2017.

Mathworks.

What Is the Genetic Algorithm?.

Morejudo, S. H. et al.

Direct conversion of Methane to aromatics in a catalytic co-ionic membrane reactor.

Science, Vol. 353, pp. 563–566, 2016.

Myung, J.-h, Neagu, D., Miller, D. N. & Irvine, J. T. S.

Switching on electrocatalytic activity in solid oxide cells.

Nature, Vol. 537, pp. 528–531, 2016.

Norby, T.

Solid-state protonic conductors: principles, properties, progress and prospects.

Solid State Ionics, Vol. 125, pp. 1–11, 1999.

Richart B.S.

Análisis y propuestas de mejora de la red de abastecimiento de agua potable del Área Metropolitana de València en el subsistema Paterna-Bétera.
2022.

Sengodan, S. et al.

Layered oxygen-deficient double perovskite as an efficient and stable anode for direct hydrocarbon solid oxide fuel cells.

Nature Materials, Vol. 14, pp. 205–209, 2015.

Swagelok.

Stainless Steel Seamless Tubing and Tube Support Systems.

THE EUROPEAN PARLIAMENT

Commission regulation (EU) 2017/2400.

United Nations

Department of Economic and Social Affairs.

World Population Prospects. 2019.

U.S. Energy Information Administration.
International Energy Outlook 2021, 10 2021.

Annex I

Stage 1 - Complete results summary

This annex includes the simulation results for the thermal equilibrium condition that were not presented in Section 4.1.7.

Table I.1. Stage 1 additional results Part 1.

SF	NH3 Flow [kg/h]	T _{op} [K]	I _{cell} [A/cm ²]	E _{cell} [V]	P _{el} [kW]	Ph _{CMR} [kW]	Q _{HXN2} [kW]	Q _{HXH2} [kW]	P _{H2} [kW]	P _{FCS} [kW]	P _{net} [kW]	Eff _{thermal} [-]	Eff _{H2} [-]
0.5	1.5	292	0.0173	0.0701	0.49	-0.78	-0.01	0.00					
	2.5	290	0.0288	0.1115	1.30	-0.82	-0.01	0.00					
	5	302	0.0577	0.2149	5.02	0.77	0.03	0.00					
	10	675	0.1153	0.4130	19.28	10.79	0.44	2.59	58.8	29.4	10.1	0.195	0.825
	20	769	0.2307	0.3493	32.62	15.39	1.09	5.88	117.6	58.8	26.2	0.252	0.861
	30.3	805	0.3495	0.3269	46.25	19.90	1.72	9.22	178.2	89.1	42.9	0.272	0.874
	40	881	0.4614	0.3171	59.22	24.20	2.35	12.40	235.3	117.6	58.4	0.281	0.880
	50	922	0.5767	0.3113	72.68	28.64	2.96	15.75	294.1	147.0	74.4	0.286	0.884
	60	958	0.6921	0.3077	86.21	33.09	3.53	19.13	352.9	176.5	90.2	0.289	0.886
	70	990	0.8074	0.3055	99.84	37.58	4.08	22.60	411.7	205.9	106.0	0.291	0.888
	80	1020	0.9228	0.3039	113.53	42.07	4.59	26.21	470.5	235.3	121.7	0.293	0.889
	90	1047	1.0381	0.3028	127.27	46.57	5.06	29.95	529.4	264.7	137.4	0.294	0.889
100	1072	1.1535	0.3019	140.98	50.99	5.62	33.84	588.2	294.1	153.1	0.294	0.890	
1	1.5	290	0.0087	0.0390	0.27	-1.00	-0.01	-0.01					
	2.5	286	0.0144	0.0597	0.70	-1.43	-0.01	0.00					
	5	284	0.0289	0.1115	2.60	-1.64	-0.02	0.01					
	10	304	0.0577	0.2150	10.04	1.55	0.00	0.08					
	20	679	0.1154	0.3973	37.10	20.10	0.85	4.73	117.6	58.8	21.7	0.209	0.834
	30.3	732	0.1748	0.3605	51.00	25.05	1.54	7.40	178.2	89.1	38.1	0.242	0.855
	40	771	0.2308	0.3425	63.98	29.51	2.23	9.92	235.3	117.6	53.7	0.258	0.865
	50	805	0.2885	0.3309	77.24	33.95	2.88	12.59	294.1	147.0	69.8	0.268	0.872
	60	834	0.3462	0.3231	90.52	38.34	3.51	15.28	352.9	176.5	85.9	0.275	0.877
	70	860	0.4039	0.3176	103.81	42.71	4.12	18.02	411.7	205.9	102.1	0.280	0.880
	80	883	0.4616	0.3135	117.10	47.04	4.74	20.84	470.5	235.3	118.2	0.284	0.883
	90	904	0.5193	0.3103	130.40	51.33	5.35	23.78	529.4	264.7	134.3	0.287	0.885
100	924	0.5770	0.3077	143.68	55.58	5.96	26.83	588.2	294.1	150.4	0.289	0.886	

Table I.2. Stage 1 additional results Part 2.

SF	NH3 Flow [kg/h]	T_op [K]	I_cell [A/cm2]	E_cell [V]	P_el [kW]	Ph_CMV [kW]	Q_HXN2 [kW]	Q_HXH2 [kW]	P H2 [kW]	P FCS [kW]	P net [kW]	Eff_thermal [-]	Eff_H2 [-]
1.5	1.5	290	0.0058	0.0287	0.20	-1.07	0.00	-0.01					
	2.5	287	0.0096	0.0425	0.50	-1.63	0.00	-0.01					
	5	280	0.0192	0.0770	1.80	-2.45	0.00	-0.02					
	10	282	0.0385	0.1460	6.82	-1.67	0.02	-0.05					
	20	365	0.0769	0.2840	26.52	9.54	0.03	0.84					
	30.3	682	0.1165	0.3905	55.25	29.49	1.21	6.50	178.2	89.1	33.9	0.215	0.837
	40	717	0.1538	0.3666	68.47	34.28	1.75	8.71	235.3	117.6	49.2	0.236	0.851
	50	747	0.1923	0.3507	81.88	38.96	2.26	11.05	294.1	147.0	65.2	0.251	0.860
	60	772	0.2308	0.3398	95.21	43.51	2.75	13.42	352.9	176.5	81.2	0.260	0.867
	70	795	0.2692	0.3320	108.50	47.98	3.23	15.82	411.7	205.9	97.4	0.267	0.871
	80	816	0.3077	0.3259	121.75	52.37	3.71	18.30	470.5	235.3	113.5	0.273	0.875
	90	835	0.3462	0.3212	134.97	56.7	4.19	20.87	529.4	264.7	129.7	0.277	0.878
100	852	0.3846	0.3173	148.15	60.96	4.67	23.54	588.2	294.1	145.9	0.281	0.880	
2	1.5	285	0.0043	0.0235	0.16	-1.11	0.00	-0.01					
	2.5	282	0.0072	0.0339	0.40	-1.73	0.00	-0.01					
	5	280	0.0144	0.0597	1.39	-2.85	0.01	-0.27					
	10	275	0.0289	0.1115	5.21	-3.28	0.03	-0.10					
	20	305	0.0577	0.2150	20.08	3.10	0.01	0.16					
	30.3	462	0.0874	0.3217	45.51	19.78	0.14	2.76					
	40	681	0.1154	0.3882	72.50	38.49	1.45	7.94	235.3	117.6	45.1	0.217	0.839
	50	709	0.1443	0.3688	86.10	43.42	1.87	10.07	294.1	147.0	60.9	0.234	0.850
	60	733	0.1731	0.3553	99.55	48.14	2.28	12.23	352.9	176.5	76.9	0.246	0.858
	70	754	0.2020	0.3454	112.90	52.74	2.68	14.44	411.7	205.9	93.0	0.255	0.863
	80	773	0.2308	0.3378	126.18	57.23	3.08	16.70	470.5	235.3	109.1	0.262	0.868
	90	790	0.2597	0.3317	139.39	61.63	3.47	19.04	529.4	264.7	125.3	0.268	0.872
100	807	0.2885	0.3267	152.55	65.94	3.88	21.48	588.2	294.1	141.5	0.272	0.875	

Annex II

Stage 2 - Complete results summary

This annex includes the simulation results for the simulations that were not presented in Section 4.2.3.

II. Additional Tables

Table II.1. Stage 2 – Results for SF0.05.

SF	NH3 Flow [kg/h]	T_target [K]	I_cell [A/cm ²]	E_cell [V]	P_el [kW]	Ph_CM _R [kW]	Conversion [-]	Extraction [-]	P_total [kW]	P_aux [kW]	X_3 [-]	X_2 [-]	X_1 [-]	Q_HXN2 [kW]	Q_HXH2 [kW]	P_H2 [kW]	P_FCS [kW]	P_net [kW]	E_sp [kWh/kgH ₂]	Eff_thermal [-]	Eff_H2 [-]
0.05	2.5	600	0.2860	1.0342	12.07	9.95	99.8727	98.9835	4.54	-7.53	1.000	1.000	0.708	155.28	529.28	14.70	7.35				
	2.5	800	0.2861	0.3400	3.97	1.81	99.9000	99.0000	6.16	2.19	1.000	1.000	1.000	155.84	882.43	14.70	7.35	1.19	13.96	0.092	0.767
	2.5	1000	0.2861	0.1111	1.30	-0.93	99.9001	99.0000	7.71	6.41	1.000	1.000	1.000	196.41	1273.70	14.70	7.35				
	2.5	1200	0.2861	0.0587	0.69	-1.60	99.9000	99.0000	9.04	8.35	1.000	1.000	1.000	251.48	1520.79	14.70	7.35				
	5	600	0.5569	2.0033	45.52	41.39	97.2325	98.8190	6.69	-38.83	1.000	1.000	0.627	204.80	1025.87	29.41	14.70				
	5	800	0.5722	0.6706	15.66	11.33	99.9000	99.0000	8.46	-7.20	1.000	1.000	1.000	220.76	1761.10	29.41	14.70				
	5	1000	0.5722	0.2104	4.91	0.46	99.9001	99.0000	10.02	5.11	1.000	1.000	1.000	250.42	2442.26	29.41	14.70	4.69	11.35	0.180	0.817
	5	1200	0.5722	0.1033	2.41	-2.17	99.9000	99.0000	11.34	8.93	1.000	1.000	1.000	289.54	2937.08	29.41	14.70	3.36	12.86	0.129	0.788
	10	600	0.9901	3.5446	143.19	100.00	86.4318	98.4777	46.35	-96.84	0.992	0.480	0.153	38.73	602.95	58.82	29.41				
	10	600	0.9901	3.5446	143.19	100.00	86.4318	98.4777	46.70	-96.50	1.000	0.828	0.523	261.14	1793.83	58.82	29.41				
	10	800	1.1444	1.3318	62.18	53.53	99.9000	99.0000	13.12	-49.06	1.000	1.000	1.000	357.31	3446.33	58.82	29.41				
	10	1000	1.1444	0.4090	19.10	10.19	99.9000	99.0000	14.85	-4.25	1.000	1.000	1.000	399.66	4635.35	58.82	29.41				
	10	1200	1.1444	0.1923	8.98	-0.18	99.9001	99.0000	16.18	7.20	1.000	1.000	1.000	398.57	5772.37	58.82	29.41	13.23	9.17	0.254	0.863
	20	600	2.2889	8.2131	766.99	100.00	99.9003	99.0000	672.62	-94.37	1.000	0.728	0.530	497.23	3725.99	117.64	58.82				
	20	800	2.2889	2.6540	247.85	100.00	99.9000	99.0000	154.48	-93.37	1.000	1.000	0.934	974.61	6288.15	117.64	58.82				
	20	1000	2.2889	0.8061	75.28	57.47	99.9001	99.0000	25.82	-49.46	1.000	1.000	1.000	870.06	8517.46	117.64	58.82				
	20	1200	2.2889	0.3705	34.60	16.27	99.9001	99.0000	27.26	-7.33	1.000	1.000	1.000	873.77	10599.97	117.64	58.82				
	30.3	600	3.4676	12.4431	1760.44	100.00	99.9002	99.0000	1668.68	-91.76	1.000	0.617	0.460	709.01	5079.45	178.22	89.11				
	30.3	800	3.4676	4.0160	568.18	100.00	99.9000	99.0000	477.46	-90.72	1.000	1.000	0.830	1835.20	8608.44	178.22	89.11				
	30.3	1000	3.4676	1.2152	171.93	100.00	99.9001	99.0000	83.18	-88.75	1.000	1.000	1.000	1476.75	11870.02	178.22	89.11				
	30.3	1200	3.4676	0.5539	78.37	50.61	99.9001	99.0000	40.11	-38.26	1.000	1.000	1.000	1543.44	14852.02	178.22	89.11				
	40	600	4.5778	16.4267	3068.05	100.00	99.9004	99.0000	2978.75	-89.30	1.000	0.545	0.410	776.38	6212.94	235.27	117.64				
	40	800	4.5777	5.2986	989.63	100.00	99.9000	99.0000	901.69	-87.94	1.000	1.000	0.756	2488.44	10553.98	235.27	117.64				
	40	1000	4.5777	1.6005	298.92	100.00	99.9000	99.0000	213.39	-85.53	1.000	1.000	1.000	2078.04	14814.61	235.27	117.64				
	40	1200	4.5777	0.7267	135.73	99.08	99.9001	99.0000	52.46	-83.26	1.000	1.000	1.000	2210.99	18549.92	235.27	117.64				
50	600	5.7222	20.5334	4793.84	100.00	99.9002	99.0000	4707.04	-86.80	1.000	0.495	0.370	795.22	7323.49	294.09	147.04					
50	800	5.7222	6.6209	1545.74	100.00	99.9000	99.0000	1460.77	-84.97	1.000	0.940	0.699	2839.60	12444.42	294.09	147.04					
50	1000	5.7222	1.9976	466.37	100.00	99.9002	99.0000	384.24	-82.13	1.000	1.000	1.000	2699.84	17686.45	294.09	147.04					
50	1200	5.7222	0.9048	211.24	100.00	99.9001	99.0000	130.84	-80.40	1.000	1.000	1.000	2933.88	22203.34	294.09	147.04					

Table II.2. Stage 2 – Results for SF0.1.

SF	NH3 Flow [kg/h]	T_target [K]	I_cell [A/cm2]	E_cell [V]	P_el [kW]	Ph_CM [kW]	Conversion [-]	Extraction [-]	P_total [kW]	P_aux [kW]	X_3 [-]	X_2 [-]	X_1 [-]	Q_HXN2 [kW]	Q_HXH2 [kW]	P_H2 [kW]	P_FCS [kW]	P_net [kW]	E_sp [kWh/kgH2]	Eff_thermal [-]	Eff_H2 [-]
0.1	2.5	600	0.1438	0.5238	6.12	3.99	99.9000	99.0000	5.34	-0.78	1.000	1.000	0.708	155.29	529.51	14.70	7.35				
	2.5	800	0.1438	0.1756	2.05	-0.11	99.9004	99.0000	7.49	5.44	1.000	1.000	1.000	155.84	882.44	14.70	7.35				
	2.5	1000	0.1438	0.0617	0.72	-1.51	99.9001	99.0000	9.57	8.85	1.000	1.000	1.000	196.41	1273.70	14.70	7.35				
	2.5	1200	0.1438	0.0366	0.43	-1.86	99.9001	99.0000	11.43	11.00	1.000	1.000	1.000	251.48	1520.79	14.70	7.35				
	5	600	0.2874	1.0392	24.25	20.01	99.8688	98.9831	7.59	-16.66	1.000	1.000	0.644	207.60	1055.30	29.41	14.70				
	5	800	0.2875	0.3417	7.98	3.65	99.9002	99.0000	9.79	1.81	1.000	1.000	1.000	220.76	1761.11	29.41	14.70	4.92	11.09	0.189	0.822
	5	1000	0.2875	0.1116	2.61	-1.85	99.9000	99.0000	11.88	9.27	1.000	1.000	1.000	250.42	2442.26	29.41	14.70	2.83	13.46	0.109	0.776
	5	1200	0.2875	0.0590	1.38	-3.20	99.9000	99.0000	13.73	12.36	1.000	1.000	1.000	289.54	2937.08	29.41	14.70	0.97	15.56	0.037	0.740
	10	600	0.5594	2.0122	91.41	83.15	97.1900	98.8170	12.42	-78.99	1.000	0.883	0.590	280.16	2011.31	58.82	29.41				
	10	800	0.5750	0.6739	31.47	22.81	99.9000	99.0000	14.45	-17.02	1.000	1.000	1.000	357.31	3446.33	58.82	29.41				
	10	1000	0.5750	0.2114	9.87	0.96	99.9000	99.0000	16.71	6.84	1.000	1.000	1.000	399.66	4635.35	58.82	29.41	12.70	9.47	0.244	0.856
	10	1200	0.5750	0.1037	4.84	-4.32	99.9000	99.0000	18.57	13.73	1.000	1.000	1.000	398.57	5772.37	58.82	29.41	10.84	10.52	0.208	0.833
	20	600	0.9938	3.5574	287.05	100.00	86.3216	98.4751	193.77	-93.29	1.000	0.664	0.466	452.12	3307.51	117.64	58.82				
	20	800	1.1501	1.3383	124.98	100.00	99.9000	99.0000	32.93	-92.05	1.000	1.000	0.934	974.61	6288.15	117.64	58.82				
	20	1000	1.1501	0.4110	38.38	20.56	99.9002	99.0000	27.68	-10.69	1.000	1.000	1.000	870.05	8517.47	117.64	58.82				
	20	1200	1.1501	0.1932	18.04	-0.28	99.9001	99.0000	29.65	11.61	1.000	1.000	1.000	873.77	10599.97	117.64	58.82	29.16	8.40	0.280	0.880
	30.3	600	1.3204	4.7150	505.54	100.00	75.7077	98.2568	415.19	-90.35	1.000	0.519	0.367	614.97	4158.94	178.22	89.11				
	30.3	800	1.7424	2.0226	286.16	100.00	99.9000	99.0000	196.76	-89.40	1.000	1.000	0.830	1835.20	8608.44	178.22	89.11				
	30.3	1000	1.7424	0.6165	87.22	60.23	99.9001	99.0000	40.09	-47.13	1.000	1.000	1.000	1476.75	11870.02	178.22	89.11				
	30.3	1200	1.7424	0.2854	40.38	12.62	99.9001	99.0000	42.50	2.12	1.000	1.000	1.000	1543.44	14852.01	178.22	89.11	46.61	7.95	0.296	0.891
	40	600	2.3002	8.2535	1541.54	100.00	99.9004	99.0000	1453.03	-88.51	1.000	0.545	0.410	776.38	6212.94	235.27	117.64				
	40	800	2.3001	2.6671	498.13	100.00	99.9000	99.0000	411.52	-86.61	1.000	1.000	0.756	2488.44	10553.98	235.27	117.64				
	40	1000	2.3002	0.8101	151.30	100.00	99.9002	99.0000	67.62	-83.67	1.000	1.000	1.000	2078.04	14814.62	235.27	117.64				
	40	1200	2.3001	0.3722	69.52	32.87	99.9001	99.0000	54.85	-14.67	1.000	1.000	1.000	2210.99	18549.92	235.27	117.64				
	50	600	2.8752	10.3170	2408.67	100.00	99.9001	99.0000	2322.67	-86.00	1.000	0.495	0.370	795.22	7323.49	294.09	147.04				
	50	800	2.8752	3.3315	777.78	100.00	99.9000	99.0000	694.14	-83.64	1.000	0.940	0.699	2839.60	12444.42	294.09	147.04				
	50	1000	2.8752	1.0096	235.71	100.00	99.9002	99.0000	155.44	-80.28	1.000	1.000	1.000	2699.84	17686.45	294.09	147.04				
	50	1200	2.8752	0.4617	107.79	61.99	99.9000	99.0000	67.79	-40.00	1.000	1.000	1.000	2933.88	22203.33	294.09	147.04				
	60	600	3.4502	12.3806	3468.53	100.00	99.9004	99.0000	3385.01	-83.51	1.000	0.459	0.336	790.31	8391.24	352.91	176.45				
	60	800	3.4502	3.9958	1119.47	100.00	99.9000	99.0000	1038.81	-80.65	1.000	0.881	0.651	3102.20	14234.78	352.91	176.45				
	60	1000	3.4502	1.2092	338.76	100.00	99.9002	99.0000	261.83	-76.93	1.000	1.000	1.000	3275.81	20388.48	352.91	176.45				
	60	1200	3.4502	0.5512	154.43	99.46	99.9000	99.0000	80.71	-73.71	1.000	1.000	1.000	3579.64	25718.86	352.91	176.45				
80	600	4.6003	16.5076	6166.33	100.00	99.9004	99.0000	6087.69	-78.64	1.000	0.414	0.286	751.42	10531.04	470.54	235.27					
80	800	4.6003	5.3246	1988.98	100.00	99.9000	99.0000	1914.24	-74.74	1.000	0.799	0.578	3482.95	17688.46	470.54	235.27					
80	1000	4.6003	1.6083	600.76	100.00	99.9002	99.0000	530.35	-70.41	1.000	1.000	0.940	4813.88	25385.39	470.54	235.27					
80	1200	4.6003	0.7302	272.76	100.00	99.9001	99.0000	205.91	-66.85	1.000	1.000	1.000	4756.83	32616.53	470.54	235.27					

Table II.3. Stage 2 – Results for SF0.2.

SF	NH3 Flow [kg/h]	T_target [K]	I_cell [A/cm2]	E_cell [V]	P_el [kW]	Ph_CMV [kW]	Conversion [-]	Extraction [-]	P_total [kW]	P_aux [kW]	X_3 [-]	X_2 [-]	X_1 [-]	Q_HXN2 [kW]	Q_HXH2 [kW]	P_H2 [kW]	P_FCS [kW]	P_net [kW]	E_sp [kWh/kgH2]	Eff_thermal [-]	Eff_H2 [-]
0.2	5	673	0.1441	0.5251	12.26	8.01	99.9000	99.0000	9.72	-2.54	1.000	1.000	0.764	269.52	1231.74	29.41	14.70				
	5	775	0.1441	0.2113	4.93	0.62	99.9000	99.0000	11.70	6.76	1.000	1.000	1.000	218.53	1673.52	29.41	14.70	3.01	13.26	0.116	0.780
	5	900	0.1441	0.0960	2.24	-2.15	99.9002	99.0000	13.61	11.37	1.000	1.000	1.000	235.51	2105.57	29.41	14.70	1.09	15.43	0.042	0.742
	5	1025	0.1441	0.0566	1.32	-3.15	99.9001	99.0000	15.45	14.12	1.000	1.000	1.000	252.94	2529.66	29.41	14.70				
	5	1150	0.1441	0.0403	0.94	-3.61	99.9002	99.0000	17.19	16.25	1.000	1.000	1.000	277.75	2830.38	29.41	14.70				
	10	673	0.2881	1.0418	48.63	40.14	99.8668	98.9829	14.51	-34.12	1.000	1.000	0.715	385.32	2412.39	58.82	29.41				
	10	775	0.2882	0.4135	19.31	10.69	99.9001	99.0000	16.32	-2.98	1.000	1.000	0.986	353.24	3283.68	58.82	29.41				
	10	900	0.2882	0.1814	8.47	-0.31	99.9002	99.0000	18.36	9.90	1.000	1.000	1.000	378.31	4073.86	58.82	29.41	11.04	10.41	0.212	0.836
	10	1025	0.2882	0.1011	4.72	-4.22	99.9002	99.0000	20.30	15.58	1.000	1.000	1.000	403.54	4772.71	58.82	29.41	9.11	11.50	0.175	0.814
	10	1150	0.2882	0.0670	3.13	-5.97	99.9001	99.0000	22.06	18.93	1.000	1.000	1.000	406.01	5479.77	58.82	29.41	7.35	12.50	0.141	0.794
	20	673	0.5607	2.0167	183.18	166.66	97.1685	98.8160	87.66	-95.52	1.000	0.941	0.681	900.36	4657.74	117.64	58.82				
	20	775	0.5765	0.8178	76.37	59.13	99.9000	99.0000	27.10	-49.28	1.000	1.000	0.883	1070.05	5962.88	117.64	58.82				
	20	900	0.5765	0.3521	32.88	15.32	99.9002	99.0000	29.29	-3.59	1.000	1.000	1.000	840.20	7441.42	117.64	58.82				
	20	1025	0.5765	0.1900	17.75	-0.13	99.9001	99.0000	31.28	13.53	1.000	1.000	1.000	874.95	8789.04	117.64	58.82	27.54	8.86	0.265	0.870
	20	1150	0.5765	0.1204	11.25	-6.95	99.9001	99.0000	33.11	21.86	1.000	1.000	1.000	882.54	10087.59	117.64	58.82	25.71	9.38	0.247	0.858
	30.3	673	0.8733	1.3062	184.79	158.70	99.9000	99.0000	84.79	-100.00	1.000	1.000	0.775	1855.02	8066.78	178.22	89.11				
	30.3	775	0.8733	1.2090	171.05	144.92	99.9000	99.0000	88.07	-82.99	1.000	1.000	0.789	1892.03	8219.75	178.22	89.11				
	30.3	900	0.8733	0.5279	74.69	48.09	99.9002	99.0000	41.32	-33.37	1.000	1.000	1.000	1411.18	10393.89	178.22	89.11				
	30.3	1025	0.8733	0.2817	39.85	12.76	99.9002	99.0000	43.78	3.93	1.000	1.000	1.000	1493.97	12237.77	178.22	89.11	45.33	8.19	0.288	0.885
	30.3	1150	0.8733	0.1754	24.82	-2.75	99.9001	99.0000	45.90	21.08	1.000	1.000	1.000	1545.14	14100.66	178.22	89.11	43.21	8.58	0.274	0.876
	40	673	1.1529	0.8138	151.99	117.01	99.9000	99.0000	51.99	-100.00	1.000	1.000	0.895	2408.39	12210.27	235.27	117.64				
	40	775	1.1529	0.8138	151.99	117.00	99.9000	99.0000	51.99	-100.00	1.000	1.000	0.895	2408.37	12210.37	235.27	117.64				
	40	900	1.1529	0.6935	129.53	94.41	99.9000	99.0000	52.75	-76.77	1.000	1.000	0.947	2220.54	12821.82	235.27	117.64				
	40	1025	1.1529	0.3679	68.72	32.97	99.9002	99.0000	55.72	-13.00	1.000	1.000	1.000	2102.68	15276.87	235.27	117.64				
	40	1150	1.1529	0.2272	42.44	6.05	99.9001	99.0000	58.17	15.73	1.000	1.000	1.000	2199.66	17598.51	235.27	117.64	59.46	8.24	0.286	0.884
	50	673	1.4411	0.7094	165.61	121.49	99.9003	99.0000	65.61	-100.00	1.000	1.000	0.950	2869.79	16084.76	294.09	147.04				
	50	775	1.4411	0.7094	165.61	121.49	99.9003	99.0000	65.61	-100.00	1.000	1.000	0.950	2869.79	16084.76	294.09	147.04				
	50	900	1.4411	0.7094	165.61	121.49	99.9003	99.0000	65.61	-100.00	1.000	1.000	0.950	2869.79	16084.76	294.09	147.04				
	50	1025	1.4411	0.4569	106.67	61.97	99.9002	99.0000	68.12	-38.54	1.000	1.000	1.000	2734.51	18249.82	294.09	147.04				
	50	1150	1.4411	0.2806	65.52	20.03	99.9000	99.0000	70.99	5.48	1.000	1.000	1.000	2894.90	21060.21	294.09	147.04	76.05	8.05	0.292	0.888
	60	673	1.7294	0.6405	179.43	126.07	99.9001	99.0000	79.43	-100.00	1.000	1.000	1.000	3264.78	20129.35	352.91	176.45				
	60	775	1.7294	0.6405	179.43	126.07	99.9001	99.0000	79.43	-100.00	1.000	1.000	1.000	3264.78	20129.35	352.91	176.45				
	60	900	1.7294	0.6405	179.43	126.07	99.9001	99.0000	79.43	-100.00	1.000	1.000	1.000	3264.78	20129.35	352.91	176.45				
	60	1025	1.7294	0.5458	152.92	99.29	99.9001	99.0000	80.48	-72.44	1.000	1.000	1.000	3310.19	21063.26	352.91	176.45				
	60	1150	1.7294	0.3340	93.58	39.00	99.9000	99.0000	83.78	-9.81	1.000	1.000	1.000	3514.37	24385.96	352.91	176.45				
	80	673	2.3058	0.5551	207.35	135.20	99.9002	99.0000	107.35	-100.00	1.000	1.000	1.000	4556.30	28666.63	470.54	235.27				
	80	775	2.3058	0.5551	207.35	135.20	99.9002	99.0000	107.35	-100.00	1.000	1.000	1.000	4556.30	28666.63	470.54	235.27				
	80	900	2.3058	0.5551	207.35	135.20	99.9002	99.0000	107.35	-100.00	1.000	1.000	1.000	4556.30	28666.63	470.54	235.27				
	80	1025	2.3058	0.5551	207.35	135.20	99.9002	99.0000	107.35	-100.00	1.000	1.000	1.000	4556.30	28666.63	470.54	235.27				
	80	1150	2.3058	0.4408	164.67	91.90	99.9000	99.0000	109.25	-55.42	1.000	1.000	1.000	4673.89	30855.21	470.54	235.27				
100	673	2.8823	0.5040	235.32	144.04	99.9002	99.0000	135.32	-100.00	1.000	1.000	1.000	5842.68	38403.51	588.18	294.09					
100	775	2.8823	0.5040	235.32	144.04	99.9002	99.0000	135.32	-100.00	1.000	1.000	1.000	5842.68	38403.51	588.18	294.09					
100	900	2.8823	0.5040	235.32	144.04	99.9002	99.0000	135.32	-100.00	1.000	1.000	1.000	5842.68	38403.51	588.18	294.09					
100	1025	2.8823	0.5040	235.32	144.04	99.9002	99.0000	135.32	-100.00	1.000	1.000	1.000	5842.68	38403.51	588.18	294.09					
100	1150	2.8823	0.5040	235.32	144.04	99.9002	99.0000	135.32	-100.00	1.000	1.000	1.000	5842.68	38403.51	588.18	294.09					

Table II.4. Stage 2 – Results for SF0.3.

SF	NH3 Flow [kg/h]	T_target [K]	I_cell [A/cm2]	E_cell [V]	P_el [kW]	Ph_CMV [kW]	Conversion [-]	Extraction [-]	P_total [kW]	P_aux [kW]	X_3 [-]	X_2 [-]	X_1 [-]	Q_HXN2 [kW]	Q_HXH2 [kW]	P H2 [kW]	P FCS [kW]	P net [kW]	E_sp [kWh/kgH2]	Eff_thermal [-]	Eff_H2 [-]
0.3	5	673	0.0962	0.3530	8.24	4.00	99.9000	99.0000	11.19	2.94	1.000	1.000	0.764	269.52	1231.74	29.41	14.70	3.52	12.68	0.135	0.791
	5	775	0.0962	0.1441	3.36	-0.95	99.9003	99.0000	13.68	10.32	1.000	1.000	1.000	218.53	1673.52	29.41	14.70	1.02	15.51	0.039	0.741
	5	900	0.0962	0.0676	1.58	-2.81	99.9000	99.0000	16.12	14.54	1.000	1.000	1.000	235.51	2105.57	29.41	14.70				
	5	1025	0.0962	0.0418	0.98	-3.49	99.9002	99.0000	18.48	17.50	1.000	1.000	1.000	252.94	2529.66	29.41	14.70				
	5	1150	0.0962	0.0314	0.73	-3.81	99.9001	99.0000	20.75	20.01	1.000	1.000	1.000	277.75	2830.38	29.41	14.70				
	10	673	0.1923	0.6981	32.60	24.10	99.9000	99.0000	15.98	-16.62	1.000	1.000	0.716	385.42	2413.53	58.82	29.41				
	10	775	0.1923	0.2789	13.02	4.40	99.9002	99.0000	18.31	5.28	1.000	1.000	0.986	353.24	3283.69	58.82	29.41	11.10	10.38	0.213	0.837
	10	900	0.1923	0.1246	5.82	-2.96	99.9002	99.0000	20.87	15.06	1.000	1.000	1.000	378.31	4073.86	58.82	29.41	8.53	11.83	0.164	0.807
	10	1025	0.1923	0.0715	3.34	-5.60	99.9000	99.0000	23.33	19.99	1.000	1.000	1.000	403.54	4772.71	58.82	29.41	6.08	13.22	0.117	0.781
	10	1150	0.1923	0.0493	2.30	-6.80	99.9001	99.0000	25.61	23.31	1.000	1.000	1.000	406.01	5479.77	58.82	29.41	3.80	14.51	0.073	0.758
	20	673	0.3830	1.3670	127.11	110.20	99.4706	98.9478	27.11	-100.00	1.000	0.919	0.674	826.03	4648.67	117.64	58.82				
	20	775	0.3846	0.5487	51.24	34.00	99.9001	99.0000	29.08	-22.16	1.000	1.000	0.883	1070.05	5962.88	117.64	58.82				
	20	900	0.3846	0.2385	22.27	4.71	99.9002	99.0000	31.80	9.53	1.000	1.000	1.000	840.20	7441.42	117.64	58.82	27.01	9.01	0.260	0.866
	20	1025	0.3846	0.1308	12.22	-5.66	99.9002	99.0000	34.31	22.09	1.000	1.000	1.000	874.95	8789.04	117.64	58.82	24.51	9.72	0.236	0.851
	20	1150	0.3846	0.0849	7.93	-10.27	99.9001	99.0000	36.66	28.74	1.000	1.000	1.000	882.54	10087.59	117.64	58.82	22.15	10.39	0.213	0.836
	30.3	673	0.5827	0.9908	140.18	114.15	99.9000	99.0000	40.18	-100.00	1.000	0.991	0.739	1676.23	7759.13	178.22	89.11				
	30.3	775	0.5827	0.8266	116.94	90.82	99.9000	99.0000	40.62	-76.32	1.000	1.000	0.781	1823.10	8158.78	178.22	89.11				
	30.3	900	0.5827	0.3558	50.34	23.73	99.9003	99.0000	43.83	-6.50	1.000	1.000	1.000	1411.18	10393.90	178.22	89.11				
	30.3	1025	0.5827	0.1920	27.16	0.08	99.9002	99.0000	46.81	19.65	1.000	1.000	1.000	1493.97	12237.77	178.22	89.11	42.30	8.75	0.268	0.872
	30.3	1150	0.5827	0.1216	17.20	-10.36	99.9000	99.0000	49.45	32.25	1.000	1.000	1.000	1545.14	14100.66	178.22	89.11	39.66	9.25	0.252	0.861
	40	673	0.7692	0.8175	152.68	118.00	99.9001	99.0000	52.68	-100.00	1.000	1.000	0.780	2587.09	10843.29	235.27	117.64				
	40	775	0.7692	0.8175	152.68	118.00	99.9001	99.0000	52.68	-100.00	1.000	1.000	0.780	2587.09	10843.29	235.27	117.64				
	40	900	0.7692	0.4663	87.09	51.97	99.9001	99.0000	55.26	-31.82	1.000	1.000	0.947	2220.54	12821.83	235.27	117.64				
	40	1025	0.7692	0.2495	46.61	10.85	99.9000	99.0000	58.75	12.14	1.000	1.000	1.000	2102.69	15276.86	235.27	117.64	58.88	8.32	0.283	0.882
	40	1150	0.7692	0.1561	29.16	-7.23	99.9001	99.0000	61.73	32.57	1.000	1.000	1.000	2199.66	17598.51	235.27	117.64	55.91	8.75	0.269	0.872
	50	673	0.9616	0.7106	165.90	122.21	99.9000	99.0000	65.90	-100.00	1.000	1.000	0.819	3246.79	14217.63	294.09	147.04				
	50	775	0.9616	0.7106	165.90	122.21	99.9000	99.0000	65.90	-100.00	1.000	1.000	0.819	3246.79	14217.63	294.09	147.04				
	50	900	0.9616	0.5802	135.45	91.55	99.9000	99.0000	67.03	-68.42	1.000	1.000	0.883	3117.98	15124.20	294.09	147.04				
	50	1025	0.9616	0.3089	72.11	27.42	99.9001	99.0000	71.16	-0.96	1.000	1.000	1.000	2734.51	18249.81	294.09	147.04				
	50	1150	0.9616	0.1918	44.77	-0.71	99.9001	99.0000	74.55	29.78	1.000	1.000	1.000	2894.90	21060.22	294.09	147.04	72.49	8.45	0.279	0.879
	60	673	1.1539	0.6402	179.36	126.58	99.9003	99.0000	79.36	-100.00	1.000	1.000	0.855	3837.23	17724.30	352.91	176.45				
	60	775	1.1539	0.6402	179.36	126.58	99.9003	99.0000	79.36	-100.00	1.000	1.000	0.855	3837.23	17724.30	352.91	176.45				
	60	900	1.1539	0.6402	179.36	126.58	99.9003	99.0000	79.36	-100.00	1.000	1.000	0.855	3837.23	17724.30	352.91	176.45				
	60	1025	1.1539	0.3682	103.16	49.53	99.9002	99.0000	83.51	-19.65	1.000	1.000	1.000	3310.18	21063.27	352.91	176.45				
	60	1150	1.1539	0.2274	63.71	9.13	99.9001	99.0000	87.33	23.62	1.000	1.000	1.000	3514.37	24385.97	352.91	176.45	89.12	8.25	0.286	0.884
	80	673	1.5385	0.5537	206.84	135.62	99.9001	99.0000	106.84	-100.00	1.000	1.000	0.934	4841.40	25261.90	470.54	235.27				
	80	775	1.5385	0.5537	206.84	135.62	99.9001	99.0000	106.84	-100.00	1.000	1.000	0.934	4841.40	25261.90	470.54	235.27				
	80	900	1.5385	0.5537	206.84	135.62	99.9001	99.0000	106.84	-100.00	1.000	1.000	0.934	4841.40	25261.90	470.54	235.27				
	80	1025	1.5385	0.4869	181.89	110.38	99.9000	99.0000	108.13	-73.76	1.000	1.000	0.990	4573.28	26385.52	470.54	235.27				
	80	1150	1.5385	0.2987	111.57	38.79	99.9001	99.0000	112.81	1.24	1.000	1.000	1.000	4673.89	30855.22	470.54	235.27	122.46	7.99	0.294	0.890
100	673	1.9231	0.5028	234.76	144.82	99.9001	99.0000	134.76	-100.00	1.000	1.000	1.000	5652.97	33614.62	588.18	294.09					
100	775	1.9231	0.5028	234.76	144.82	99.9001	99.0000	134.76	-100.00	1.000	1.000	1.000	5652.97	33614.62	588.18	294.09					
100	900	1.9231	0.5028	234.76	144.82	99.9001	99.0000	134.76	-100.00	1.000	1.000	1.000	5652.97	33614.62	588.18	294.09					
100	1025	1.9231	0.5028	234.76	144.82	99.9001	99.0000	134.76	-100.00	1.000	1.000	1.000	5652.97	33614.62	588.18	294.09					
100	1150	1.9231	0.3699	172.73	81.76	99.9001	99.0000	138.11	-34.62	1.000	1.000	1.000	5791.75	37320.60	588.18	294.09					

Table II.5. Stage 2 – Results for SF0.4.

SF	NH3 Flow [kg/h]	T_target [K]	I_cell [A/cm2]	E_cell [V]	P_el [kW]	Ph_CMV [kW]	Conversion [-]	Extraction [-]	P_total [kW]	P_aux [kW]	X_3 [-]	X_2 [-]	X_1 [-]	Q_HXN2 [kW]	Q_HXH2 [kW]	P_H2 [kW]	P_FCS [kW]	P_net [kW]	E_sp [kWh/kgH2]	Eff_thermal [-]	Eff_H2 [-]
0.4	5	673	0.0721	0.2665	6.22	1.98	99.9000	99.0000	12.58	6.36	1.000	1.000	0.764	269.52	1231.74	29.41	14.70	2.12	14.26	0.082	0.762
	5	775	0.0721	0.1103	2.57	-1.74	99.9004	99.0000	15.58	13.01	1.000	1.000	1.000	218.53	1673.52	29.41	14.70				
	5	900	0.0721	0.0533	1.25	-3.14	99.9002	99.0000	18.52	17.27	1.000	1.000	1.000	235.51	2105.57	29.41	14.70				
	5	1025	0.0721	0.0344	0.80	-3.67	99.9000	99.0000	21.37	20.57	1.000	1.000	1.000	252.94	2529.66	29.41	14.70				
	5	1150	0.0721	0.0270	0.63	-3.92	99.9000	99.0000	24.14	23.51	1.000	1.000	1.000	277.75	2830.37	29.41	14.70				
	10	673	0.1441	0.5251	24.52	16.03	99.9000	99.0000	17.37	-7.15	1.000	1.000	0.716	385.42	2413.53	58.82	29.41				
	10	775	0.1441	0.2113	9.87	1.25	99.9000	99.0000	20.21	10.34	1.000	1.000	0.986	353.24	3283.68	58.82	29.41	9.20	11.45	0.177	0.815
	10	900	0.1441	0.0960	4.48	-4.30	99.9002	99.0000	23.27	18.79	1.000	1.000	1.000	378.31	4073.85	58.82	29.41	6.14	13.19	0.118	0.781
	10	1025	0.1441	0.0566	2.64	-6.30	99.9001	99.0000	26.23	23.58	1.000	1.000	1.000	403.54	4772.71	58.82	29.41	3.18	14.86	0.061	0.752
	10	1150	0.1441	0.0403	1.88	-7.21	99.9002	99.0000	29.01	27.12	1.000	1.000	1.000	406.01	5479.77	58.82	29.41	0.40	16.44	0.008	0.726
	20	673	0.2881	1.0418	97.25	80.28	99.8668	98.9829	28.20	-69.06	1.000	0.858	0.629	717.51	4357.00	117.64	58.82				
	20	775	0.2882	0.4135	38.61	21.37	99.9001	99.0000	30.98	-7.63	1.000	1.000	0.883	1070.05	5962.88	117.64	58.82				
	20	900	0.2882	0.1814	16.94	-0.62	99.9002	99.0000	34.20	17.26	1.000	1.000	1.000	840.20	7441.43	117.64	58.82	24.62	9.69	0.237	0.851
	20	1025	0.2882	0.1011	9.44	-8.44	99.9002	99.0000	37.21	27.77	1.000	1.000	1.000	874.94	8789.04	117.64	58.82	21.61	10.54	0.208	0.833
	20	1150	0.2882	0.0670	6.26	-11.94	99.9001	99.0000	40.06	33.80	1.000	1.000	1.000	882.54	10087.59	117.64	58.82	18.76	11.35	0.180	0.817
	30.3	673	0.4367	0.9980	141.20	115.29	99.9000	99.0000	41.20	-100.00	1.000	0.907	0.676	1457.88	7163.81	178.22	89.11				
	30.3	775	0.4367	0.6217	87.96	61.84	99.9000	99.0000	42.52	-45.44	1.000	1.000	0.781	1823.10	8158.78	178.22	89.11				
	30.3	900	0.4367	0.2693	38.10	11.50	99.9003	99.0000	46.23	8.13	1.000	1.000	1.000	1411.18	10393.90	178.22	89.11	42.88	8.65	0.272	0.875
	30.3	1025	0.4367	0.1469	20.78	-6.30	99.9001	99.0000	49.70	28.92	1.000	1.000	1.000	1493.97	12237.77	178.22	89.11	39.41	9.30	0.250	0.860
	30.3	1150	0.4367	0.0945	13.37	-14.19	99.9002	99.0000	52.84	39.47	1.000	1.000	1.000	1545.14	14100.67	178.22	89.11	36.26	9.88	0.230	0.847
	40	673	0.5765	0.8229	153.70	119.22	99.9000	99.0000	53.70	-100.00	1.000	0.953	0.709	2265.60	9977.74	235.27	117.64				
	40	775	0.5765	0.8178	152.74	118.26	99.9000	99.0000	53.72	-99.02	1.000	0.955	0.710	2272.44	9995.28	235.27	117.64				
	40	900	0.5765	0.3521	65.76	30.64	99.9002	99.0000	57.66	-8.10	1.000	1.000	0.947	2220.54	12821.83	235.27	117.64				
	40	1025	0.5765	0.1900	35.49	-0.26	99.9001	99.0000	61.65	26.15	1.000	1.000	1.000	2102.68	15276.86	235.27	117.64	55.99	8.73	0.269	0.873
	40	1150	0.5765	0.1204	22.49	-13.90	99.9001	99.0000	65.12	42.63	1.000	1.000	1.000	2199.66	17598.51	235.27	117.64	52.51	9.23	0.252	0.861
	50	673	0.7206	0.7140	166.69	123.28	99.9000	99.0000	66.69	-100.00	1.000	0.993	0.740	3085.92	13052.90	294.09	147.04				
	50	775	0.7206	0.7140	166.69	123.28	99.9000	99.0000	66.69	-100.00	1.000	0.993	0.740	3085.92	13052.90	294.09	147.04				
	50	900	0.7206	0.4374	102.13	58.23	99.9001	99.0000	69.43	-32.70	1.000	1.000	0.883	3117.98	15124.20	294.09	147.04				
	50	1025	0.7206	0.2345	54.75	10.06	99.9002	99.0000	74.05	19.30	1.000	1.000	1.000	2734.51	18249.82	294.09	147.04	72.99	8.39	0.281	0.880
	50	1150	0.7206	0.1471	34.35	-11.14	99.9000	99.0000	77.94	43.59	1.000	1.000	1.000	2894.90	21060.21	294.09	147.04	69.10	8.83	0.266	0.870
	60	673	0.8647	0.6420	179.85	127.43	99.9001	99.0000	79.85	-100.00	1.000	1.000	0.767	3913.93	16243.86	352.91	176.45				
	60	775	0.8647	0.6420	179.85	127.43	99.9001	99.0000	79.85	-100.00	1.000	1.000	0.767	3913.93	16243.86	352.91	176.45				
	60	900	0.8647	0.5228	146.47	93.79	99.9001	99.0000	81.22	-65.24	1.000	1.000	0.829	3891.58	17288.95	352.91	176.45				
	60	1025	0.8647	0.2790	78.16	24.53	99.9001	99.0000	86.40	8.24	1.000	1.000	1.000	3310.19	21063.26	352.91	176.45	90.05	8.16	0.289	0.886
	60	1150	0.8647	0.1738	48.70	-5.88	99.9002	99.0000	90.73	42.03	1.000	1.000	1.000	3514.37	24385.98	352.91	176.45	85.73	8.57	0.275	0.876
	80	673	1.1529	0.5537	206.85	136.20	99.9001	99.0000	106.85	-100.00	1.000	1.000	0.825	5130.53	23037.25	470.54	235.27				
	80	775	1.1529	0.5537	206.85	136.20	99.9001	99.0000	106.85	-100.00	1.000	1.000	0.825	5130.53	23037.25	470.54	235.27				
	80	900	1.1529	0.5537	206.85	136.20	99.9001	99.0000	106.85	-100.00	1.000	1.000	0.825	5130.53	23037.25	470.54	235.27				
	80	1025	1.1529	0.3679	137.44	65.93	99.9002	99.0000	111.03	-26.42	1.000	1.000	0.990	4573.27	26385.55	470.54	235.27				
	80	1150	1.1529	0.2272	84.88	12.10	99.9001	99.0000	116.20	31.32	1.000	1.000	1.000	4673.89	30855.21	470.54	235.27	119.07	8.23	0.286	0.884
100	673	1.4411	0.5017	234.27	145.15	99.9002	99.0000	134.27	-100.00	1.000	1.000	0.899	6143.93	30548.03	588.18	294.09					
100	775	1.4411	0.5017	234.27	145.15	99.9002	99.0000	134.27	-100.00	1.000	1.000	0.899	6143.93	30548.03	588.18	294.09					
100	900	1.4411	0.5017	234.27	145.15	99.9002	99.0000	134.27	-100.00	1.000	1.000	0.899	6143.93	30548.03	588.18	294.09					
100	1025	1.4411	0.4569	213.33	123.95	99.9002	99.0000	135.43	-77.91	1.000	1.000	0.941	6012.80	31535.14	588.18	294.09					
100	1150	1.4411	0.2806	131.04	40.06	99.9000	99.0000	141.50	10.46	1.000	1.000	1.000	5791.75	37320.58	588.18	294.09	152.59	8.02	0.293	0.889	

Table II.6. Stage 2 – Results for SF0.5.

SF	NH3 Flow [kg/h]	T_target [K]	I_cell [A/cm2]	E_cell [V]	P_el [kW]	Ph_CMV [kW]	Conversion [-]	Extraction [-]	P_total [kW]	P_aux [kW]	X_3 [-]	X_2 [-]	X_1 [-]	Q_HXN2 [kW]	Q_HXH2 [kW]	P H2 [kW]	P FCS [kW]	P net [kW]	E_sp [kWh/kgH2]	Eff_thermal [-]	Eff_H2 [-]
0.5	5	673	0.0577	0.2149	5.02	0.77	99.9000	99.0000	13.93	8.91	1.000	1.000	0.764	269.52	1231.74	29.41	14.70	0.78	15.78	0.030	0.737
	5	775	0.0577	0.0901	2.10	-2.21	99.9002	99.0000	17.40	15.30	1.000	1.000	1.000	218.53	1673.52	29.41	14.70				
	5	900	0.0577	0.0448	1.05	-3.34	99.9002	99.0000	20.82	19.77	1.000	1.000	1.000	235.51	2105.57	29.41	14.70				
	5	1025	0.0577	0.0299	0.70	-3.77	99.9002	99.0000	24.15	23.46	1.000	1.000	1.000	252.94	2529.66	29.41	14.70				
	5	1150	0.0577	0.0243	0.57	-3.98	99.9001	99.0000	27.40	26.84	1.000	1.000	1.000	277.75	2830.38	29.41	14.70				
	10	673	0.1153	0.4219	19.70	11.21	99.9000	99.0000	18.72	-0.98	1.000	1.000	0.716	385.42	2413.53	58.82	29.41				
	10	775	0.1153	0.1710	7.98	-0.64	99.9001	99.0000	22.03	14.05	1.000	1.000	0.986	353.24	3283.68	58.82	29.41	7.38	12.48	0.142	0.795
	10	900	0.1153	0.0790	3.69	-5.09	99.9003	99.0000	25.57	21.88	1.000	1.000	1.000	378.31	4073.86	58.82	29.41	3.84	14.49	0.074	0.758
	10	1025	0.1153	0.0477	2.23	-6.71	99.9000	99.0000	29.01	26.78	1.000	1.000	1.000	403.54	4772.71	58.82	29.41	0.40	16.44	0.008	0.726
	10	1150	0.1153	0.0350	1.63	-7.46	99.9001	99.0000	32.27	30.64	1.000	1.000	1.000	406.01	5479.77	58.82	29.41				
	20	673	0.2307	0.8358	78.05	61.07	99.9000	99.0000	29.54	-48.51	1.000	0.858	0.629	717.71	4358.71	117.64	58.82				
	20	775	0.2307	0.3328	31.08	13.84	99.9000	99.0000	32.80	1.72	1.000	1.000	0.883	1070.05	5962.88	117.64	58.82	26.02	9.29	0.250	0.860
	20	900	0.2307	0.1473	13.76	-3.80	99.9001	99.0000	36.50	22.75	1.000	1.000	1.000	840.20	7441.42	117.64	58.82	22.32	10.34	0.215	0.837
	20	1025	0.2307	0.0833	7.78	-10.09	99.9001	99.0000	39.99	32.21	1.000	1.000	1.000	874.95	8789.04	117.64	58.82	18.83	11.33	0.181	0.817
	20	1150	0.2307	0.0564	5.26	-12.93	99.9001	99.0000	43.32	38.06	1.000	1.000	1.000	882.54	10087.59	117.64	58.82	15.50	12.27	0.149	0.799
	30.3	673	0.3495	1.0047	142.14	116.32	99.9000	99.0000	42.14	-100.00	1.000	0.848	0.632	1303.28	6742.12	178.22	89.11				
	30.3	775	0.3495	0.4995	70.66	44.54	99.9000	99.0000	44.34	-26.32	1.000	1.000	0.781	1823.10	8158.78	178.22	89.11				
	30.3	900	0.3495	0.2177	30.80	4.19	99.9002	99.0000	48.53	17.73	1.000	1.000	1.000	1411.18	10393.89	178.22	89.11	40.58	9.08	0.258	0.865
	30.3	1025	0.3495	0.1200	16.98	-10.11	99.9000	99.0000	52.48	35.51	1.000	1.000	1.000	1493.97	12237.76	178.22	89.11	36.62	9.82	0.232	0.848
	30.3	1150	0.3495	0.0784	11.09	-16.48	99.9001	99.0000	56.11	45.02	1.000	1.000	1.000	1545.14	14100.66	178.22	89.11	33.00	10.49	0.209	0.834
	40	673	0.4614	0.8281	154.67	120.33	99.9000	99.0000	54.67	-100.00	1.000	0.887	0.659	2024.57	9367.03	235.27	117.64				
	40	775	0.4614	0.6564	122.60	88.11	99.9001	99.0000	55.54	-67.06	1.000	0.955	0.710	2272.44	9995.28	235.27	117.64				
	40	900	0.4614	0.2839	53.03	17.91	99.9000	99.0000	59.96	6.93	1.000	1.000	0.947	2220.54	12821.82	235.27	117.64	57.67	8.49	0.277	0.878
	40	1025	0.4614	0.1545	28.86	-6.89	99.9000	99.0000	64.43	35.57	1.000	1.000	1.000	2102.69	15276.86	235.27	117.64	53.21	9.13	0.256	0.864
	40	1150	0.4614	0.0991	18.51	-17.88	99.9000	99.0000	68.39	49.87	1.000	1.000	1.000	2199.66	17598.51	235.27	117.64	49.25	9.69	0.237	0.851
	50	673	0.5767	0.7181	167.65	124.44	99.9001	99.0000	67.65	-100.00	1.000	0.922	0.684	2752.28	12229.70	294.09	147.04				
	50	775	0.5767	0.7181	167.65	124.44	99.9001	99.0000	67.65	-100.00	1.000	0.922	0.684	2752.28	12229.70	294.09	147.04				
	50	900	0.5767	0.3523	82.24	38.34	99.9003	99.0000	71.73	-10.51	1.000	1.000	0.883	3117.97	15124.22	294.09	147.04				
	50	1025	0.5767	0.1901	44.39	-0.30	99.9002	99.0000	76.83	32.45	1.000	1.000	1.000	2734.51	18249.82	294.09	147.04	70.21	8.71	0.270	0.873
	50	1150	0.5767	0.1205	28.13	-17.36	99.9000	99.0000	81.21	53.08	1.000	1.000	1.000	2894.90	21060.21	294.09	147.04	65.84	9.20	0.253	0.862
	60	673	0.6921	0.6452	180.76	128.60	99.9001	99.0000	80.76	-100.00	1.000	0.952	0.706	3496.59	15197.49	352.91	176.45				
	60	775	0.6921	0.6452	180.76	128.60	99.9001	99.0000	80.76	-100.00	1.000	0.952	0.706	3496.59	15197.49	352.91	176.45				
	60	900	0.6921	0.4206	117.83	65.15	99.9000	99.0000	83.53	-34.30	1.000	1.000	0.829	3891.58	17288.94	352.91	176.45				
	60	1025	0.6921	0.2257	63.24	9.61	99.9001	99.0000	89.18	25.95	1.000	1.000	1.000	3310.19	21063.26	352.91	176.45	87.27	8.42	0.280	0.880
	60	1150	0.6921	0.1419	39.74	-14.84	99.9002	99.0000	93.99	54.25	1.000	1.000	1.000	3514.37	24385.98	352.91	176.45	82.47	8.88	0.264	0.869
	80	673	0.9228	0.5550	207.31	137.06	99.9003	99.0000	107.31	-100.00	1.000	1.000	0.752	5026.25	21498.44	470.54	235.27				
	80	775	0.9228	0.5550	207.31	137.06	99.9003	99.0000	107.31	-100.00	1.000	1.000	0.752	5026.25	21498.44	470.54	235.27				
	80	900	0.9228	0.5550	207.31	137.06	99.9003	99.0000	107.31	-100.00	1.000	1.000	0.752	5026.25	21498.44	470.54	235.27				
	80	1025	0.9228	0.2969	110.91	39.40	99.9000	99.0000	113.81	2.90	1.000	1.000	0.990	4573.28	26385.52	470.54	235.27	121.46	8.06	0.292	0.888
	80	1150	0.9228	0.1846	68.95	-3.82	99.9001	99.0000	119.46	50.51	1.000	1.000	1.000	4673.89	30855.22	470.54	235.27	115.81	8.46	0.278	0.879
100	673	1.1535	0.5018	234.32	145.77	99.9002	99.0000	134.32	-100.00	1.000	1.000	0.810	6241.64	28430.63	588.18	294.09					
100	775	1.1535	0.5018	234.32	145.77	99.9002	99.0000	134.32	-100.00	1.000	1.000	0.810	6241.64	28430.63	588.18	294.09					
100	900	1.1535	0.5018	234.32	145.77	99.9002	99.0000	134.32	-100.00	1.000	1.000	0.810	6241.64	28430.63	588.18	294.09					
100	1025	1.1535	0.3681	171.88	82.50	99.9001	99.0000	138.21	-33.67	1.000	1.000	0.941	6012.81	31535.11	588.18	294.09					
100	1150	1.1535	0.2273	106.15	15.18	99.9002	99.0000	144.76	38.61	1.000	1.000	1.000	5791.75	37320.61	588.18	294.09	149.32	8.20	0.287	0.885	

Table II.7. Stage 2 – Results for SF1.

SF	NH3 Flow [kg/h]	T_target [K]	I_cell [A/cm2]	E_cell [V]	P_el [kW]	Ph_CMRR [kW]	Conversion [-]	Extraction [-]	P_total [kW]	P_aux [kW]	X_3 [-]	X_2 [-]	X_1 [-]	Q_HXN2 [kW]	Q_HXH2 [kW]	P_H2 [kW]	P_FCS [kW]	P_net [kW]	E_sp [kWh/kgH2]	Eff_thermal [-]	Eff_H2 [-]
1	5	673	0.0289	0.1115	2.60	-1.64	99.9000	99.0000	20.27	17.67	1.000	1.000	0.764	269.52	1231.74	29.41	14.70				
	5	775	0.0289	0.0497	1.16	-3.15	99.9002	99.0000	26.02	24.86	1.000	1.000	1.000	218.53	1673.52	29.41	14.70				
	5	900	0.0289	0.0277	0.65	-3.74	99.9003	99.0000	31.70	31.05	1.000	1.000	1.000	235.51	2105.58	29.41	14.70				
	5	1025	0.0289	0.0210	0.49	-3.98	99.9001	99.0000	37.30	36.81	1.000	1.000	1.000	252.94	2529.66	29.41	14.70				
	5	1150	0.0289	0.0190	0.44	-4.11	99.9002	99.0000	42.82	42.37	1.000	1.000	1.000	277.75	2830.38	29.41	14.70				
	10	673	0.0577	0.2150	10.04	1.55	99.9000	99.0000	25.06	15.02	1.000	1.000	0.716	385.42	2413.53	58.82	29.41	4.34	14.20	0.084	0.763
	10	775	0.0577	0.0901	4.21	-4.41	99.9005	99.0000	30.64	26.43	1.000	1.000	0.986	353.23	3283.70	58.82	29.41				
	10	900	0.0577	0.0448	2.09	-6.69	99.9000	99.0000	36.45	34.36	1.000	1.000	1.000	378.31	4073.85	58.82	29.41				
	10	1025	0.0577	0.0299	1.40	-7.54	99.9001	99.0000	42.15	40.76	1.000	1.000	1.000	403.54	4772.71	58.82	29.41				
	10	1150	0.0577	0.0243	1.14	-7.96	99.9000	99.0000	47.68	46.55	1.000	1.000	1.000	406.01	5479.76	58.82	29.41				
	20	673	0.1154	0.4221	39.42	22.44	99.9000	99.0000	35.89	-3.53	1.000	0.858	0.629	717.71	4358.71	117.64	58.82				
	20	775	0.1154	0.1711	15.98	-1.27	99.9000	99.0000	41.42	25.44	1.000	1.000	0.883	1070.05	5962.88	117.64	58.82	17.40	11.73	0.167	0.809
	20	900	0.1154	0.0790	7.38	-10.18	99.9001	99.0000	47.38	40.00	1.000	1.000	1.000	840.20	7441.42	117.64	58.82	11.44	13.42	0.110	0.777
	20	1025	0.1154	0.0478	4.46	-13.42	99.9001	99.0000	53.13	48.67	1.000	1.000	1.000	874.95	8789.04	117.64	58.82	5.68	15.05	0.055	0.749
	20	1150	0.1154	0.0350	3.27	-14.93	99.9002	99.0000	58.73	55.46	1.000	1.000	1.000	882.54	10087.59	117.64	58.82	0.09	16.64	0.001	0.723
	30.3	673	0.1748	0.6354	89.89	64.16	99.9000	99.0000	47.30	-42.59	1.000	0.737	0.549	1014.03	5944.28	178.22	89.11				
	30.3	775	0.1748	0.2544	36.00	9.88	99.9001	99.0000	52.95	16.96	1.000	1.000	0.781	1823.10	8158.78	178.22	89.11	36.15	9.90	0.229	0.847
	30.3	900	0.1748	0.1142	16.16	-10.44	99.9003	99.0000	59.41	43.25	1.000	1.000	1.000	1411.18	10393.90	178.22	89.11	29.70	11.11	0.188	0.821
	30.3	1025	0.1748	0.0661	9.35	-17.73	99.9001	99.0000	65.63	56.28	1.000	1.000	1.000	1493.97	12237.76	178.22	89.11	23.48	12.27	0.149	0.798
	30.3	1150	0.1748	0.0460	6.51	-21.05	99.9002	99.0000	71.52	65.01	1.000	1.000	1.000	1545.14	14100.67	178.22	89.11	17.59	13.38	0.112	0.778
	40	673	0.2308	0.8362	156.18	122.22	99.9000	99.0000	58.10	-98.09	1.000	0.659	0.492	1180.59	7269.77	235.27	117.64				
	40	775	0.2308	0.3330	62.19	27.70	99.9001	99.0000	64.16	1.97	1.000	0.955	0.710	2272.44	9995.27	235.27	117.64	53.48	9.09	0.257	0.864
	40	900	0.2308	0.1474	27.52	-7.59	99.9002	99.0000	70.84	43.32	1.000	1.000	0.947	2220.53	12821.84	235.27	117.64	46.79	10.04	0.225	0.844
	40	1025	0.2308	0.0834	15.57	-20.18	99.9000	99.0000	77.57	62.00	1.000	1.000	1.000	2102.69	15276.86	235.27	117.64	40.06	10.99	0.193	0.824
	40	1150	0.2308	0.0564	10.53	-25.86	99.9000	99.0000	83.80	73.27	1.000	1.000	1.000	2199.66	17598.51	235.27	117.64	33.84	11.87	0.163	0.806
	50	673	0.2885	0.7373	172.14	129.46	99.9000	99.0000	72.14	-100.00	1.000	0.730	0.540	1855.35	10041.84	294.09	147.04				
	50	775	0.2885	0.4139	96.63	53.53	99.9000	99.0000	75.69	-20.94	1.000	0.883	0.654	2570.57	11784.18	294.09	147.04				
	50	900	0.2885	0.1815	42.38	-1.51	99.9002	99.0000	82.61	40.23	1.000	1.000	0.883	3117.97	15124.21	294.09	147.04	64.43	9.36	0.248	0.858
	50	1025	0.2885	0.1012	23.62	-21.07	99.9002	99.0000	89.98	66.36	1.000	1.000	1.000	2734.51	18249.82	294.09	147.04	57.07	10.20	0.219	0.840
	50	1150	0.2885	0.0671	15.66	-29.83	99.9001	99.0000	96.62	80.96	1.000	1.000	1.000	2894.90	21060.22	294.09	147.04	50.43	10.95	0.194	0.825
	60	673	0.3462	0.6611	185.23	133.77	99.9000	99.0000	85.23	-100.00	1.000	0.750	0.550	2359.72	12436.07	352.91	176.45				
	60	775	0.3462	0.4948	138.63	86.91	99.9000	99.0000	87.22	-51.41	1.000	0.826	0.608	2792.55	13483.80	352.91	176.45				
	60	900	0.3462	0.2157	60.44	7.76	99.9003	99.0000	94.41	33.97	1.000	1.000	0.829	3891.57	17288.96	352.91	176.45	82.05	8.92	0.263	0.868
	60	1025	0.3462	0.1190	33.33	-20.30	99.9000	99.0000	102.33	69.00	1.000	1.000	1.000	3310.19	21063.26	352.91	176.45	74.12	9.66	0.238	0.852
	60	1150	0.3462	0.0778	21.79	-32.80	99.9000	99.0000	109.40	87.61	1.000	1.000	1.000	3514.37	24385.97	352.91	176.45	67.05	10.33	0.215	0.837
	80	673	0.4616	0.5661	211.48	111.48	99.9001	99.0000	111.48	-100.00	1.000	0.787	0.569	3396.27	17477.77	470.54	235.27				
	80	775	0.4616	0.5661	211.48	142.31	99.9001	99.0000	111.48	-100.00	1.000	0.787	0.569	3396.27	17477.77	470.54	235.27				
	80	900	0.4616	0.2841	106.11	35.88	99.9002	99.0000	118.16	12.04	1.000	1.000	0.750	5015.67	21471.81	470.54	235.27	117.12	8.37	0.282	0.881
	80	1025	0.4616	0.1546	57.75	-13.76	99.9001	99.0000	126.95	69.20	1.000	1.000	0.990	4573.27	26385.54	470.54	235.27	108.32	8.99	0.260	0.867
	80	1150	0.4616	0.0992	37.04	-35.74	99.9001	99.0000	134.88	97.84	1.000	1.000	1.000	4673.89	30855.22	470.54	235.27	100.39	9.55	0.241	0.854
100	673	0.5770	0.5092	237.78	150.74	99.9000	99.0000	137.78	-100.00	1.000	0.826	0.595	4479.47	22976.18	588.18	294.09					
100	775	0.5770	0.5092	237.78	150.74	99.9000	99.0000	137.78	-100.00	1.000	0.826	0.595	4479.47	22976.18	588.18	294.09					
100	900	0.5770	0.3524	164.56	76.76	99.9001	99.0000	142.01	-22.55	1.000	0.944	0.698	5550.81	25674.68	588.18	294.09					
100	1025	0.5770	0.1902	88.82	-0.57	99.9001	99.0000	151.35	62.54	1.000	1.000	0.941	6012.81	31535.11	588.18	294.09	142.73	8.58	0.274	0.876	
100	1150	0.5770	0.1267	59.17	-31.61	99.9000	99.0000	159.17	100.00	1.000	1.000	1.000	5763.32	36612.56	588.18	294.09	134.92	9.02	0.259	0.866	

Table II.8. Stage 2 – Results for SF1.5.

SF	NH3 Flow [kg/h]	T_target [K]	I_cell [A/cm2]	E_cell [V]	P_el [kW]	Ph_CMV [kW]	Conversion [-]	Extraction [-]	P_total [kW]	P_aux [kW]	X_3 [-]	X_2 [-]	X_1 [-]	Q_HXN2 [kW]	Q_HXH2 [kW]	P H2 [kW]	P FCS [kW]	P net [kW]	E_sp [kWh/kgH2]	Eff_thermal [K]	Eff_H2 [K]
1.5	5	673	0.0192	0.0770	1.80	-2.45	99.9000	99.0000	26.31	24.51	1.000	1.000	0.764	269.52	1231.74	29.41	14.70				
	5	775	0.0192	0.0362	0.84	-3.47	99.9003	99.0000	34.20	33.36	1.000	1.000	1.000	218.53	1673.52	29.41	14.70				
	5	900	0.0192	0.0221	0.51	-3.88	99.9002	99.0000	42.04	41.53	1.000	1.000	1.000	235.51	2105.57	29.41	14.70				
	5	1025	0.0192	0.0181	0.42	-4.05	99.9002	99.0000	49.80	49.38	1.000	1.000	1.000	252.94	2529.66	29.41	14.70				
	5	1150	0.0192	0.0172	0.40	-4.15	99.9002	99.0000	57.47	57.07	1.000	1.000	1.000	277.75	2830.38	29.41	14.70				
	10	673	0.0385	0.1460	6.82	-1.67	99.9000	99.0000	31.10	24.28	1.000	1.000	0.716	385.42	2413.53	58.82	29.41				
	10	775	0.0385	0.0631	2.95	-5.67	99.9001	99.0000	38.83	35.88	1.000	1.000	0.986	353.24	3283.69	58.82	29.41				
	10	900	0.0385	0.0334	1.56	-7.22	99.9002	99.0000	46.79	45.23	1.000	1.000	1.000	378.31	4073.86	58.82	29.41				
	10	1025	0.0385	0.0240	1.12	-7.82	99.9001	99.0000	54.65	53.53	1.000	1.000	1.000	403.54	4772.71	58.82	29.41				
	10	1150	0.0385	0.0207	0.97	-8.13	99.9001	99.0000	62.33	61.36	1.000	1.000	1.000	406.01	5479.77	58.82	29.41				
	20	673	0.0769	0.2840	26.52	9.54	99.9000	99.0000	41.92	15.40	1.000	0.858	0.629	717.71	4358.71	117.64	58.82	16.89	11.88	0.162	0.806
	20	775	0.0769	0.1171	10.93	-6.31	99.9004	99.0000	49.60	38.67	1.000	1.000	0.883	1070.04	5962.90	117.64	58.82	9.21	14.05	0.089	0.766
	20	900	0.0769	0.0562	5.25	-12.31	99.9003	99.0000	57.72	52.47	1.000	1.000	1.000	840.20	7441.43	117.64	58.82	1.09	16.35	0.011	0.727
	20	1025	0.0769	0.0359	3.35	-14.53	99.9000	99.0000	65.63	62.28	1.000	1.000	1.000	874.95	8789.03	117.64	58.82				
	20	1150	0.0769	0.0279	2.60	-15.59	99.9001	99.0000	73.38	70.78	1.000	1.000	1.000	882.54	10087.59	117.64	58.82				
	30.3	673	0.1165	0.4262	60.30	34.57	99.9000	99.0000	53.33	-6.96	1.000	0.737	0.549	1014.03	5944.28	178.22	89.11				
	30.3	775	0.1165	0.1727	24.43	-1.69	99.9001	99.0000	61.14	36.71	1.000	1.000	0.781	1823.10	8158.78	178.22	89.11	27.97	11.43	0.178	0.815
	30.3	900	0.1165	0.0797	11.27	-15.33	99.9002	99.0000	69.75	58.48	1.000	1.000	1.000	1411.18	10393.89	178.22	89.11	19.36	13.04	0.123	0.784
	30.3	1025	0.1165	0.0481	6.81	-20.28	99.9000	99.0000	78.13	71.32	1.000	1.000	1.000	1493.97	12237.76	178.22	89.11	10.98	14.61	0.070	0.756
	30.3	1150	0.1165	0.0352	4.98	-22.58	99.9001	99.0000	86.17	81.19	1.000	1.000	1.000	1545.14	14100.66	178.22	89.11	2.94	16.12	0.019	0.731
	40	673	0.1538	0.5601	104.60	70.64	99.9000	99.0000	64.13	-40.47	1.000	0.659	0.492	1180.59	7269.77	235.27	117.64				
	40	775	0.1538	0.2250	42.02	7.54	99.9002	99.0000	72.34	30.32	1.000	0.955	0.710	2272.44	9995.28	235.27	117.64	45.29	10.25	0.218	0.839
	40	900	0.1538	0.1018	19.01	-16.11	99.9002	99.0000	81.18	62.17	1.000	1.000	0.947	2220.53	12821.83	235.27	117.64	36.45	11.50	0.175	0.814
	40	1025	0.1538	0.0596	11.14	-24.62	99.9001	99.0000	90.07	78.93	1.000	1.000	1.000	2102.68	15276.87	235.27	117.64	27.57	12.76	0.133	0.789
	40	1150	0.1538	0.0421	7.87	-28.52	99.9001	99.0000	98.45	90.58	1.000	1.000	1.000	2199.66	17598.51	235.27	117.64	19.19	13.95	0.092	0.768
	50	673	0.1923	0.6981	162.98	120.52	99.9000	99.0000	75.22	-87.75	1.000	0.601	0.446	1261.21	8570.25	294.09	147.04				
	50	775	0.1923	0.2789	65.12	22.02	99.9002	99.0000	83.87	18.75	1.000	0.883	0.654	2570.57	11784.19	294.09	147.04	63.17	9.51	0.243	0.855
	50	900	0.1923	0.1246	29.08	-14.82	99.9002	99.0000	92.95	63.87	1.000	1.000	0.883	3117.97	15124.21	294.09	147.04	54.09	10.53	0.208	0.833
	50	1025	0.1923	0.0715	16.69	-28.00	99.9000	99.0000	102.48	85.79	1.000	1.000	1.000	2734.51	18249.81	294.09	147.04	44.57	11.61	0.171	0.811
	50	1150	0.1923	0.0503	11.75	-33.68	99.9001	99.0000	111.75	100.00	1.000	1.000	1.000	2885.60	20860.28	294.09	147.04	35.29	12.67	0.136	0.791
	60	673	0.2308	0.6760	189.40	138.29	99.9000	99.0000	89.40	-100.00	1.000	0.651	0.477	1807.28	11091.09	352.91	176.45				
	60	775	0.2308	0.3329	93.26	41.54	99.9001	99.0000	95.41	2.15	1.000	0.826	0.608	2792.55	13483.80	352.91	176.45	81.04	9.01	0.260	0.866
	60	900	0.2308	0.1473	41.28	-11.40	99.9003	99.0000	104.75	63.47	1.000	1.000	0.829	3891.57	17288.97	352.91	176.45	71.70	9.89	0.230	0.847
	60	1025	0.2308	0.0834	23.35	-30.28	99.9001	99.0000	114.83	91.47	1.000	1.000	1.000	3310.19	21063.26	352.91	176.45	61.63	10.84	0.198	0.827
	60	1150	0.2308	0.0688	19.29	-34.77	99.9002	99.0000	119.29	100.00	1.000	1.000	1.000	3401.24	22531.77	352.91	176.45	57.17	11.27	0.183	0.818
	80	673	0.3077	0.5774	215.68	147.05	99.9000	99.0000	115.68	-100.00	1.000	0.682	0.486	2608.77	15561.93	470.54	235.27				
	80	775	0.3077	0.4408	164.66	95.69	99.9000	99.0000	118.41	-46.25	1.000	0.748	0.538	3102.90	16764.52	470.54	235.27				
	80	900	0.3077	0.1929	72.06	1.82	99.9003	99.0000	128.50	56.44	1.000	1.000	0.750	5015.67	21471.81	470.54	235.27	106.77	9.10	0.257	0.864
	80	1025	0.3077	0.1071	40.01	-31.50	99.9001	99.0000	139.45	99.44	1.000	1.000	0.990	4573.28	26385.53	470.54	235.27	95.82	9.88	0.230	0.847
	80	1150	0.3077	0.1062	39.66	-31.87	99.9001	99.0000	139.66	100.00	1.000	1.000	0.995	4549.89	26475.59	470.54	235.27	95.61	9.89	0.230	0.847
100	673	0.3846	0.5180	241.86	155.56	99.9000	99.0000	141.86	-100.00	1.000	0.715	0.500	3449.40	20413.21	588.18	294.09					
100	775	0.3846	0.5180	241.86	155.56	99.9000	99.0000	141.86	-100.00	1.000	0.715	0.500	3449.40	20413.20	588.18	294.09					
100	900	0.3846	0.2385	111.35	23.55	99.9002	99.0000	152.35	41.00	1.000	0.944	0.698	5550.81	25674.69	588.18	294.09	141.74	8.63	0.273	0.875	
100	1025	0.3846	0.1351	63.10	-26.19	99.9002	99.0000	163.10	100.00	1.000	1.000	0.925	6077.57	31157.54	588.18	294.09	130.99	9.24	0.252	0.861	
100	1150	0.3846	0.1351	63.10	-26.19	99.9002	99.0000	163.10	100.00	1.000	1.000	0.925	6077.57	31157.54	588.18	294.09	130.99	9.24	0.252	0.861	

Table II.9. Stage 2 – Results for SF2.

SF	NH3 Flow [kg/h]	T_target [K]	I_cell [A/cm2]	E_cell [V]	P_el [kW]	Ph_CMV [kW]	Conversion [-]	Extraction [-]	P_total [kW]	P_aux [kW]	X_3 [-]	X_2 [-]	X_1 [-]	Q_HXN2 [kW]	Q_HXH2 [kW]	P_H2 [kW]	P_FCS [kW]	P_net [kW]	E_sp [kWh/kgH2]	Eff_thermal [-]	Eff_H2 [-]
2	2.5	600	0.0072	0.0339	0.40	-1.73	99.9000	99.0000	10.41	10.01	0.996	0.809	0.322	37.55	177.62	14.70	7.35				
	2.5	800	0.0072	0.0339	0.40	-1.73	99.9000	99.0000	25.95	25.56	1.000	1.000	0.708	155.29	529.51	14.70	7.35				
	2.5	1000	0.0072	0.0143	0.17	-2.06	99.9002	99.0000	57.67	57.51	1.000	1.000	1.000	196.41	1273.71	14.70	7.35				
	2.5	1200	0.0072	0.0153	0.18	-2.11	100.0000	99.0000	73.28	73.10	1.000	1.000	1.000	251.37	1521.55	14.70	7.35				
	5	600	0.0144	0.0597	1.39	-2.85	99.9001	99.0000	13.14	11.74	0.993	0.682	0.220	41.25	354.09	29.41	14.70	1.57	14.89	0.060	0.751
	5	800	0.0144	0.0261	0.61	-3.72	99.9004	99.0000	44.15	43.54	1.000	1.000	1.000	220.76	1761.11	29.41	14.70				
	5	1000	0.0144	0.0169	0.39	-4.06	99.9000	99.0000	59.98	59.59	1.000	1.000	1.000	250.42	2442.26	29.41	14.70				
	5	1200	0.0144	0.0164	0.38	-4.20	100.0000	99.0000	75.59	75.20	1.000	1.000	1.000	289.32	2938.29	29.41	14.70				
	10	600	0.0289	0.1115	5.21	-3.28	99.9000	99.0000	18.70	13.49	0.993	0.497	0.180	38.65	692.29	58.82	29.41	10.71	10.60	0.206	0.832
	10	800	0.0289	0.0428	2.00	-6.65	99.9004	99.0000	48.81	46.81	1.000	1.000	1.000	357.31	3446.34	58.82	29.41				
	10	1000	0.0289	0.0219	1.02	-7.89	99.9001	99.0000	64.81	63.79	1.000	1.000	1.000	399.66	4635.35	58.82	29.41				
	10	1200	0.0289	0.0187	0.87	-8.29	99.9002	99.0000	80.42	79.55	1.000	1.000	1.000	398.57	5772.38	58.82	29.41				
	20	600	0.0577	0.2150	20.08	3.10	99.9000	99.0000	29.96	9.88	0.991	0.309	0.153	53.25	1253.56	117.64	58.82	28.86	8.49	0.277	0.878
	20	800	0.0577	0.2150	20.08	3.10	99.9000	99.0000	44.03	23.95	1.000	0.728	0.530	497.22	3725.98	117.64	58.82	14.79	12.47	0.142	0.795
	20	1000	0.0577	0.0319	2.98	-14.84	99.9000	99.0000	75.79	72.81	1.000	1.000	1.000	870.06	8517.46	117.64	58.82				
	20	1200	0.0577	0.0232	2.17	-16.16	99.9000	99.0000	91.50	89.34	1.000	1.000	1.000	873.77	10599.96	117.64	58.82				
	30.3	600	0.0874	0.3217	45.51	19.78	99.9000	99.0000	41.67	-3.84	0.989	0.227	0.129	86.82	1731.82	178.22	89.11				
	30.3	800	0.0874	0.1105	15.63	-10.59	99.9004	99.0000	71.18	55.55	1.000	1.000	0.830	1835.19	8608.46	178.22	89.11	17.93	13.31	0.114	0.779
	30.3	1000	0.0874	0.0422	5.97	-21.02	99.9002	99.0000	88.20	82.23	1.000	1.000	1.000	1476.75	11870.03	178.22	89.11	0.91	16.49	0.006	0.725
	30.3	1200	0.0874	0.0288	4.07	-23.58	99.9001	99.0000	104.07	100.00	1.000	1.000	1.000	1546.12	14453.46	178.22	89.11				
	40	600	0.1154	0.4221	78.84	44.87	99.9000	99.0000	52.74	-26.10	0.988	0.186	0.111	92.57	2139.32	235.27	117.64				
	40	800	0.1154	0.1428	26.67	-7.94	99.9001	99.0000	82.36	55.68	1.000	1.000	0.756	2488.44	10553.99	235.27	117.64	35.28	11.67	0.170	0.810
	40	1000	0.1154	0.0519	9.69	-25.93	99.9001	99.0000	100.06	90.36	1.000	1.000	1.000	2078.04	14814.61	235.27	117.64	17.58	14.17	0.085	0.764
	40	1200	0.1154	0.0408	7.62	-28.42	99.9001	99.0000	107.62	100.00	1.000	1.000	1.000	2154.01	16304.45	235.27	117.64	10.02	15.25	0.048	0.745
	50	600	0.1443	0.5256	122.72	80.26	99.9000	99.0000	64.16	-58.56	0.987	0.161	0.096	93.84	2537.89	294.09	147.04				
	50	800	0.1443	0.1761	41.12	-2.14	99.9000	99.0000	93.98	52.86	1.000	0.940	0.699	2839.60	12444.42	294.09	147.04	53.06	10.65	0.204	0.831
	50	1000	0.1443	0.0619	14.45	-30.08	99.9002	99.0000	112.36	97.91	1.000	1.000	1.000	2699.84	17686.45	294.09	147.04	34.68	12.73	0.133	0.790
	50	1200	0.1443	0.0589	13.76	-30.87	99.9001	99.0000	113.76	100.00	1.000	1.000	1.000	2718.93	17995.72	294.09	147.04	33.29	12.89	0.128	0.787
	60	600	0.1731	0.6292	176.27	100.00	99.9000	99.0000	100.90	-75.37	0.987	0.145	0.083	91.97	2942.54	352.91	176.45				
	60	800	0.1731	0.2095	58.69	6.77	99.9001	99.0000	105.62	46.93	1.000	0.881	0.651	3102.20	14234.78	352.91	176.45	70.83	9.98	0.227	0.845
	60	1000	0.1731	0.0794	22.24	-31.01	99.9002	99.0000	122.24	100.00	1.000	1.000	0.973	3400.07	19655.67	352.91	176.45	54.21	11.55	0.174	0.813
	60	1200	0.1731	0.0794	22.24	-31.01	99.9002	99.0000	122.24	100.00	1.000	1.000	0.973	3400.07	19655.69	352.91	176.45	54.21	11.55	0.174	0.813
80	600	0.2308	0.8362	312.37	100.00	99.9000	99.0000	242.79	-69.58	0.986	0.130	0.062	82.82	3798.22	470.54	235.27					
80	800	0.2308	0.2762	103.16	33.93	99.9000	99.0000	128.84	25.68	1.000	0.799	0.578	3482.95	17688.46	470.54	235.27	106.43	9.13	0.256	0.864	
80	1000	0.2308	0.1161	43.36	-27.35	99.9001	99.0000	143.36	100.00	1.000	1.000	0.837	5119.00	23290.67	470.54	235.27	91.91	10.15	0.221	0.841	
80	1200	0.2308	0.1161	43.36	-27.35	99.9001	99.0000	143.36	100.00	1.000	1.000	0.837	5119.00	23290.67	470.54	235.27	91.91	10.15	0.221	0.841	
100	600	0.2884	1.0428	486.73	100.00	99.8660	98.9828	422.86	-63.88	0.985	0.124	0.046	68.75	4733.41	588.18	294.09					
100	800	0.2885	0.3428	160.07	73.55	99.9001	99.0000	151.83	-8.24	1.000	0.748	0.528	3759.70	21185.43	588.18	294.09					
100	1000	0.2885	0.1437	67.09	-21.28	99.9001	99.0000	167.09	100.00	1.000	1.000	0.782	6213.27	27752.19	588.18	294.09	127.00	9.47	0.244	0.856	
100	1200	0.2885	0.1437	67.09	-21.28	99.9001	99.0000	167.09	100.00	1.000	1.000	0.782	6213.27	27752.19	588.18	294.09	127.00	9.47	0.244	0.856	

II.2 Additional Plots

II.2.1 Hydrogen Generation Specific Energy

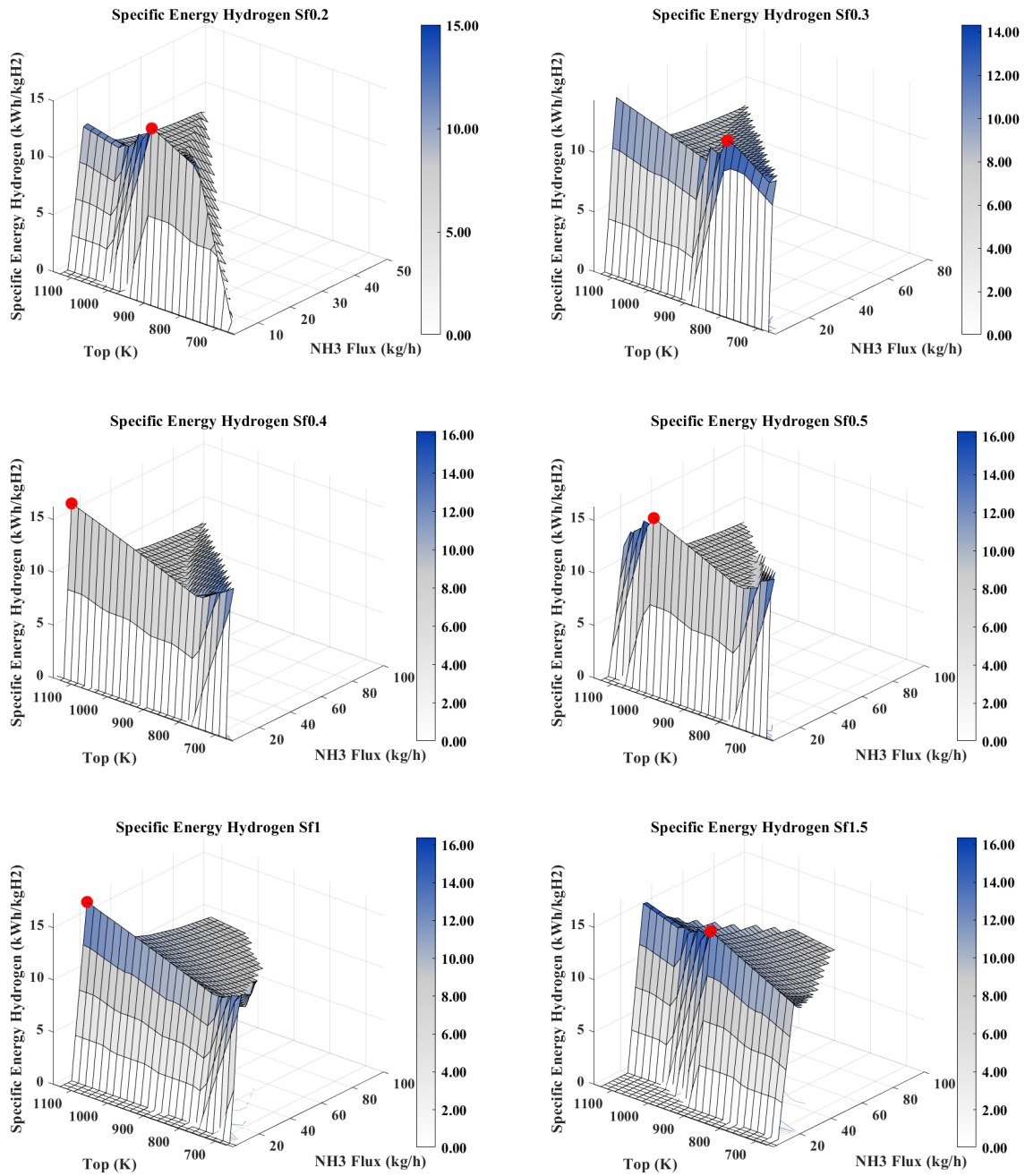


Figure II.1. Stage 2 – Hydrogen Generation Specific Energy summary.

II.2.2 Hydrogen Efficiency

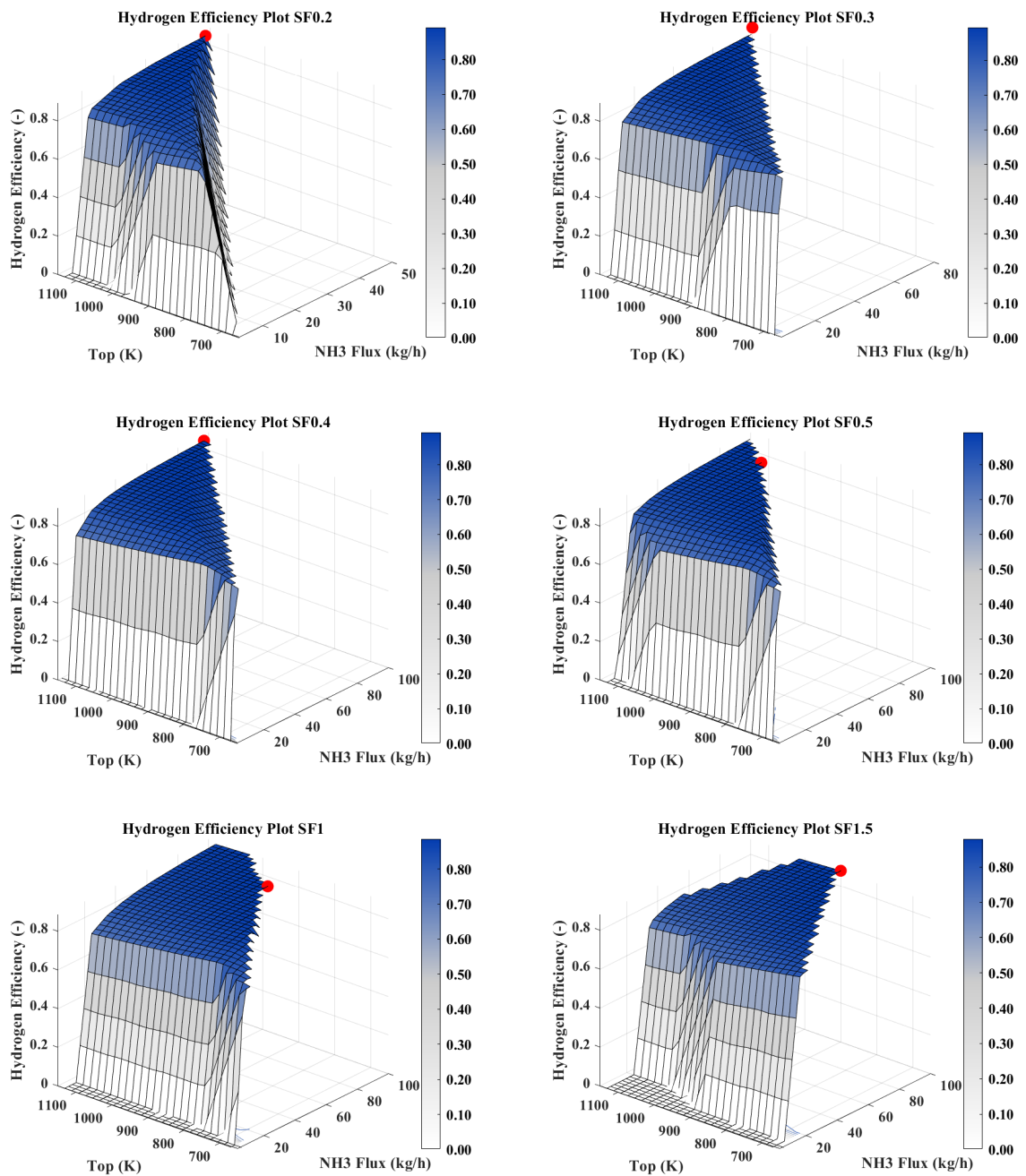


Figure II.2. Stage 2 – Hydrogen Efficiency summary.

Annex III

Stage 3 - Complete results summary

This annex includes the simulation results for the heat exchangers that were not presented in Section 4.3.

III.1 Additional HXN2 Temperature Tables

Table III.1. HXN2 Temperature results for SF0.2.

SF	Flow [kg/h]	T_target [K]	X_3 [-]	X_2 [-]	X_1 [-]	Q_HXN2 [kW]	T_NH3in [K]	T_NH3out [K]	T_N2in [K]	T_N2out [K]	$\Delta T1_N2$ [K]	$\Delta T2_N2$ [K]	DMLT_N2 [K]
0.2	2.5	673	1.000	1.000	0.822	179.90	298.64	438.28	562.38	316.26			
	2.5	775	1.000	1.000	1.000	152.78	312.11	555.88	680.52	475.46			
	2.5	900	1.000	1.000	1.000	176.98	413.58	664.54	797.79	565.15			
	2.5	1025	1.000	1.000	1.000	201.25	516.86	754.83	912.28	653.40			
	2.5	1150	1.000	1.000	1.000	235.66	590.50	818.85	1023.33	725.84			
	5	673	1.000	1.000	0.764	269.52	299.09	381.85	499.64	314.64			
	5	775	1.000	1.000	1.000	218.53	307.57	511.12	613.51	465.79	158.21	102.39	128.29
	5	900	1.000	1.000	1.000	235.51	419.10	629.00	721.55	565.48	146.38	92.55	117.41
	5	1025	1.000	1.000	1.000	252.94	525.90	724.92	821.34	657.12			
	5	1150	1.000	1.000	1.000	277.75	607.12	794.54	911.82	734.71			
	10	673	1.000	1.000	0.715	385.32	300.57	305.52	452.90	320.44			
	10	775	1.000	1.000	0.986	353.24	301.37	424.82	558.14	437.94			
	10	900	1.000	1.000	1.000	378.31	402.42	550.57	671.58	545.32	142.89	121.01	131.65
	10	1025	1.000	1.000	1.000	403.54	502.60	650.25	766.60	634.51	131.91	116.36	123.97
	10	1150	1.000	1.000	1.000	406.01	597.53	733.64	847.48	716.90	119.37	113.84	116.58
	20	673	1.000	0.941	0.681	900.36	305.34	298.45	496.89	357.43			
	20	775	1.000	1.000	0.883	1070.05	307.20	367.67	587.01	405.00			
	20	900	1.000	1.000	1.000	840.20	354.57	463.10	682.56	542.47			
	20	1025	1.000	1.000	1.000	874.95	450.69	561.17	769.76	626.48	175.79	208.60	191.73
	20	1150	1.000	1.000	1.000	882.54	541.55	646.03	843.60	701.39	159.83	197.57	178.04
	30.3	673	1.000	1.000	0.775	1855.02	313.18	316.12	599.50	402.46			
	30.3	775	1.000	1.000	0.789	1892.03	313.41	323.25	606.25	404.83			
	30.3	900	1.000	1.000	1.000	1411.18	324.01	405.42	701.18	546.23			
	30.3	1025	1.000	1.000	1.000	1493.97	403.58	499.66	791.30	630.27	226.68	291.64	257.80
	30.3	1150	1.000	1.000	1.000	1545.14	490.12	586.78	866.91	703.00	212.89	280.14	244.98
	40	673	1.000	1.000	0.895	2408.39	322.18	358.28	697.40	496.05			
	40	775	1.000	1.000	0.895	2408.37	322.18	358.29	697.40	496.05			
	40	900	1.000	1.000	0.947	2220.54	322.99	374.20	717.77	533.17			
	40	1025	1.000	1.000	1.000	2102.68	378.57	461.60	808.86	637.63			
	40	1150	1.000	1.000	1.000	2199.66	458.10	547.49	885.34	709.04	250.94	337.84	292.24
	50	673	1.000	1.000	0.950	2869.79	330.04	372.73	751.35	561.71			
	50	775	1.000	1.000	0.950	2869.79	330.04	372.73	751.35	561.71			
	50	900	1.000	1.000	0.950	2869.79	330.04	372.73	751.35	561.71			
	50	1025	1.000	1.000	1.000	2734.51	363.11	433.34	820.75	642.94			
	50	1150	1.000	1.000	1.000	2894.90	436.38	519.20	902.94	717.84	281.46	383.74	329.96
	60	673	1.000	1.000	1.000	3264.78	337.86	385.32	792.31	614.31			
	60	775	1.000	1.000	1.000	3264.78	337.86	385.32	792.31	614.31			
	60	900	1.000	1.000	1.000	3264.78	337.86	385.32	792.31	614.31			
	60	1025	1.000	1.000	1.000	3310.19	353.70	409.61	819.20	639.73			
	60	1150	1.000	1.000	1.000	3514.37	421.17	495.52	905.80	718.62			
80	673	1.000	1.000	1.000	4556.30	373.58	419.19	860.16	676.43				
80	775	1.000	1.000	1.000	4556.30	373.58	419.19	860.16	676.43				
80	900	1.000	1.000	1.000	4556.30	373.58	419.19	860.16	676.43				
80	1025	1.000	1.000	1.000	4556.30	373.58	419.19	860.16	676.43				
80	1150	1.000	1.000	1.000	4673.89	404.82	461.54	902.52	715.69				
100	673	1.000	1.000	1.000	5842.68	412.40	457.48	914.76	728.42				
100	775	1.000	1.000	1.000	5842.68	412.40	457.48	914.76	728.42				
100	900	1.000	1.000	1.000	5842.68	412.40	457.48	914.76	728.42				
100	1025	1.000	1.000	1.000	5842.68	412.40	457.48	914.76	728.42				
100	1150	1.000	1.000	1.000	5842.68	412.40	457.48	914.76	728.42				

Table III.2. HXN2 Temperature results for SF0.4.

SF	Flow [kg/h]	T_target [K]	X_3 [-]	X_2 [-]	X_1 [-]	Q_HXN2 [kW]	T_NH3in [K]	T_NH3out [K]	T_N2in [K]	T_N2out [K]	ΔT1_N2 [K]	ΔT2_N2 [K]	DMLT_N2 [K]
0.4	2.5	673	1.000	1.000	0.822	179.90	298.64	438.28	562.38	316.26			
	2.5	775	1.000	1.000	1.000	152.78	312.11	555.88	680.52	475.46			
	2.5	900	1.000	1.000	1.000	176.98	413.58	664.54	797.79	565.15			
	2.5	1025	1.000	1.000	1.000	201.25	516.86	754.83	912.28	653.40			
	2.5	1150	1.000	1.000	1.000	235.66	590.50	818.85	1023.33	725.84			
	5	673	1.000	1.000	0.764	269.52	299.09	381.85	499.64	314.64	15.55	117.79	50.49
	5	775	1.000	1.000	1.000	218.53	307.58	511.12	613.51	465.79			
	5	900	1.000	1.000	1.000	235.51	419.10	629.00	721.55	565.48			
	5	1025	1.000	1.000	1.000	252.94	525.90	724.92	821.34	657.12			
	5	1150	1.000	1.000	1.000	277.75	607.12	794.54	911.82	734.71			
	10	673	1.000	1.000	0.716	385.42	300.57	305.63	452.94	320.44			
	10	775	1.000	1.000	0.986	353.24	301.37	424.82	558.14	437.94	136.56	133.32	134.93
	10	900	1.000	1.000	1.000	378.31	402.42	550.57	671.58	545.32	142.89	121.01	131.65
	10	1025	1.000	1.000	1.000	403.54	502.60	650.25	766.60	634.51	131.91	116.36	123.97
	10	1150	1.000	1.000	1.000	406.01	597.53	733.64	847.48	716.90	119.37	113.84	116.58
	20	673	1.000	0.858	0.629	717.51	304.91	298.45	468.04	344.88			
	20	775	1.000	1.000	0.883	1070.05	307.20	367.67	587.01	405.00			
	20	900	1.000	1.000	1.000	840.20	354.57	463.10	682.56	542.47	187.90	219.46	203.28
	20	1025	1.000	1.000	1.000	874.94	450.69	561.17	769.76	626.48	175.79	208.60	191.73
	20	1150	1.000	1.000	1.000	882.54	541.55	646.03	843.60	701.39	159.83	197.57	178.04
	30.3	673	1.000	0.907	0.676	1457.88	311.84	298.45	547.47	383.10			
	30.3	775	1.000	1.000	0.781	1823.10	313.28	316.81	601.66	397.13			
	30.3	900	1.000	1.000	1.000	1411.18	324.01	405.42	701.18	546.23	222.22	295.76	257.24
	30.3	1025	1.000	1.000	1.000	1493.97	403.58	499.66	791.30	630.27	226.68	291.64	257.80
	30.3	1150	1.000	1.000	1.000	1545.14	490.12	586.78	866.91	703.00	212.89	280.14	244.98
	40	673	1.000	0.953	0.709	2265.60	318.80	298.45	608.75	416.55			
	40	775	1.000	0.955	0.710	2272.44	318.82	298.45	609.55	416.79			
	40	900	1.000	1.000	0.947	2220.54	322.99	374.20	717.77	533.17			
	40	1025	1.000	1.000	1.000	2102.68	378.57	461.60	808.86	637.63	259.06	347.27	301.01
	40	1150	1.000	1.000	1.000	2199.66	458.10	547.49	885.34	709.04	250.94	337.84	292.24
	50	673	1.000	0.993	0.740	3085.92	325.79	298.46	652.84	444.66			
	50	775	1.000	0.993	0.740	3085.92	325.79	298.46	652.84	444.66			
	50	900	1.000	1.000	0.883	3117.98	328.81	351.69	722.89	515.28			
	50	1025	1.000	1.000	1.000	2734.51	363.11	433.34	820.75	642.94	279.82	387.41	330.70
	50	1150	1.000	1.000	1.000	2894.90	436.38	519.20	902.94	717.84	281.46	383.74	329.96
	60	673	1.000	1.000	0.767	3913.93	332.35	309.10	688.81	469.99			
	60	775	1.000	1.000	0.767	3913.93	332.35	309.10	688.81	469.99			
	60	900	1.000	1.000	0.829	3891.58	333.83	331.66	719.25	502.99			
	60	1025	1.000	1.000	1.000	3310.19	353.70	409.61	819.20	639.73	286.03	409.59	344.12
	60	1150	1.000	1.000	1.000	3514.37	421.17	495.52	905.80	718.62	297.45	410.28	350.85
80	673	1.000	1.000	0.825	5130.53	344.49	327.19	745.03	532.37				
80	775	1.000	1.000	0.825	5130.53	344.49	327.19	745.03	532.37				
80	900	1.000	1.000	0.825	5130.53	344.49	327.19	745.03	532.37				
80	1025	1.000	1.000	0.990	4573.27	348.15	377.24	813.07	626.73				
80	1150	1.000	1.000	1.000	4673.89	404.82	461.54	902.52	715.69	310.87	440.98	372.14	
100	673	1.000	1.000	0.899	6143.93	355.39	346.44	791.10	589.55				
100	775	1.000	1.000	0.899	6143.93	355.39	346.44	791.10	589.55				
100	900	1.000	1.000	0.899	6143.93	355.39	346.44	791.10	589.55				
100	1025	1.000	1.000	0.941	6012.80	356.34	358.76	807.56	611.12				
100	1150	1.000	1.000	1.000	5791.75	400.24	440.88	899.00	713.68	313.44	458.12	381.21	

Table III.3. HXN2 Temperature results for SF0.5.

SF	Flow [kg/h]	T_target [K]	X_3 [-]	X_2 [-]	X_1 [-]	Q_HXN2 [kW]	T_NH3in [K]	T_NH3out [K]	T_N2in [K]	T_N2out [K]	$\Delta T1_{N2}$ [K]	$\Delta T2_{N2}$ [K]	DMLT_N2 [K]
0.5	2.5	673	1.000	1.000	0.822	179.90	298.64	438.28	562.38	316.26			
	2.5	775	1.000	1.000	1.000	152.78	312.11	555.88	680.52	475.46			
	2.5	900	1.000	1.000	1.000	176.98	413.58	664.54	797.79	565.15			
	2.5	1025	1.000	1.000	1.000	201.25	516.86	754.83	912.28	653.40			
	2.5	1150	1.000	1.000	1.000	235.66	590.50	818.85	1023.33	725.84			
	5	673	1.000	1.000	0.764	269.52	299.09	381.85	499.64	314.64	15.55	117.79	50.49
	5	775	1.000	1.000	1.000	218.53	307.58	511.12	613.51	465.79			
	5	900	1.000	1.000	1.000	235.51	419.10	629.00	721.55	565.48			
	5	1025	1.000	1.000	1.000	252.94	525.90	724.92	821.34	657.12			
	5	1150	1.000	1.000	1.000	277.75	607.12	794.54	911.82	734.71			
	10	673	1.000	1.000	0.716	385.42	300.57	305.63	452.94	320.44			
	10	775	1.000	1.000	0.986	353.24	301.37	424.82	558.14	437.94	136.56	133.32	134.93
	10	900	1.000	1.000	1.000	378.31	402.42	550.57	671.58	545.32	142.89	121.01	131.65
	10	1025	1.000	1.000	1.000	403.54	502.60	650.25	766.60	634.51	131.91	116.36	123.97
	10	1150	1.000	1.000	1.000	406.01	597.53	733.64	847.48	716.90			
	20	673	1.000	0.858	0.629	717.71	304.92	298.45	468.08	344.88			
	20	775	1.000	1.000	0.883	1070.05	307.20	367.67	587.01	405.00	97.80	219.35	150.48
	20	900	1.000	1.000	1.000	840.20	354.57	463.10	682.56	542.47	187.90	219.46	203.28
	20	1025	1.000	1.000	1.000	874.95	450.69	561.17	769.76	626.48	175.79	208.60	191.73
	20	1150	1.000	1.000	1.000	882.54	541.55	646.03	843.60	701.39	159.83	197.57	178.04
	30.3	673	1.000	0.848	0.632	1303.28	311.18	298.45	523.77	376.60			
	30.3	775	1.000	1.000	0.781	1823.10	313.28	316.81	601.66	397.13			
	30.3	900	1.000	1.000	1.000	1411.18	324.01	405.42	701.18	546.23	222.22	295.76	257.24
	30.3	1025	1.000	1.000	1.000	1493.97	403.58	499.66	791.30	630.27	226.68	291.64	257.80
	30.3	1150	1.000	1.000	1.000	1545.14	490.12	586.78	866.91	703.00	212.89	280.14	244.98
	40	673	1.000	0.887	0.659	2024.57	317.87	298.45	580.27	408.02			
	40	775	1.000	0.955	0.710	2272.44	318.82	298.45	609.55	416.79			
	40	900	1.000	1.000	0.947	2220.54	322.99	374.20	717.77	533.17	210.18	343.57	271.43
	40	1025	1.000	1.000	1.000	2102.69	378.57	461.60	808.86	637.63	259.06	347.27	301.02
	40	1150	1.000	1.000	1.000	2199.66	458.10	547.49	885.34	709.04	250.94	337.84	292.24
	50	673	1.000	0.922	0.684	2752.28	324.67	298.46	620.64	434.28			
	50	775	1.000	0.922	0.684	2752.28	324.67	298.46	620.64	434.28			
	50	900	1.000	1.000	0.883	3117.97	328.81	351.69	722.89	515.28			
	50	1025	1.000	1.000	1.000	2734.51	363.11	433.34	820.75	642.94	279.82	387.41	330.70
	50	1150	1.000	1.000	1.000	2894.90	436.38	519.20	902.94	717.84	281.46	383.74	329.96
	60	673	1.000	0.952	0.706	3496.59	331.05	298.46	654.19	457.85			
	60	775	1.000	0.952	0.706	3496.59	331.05	298.46	654.19	457.85			
	60	900	1.000	1.000	0.829	3891.58	333.83	331.66	719.25	502.99			
	60	1025	1.000	1.000	1.000	3310.19	353.70	409.61	819.20	639.73	286.03	409.59	344.12
	60	1150	1.000	1.000	1.000	3514.37	421.17	495.52	905.80	718.62	297.45	410.28	350.85
	80	673	1.000	1.000	0.752	5026.25	342.66	301.03	709.14	499.36			
	80	775	1.000	1.000	0.752	5026.25	342.66	301.03	709.14	499.36			
	80	900	1.000	1.000	0.752	5026.25	342.66	301.03	709.14	499.36			
	80	1025	1.000	1.000	0.990	4573.28	348.15	377.24	813.07	626.73	278.57	435.83	351.36
	80	1150	1.000	1.000	1.000	4673.89	404.82	461.54	902.52	715.69	310.87	440.98	372.14
	100	673	1.000	1.000	0.810	6241.64	353.21	318.69	753.30	546.82			
	100	775	1.000	1.000	0.810	6241.64	353.21	318.69	753.30	546.82			
	100	900	1.000	1.000	0.810	6241.64	353.21	318.69	753.30	546.82			
100	1025	1.000	1.000	0.941	6012.81	356.34	358.76	807.56	611.12				
100	1150	1.000	1.000	1.000	5791.75	400.24	440.88	899.00	713.68	313.44	458.12	381.21	

Table III.4. HXN2 Temperature results for SF1.

SF	Flow [kg/h]	T_target [K]	X_3 [-]	X_2 [-]	X_1 [-]	Q_HXN2 [kW]	T_NH3in [K]	T_NH3out [K]	T_N2in [K]	T_N2out [K]	ΔT1_N2 [K]	ΔT2_N2 [K]	DMLT_N2 [K]
1	2.5	673	1.000	1.000	0.822	179.90	298.64	438.28	562.38	316.26			
	2.5	775	1.000	1.000	1.000	152.78	312.11	555.88	680.52	475.46			
	2.5	900	1.000	1.000	1.000	176.98	413.58	664.54	797.79	565.15			
	2.5	1025	1.000	1.000	1.000	201.25	516.86	754.83	912.28	653.40			
	2.5	1150	1.000	1.000	1.000	235.66	590.50	818.85	1023.33	725.84			
	5	673	1.000	1.000	0.764	269.52	299.09	381.85	499.64	314.64			
	5	775	1.000	1.000	1.000	218.53	307.58	511.12	613.51	465.79			
	5	900	1.000	1.000	1.000	235.51	419.10	629.00	721.55	565.48			
	5	1025	1.000	1.000	1.000	252.94	525.90	724.92	821.34	657.12			
	5	1150	1.000	1.000	1.000	277.75	607.12	794.54	911.82	734.71			
	10	673	1.000	1.000	0.716	385.42	300.57	305.63	452.94	320.44	19.87	147.31	63.61
	10	775	1.000	1.000	0.986	353.23	301.37	424.82	558.14	437.94			
	10	900	1.000	1.000	1.000	378.31	402.42	550.57	671.58	545.32			
	10	1025	1.000	1.000	1.000	403.54	502.60	650.25	766.60	634.51			
	10	1150	1.000	1.000	1.000	406.01	597.53	733.64	847.48	716.90			
	20	673	1.000	0.858	0.629	717.71	304.92	298.45	468.08	344.88			
	20	775	1.000	1.000	0.883	1070.05	307.20	367.67	587.01	405.00	97.80	219.35	150.48
	20	900	1.000	1.000	1.000	840.20	354.57	463.10	682.56	542.47	187.90	219.46	203.28
	20	1025	1.000	1.000	1.000	874.95	450.69	561.17	769.76	626.48	175.79	208.60	191.73
	20	1150	1.000	1.000	1.000	882.54	541.56	646.03	843.60	701.39	159.83	197.57	178.04
	30.3	673	1.000	0.737	0.549	1014.03	309.91	298.45	478.13	363.36			
	30.3	775	1.000	1.000	0.781	1823.10	313.28	316.81	601.66	397.13	83.85	284.85	164.36
	30.3	900	1.000	1.000	1.000	1411.18	324.01	405.42	701.18	546.23	222.22	295.76	257.24
	30.3	1025	1.000	1.000	1.000	1493.97	403.58	499.66	791.30	630.27	226.68	291.64	257.80
	30.3	1150	1.000	1.000	1.000	1545.14	490.12	586.78	866.91	703.00	212.89	280.14	244.98
	40	673	1.000	0.659	0.492	1180.59	314.44	298.45	473.96	372.74			
	40	775	1.000	0.955	0.710	2272.44	318.82	298.45	609.55	416.79	97.96	311.10	184.45
	40	900	1.000	1.000	0.947	2220.53	322.99	374.20	717.77	533.17	210.18	343.57	271.44
	40	1025	1.000	1.000	1.000	2102.69	378.57	461.60	808.86	637.63	259.06	347.27	301.02
	40	1150	1.000	1.000	1.000	2199.66	458.10	547.49	885.34	709.04	250.94	337.84	292.24
	50	673	1.000	0.730	0.540	1855.35	321.35	298.45	529.06	402.26			
	50	775	1.000	0.883	0.654	2570.57	324.01	298.46	602.72	428.31			
	50	900	1.000	1.000	0.883	3117.97	328.81	351.69	722.89	515.28	186.48	371.20	268.32
	50	1025	1.000	1.000	1.000	2734.51	363.11	433.34	820.75	642.94	279.82	387.41	330.70
	50	1150	1.000	1.000	1.000	2894.90	436.39	519.20	902.94	717.84	281.46	383.74	329.96
	60	673	1.000	0.750	0.550	2359.72	327.15	298.46	555.30	421.30			
	60	775	1.000	0.826	0.608	2792.55	328.71	298.46	594.06	436.13			
	60	900	1.000	1.000	0.829	3891.57	333.83	331.66	719.25	502.99	169.16	387.59	263.45
	60	1025	1.000	1.000	1.000	3310.19	353.70	409.61	819.20	639.73	286.03	409.59	344.12
	60	1150	1.000	1.000	1.000	3514.37	421.17	495.52	905.80	718.62	297.45	410.28	350.85
80	673	1.000	0.787	0.569	3396.27	337.87	298.46	598.71	454.91				
80	775	1.000	0.787	0.569	3396.27	337.87	298.46	598.71	454.91				
80	900	1.000	1.000	0.750	5015.67	342.63	300.47	708.46	499.11	156.47	407.99	262.44	
80	1025	1.000	1.000	0.990	4573.27	348.15	377.24	813.07	626.73	278.57	435.83	351.36	
80	1150	1.000	1.000	1.000	4673.89	404.82	461.54	902.52	715.69	310.87	440.98	372.14	
100	673	1.000	0.826	0.595	4479.47	347.51	298.46	635.50	484.63				
100	775	1.000	0.826	0.595	4479.47	347.51	298.46	635.50	484.63				
100	900	1.000	0.944	0.698	5550.81	350.41	298.46	697.02	511.66				
100	1025	1.000	1.000	0.941	6012.81	356.34	358.76	807.56	611.12	254.78	448.80	342.68	
100	1150	1.000	1.000	1.000	5763.32	392.62	430.04	888.35	703.53	310.92	458.31	379.86	

Table III.7. HXN2 UA calculation tables for SF0.5.

SF	Tm_NH3 [K]	k_NH3 [W/m²K]	μ_NH3 [Pa·s]	ReD_NH3 [-] (Ø=2mm)	Pr_NH3 [-]	NuD_NH3 [-] (Ø=2mm)	h_NH3 [W/m²K]	Rconv_int [K/W]	Rcond [K/W]	Øint [mm]	Øext [mm]	Area [m²]	Tm_N2 [K]	rho_N2 [kg/m³]	v_N2 [m/s]	h_N2 [W/m²K]	Rconv_ext [K/W]	UA [K/W]
										16	18							
										16	18							
										16	18							
										16	18							
										16	18							
	340.468	0.031	1.17E-05	7539.82	0.97	28.75	443.6	0.359	0.004	16	18	1.3E-04	499.6	6.800	1.2901486	2.99	35.537	0.028
										16	18							
										16	18							
										16	18							
										16	18							
										16	18							
	363.096	0.033	1.25E-05	14114.36	0.94	46.76	778.6	0.204	0.004	16	18	1.3E-04	558.1	6.070	2.8905178	6.12	17.333	0.057
	476.497	0.050	1.71E-05	10345.08	0.85	35.12	886.6	0.180	0.004	16	18	1.3E-04	671.6	5.036	3.4839802	7.23	14.679	0.067
	576.422	0.066	2.10E-05	8436.97	0.85	29.85	989.8	0.161	0.004	16	18	1.3E-04	766.6	4.416	3.9736437	8.13	13.058	0.076
										16	18							
										16	18							
										16	18							
										16	18							
	337.436	0.030	1.15E-05	30682.54	0.98	88.77	1344.5	0.118	0.004	16	18	1.3E-04	587.0	5.761	6.0908880	11.88	8.929	0.110
	408.833	0.040	1.43E-05	24689.54	0.89	71.57	1415.6	0.112	0.004	16	18	1.3E-04	682.6	4.963	7.0711592	13.57	7.818	0.126
	505.926	0.055	1.83E-05	19361.56	0.85	57.82	1601.3	0.099	0.004	16	18	1.3E-04	769.8	4.416	7.9472873	15.06	7.046	0.140
	593.795	0.068	2.15E-05	16428.73	0.86	51.00	1745.6	0.091	0.004	16	18	1.3E-04	843.6	4.024	8.7198196	16.35	6.488	0.152
										16	18							
										16	18							
										16	18							
	364.715	0.033	1.25E-05	42766.51	0.94	113.50	1890.0	0.084	0.004	16	18	1.3E-04	701.2	4.822	11.0251640	20.15	5.265	0.187
	451.622	0.046	1.61E-05	33260.19	0.86	89.76	2085.1	0.076	0.004	16	18	1.3E-04	791.3	4.277	12.4303118	22.42	4.732	0.208
	538.446	0.060	1.94E-05	27579.87	0.84	76.70	2309.8	0.069	0.004	16	18	1.3E-04	866.9	3.909	13.6005228	24.29	4.368	0.225
										16	18							
										16	18							
										16	18							
	348.593	0.031	1.19E-05	59302.09	0.96	149.03	2343.7	0.068	0.004	16	18	1.3E-04	717.8	4.722	14.8638409	26.29	4.036	0.243
	420.083	0.042	1.49E-05	47403.52	0.88	120.06	2508.1	0.063	0.004	16	18	1.3E-04	808.9	4.198	16.7184573	29.19	3.635	0.270
	502.796	0.055	1.81E-05	39140.95	0.85	101.56	2771.4	0.057	0.004	16	18	1.3E-04	885.3	3.821	18.3660658	31.74	3.343	0.294
										16	18							
										16	18							
										16	18							
	398.228	0.038	1.39E-05	63487.77	0.89	152.93	2913.4	0.055	0.004	16	18	1.3E-04	820.8	4.122	21.2844158	36.19	2.932	0.334
	477.790	0.050	1.71E-05	51725.41	0.85	127.26	3212.9	0.050	0.004	16	18	1.3E-04	902.9	3.758	23.3436498	39.29	2.701	0.363
										16	18							
										16	18							
										16	18							
										16	18							
	381.655	0.036	1.33E-05	79609.32	0.91	184.52	3318.3	0.048	0.004	16	18	1.3E-04	819.2	4.147	25.3867047	42.33	2.506	0.391
	458.342	0.047	1.63E-05	65062.11	0.86	153.39	3624.4	0.044	0.004	16	18	1.3E-04	905.8	3.738	28.1667717	46.43	2.285	0.429
										16	18							
										16	18							
										16	18							
	362.606	0.033	1.25E-05	112914.89	0.94	246.78	4109.5	0.039	0.004	16	18	1.3E-04	813.1	4.172	33.6428751	54.39	1.951	0.502
	433.179	0.043	1.53E-05	92350.06	0.87	204.13	4420.8	0.036	0.004	16	18	1.3E-04	902.5	3.758	37.3498398	59.69	1.778	0.550
										16	18							
										16	18							
										16	18							
										16	18							
	420.558	0.042	1.49E-05	118508.80	0.88	249.88	5220.4	0.030	0.004	16	18	1.3E-04	899.0	3.779	46.4303281	72.45	1.465	0.667

Table III.11. HXN2 Tube number calculation tables for SF0.5.

SF	U = 100 [W/m2K]			U = 300 [W/m2K]			U = 500 [W/m2K]			U = 1000 [W/m2K]			U = 1500 [W/m2K]		
	A_DMLT [m ²]	NT_N2 [-]	A_DB [m ²]	A_DMLT [m ²]	NT_N2 [-]	A_DB [m ²]	A_DMLT [m ²]	NT_N2 [-]	A_DB [m ²]	A_DMLT [m ²]	NT_N2 [-]	A_DB [m ²]	A_DMLT [m ²]	NT_N2 [-]	A_DB [m ²]
	0.0534	7	0.0003	0.0178	3	0.0001	0.0107	2	0.0001	0.0053	1	0.0000	0.0036	1	0.0000
	0.0262	4	0.0006	0.0087	2	0.0002	0.0052	1	0.0001	0.0026	1	0.0001	0.0017	1	0.0000
	0.0287	4	0.0007	0.0096	2	0.0002	0.0057	1	0.0001	0.0029	1	0.0001	0.0019	1	0.0000
	0.0326	5	0.0008	0.0109	2	0.0003	0.0065	1	0.0002	0.0033	1	0.0001	0.0022	1	0.0001
	0.0711	10	0.0011	0.0237	4	0.0004	0.0142	2	0.0002	0.0071	1	0.0001	0.0047	1	0.0001
	0.0413	6	0.0013	0.0138	2	0.0004	0.0083	2	0.0003	0.0041	1	0.0001	0.0028	1	0.0001
	0.0456	6	0.0014	0.0152	2	0.0005	0.0091	2	0.0003	0.0046	1	0.0001	0.0030	1	0.0001
	0.0496	7	0.0015	0.0165	3	0.0005	0.0099	2	0.0003	0.0050	1	0.0002	0.0033	1	0.0001
	0.0549	7	0.0019	0.0183	3	0.0006	0.0110	2	0.0004	0.0055	1	0.0002	0.0037	1	0.0001
	0.0580	8	0.0021	0.0193	3	0.0007	0.0116	2	0.0004	0.0058	1	0.0002	0.0039	1	0.0001
	0.0631	9	0.0023	0.0210	3	0.0008	0.0126	2	0.0005	0.0063	1	0.0002	0.0042	1	0.0002
	0.0818	11	0.0024	0.0273	4	0.0008	0.0164	3	0.0005	0.0082	2	0.0002	0.0055	1	0.0002
	0.0699	9	0.0027	0.0233	3	0.0009	0.0140	2	0.0005	0.0070	1	0.0003	0.0047	1	0.0002
	0.0753	10	0.0029	0.0251	4	0.0010	0.0151	2	0.0006	0.0075	1	0.0003	0.0050	1	0.0002
	0.0827	11	0.0033	0.0276	4	0.0011	0.0165	3	0.0007	0.0083	2	0.0003	0.0055	1	0.0002
	0.0877	12	0.0036	0.0292	4	0.0012	0.0175	3	0.0007	0.0088	2	0.0004	0.0058	1	0.0002
	0.0962	13	0.0039	0.0321	5	0.0013	0.0192	3	0.0008	0.0096	2	0.0004	0.0064	1	0.0003
	0.1002	13	0.0043	0.0334	5	0.0014	0.0200	3	0.0009	0.0100	2	0.0004	0.0067	1	0.0003
	0.1302	17	0.0050	0.0434	6	0.0017	0.0260	4	0.0010	0.0130	2	0.0005	0.0087	2	0.0003
	0.1256	16	0.0055	0.0419	6	0.0018	0.0251	4	0.0011	0.0126	2	0.0006	0.0084	2	0.0004
	0.1519	20	0.0067	0.0506	7	0.0022	0.0304	4	0.0013	0.0152	2	0.0007	0.0101	2	0.0004

III.4 Additional Results for HXH2

Table III.13. HXH2 Additional results for SF0.2.

SF	Flow	T_target	X_3	X_2	X_1	Q_HXH2	T_NH3in	T_NH3out	T_H2in	T_H2out	ΔT1	ΔT2	LMTD	A_H2	Tube Number	h_H2out	Q_H2-Air
	[kg/h]	[K]	[-]	[-]	[-]	[kW]	[K]	[K]	[K]	[K]	[K]	[K]	[K]	[m2]	[-]	[kJ/kg]	[kW]
0.2	2.5	673	1.000	1.000	0.822	617.77	298.72	298.64	649.99	298.30						3931	-0.11
	2.5	775	1.000	1.000	1.000	839.40	298.81	312.11	774.99	298.23						3930	-0.11
	2.5	900	1.000	1.000	1.000	1059.78	298.93	413.58	900.00	300.01						3955	-0.10
	2.5	1025	1.000	1.000	1.000	1326.17	299.04	516.86	1025.00	276.64						3623	-0.14
	2.5	1150	1.000	1.000	1.000	1467.62	299.12	590.50	1149.99	327.42						4348	-0.06
	5	673	1.000	1.000	0.764	1231.74	299.33	299.09	650.00	299.31						3945	-0.21
	5	775	1.000	1.000	1.000	1673.52	299.68	307.57	775.00	299.64	0.05	467.43	50.72	0.009	2	3950	-0.21
	5	900	1.000	1.000	1.000	2105.57	300.20	419.10	900.00	303.89	3.69	480.90	98.00	0.012	2	4011	-0.19
	5	1025	1.000	1.000	1.000	2529.66	300.64	525.90	1025.00	311.97						4126	-0.17
	5	1150	1.000	1.000	1.000	2830.38	300.94	607.12	1150.00	357.25						4778	-0.01
	10	673	1.000	1.000	0.715	2412.39	299.10	300.57	650.01	306.48						4048	-0.37
	10	775	1.000	1.000	0.986	3283.68	301.79	301.37	775.01	308.74						4080	-0.35
	10	900	1.000	1.000	1.000	4073.86	303.70	402.42	900.02	323.61	19.91	497.59	148.41	0.021	3	4293	-0.25
	10	1025	1.000	1.000	1.000	4772.71	304.94	502.60	1025.02	353.03	48.09	522.42	198.85	0.026	4	4717	-0.04
	10	1150	1.000	1.000	1.000	5479.77	306.09	597.53	1150.02	382.92	76.84	552.49	241.11	0.031	4	5151	0.17
	20	673	1.000	0.941	0.681	4657.74	292.95	305.34	670.32	342.89						4571	-0.23
	20	775	1.000	1.000	0.883	5962.88	293.65	307.20	775.10	352.17						4705	-0.10
	20	900	1.000	1.000	1.000	7441.42	295.31	354.57	900.12	374.18						5023	0.22
	20	1025	1.000	1.000	1.000	8789.04	297.75	450.69	1025.15	406.99	109.24	574.47	280.28	0.031	4	5499	0.68
	20	1150	1.000	1.000	1.000	10087.59	300.21	541.55	1150.18	445.21	144.99	608.63	323.20	0.038	5	6052	1.23
	30.3	673	1.000	1.000	0.775	8066.78	291.77	313.18	768.60	392.90						5295	0.73
	30.3	775	1.000	1.000	0.789	8219.75	291.80	313.41	778.04	394.19						5314	0.76
	30.3	900	1.000	1.000	1.000	10393.89	292.31	324.01	900.37	415.75						5626	1.22
	30.3	1025	1.000	1.000	1.000	12237.77	293.23	403.58	1025.45	457.95	164.72	621.87	344.11	0.032	5	6237	2.13
	30.3	1150	1.000	1.000	1.000	14100.66	294.20	490.12	1150.55	501.10	206.90	660.43	390.76	0.038	5	6863	3.06
	40	673	1.000	1.000	0.895	12210.27	291.23	322.18	874.14	442.70						6016	2.38
	40	775	1.000	1.000	0.895	12210.37	291.23	322.18	874.14	442.70						6016	2.38
	40	900	1.000	1.000	0.947	12821.82	291.29	322.99	900.74	448.16						6095	2.54
	40	1025	1.000	1.000	1.000	15276.87	291.73	378.57	1025.90	489.67						6697	3.72
	40	1150	1.000	1.000	1.000	17598.51	292.21	458.10	1151.09	537.80	245.59	692.99	431.29	0.040	6	7395	5.08
	50	673	1.000	1.000	0.950	16084.76	290.84	330.04	936.46	483.16						6602	4.41
	50	775	1.000	1.000	0.950	16084.76	290.84	330.04	936.46	483.16						6602	4.41
	50	900	1.000	1.000	0.950	16084.76	290.84	330.04	936.46	483.16						6602	4.41
	50	1025	1.000	1.000	1.000	18249.82	291.03	363.11	1026.54	514.42						7056	5.52
	50	1150	1.000	1.000	1.000	21060.21	291.34	436.38	1151.87	565.27	273.93	715.49	459.91	0.043	6	7794	7.33
	60	673	1.000	1.000	1.000	20129.35	290.81	337.86	992.67	521.33						7156	6.92
	60	775	1.000	1.000	1.000	20129.35	290.81	337.86	992.67	521.33						7156	6.92
	60	900	1.000	1.000	1.000	20129.35	290.81	337.86	992.67	521.33						7156	6.92
	60	1025	1.000	1.000	1.000	21063.26	290.88	353.70	1027.36	535.10						7356	7.51
	60	1150	1.000	1.000	1.000	24385.96	291.13	421.17	1152.88	587.30						8114	9.74
80	673	1.000	1.000	1.000	28666.63	291.01	373.58	1093.10	593.01						8197	13.31	
80	775	1.000	1.000	1.000	28666.63	291.01	373.58	1093.10	593.01						8197	13.31	
80	900	1.000	1.000	1.000	28666.63	291.01	373.58	1093.10	593.01						8197	13.31	
80	1025	1.000	1.000	1.000	28666.63	291.01	373.58	1093.10	593.01						8197	13.31	
80	1150	1.000	1.000	1.000	30855.21	291.12	404.82	1155.56	619.55						8583	14.83	
100	673	1.000	1.000	1.000	38403.51	291.29	412.40	1183.57	651.31						9045	20.80	
100	775	1.000	1.000	1.000	38403.51	291.29	412.40	1183.57	651.31						9045	20.80	
100	900	1.000	1.000	1.000	38403.51	291.29	412.40	1183.57	651.31						9045	20.80	
100	1025	1.000	1.000	1.000	38403.51	291.29	412.40	1183.57	651.31						9045	20.80	
100	1150	1.000	1.000	1.000	38403.51	291.29	412.40	1183.57	651.31						9045	20.80	

Table III.14. HXH2 Additional results for SF0.4.

SF	Flow [kg/h]	T_target [K]	X_3 [-]	X_2 [-]	X_1 [-]	Q_HXH2 [kW]	T_NH3in [K]	T_NH3out [K]	T_H2in [K]	T_H2out [K]	ΔT1 [K]	ΔT2 [K]	LMTD [K]	A_H2 [m2]	Tube Number [-]	h_H2out [kJ/kg]	Q_H2-Air [kW]	HX
0.4	2.5	673	1.000	1.000	0.822	617.77	298.72	298.64	649.99	298.30						3931	-0.11	
	2.5	775	1.000	1.000	1.000	839.40	298.81	312.11	774.99	298.23						3930	-0.11	
	2.5	900	1.000	1.000	1.000	1059.78	298.93	413.58	900.00	300.01						3955	-0.10	
	2.5	1025	1.000	1.000	1.000	1326.17	299.04	516.86	1025.00	276.64						3623	-0.14	
	2.5	1150	1.000	1.000	1.000	1467.62	299.12	590.50	1149.99	327.42						4348	-0.06	
	5	673	1.000	1.000	0.764	1231.74	299.33	299.09	650.00	299.31	0.02	350.91	36.01	0.016	3	3945	-0.21	
	5	775	1.000	1.000	1.000	1673.52	299.68	307.58	775.00	299.64						3950	-0.21	
	5	900	1.000	1.000	1.000	2105.57	300.20	419.10	900.00	303.89						4011	-0.19	
	5	1025	1.000	1.000	1.000	2529.66	300.64	525.90	1025.00	311.97						4126	-0.17	
	5	1150	1.000	1.000	1.000	2830.37	300.94	607.12	1150.00	357.25						4778	-0.01	
	10	673	1.000	1.000	0.716	2413.53	299.11	300.57	650.01	306.49						4048	-0.37	
	10	775	1.000	1.000	0.986	3283.68	301.79	301.37	775.01	308.74	6.96	473.64	110.57	0.016	3	4080	-0.35	
	10	900	1.000	1.000	1.000	4073.85	303.70	402.42	900.02	323.61	19.91	497.59	148.41	0.021	3	4293	-0.25	
	10	1025	1.000	1.000	1.000	4772.71	304.94	502.60	1025.02	353.03	48.09	522.42	198.85	0.026	4	4717	-0.04	
	10	1150	1.000	1.000	1.000	5479.77	306.09	597.53	1150.02	382.92	76.84	552.49	241.11	0.031	4	5151	0.17	
	20	673	1.000	0.858	0.629	4357.00	292.75	304.91	650.08	340.15						4531	-0.27	
	20	775	1.000	1.000	0.883	5962.88	293.65	307.20	775.10	352.17						4705	-0.10	
	20	900	1.000	1.000	1.000	7441.43	295.31	354.57	900.12	374.18	78.87	545.55	241.31	0.024	4	5023	0.22	
	20	1025	1.000	1.000	1.000	8789.04	297.75	450.69	1025.15	406.99	109.24	574.47	280.28	0.031	4	5499	0.68	
	20	1150	1.000	1.000	1.000	10087.59	300.21	541.55	1150.18	445.21	144.99	608.63	323.20	0.038	5	6052	1.23	
	30.3	673	1.000	0.907	0.676	7163.81	291.57	311.84	719.70	383.96						5166	0.54	
	30.3	775	1.000	1.000	0.781	8158.78	291.78	313.28	775.30	393.46						5303	0.74	
	30.3	900	1.000	1.000	1.000	10393.90	292.31	324.01	900.37	415.75	123.44	576.35	293.92	0.027	4	5626	1.22	
	30.3	1025	1.000	1.000	1.000	12237.77	293.23	403.58	1025.45	457.95	164.72	621.87	344.11	0.032	5	6237	2.13	
	30.3	1150	1.000	1.000	1.000	14100.67	294.20	490.12	1150.55	501.10	206.90	660.43	390.76	0.038	5	6863	3.06	
	40	673	1.000	0.953	0.709	9977.74	291.00	318.80	774.81	421.22						5705	1.77	
	40	775	1.000	0.955	0.710	9995.28	291.00	318.82	775.60	421.39						5707	1.78	
	40	900	1.000	1.000	0.947	12821.83	291.29	322.99	900.74	448.16						6095	2.54	
	40	1025	1.000	1.000	1.000	15276.86	291.73	378.57	1025.90	489.67	197.95	647.33	379.27	0.034	5	6697	3.72	
	40	1150	1.000	1.000	1.000	17598.51	292.21	458.10	1151.09	537.80	245.59	692.99	431.29	0.040	6	7395	5.08	
	50	673	1.000	0.993	0.740	13052.90	290.66	325.79	824.01	454.60						6189	3.40	
	50	775	1.000	0.993	0.740	13052.90	290.66	325.79	824.01	454.60						6189	3.40	
	50	900	1.000	1.000	0.883	15124.20	290.78	328.81	901.27	474.41						6476	4.10	
	50	1025	1.000	1.000	1.000	18249.82	291.03	363.11	1026.54	514.42	223.38	663.42	404.25	0.037	5	7056	5.52	
	50	1150	1.000	1.000	1.000	21060.21	291.34	436.38	1151.87	565.27	273.93	715.49	459.91	0.043	6	7794	7.33	
	60	673	1.000	1.000	0.767	16243.86	290.63	332.35	867.86	485.45						6636	5.39	
	60	775	1.000	1.000	0.767	16243.86	290.63	332.35	867.86	485.45						6636	5.39	
	60	900	1.000	1.000	0.829	17288.95	290.68	333.83	901.97	495.51						6782	5.82	
	60	1025	1.000	1.000	1.000	21063.26	290.88	353.70	1027.36	535.10	244.22	673.66	423.24	0.041	6	7356	7.51	
	60	1150	1.000	1.000	1.000	24385.98	291.13	421.17	1152.88	587.30	296.18	731.71	481.56	0.046	6	8114	9.74	
80	673	1.000	1.000	0.825	23037.25	290.79	344.49	944.51	539.39						7418	10.26		
80	775	1.000	1.000	0.825	23037.25	290.79	344.49	944.51	539.39						7418	10.26		
80	900	1.000	1.000	0.825	23037.25	290.79	344.49	944.51	539.39						7418	10.26		
80	1025	1.000	1.000	0.990	26385.55	290.90	348.15	1029.60	567.59						7827	11.86		
80	1150	1.000	1.000	1.000	30855.21	291.12	404.82	1155.56	619.55	328.43	750.74	510.82	0.055	8	8583	14.83		
100	673	1.000	1.000	0.899	30548.03	291.00	355.39	1011.68	583.59						8060	15.97		
100	775	1.000	1.000	0.899	30548.03	291.00	355.39	1011.68	583.59						8060	15.97		
100	900	1.000	1.000	0.899	30548.03	291.00	355.39	1011.68	583.59						8060	15.97		
100	1025	1.000	1.000	0.941	31535.14	291.03	356.34	1032.57	591.20						8170	16.51		
100	1150	1.000	1.000	1.000	37320.58	291.25	400.24	1159.13	640.99	349.74	758.89	528.17	0.065	9	8895	20.06		

Table III.15. HXH2 Additional results for SF0.5.

SF	Flow [kg/h]	T_target [K]	X_3 [-]	X_2 [-]	X_1 [-]	Q_HXH2 [kW]	T_NH3in [K]	T_NH3out [K]	T_H2in [K]	T_H2out [K]	ΔT1 [K]	ΔT2 [K]	LMTD [K]	A_H2 [m2]	Tube Number [-]	h_H2out [kJ/kg]	Q_H2-Air [kW]	HX
0.5	2.5	673	1.000	1.000	0.822	617.77	298.72	298.64	649.99	298.30						3931	-0.11	
	2.5	775	1.000	1.000	1.000	839.40	298.81	312.11	774.99	298.23						3930	-0.11	
	2.5	900	1.000	1.000	1.000	1059.78	298.93	413.58	900.00	300.01						3955	-0.10	
	2.5	1025	1.000	1.000	1.000	1326.18	299.04	516.86	1025.00	276.64						3623	-0.14	
	2.5	1150	1.000	1.000	1.000	1467.62	299.12	590.50	1149.99	327.42						4348	-0.06	
	5	673	1.000	1.000	0.764	1231.74	299.33	299.09	650.00	299.31	0.02	350.91	36.01	0.02	3	3945	-0.21	
	5	775	1.000	1.000	1.000	1673.52	299.68	307.58	775.00	299.64						3950	-0.21	
	5	900	1.000	1.000	1.000	2105.57	300.20	419.10	900.00	303.89						4011	-0.19	
	5	1025	1.000	1.000	1.000	2529.66	300.64	525.90	1025.00	311.97						4126	-0.17	
	5	1150	1.000	1.000	1.000	2830.38	300.94	607.12	1150.00	357.25						4778	-0.01	
	10	673	1.000	1.000	0.716	2413.53	299.11	300.57	650.01	306.49						4048	-0.37	
	10	775	1.000	1.000	0.986	3283.68	301.79	301.37	775.01	308.74	6.96	473.64	110.57	0.02	3	4080	-0.35	
	10	900	1.000	1.000	1.000	4073.86	303.70	402.42	900.02	323.61	19.91	497.59	148.41	0.02	3	4293	-0.25	
	10	1025	1.000	1.000	1.000	4772.71	304.94	502.60	1025.02	353.03	48.09	522.42	198.85	0.03	4	4717	-0.04	
	10	1150	1.000	1.000	1.000	5479.77	306.09	597.53	1150.02	382.92						5151	0.17	
	20	673	1.000	0.858	0.629	4358.71	292.75	304.92	650.08	340.18						4532	-0.26	
	20	775	1.000	1.000	0.883	5962.88	293.65	307.20	775.10	352.17	58.52	467.90	196.92	0.03	4	4705	-0.10	
	20	900	1.000	1.000	1.000	7441.42	295.31	354.57	900.12	374.18	78.87	545.55	241.31	0.02	4	5023	0.22	
	20	1025	1.000	1.000	1.000	8789.04	297.75	450.69	1025.15	406.99	109.24	574.47	280.28	0.03	4	5499	0.68	
	20	1150	1.000	1.000	1.000	10087.59	300.21	541.55	1150.18	445.21	144.99	608.63	323.20	0.04	5	6052	1.23	
	30.3	673	1.000	0.848	0.632	6742.12	291.48	311.18	695.80	379.70						5104	0.45	
	30.3	775	1.000	1.000	0.781	8158.78	291.78	313.28	775.30	393.46						5303	0.74	
	30.3	900	1.000	1.000	1.000	10393.89	292.31	324.01	900.37	415.75	123.44	576.35	293.92	0.03	4	5626	1.22	
	30.3	1025	1.000	1.000	1.000	12237.76	293.23	403.58	1025.45	457.95	164.72	621.87	344.11	0.03	5	6237	2.13	
	30.3	1150	1.000	1.000	1.000	14100.66	294.20	490.12	1150.55	501.10	206.90	660.43	390.76	0.04	5	6863	3.06	
	40	673	1.000	0.887	0.659	9367.03	290.93	317.87	747.21	415.04						5615	1.60	
	40	775	1.000	0.955	0.710	9995.28	291.00	318.82	775.60	421.39						5707	1.78	
	40	900	1.000	1.000	0.947	12821.82	291.29	322.99	900.74	448.16	156.87	577.75	322.83	0.03	5	6095	2.54	
	40	1025	1.000	1.000	1.000	15276.86	291.73	378.57	1025.90	489.67	197.95	647.33	379.27	0.03	5	6697	3.72	
	40	1150	1.000	1.000	1.000	17598.51	292.21	458.10	1151.09	537.80	245.59	692.99	431.29	0.04	6	7395	5.08	
	50	673	1.000	0.922	0.684	12229.70	290.61	324.67	792.94	446.52						6071	3.11	
	50	775	1.000	0.922	0.684	12229.70	290.61	324.67	792.94	446.52						6071	3.11	
	50	900	1.000	1.000	0.883	15124.22	290.78	328.81	901.27	474.41						6476	4.10	
	50	1025	1.000	1.000	1.000	18249.82	291.03	363.11	1026.54	514.42	223.38	663.42	404.25	0.04	5	7056	5.52	
	50	1150	1.000	1.000	1.000	21060.21	291.34	436.38	1151.87	565.27	273.93	715.49	459.91	0.04	6	7794	7.33	
	60	673	1.000	0.952	0.706	15197.49	290.59	331.05	833.56	475.37						6489	4.96	
	60	775	1.000	0.952	0.706	15197.49	290.59	331.05	833.56	475.37						6489	4.96	
	60	900	1.000	1.000	0.829	17288.94	290.68	333.83	901.97	495.51						6782	5.82	
	60	1025	1.000	1.000	1.000	21063.26	290.88	353.70	1027.36	535.10	244.22	673.66	423.24	0.04	6	7356	7.51	
	60	1150	1.000	1.000	1.000	24385.98	291.13	421.17	1152.88	587.30	296.18	731.71	481.56	0.05	6	8114	9.74	
	80	673	1.000	1.000	0.752	21498.44	290.73	342.66	904.51	525.72						7220	9.48	
	80	775	1.000	1.000	0.752	21498.44	290.73	342.66	904.51	525.72						7220	9.48	
	80	900	1.000	1.000	0.752	21498.44	290.73	342.66	904.51	525.72						7220	9.48	
	80	1025	1.000	1.000	0.990	26385.52	290.90	348.15	1029.60	567.59	276.68	681.44	449.06	0.05	7	7827	11.86	
	80	1150	1.000	1.000	1.000	30855.22	291.12	404.82	1155.56	619.55	328.43	750.74	510.82	0.06	8	8583	14.83	
	100	673	1.000	1.000	0.810	28430.63	290.93	353.21	966.31	566.94						7818	14.79	
	100	775	1.000	1.000	0.810	28430.63	290.93	353.21	966.31	566.94						7818	14.79	
	100	900	1.000	1.000	0.810	28430.63	290.93	353.21	966.31	566.94						7818	14.79	
	100	1025	1.000	1.000	0.941	31535.11	291.03	356.34	1032.57	591.20						8170	16.51	
	100	1150	1.000	1.000	1.000	37320.61	291.25	400.24	1159.13	640.99	349.74	758.89	528.17	0.07	9	8895	20.06	

Table III.16. HXH2 Additional results for SF1.

SF	Flow [kg/h]	T_target [K]	X_3 [-]	X_2 [-]	X_1 [-]	Q_HXH2 [kW]	T_NH3in [K]	T_NH3out [K]	T_H2in [K]	T_H2out [K]	ΔT1 [K]	ΔT2 [K]	LMTD [K]	A_H2 [m2]	Tube Number [-]	h_H2out [kJ/kg]	Q_H2-Air [kW]	
1	2.5	673	1.000	1.000	0.822	617.77	298.72	298.64	649.99	298.30						3931	-0.11	
	2.5	775	1.000	1.000	1.000	839.40	298.81	312.11	774.99	298.23						3930	-0.11	
	2.5	900	1.000	1.000	1.000	1059.78	298.93	413.58	900.00	300.01						3955	-0.10	
	2.5	1025	1.000	1.000	1.000	1326.17	299.04	516.86	1025.00	298.64						3623	-0.14	
	2.5	1150	1.000	1.000	1.000	1467.62	299.12	590.50	1149.99	327.42						4348	-0.06	
	5	673	1.000	1.000	0.764	1231.74	299.33	299.09	650.00	299.31							3945	-0.21
	5	775	1.000	1.000	1.000	1673.52	299.68	307.58	775.00	299.64							3950	-0.21
	5	900	1.000	1.000	1.000	2105.58	300.20	419.10	900.00	303.89							4011	-0.19
	5	1025	1.000	1.000	1.000	2529.66	300.64	525.90	1025.00	311.97							4126	-0.17
	5	1150	1.000	1.000	1.000	2830.38	300.94	607.12	1150.00	357.25							4778	-0.01
	10	673	1.000	1.000	0.716	2413.53	299.11	300.57	650.01	306.49	7.38	349.44	88.68	0.025	4	4048	-0.37	
	10	775	1.000	1.000	0.986	3283.70	301.79	301.37	775.01	308.74							4080	-0.35
	10	900	1.000	1.000	1.000	4073.85	303.70	402.42	900.02	323.61							4293	-0.25
	10	1025	1.000	1.000	1.000	4772.71	304.94	502.60	1025.02	353.03							4717	-0.04
	10	1150	1.000	1.000	1.000	5479.76	306.09	597.53	1150.02	382.92							5151	0.17
	20	673	1.000	0.858	0.629	4358.71	292.75	304.92	650.08	340.18							4532	-0.26
	20	775	1.000	1.000	0.883	5962.88	293.65	307.20	775.10	352.17	58.52	467.90	196.92	0.026	4	4705	-0.10	
	20	900	1.000	1.000	1.000	7441.42	295.31	354.57	900.12	374.18	78.87	545.55	241.31	0.024	4	5023	0.22	
	20	1025	1.000	1.000	1.000	8789.04	297.75	450.69	1025.15	406.99	109.24	574.47	280.28	0.031	4	5499	0.68	
	20	1150	1.000	1.000	1.000	10087.59	300.21	541.56	1150.18	445.21	144.99	608.63	323.20	0.038	5	6052	1.23	
	30.3	673	1.000	0.737	0.549	5944.28	291.31	309.91	650.24	371.42							4983	0.27
	30.3	775	1.000	1.000	0.781	8158.78	291.78	313.28	775.30	393.46	101.68	462.02	238.05	0.033	5	5303	0.74	
	30.3	900	1.000	1.000	1.000	10393.90	292.31	324.01	900.37	415.75	123.44	576.35	293.92	0.027	4	5626	1.22	
	30.3	1025	1.000	1.000	1.000	12237.76	293.23	403.58	1025.45	457.95	164.72	621.87	344.11	0.032	5	6237	2.13	
	30.3	1150	1.000	1.000	1.000	14100.67	294.20	490.12	1150.55	501.10	206.90	660.43	390.76	0.038	5	6863	3.06	
	40	673	1.000	0.659	0.492	7269.77	290.71	314.44	650.47	392.13							5284	0.95
	40	775	1.000	0.955	0.710	9995.27	291.00	318.82	775.60	421.39	130.40	456.77	260.35	0.036	5	5707	1.78	
	40	900	1.000	1.000	0.947	12821.84	291.29	322.99	900.74	448.16	156.87	577.75	322.83	0.031	5	6095	2.54	
	40	1025	1.000	1.000	1.000	15276.86	291.73	378.57	1025.90	489.67	197.95	647.33	379.27	0.034	5	6697	3.72	
	40	1150	1.000	1.000	1.000	17598.51	292.21	458.10	1151.09	537.80	245.59	692.99	431.29	0.040	6	7395	5.08	
	50	673	1.000	0.730	0.540	10041.84	290.49	321.35	708.79	423.71							5741	2.30
	50	775	1.000	0.883	0.654	11784.18	290.59	324.01	776.02	442.04							6007	2.95
	50	900	1.000	1.000	0.883	15124.21	290.78	328.81	901.27	474.41	183.63	572.47	341.98	0.038	5	6476	4.10	
	50	1025	1.000	1.000	1.000	18249.82	291.03	363.11	1026.54	514.42	223.38	663.42	404.25	0.037	5	7056	5.52	
	50	1150	1.000	1.000	1.000	21060.22	291.34	436.39	1151.87	565.27	273.93	715.49	459.91	0.043	6	7794	7.33	
	60	673	1.000	0.750	0.550	12436.07	290.47	327.15	741.29	447.35							6083	3.77
	60	775	1.000	0.826	0.608	13483.80	290.51	328.71	776.56	458.18							6240	4.23
	60	900	1.000	1.000	0.829	17288.96	290.68	333.83	901.97	495.51	204.84	568.14	356.12	0.044	6	6782	5.82	
	60	1025	1.000	1.000	1.000	21063.26	290.88	353.70	1027.36	535.10	244.22	673.66	423.24	0.041	6	7356	7.51	
	60	1150	1.000	1.000	1.000	24385.97	291.13	421.17	1152.88	587.30	296.17	731.71	481.56	0.046	6	8114	9.74	
80	673	1.000	0.787	0.569	17477.77	290.60	337.87	797.44	488.25							6676	7.35	
80	775	1.000	0.787	0.569	17477.77	290.60	337.87	797.44	488.25							6676	7.35	
80	900	1.000	1.000	0.750	21471.81	290.73	342.63	903.81	525.48	234.75	561.18	374.55	0.055	7	7216	9.47		
80	1025	1.000	1.000	0.990	26385.54	290.90	348.15	1029.60	567.59	276.68	681.44	449.06	0.050	7	7827	11.86		
80	1150	1.000	1.000	1.000	30855.22	291.12	404.82	1155.56	619.55	328.43	750.74	510.82	0.055	8	8583	14.83		
100	673	1.000	0.826	0.595	22976.18	290.77	347.51	845.83	521.31							7156	11.54	
100	775	1.000	0.826	0.595	22976.18	290.77	347.51	845.83	521.31							7156	11.54	
100	900	1.000	0.944	0.698	25674.68	290.85	350.41	906.14	544.42							7491	13.18	
100	1025	1.000	1.000	0.941	31535.11	291.03	356.34	1032.57	591.20	300.18	676.23	463.03	0.061	8	8170	16.51		
100	1150	1.000	1.000	1.000	36612.56	291.22	392.62	1143.24	634.38	343.16	750.62	520.58	0.064	9	8799	19.59		

Annex IV

**Controls for the
CMR - FC MVM**

IV.1 CMR Dynamics Function

```
function Top = Top_Dynamics(Top_max_eff, flow_i, flow_i0, dt, Top)

if flow_i > flow_i0
    if Top < Top_max_eff
        gain_asc = (Top_max_eff - Top) / (2250 * (1-(flow_i^1.1/80)/2));
        Top = Top + gain_asc * dt;
    elseif Top > Top_max_eff
        gain_desc = - (Top - Top_max_eff) / (1400 * (1+(5/flow_i^0.15)/1.5));
        Top = Top + gain_desc * dt;
    else
        Top = Top_max_eff;
    end
elseif flow_i < flow_i0
    if Top > Top_max_eff
        gain_desc = - (Top - Top_max_eff) / (1400 * (1+(5/flow_i^0.15)/1.5));
        Top = Top + gain_desc * dt;
    elseif Top < Top_max_eff
        gain_asc = (Top_max_eff - Top) / (2250 * (1-(flow_i^1.1/80)/2));
        Top = Top + gain_asc * dt;
    else
        Top = Top_max_eff;
    end
end

else
    if Top < Top_max_eff
        gain_asc = (Top_max_eff - Top) / (2250 * (1-(flow_i^1.1/80)/2));
        Top = Top + gain_asc * dt;
    elseif Top > Top_max_eff
        gain_desc = - (Top - Top_max_eff) / (1400 * (1+(5/flow_i^0.15)/1.5));
        Top = Top + gain_desc * dt;
    else
        Top = Top_max_eff;
    end
end
end
```

IV.2 Hydrogen Tank Pressure Control Function

```
function flow_i = PressureControl(mass_flow, tank_press, max_press,
press_margin, Full_flow)

if tank_press >= max_press
    flow_i = min(Full_flow);
elseif tank_press < max_press & tank_press >= (max_press - press_margin)
    flow_i = min(0.8 * mass_flow * 17/3, max(Full_flow));
elseif tank_press < (max_press - press_margin) & tank_press >= (max_press - 8 +
press_margin)
    flow_i = min(2 * mass_flow * 17/3, max(Full_flow));
else
    flow_i = max(Full_flow);
end
```

IV.3 Ideal Gas Law for Tank mass calculation

```
function [tank_mass, tank_pressure] = CMR_IdealGas(tank_mass, R_H2, tank_V,  
tank_T, dt, mass_flow)
```

```
tank_mass = tank_mass + mass_flow * dt; %Simple mass balance
```

```
tank_pressure = R_H2*103 * tank_T * tank_mass / tank_V;  
%Pressure obtained from ideal gas law [Pa]
```

```
tank_pressure = tank_pressure / 105; %Pressure converted to [bar]
```

BUDGET

BUDGET INDEX

PRICE CHART N°1 1
DECOMPOSED PRICE CHART 2
BUDGET SUMMARY 3

Price Chart N°1

NUMBER	CODE	UNIT	DESCRIPTION	PRICE
UT01	BSRA.0001	u	Software and hardware tools for the development of the various models and calculations carried out throughout the thesis. This includes licenses for MATLAB, Microsoft Office, GT-Power, and REFPROP. The hardware consists of a touchscreen laptop with an Intel i7 processor and 16 GB of RAM.	1,276.44 €
ONE THOUSAND TWO HUNDRED SEVENTY-SIX EUROS AND FORTY-FOUR CENTS				
UT02	BSRA.0002	u	Calibration and validation of the fuel cell models for the Toyota Mirai and the fuel cell owned by the IUI CMT - Clean Mobility and Thermofluids for Heavy-Duty applications.	18,360.00 €
EIGHTEEN THOUSAND THREE HUNDRED SIXTY EUROS				
UT03	BSRA.0003	u	Project follow-up meetings held up each two weeks.	2,492.59 €
TWO THOUSAND FOUR HUNDRED NINETY-TWO EUROS AND FIFTY-NINE CENTS				
UT04	BSRA.0004	u	Maintenance of the laboratory rooms where the experimental work for the development of the CMR and FC models was carried out. This includes an estimation of rental costs and consumables.	26,288.00 €
TWENTY-SIX THOUSAND TWO HUNDRED EIGHTY-EIGHT EUROS				
UT05	BSRA.0005	u	Obtaining all the results presented in the thesis and drafting the report and the budget.	21,164.00 €
TWENTY-ONE THOUSAND ONE HUNDRED SIXTY-FOUR EUROS				

Decomposed Price Chart

ACTIVITY NUMBER	CODE	UNIT	DESCRIPTION	RATE	MEASUREMENT	PRICE
UT01	BSRA.0001	u	MODEL DEVELOPMENT TOOLS		1.000	
	CMT.0001	u	MATLAB Annual Standard License	900.00	0.750	675.00
	CMT.0002	u	Microsoft 365 Monthly Standard License	11.70	8.000	93.60
	CMT.0003	u	GT-Power License	2,000.00	0.005	10.96
	CMT.0004	u	RefProp Permanent License	325.00	1.000	325.00
	CMT.0005	u	ASUS Laptop. Intel i7, 16GB RAM.	979.00	0.150	146.85
	DCC.02	%	Direct Complementary Costs	1,251.41	0.020	25.03
					TOTAL COST	1,276.44 €
UT02	BSRA.0002	u	CALIBRATION AND VALIDATION OF THE FUEL CELL MODELS		1.000	
	CMT.0006	u	Toyota Mirai FC Model Calibration and Validation	12,000.00	1.000	12,000.00
	CMT.0007	u	IUI CMT FC Model Calibration	6,000.00	1.000	6,000.00
	CDC.06	%	Direct Complementary Costs	18,000.00	0.020	360.00
					TOTAL COST	18,360.00 €
UT03	BSRA.0003	u	PROJECT FOLLOW-UP MEETINGS		16.000	
	CMT.0007	h	Project Manager	33.33	0.500	16.67
	CMT.0008	h	Project Co-Director	26.17	3.000	78.51
	CMT.0009	h	Chemical Engineer	20.56	1.000	20.56
	CMT.0010	h	Technical Industrial Engineer	12.33	3.000	37.00
	CDC.02	%	Direct Complementary Costs	152.73	0.020	3.05
					TOTAL COST	2,492.59 €
UT04	BSRA.0004	u	FACILITIES MAINTENANCE		1.000	
	CMT.0011	h	Laboratory Technician	18.89	288.000	5,440.00
	CMT.0012	u	Consumables	750,000.00	3.000	2,250,000.00
	CMT.0013	u	Room rental. Monthly	3,100.00	8.000	24,800.00
	CDC.06	%	Direct Complementary Costs	24,800.00	0.060	1,488.00
					TOTAL COST	26,288.00 €
UTD05	BSRA.0005	u	THESIS WORK		1.000	
	CMT.0010	h	Technical Industrial Engineer	12.33	1560.000	19,240.00
	CDC.10	%	Direct Complementary Costs	19,240.00	0.100	1,924.00
					TOTAL COST	21,164.00 €

Budget Summary

ACTIVITY NUMBER	DESCRIPTION	UNITS	MEASUREMENT	PRICE
UT01	MODEL DEVELOPMENT TOOLS	U	1.00	1,276.44 €
UT02	CALIBRATION AND VALIDATION OF THE FUEL CELL MODELS	U	1.00	18,360.00 €
UT03	PROJECT FOLLOW-UP MEETINGS	U	16.00	2,492.59 €
UT04	FACILITIES MAINTENANCE	U	1.00	26,288.00 €
UT05	THESIS WORK	U	1.00	21,164.00 €
EXECUTION BUDGET				69,581.03 €
13.00% General Expenses				9,045.53 €
6.00% Industrial Benefices				4,174.86 €
OVERALL INVESTMENT BUDGET				82,801.42 €
21.00% IVA				17,388.30 €
TOTAL PROJECT COST				100,189.72 €

The budget amounts to the expressed sum of ONE HUNDRED THOUSAND ONE HUNDRED EIGHTY-NINE EUROS AND SEVENTY-TWO CENTS.